

Cellular and molecular pharmacology of the lipid-sensitive channel TMEM16A/Anoctamin1



Lara Francesca Scofano

The Queen's College

University of Oxford

Thesis submitted for the degree of Doctor of Philosophy

Trinity 2022

Table of Contents

ABSTRACT.....	5
ACKNOWLEDGEMENTS	6
ABBREVIATIONS	7
LIST OF FIGURES	11
LIST OF TABLES	13
CHAPTER 1.....	14
INTRODUCTION	14
1.1 Blood vessel structure and function	15
1.1.1 Regulation of vascular tone	17
1.1.2 Regulation of contraction in vascular smooth muscle cells	20
1.2 Ion channels and membrane potential regulation in VSMCs	26
1.3 Ion channels and transporters in smooth muscle cells	28
1.3.1 K ⁺ channels	28
1.3.2 Other cation channels	30
1.3.3 Cl ⁻ channels	31
1.4 The biochemistry of the plasma membrane.....	33
1.4.1 The endocytic system	37
1.4.2 The lysosome	38
1.5 NPC gene/protein defects.....	41
1.5.1 Lipid storage in NPC disease.....	42
1.5.2 Therapeutics for NPC disease.....	43
1.6 Lipid modulation of ion channels.....	45
1.6.1 Cholesterol.....	46
1.6.2 Phosphoinositides	46
1.6.3 Sphingolipids.....	47
1.7 The lipid-sensitive TMEM16A Ca ²⁺ -activated Cl ⁻ channel	48
1.7.1 TMEM16x family.....	49
1.7.2 TMEM16A structure	52
1.7.3 TMEM16A biophysical properties	54
1.8 TMEM16A role in vascular smooth muscle contraction.....	55
1.9 TMEM16A pharmacology	57
1.10 Potential role for TMEM16A in vascular disease.....	59
1.10.1 Hypertension.....	59
1.10.2 Microcirculation in the brain.....	60
1.11 Hypothesis and aims	63
CHAPTER 2.....	64
METHODS.....	64
2.1 Chemicals and reagents	65
2.2 Animals.....	65
2.3 Cell preparation	66
2.3.1 Cell lines.....	66
2.3.2 Cell culture	67
2.3.3 Cell transfection.....	67
2.3.4 Native smooth muscle cells isolation	68
2.4 Molecular Biology	70
2.4.1 Bacterial transformation	70

2.4.2	DNA extraction and purification.....	71
2.4.3	Site directed mutagenesis and primer design.....	72
2.5	Patch-clamp electrophysiology.....	74
2.5.1	Patch-clamp experimental set up.....	76
2.5.2	Patch-clamp configurations.....	78
2.5.3	Perfusion system	79
2.5.4	Stimulation protocols	80
2.5.5	Solutions for electrophysiology	81
2.5.6	Noise analysis	84
2.6	Wire myography	85
2.6.1	Wire myography experimental setup.....	86
2.6.2	Normalisation theory.....	87
2.6.3	Normalisation procedure	88
2.6.4	Wire myography experimental design	88
2.6.5	Wire myography solutions	89
2.6.6	[PE]-tension relationship analysis	91
2.7	Cortical slices preparation	91
2.8	Imaging.....	92
2.8.1	Immunocytochemistry & Immunocytochemistry	92
2.8.2	Live Imaging.....	93
2.8.3	Calcium imaging.....	94
2.8.4	Cortical slice capillary pericyte imaging	94
2.9	Imaging analysis	95
2.10	Data & statistical analysis	96
2.10.1	Experimental design.....	97
2.10.2	Randomisation	97
2.10.3	Operator blinding.....	98
2.11	Contribution to work	98
CHAPTER 3.....		99
TMEM16A CHARACTERISATION.....		99
3.1	Functional and cellular properties of TMEM16 channels.....	100
3.2	Electrophysiological profile of TMEM16A	101
3.3	Other TMEM16x family members expressed in the vasculature	104
3.3.1	Electrophysiological profile and cellular expression of TMEM16B	104
3.3.2	Electrophysiological profile and cellular expression of TMEM16F	106
3.3.3	Electrophysiological profile and cellular expression of TMEM16K	108
3.4	Pharmacology of TMEM16A channels.....	110
3.4.1	Ani9 is a selective TMEM16A inhibitor.....	110
3.4.2	AUT11813 and AUT11814 as TMEM16A inhibitors.....	113
3.5	TMEM16A functional role in the vasculature	115
3.5.1	TMEM16A-mediated mouse aortic contractility.....	115
3.5.2	TMEM16A-mediated rat aortic contractility	117
3.6	Discussion.....	119
3.6.1	Properties of cloned TMEM16A-mediated currents and other TMEM16x family members	119
3.6.2	Action of the TMEM16A-inhibitors in heterologous system.....	122
3.6.3	Features of TMEM16A-mediated vessel contraction in the aorta.....	122
CHAPTER 4.....		125
CONTROL OF TMEM16A ACTIVITY BY THE LYSOSOMAL NPC1 PROTEIN.....		125
4.1	NPC1 modulation of TMEM16A channel properties	126

4.1.1	NPC1 inhibition impairs cholesterol distribution	127
4.1.2	Pharmacological NPC1 inhibition or genetic <i>Npc1</i> deletion enhances TMEM16A currents.....	128
4.1.3	Treatment with β CD or NPC1 re-introduction rescues TMEM16A activation	135
4.1.4	TMEM16A response to α 1 adrenergic-receptors is modulated by NPC1	137
4.1.5	TMEM16A gating is affected during NPC1 inhibition.....	140
4.2	Sphingosine does not affect in TMEM16A activation by NPC1	142
4.3	The action of NPC1 on the TMEM16A channel involves PIP ₂	144
4.3.1	DrVSP-mediated PIP ₂ depletion prevents NPC1 modulation of TMEM16A	147
4.3.2	Scavenging PIP ₂ with neomycin prevents NPC1 modulation of TMEM16A	149
4.3.3	A PIP ₂ -insensitive TMEM16A mutant channel is also insensitive to NPC1	150
4.3.4	Plasmalemmal PIP ₂ level is increased during NPC1 inhibition	153
4.4	TMEM16A modulation by NPC1 is not affected by the KCNE1 auxiliary subunit.....	155
4.5	Discussion.....	157
4.5.1	TMEM16A current is activated by NPC1 inhibition	158
4.5.2	TME161A activation by NPC1 inhibition can be corrected by β CD and <i>Npc1</i> re-introduction	158
4.5.3	TMEM16A open probability is increased during NPC1 inhibition.....	159
4.5.4	Effect of α 1 adrenergic receptor stimulation during NPC1 inhibition	159
4.5.5	PIP ₂ is a potent mediator of the TMEM16A channel regulation by NPC1	160
4.5.6	PIP ₂ activates TMEM16A during NPC1 inhibition by distributing at the plasma membrane in a cholesterol-dependent manner.....	160
4.6	TMEM16A auxiliary subunit KCNE1 does not affect the channel response to NPC1 inhibition	162
4.7	Conclusions	162
CHAPTER 5.....		163
VASCULAR OVER-ACTIVITY IN <i>NPC1</i> ^{-/-} MICE RELIES ON TMEM16A POTENTIATION		163
5.1	Native TMEM16A currents in vascular smooth muscle cells are modulated by NPC1	164
5.1.1	TMEM16A current is enhanced in vascular smooth muscle cells isolated from <i>Npc1</i> ^{-/-} mice.....	165
5.2	TMEM16A modulation by NPC1 impacts arterial function	167
5.2.1	PE-mediated vessel contraction is increased in the vasculature of <i>Npc1</i> ^{-/-} mice	167
5.2.2	β CD treatment of <i>Npc1</i> ^{-/-} mice restores enhanced PE-mediated vessel contraction	173
5.2.3	Blocking TMEM16A reduces contractility of <i>Npc1</i> ^{-/-} aortas	175
5.2.4	Aortas isolated from <i>Npc1</i> ^{-/-} mice are more sensitive to changes in extracellular chloride	177
5.3	TMEM16A modulation on NPC1 affects capillary function	179
5.3.1	Pericytes density is decreased in brain slices of <i>Npc1</i> ^{-/-} mice	179
5.3.2	TMEM16A modulation of NPC1 increases capillary contractility properties in <i>Npc1</i> ^{-/-} mice	181
5.3.3	TMEM16A modulation of NPC1 increases pericytes cell death in <i>Npc1</i> ^{-/-} mice	183
5.4	Discussion.....	185
5.4.1	Electrophysiological properties of native <i>Npc1</i> ^{-/-} smooth muscle cells	185
5.4.2	Agonist-mediated contractility in <i>Npc1</i> ^{-/-} mice	186
5.4.3	TMEM16A modulates agonist-mediated contractility in <i>Npc1</i> ^{-/-} mice.....	187
5.5	TMEM16A modulation on NPC1 regulates brain capillaries function in <i>Npc1</i> ^{-/-} mice	188
5.6	Conclusions	189
CHAPTER 6.....		191
CONCLUDING REMARKS		191
PUBLICATIONS, PRESENTATIONS, POSTERS AND AWARDS.....		198
REFERENCES		199

Abstract

TMEM16A Ca^{2+} -activated Cl^- channels (CaCC) control vital functions including arterial smooth muscle tone and blood flow. The TMEM16A has a pore with regions surrounding plasmalemmal lipids, an arrangement where lipids can directly influence the ion permeation and gating of the channel. Here, it is hypothesised that TMEM16A channel may serve as a lipid sensor and couple changes in lipid metabolism to changes in cell electrical activity. It is also argued that TMEM16A channels may be indirectly modulated by the lysosome and in particular by the lysosomal lipid transporter Niemann-Pick type C 1 (NPC1) protein, given the key involvement of this organelle in the control of plasmalemmal lipid composition. Thus, it is suggested that changes in the plasmalemmal composition driven by lysosomes, can modulate the plasma membrane-residing TMEM16A channel, impacting vascular function. Indeed loss-of-function mutations in NPC1 leads to Niemann-Pick disease Type C (NPC), a neurodegenerative disorder with a range of systemic alterations, including vascular. Here, I explore the capacity of the NPC1 to control TMEM16A function, and examine the consequence of this modulation on the tone of isolated arteries, which abundantly express TMEM16A. Key results include: (i) TMEM16A currents were enhanced during NPC1 inhibition; (ii) depletion of plasmalemmal phosphatidylinositol 4,5-biphosphate (PIP_2) prevented this activation; (iii) plasmalemmal PIP_2 distribution was increased during NPC1 inhibition; (iv) aortic rings and cerebral capillaries obtained from *Npc1 null* mice showed enhanced contractility; (v) β -cyclodextrin, a drug currently studied for treating NPC disease, prevented TMEM16A activation and aortic contractility in samples obtained from *Npc1 null* mice. These results indicate that TMEM16A activity is modulated by NPC1. This regulation affects the tone of arteries. PIP_2 -dependent changes in TMEM16A activity may be the basis of vascular overactivity associated with NPC disease.

Acknowledgements

Firstly, I would like to express my sincere gratitude to Dr Paolo Tamaro. This work would have not been possible without his constant support and guidance. I am extremely grateful that during my MSc project, he saw in me the interest and perseverance to continue my project as a PhD student and since then, has always believed in me and mentored me with his meticulous attention, sincere curiosity and honest drive for scientific research. I would also like to thank Prof Frances Platt, who offered me the possibility to work in a collaboration with her lab and included me in exciting conferences and challenges for charity. I am very gratefully to Prof Platt for her mentorship, support and inspiration. A huge thanks to Dr Barbara Zonta for accepting me to Oxford in the first place, guiding me to the Tamaro's lab and supporting me on multiple occasions. Her smile and positivity have lightened up many of my days as an MSc and PhD student. Thank you to the members of Autifony Therapeutics, in particular Dr Charles Large and Dr Martin Gunthrope who gave me the opportunity to conduct my PhD project in collaboration with Autifony Therapeutics and for their feedback at all stages of the project. I am also very grateful to Autifony Therapeutics and The Queen's College for their funding.

I would like to thank incredible members and alumni of the Tamaro lab: Dr Kathryn Acheson, Dr Ria Dinsdale, Claire Pearson, Dr Zeki Ilkan, Dr Emilio Agostinelli, Dr Rumaitha Al Hosni, Zuzanna Borawska and Thibault Jouen-Tachoire. They have all been incredible colleagues and still are amazing friends. Thanks to other members of the Department of Pharmacology, in particular Dr Abigail Wilson and Dr Razik Mu-u-Min who have been and keep being part of my scientific and friend support team. A special thanks to Shruti Kochhar for her loving support, constant cheering and scientific consultations. I would also like to thank friends from my MSc in Pharmacology who kept in touch during my PhD: Karolina Weglinski, Adriana Gardner, Hanson Ng and Vicky Lee. I am also very grateful to my friends Abdul Abdulrahim, Dr Dheeya Rizmie, Othman Al Bahri and Dr Sarah Jilani as each of them has been for me an immense source of company, support and inspiration throughout my PhD.

I could have not done my PhD without the continuous love and support of my parents Paola and Pasquale, as well as the one of my new Ogunlana family, whom I am so very grateful to have come into my life.

Finally, thank you to my husband, Bo, for being on my side every step of the way. It has not been easy to reach the finish line with a pandemic in the middle of the road, but thanks to you, I now know that what I am able to achieve depends on what I allow myself to dream.

Abbreviations

[Ca ²⁺] _i	Intracellular free calcium concentration
4-AP	4-amino pyridine
ACSF	Artificial cerebrospinal fluid
Angpt1	Angiopoietin 1
Ani9	2-(4-Chloro-2-methylphenoxy)-acetic acid 2-[(2-methoxyphenyl)methylene]hydrazide
ANP	atrial natriuretic peptide
ATP	Adenosine triphosphate
Aβ	Amyloid-β
BBB	Blood-brain barrier
BK _{Ca}	Large-conductance voltage- and Ca ²⁺ -activated K ⁺ channel
BSA	Bovine albumin serum
CaCC	Ca ²⁺ activated Cl ⁻ channel
CaM	Calmodulin
cAMP	Cyclic adenosine monophosphate
Ca _v	Voltage-gated Ca ²⁺ channels
CDE	Clathrin dependent
CDI	Clathrin dependent
CFTR	Cystic fibrosis transmembrane conductance regulator
CHO	Chinese Hamster Ovary
CICR	Ca ²⁺ -induced calcium-release
CIC	Volume-activated Cl ⁻ channel
CNS	Central nervous system
COX	Cyclooxygenase
Cryo-EM	Single-particle electron cryomicroscopy
CTD	C-terminal domain
Cx	Connexin
DAG	Diacylglycerol
DAPI	4',6-diamidino-2-phenylindole
DIDS	4,4'-diisothiocyanatostilbene-2,2'-disulphonic acid

DM	Dissociation medium
DTT	Dithiothreitol
ECS	Extracellular solution
eNaC	Epithelial Na ⁺ channel
ER	Endoplasmic reticulum
ET ₁	Endothelin-1
GalCer	Galactosylceramide
GC	Guanylate cyclase
GlcCer	Glucosylceramide
GM	Monosialogangliosides
G _q PCR	G _q coupled receptor
GSL	Glycosphingolipid
HEK-293T	Human embryonic kidney 293T
IB4	Isolectin-4
ICS	Intracellular solution
IL-4	Interleukin-4
IP ₃	Inositol-3-phosphate
IP ₃	Inositol trisphosphate
IP ₃ Rs	IP ₃ receptors
K _{ATP}	ATP-activated K ⁺ channels
K _{ir}	Inwardly-rectifying K ⁺ channel
K _v	Voltage-gated K ⁺ channel
LacCer	Lactosylceramide
LB	Lysogeny broth
LDL	Low-density lipoprotein
LDL-R	Low-density lipoprotein receptor
LipA	Lysosomal acid lipase A
MES	Methanesulfonate
MIC	Mg ²⁺ -inhibitory cation channels
MLCK	Myosin light chain kinase
MLCPPT	Myosin light chain phosphatase
MOC	Manders' overlap coefficient

MONNA	N-((4-methoxy)-2-naphthyl)-5- nitroanthranilic acid
NA	Noradrenaline
NAADP	Nicotinic acid adenine dinucleotide phosphate
Na-MES	Na-methanesulfonate
NCX	Na ⁺ /Ca ²⁺ exchanger
NFA	Niflumic acid
NO	Nitric oxide
NPC	Niemann-Pick disease type C
NPC1	Niemann-Pick type C 1
NPC2	Niemann-Pick type C 2
NPPB	5-nitro-2-(phenylpropylamino)-benzoate
OGD	Oxygen- and glucose- deprived
ORAI1	Ca ²⁺ release-activated Ca ²⁺ modulator 1
P2X	ATP-ligand gated purinergic
PB	Phospholamban
PC	Phosphatidylcholine
PCC	Pearson's correlation coefficient
PE	Phenylephrine
PEdt	Phosphatidylethanolamine
PG	Phosphatidylglycerol
PGI ₂	Prostacyclin
PI	Phosphatidylinositol
PI4-K	Phosphatidylinositol 4-kinase
PIP ₂	Phosphatidyl-inositol(4,5)-bisphosphate
PIP5K	Phosphatidylinositol 4-phosphate 5-kinase
PKC	Phosphokinase-C
PLC	Phospholipase C
PMCA	Plasma membrane Ca ²⁺ ATPase
PS	Phosphatidylserine
PSS	Physiological salt solution
PUFAs	Polyunsaturated fatty acids
RND	Resistance-nodulation cell-division

RyR	Ryanodine receptor
S1P	Sphingosine-1-phosphate
SBP	Systolic blood pressure
SCAR10	Autosomal recessive spinocerebellar ataxia type 10
SERCA	Sarco(endo)plasmic reticulum calcium-ATPases
SiRNA	Short interfering RNA
SL	Sphingolipid
SOCCs	Store operated calcium channels
SR	Sarcoplasmic reticulum
STIM	Stromal-interaction molecule
SV40	Simian Virus 40
TAX ₂	Thromboxane-2
TEA	Tetraethyl ammonium
TGFβ	Transforming growth factor beta
TMDs	Transmembrane domains
TPC	Two-pore channel
TRPC	Transient receptor potential cation
UC	Unesterified cholesterol
UTP	Uridine 5'-triphosphate
VEGF	Vascular endothelial growth factor
VGCC	Voltage-gated Ca ²⁺ channel
V _m	Membrane potential
VSMCs	Vascular smooth muscle cells
β-CD	β-cyclodextrin
τ _{1/2}	Half maximal amplitude

List of Figures

Figure 1.1.1 Structural organisation of the mammalian cardiovascular system.	17
Figure 1.1.2 Ion channels and signalling pathways in VSMCs.	25
Figure 1.4.1 Lipid composition of the plasma membrane.	35
Figure 1.4.2 Lysosome mediation of cholesterol delivery to the plasma membrane.	38
Figure 1.4.3 The role of the lysosome in endocytosis, phagocytosis, and autophagy.....	40
Figure 1.7.1 TMEM16x family: scramblases and ion channels.	52
Figure 1.7.2 TMEM16A structure	54
Figure 1.8.1 Role of TMEM16A in VSMC vasoconstriction.....	57
Figure 1.9.1 Synthetic TMEM16A inhibitors.....	58
Figure 1.10.1 Pericytes surrounding capillaries in the brain.	61
Figure 2.4.1 Single point site directed mutagenesis.....	73
Figure 2.5.1 The cell membrane as a model of an electrical circuit.....	75
Figure 2.5.2 Diagrammatic representation of the whole-cell patch clamp experimental set up.....	77
Figure 2.5.3 Diagrammatic representation of recording configurations in patch-clamp electrophysiology....	79
Figure 2.5.4 Voltage stimulation protocols for patch-clamp electrophysiology recordings.	81
Figure 2.6.1 Diagrammatic representation of the wire myography set up	86
Figure 3.2.1 TMEM16A IV-relationship	102
Figure 3.2.2 TMEM16A calcium-sensitivity.	103
Figure 3.3.1 Properties of TMEM16A and TMEM16B IV-relationships.	105
Figure 3.3.2 TMEM16F time-dependent current.	107
Figure 3.3.3 TMEM16K is an intracellular channel localised at the ER.	109
Figure 3.4.1 Effect of Ani9 on cloned TMEM16A currents	111
Figure 3.4.2 Effect of Ani9 on cloned TMEM16B currents	112
Figure 3.4.3 The effects of AUT11813 and AUT11814 on whole-cell TMEM16A currents.....	114
Figure 3.5.1 The effect of Ani9 on phenylephrine-induced contraction in mouse arteries.	116
Figure 3.5.2 The effect of AUT11817, AUT11814 and Ani9 on phenylephrine-induced contraction in rat arteries.....	118
Figure 4.1.1 NPC1 inhibition or Npc1 gene deletion impairs intracellular lipid homeostasis.	128
Figure 4.1.2 TMEM16A current is enhanced during NPC1 inhibition	131
Figure 4.1.3 TMEM16B and TMEM16F activity during NPC1 inhibition.....	132
Figure 4.1.4 NPC1 co-localisation with cloned TMEM16A, TMEM16B and TMEM16F channels.....	134
Figure 4.1.5 TMEM16A activation by NPC1 is rescued by β CD treatment or NPC1 re-introduction.	136
Figure 4.1.6 Activation of TMEM16A current by α 1-adrenergic receptor activation is enhanced upon NPC1 inhibition.....	139
Figure 4.1.7 TMEM16A channel gating is modulated by NPC1 inhibition	141
Figure 4.2.1 Sphingosine secondary effect on TMEM16A activation.....	143
Figure 4.3.1 TMEM16A current is activated by diC8-PIP ₂ and reduced by PIP ₂ depletion.....	146
Figure 4.3.2 PIP ₂ depletion by DrVSP abolishes NPC1 activation of TMEM16A current.....	148
Figure 4.3.3 Neomycin sequesters PIP ₂ blocking TMEM16A current activation by NPC1	149
Figure 4.3.4 TMEM16A-R482A mutant channel is not modulated by NPC1 inhibition	151
Figure 4.3.5 Block of PLC with edelfosine enhances TMEM16A currents	152
Figure 4.3.6 PIP ₂ cellular distribution is increased at the plasma membrane during NPC1 inhibition	154
Figure 4.4.1 The TMEM16A auxiliary subunit KCNE1 does not regulate the channel modulation by NPC1. .	156
Figure 5.1.1 TMEM16A currents in VSMCs.....	166
Figure 5.2.1 PE-induced contraction in isolated aortic rings and mesenteric arteries from Npc1 ^{-/-} mice	169
Figure 5.2.2 Structural properties of isolated aortic rings from Npc1 ^{-/-} mice	171

Figure 5.2.3 Structural properties of isolated aortic rings and mesenteric arteries from <i>Npc1</i>^{-/-} mice	172
Figure 5.2.4 PE-induced contraction in aortic rings from <i>Npc1</i>^{-/-} mice treated with βCD.....	174
Figure 5.2.5 PE-induced contraction in <i>Npc1</i>^{-/-} isolated aortic rings in the presence of the TMEM16A inhibitors Ani9 or TMinh-23.....	176
Figure 5.2.6 Extracellular Cl^- in PE-induced arterial contraction in <i>Npc1</i>^{-/-} aortic rings.....	178
Figure 5.3.1 The distribution of pericytes in <i>Npc1</i>^{-/-} mice microvasculature.....	180
Figure 5.3.2 Capillary constriction in response to endothelin-1 in <i>Npc1</i>^{-/-} brain microvasculature	182
Figure 5.3.3 Pericytes cell death in <i>Npc1</i>^{-/-} brain microvasculature.	184
Figure 5.6.1 Proposed mechanism of TMEM16A activation and increased vascular contractility in a VSMC cell during NPC1 inhibition.	195

List of Tables

Table 1 VSMC ion concentrations.....	27
Table 2 Physiological salt solution (PSS)	69
Table 3 Dissociation medium (DM)	69
Table 4 Plasmid DNA.	71
Table 5 Primers designed to constitute mutant TMEM16A channels.....	73
Table 6 Extracellular solution for measurement of I_{CaCC} (ECS)	82
Table 7 Intracellular solution for measurement of I_{CaCC} (ICS).....	82
Table 8 Ca^{2+} for intracellular solution for measurement of I_{CaCC}	83
Table 9 Low EGTA intracellular solution for measurement of I_{CaCC}	83
Table 10 Physiological salt solution (PSS)	89
Table 11 High K^+ physiological salt solution (PSS).....	89
Table 12 Low Cl^- physiological salt solution (PSS)	90
Table 13 K-MES physiological salt solution (PSS)	90
Table 14 K-MES MES physiological salt solution (PSS) for variable K-MES concentrations.....	90
Table 15 Slicing solution for cortical slices	92
Table 16 Antibodies and dyes used for live and fixed staining	93
Table 17 Calcium imaging recording medium	94
Table 18 Artificial cerebrospinal fluid (aCSF) solution.....	95
Table 19 Hill-fit parameters (EC_{50} , max and h) (Eq. 13) for HEK-293T and CHO cells.	103
Table 20 Hill-fit parameters (IC_{50} , max and h) (Eq. 13) for HEK-293T cells expressing TMEM16A.....	114
Table 21 Hill-fit parameters (EC_{50} , max and h) (Eq. 13) for mouse aortic rings.	116
Table 22 Hill-fit parameters (EC_{50} , max and h) (Eq. 13) for aortic rings.	170
Table 23 Hill-fit parameters (EC_{50} , max and h) (Eq. 13) for mesenteric rings.	170
Table 24 Hill-fit parameters (EC_{50} , max and h) (Eq. 13) for aortic rings.	171
Table 25 Hill-fit parameters (EC_{50} , max and h) (Eq.13) for aortic rings in mice treated with β CD.....	174
Table 26 Hill-fit parameters (EC_{50} , max and h) (Eq.13) for aortic rings in the presence of the TMEM16A inhibitor Ani9.....	176
Table 27 Hill-fit parameters (EC_{50} , max and h) (Eq.13) for aortic rings in the presence of the TMEM16A inhibitor TMinh-23.	177

Chapter 1

Introduction

This chapter outlines the composition and function of the mammalian cardiovascular system, with emphasis on the role of ion channels in the regulation of vascular smooth muscle cells (VSMCs) contractility. This overview includes an account of the structural organisation and functions of the vessels and then continues on a cellular level, examining how the regulation of intracellular calcium affects the contractility of VSMCs. Many of the ion channels expressed in VSMCs are sensitive to plasmalemmal lipids, thus, the biochemistry of the plasma membrane is examined with focus on the function of the lysosome and particularly on the lysosomal protein NPC1 in controlling cellular lipid homeostasis. Specifically, the lipid-sensitive CaCC channel encoded by the *TMEM16A* gene, is hypothesised to play an essential role in VSMCs contraction and vascular disease.

1.1 Blood vessel structure and function

The mammalian circulation fulfils two fundamental functions: (i) distribution and (ii) exchange. Distribution refers to transport of blood to and away from a given organ. Exchange involves the diffusive passage of gasses, nutrients and waste product (i.e. CO₂, urea, lactic acid), as well as the transfer of fluids between blood and tissues (Klabunde 2012, Herring 2018). While the blood flow (i.e. cardiac output) enables the stroke volume to reach distal bodily organs rapidly, ultimately the exchange of substances with a given organ occurs *via* diffusion, in the direction determined by the local Starling forces (Klabunde 2012, Herring 2018). The circulation also fulfils a range of other functions, including transfer of heat, distributions of a range of hormones and immune responses (Klabunde 2012, Herring 2018). The circulatory system may also be the source of regulatory factors (e.g. nitric oxide (NO) produced by vascular, natriuretic peptides released by atrial myocytes, angiotensin II produced in lung endothelium etc.). Figure 1.1.1 shows the organisation of the mammalian circulatory system, where arteries distribute oxygenated blood from the heart to tissues and organs, while veins collect the blood from tissues and organs to transport it back to the heart (Pugsley and Tabrizchi 2000, Klabunde 2012, Guyton 2015). The diameter and thickness of the arteries

decrease as the distance from the heart increases (Levy 2007, Klabunde 2012). The aorta is the largest artery (25 mm diameter in humans) and is normally subjected to pressure ranging from 80 mmHg (diastolic blood pressure) to 120 mmHg (systolic blood pressure) (Wei, Galaviz et al. 2020). The wall of the aorta is especially elastic and thick (2 mm thick in humans) in order to accumulate the stroke volume during ventricular systole and discharge that volume with diastole, a process known as Windkessel effect (Levy 2007, Klabunde 2012). The thickness of the aortic wall requires specific blood flow to reach the deeper parts of the artery wall. This is obtained by a network of small vessels and capillaries called *vasa vasorum* (Heistad and Marcus 1979, Billaud, Donnenberg et al. 2017). Like the aorta, other large arteries have also a high ratio of elastin to tolerate stretch in response to diastolic and systolic blood pressure changes. The walls of small arteries and arterioles dynamically tune the local blood flow and are regulated by a range of locally-released and circulating substances (Levy 2007, Klabunde 2012). In contrast, venules and veins have a low ratio of smooth muscle cells and elastin as they return blood to the heart to lower blood pressure (Klabunde 2012, Guyton 2015).

Vascular cells include: VSMCs, endothelial cells and pericytes. VSMC from the tunica media (see below), while the endothelial cells (ECs) line the lumen of the vessels. Pericytes wrap around the endothelial cells forming the capillaries wall to regulate their diameter by constricting or relaxing in response to a wide range of stimuli (Peppiatt, Howarth et al. 2006, Attwell, Mishra et al. 2016, Hartmann, Berthiaume et al. 2021). Arteries and veins are composed by three main layers: the *tunica intima* (inner layer), *the tunica media* (middle layer) and the *tunica adventitia* (outer layer). The *tunica intima* is characterised by a monolayer of endothelial cells on the basement membrane and elastic lamina in the internal membrane (Klabunde 2012). Endothelial cells release vasoactive substances such as NO, prostacyclin, endothelin and prostanoids (Deanfield, Halcox et al. 2007, Garland, Hiley et al. 2011). The *tunica media* is composed of smooth muscle cells, elastin fibres, collagen and glycoproteins (Klabunde 2012, Guyton 2015). This layer is found in all vessels apart from capillaries and

venules (Klabunde 2012, Guyton 2015). The *tunica adventitia* is rich in collagen, fibroblasts and autonomic nerve endings which release neurotransmitters such as noradrenaline (NA), neuropeptide Y and adenosine triphosphate (ATP) regulating the vascular tone (Levy 2007, Klabunde 2012). The proportion of the different layers depends on the size and function of the blood vessels as illustrated in Figure 1.1.1.

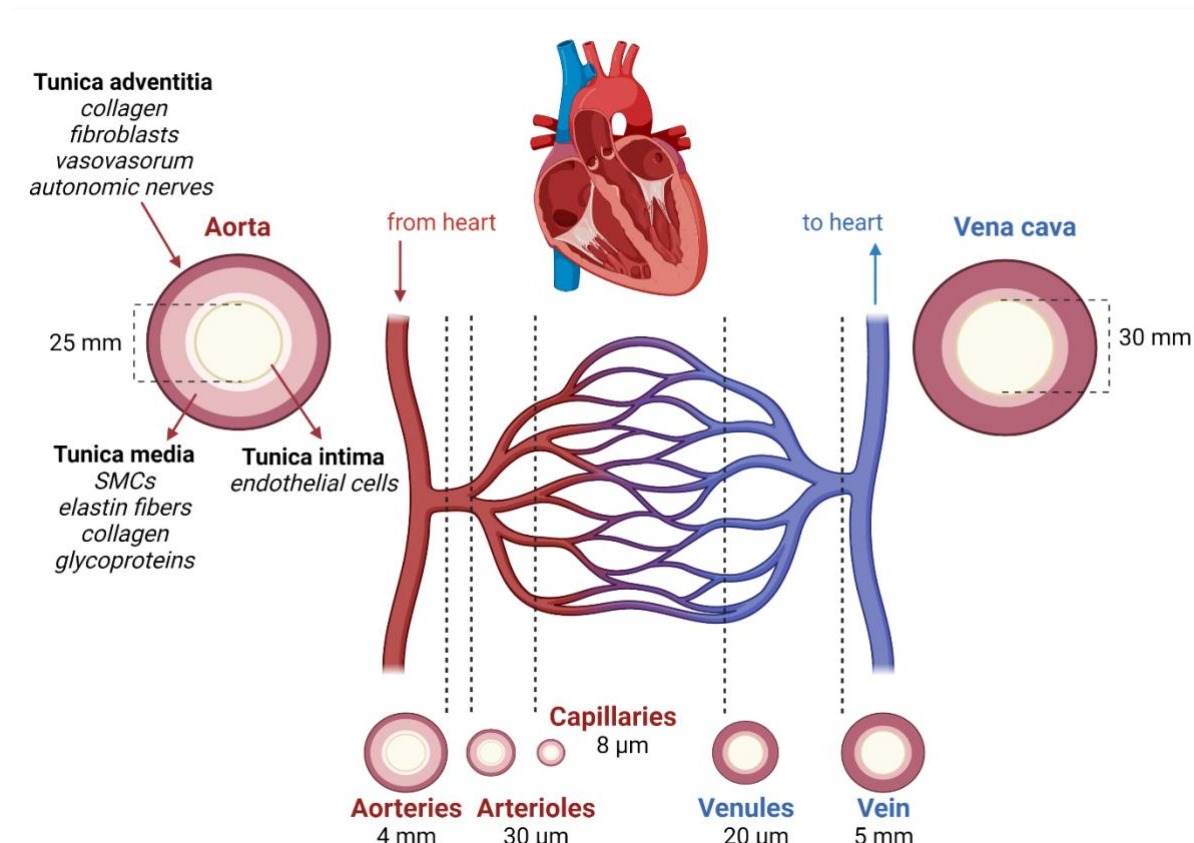


Figure 1.1.1 Structural organisation of the mammalian cardiovascular system.

Schematic illustration of the cardiovascular system. The aorta separates into arteries and arterioles. The network of capillaries connects arterioles with venules, which then collects into the veins and the vena cava. Diameter of vessels is taken from (Burton et al. 1954).

1.1.1 Regulation of vascular tone

In addition to the regulation by chemical factors, arterioles are also sensitive to mechanical forces. The 'myogenic tone' refers to arteriolar contraction in response to an increase in blood pressure (Seftel, Johnson et al. 1980, Jackson 2021). This mechanism is essential to regulate local blood flow and was first observed over than a century ago by Bayliss (Bayliss 1902).

When the luminal pressure of the vessel increases, the radial force is transmitted to the wall of the blood vessels increasing the tangential wall stress (T) which is given by Laplace law:

$$T = \frac{P \cdot r}{\Delta} \quad \text{Equation 1}$$

where P is the pressure of the lumen of the wall, r is the radius of the lumen and Δ is the thickness of the wall (Jackson 2020). An initial increase in T induces a passive dilation of the vessel that activates non-selective cation channels in VSMCs leading to calcium (Ca^{2+}) influx and contraction leading to the pressure-induced myogenic tone and reduction in local blood flow (Jackson 2020).

More generally, any factor that affect artery diameter will affect the vessel resistance to blood flow, according to the Poiseuille's law as:

$$F = \frac{\Delta P \cdot \pi \cdot r^4}{8 \cdot \eta \cdot L} \quad \text{Equation 2}$$

Where F is the blood flow, ΔP is the difference in pressure between two ends of the vessels in Pascal (arterial minus venous pressure), r is the radius of the lumen of the vessel, η is the viscosity of the blood and L is the length of the vessel. Under steady state physiological conditions, the blood viscosity and length of the vessels can be considered near constant. The apparent blood viscosity increases as the diameter of the vessel increases in a non-linear fashion (Pries, Neuhaus et al. 1992). Thus, the apparent blood viscosity is much higher in capillaries than in large arteries. The Poiseuille law was derived on the assumption that the vessel is straight and rigid tube. While this approximation does not strictly apply to blood vessels, this law remains a very useful conceptual framework, and it has been used extensively to model haemodynamic of human and animal blood vessels (Secomb 2016).

According to the Poiseuille law, a change in the diameter of the vessel is quantitatively the most important factor that modifies the blood flow to fourth power. F can be expressed using the Darcy's law as:

$$F = \frac{\Delta P}{R} \quad \text{Equation 3}$$

where R is the resistance of the vessel. It should be noted that the Darcy's law offers a good approximation of blood flow within a single organ, but the Bernulli's equation may be more suitable for calculation of blood flow in different organs since it takes into account the total mechanical energy of the blood. Combining equation 2 and 3, R is equal to:

$$R = \frac{8 \cdot \eta}{r^4 \cdot \pi} \quad \text{Equation 4}$$

The structural organisation of the vessels in an organ also affects the total resistance they provide to blood flow. The total resistance of blood vessels disposed in parallel (R_T) is equal to the sum of the reciprocal individual resistances (Levy 2007, Klabunde 2012, Guyton 2015):

$$\frac{1}{R_T} = \frac{1}{R_1} + \frac{1}{R_2} + \frac{1}{R_3} + \dots, \quad \text{Equation 5}$$

This equation implies that in a network of parallel vessels, the total resistance is less than the single lowest resistance. This is important for example in the network of capillaries. These individual vessels have the high resistance because of their small diameter. However, their total resistance is reduced as they form an intricate network of parallel vessels in the microvasculature (Levy 2007, Klabunde 2012, Guyton 2015). The second principle is that in a network of many parallel vessels, changing the resistance of one single vessel will have little

effect on the total resistance. Therefore, the various organs in the body are connected in parallel to ensure an overall low resistance to blood flow (cardiac output) and also to ensure that oxygenated blood can reach each organ simultaneously.

In contrast, vessels disposed in series are associated with a total resistance (R_T) which is equal to the sum of the individual resistances (Levy 2007, Klabunde 2012, Guyton 2015):

$$R_T = R_1 + R_2 + R_3 + \dots, \quad \text{Equation 6}$$

Therefore, for vessels disposed in series, an increase in the individual resistance can largely affect the total resistance. Arterioles, which are the primary site of resistance, have the biggest contribution to total resistance to blood flow and in the systemic circulation they are considered to provide 80% of the total peripheral resistance (Levy 2007, Klabunde 2012, Guyton 2015).

1.1.2 Regulation of contraction in vascular smooth muscle cells

VSMCs are typically 5 to 10 μm in diameter and 50 to 300 μm in length (Jackson 2021). The surface area of VSMCs is increased up to 70% by the presence of 50-90 nm invaginations known as caveolae (Parton and Simons 2007, Dart 2010). These structures play an important role in the coordination of cell excitability according to their position in relation to intracellular organelles (i.e. sarcoplasmic reticulum), and also by being enriched with specific populations of receptors, ion channels and proteins (Parton and Simons 2007, Dart 2010). VSMCs control the vascular tone in response to chemical, electrical, mechanical and metabolic stimuli (Jackson 2020). Examples of chemical stimuli are noradrenaline, ATP, angiotensin II, atrial natriuretic peptide (ANP) and vasopressin (Herring 2018). Mechanical stimuli include changes in (i) vessel wall tension, which is the trigger for the myogenic response described above or (ii) shear stress that originates from increase in blood flow and is sensed by ECs (Brozovich, Nicholson et al. 2016). Electrical and chemical stimuli from neighbouring cells may lead to

depolarisation of the VSMC membrane. This is permitted by gap-junctions between neighbouring VSMCs and between VSMCs and ECs (Garland, Hiley et al. 2011, Jackson 2021). Endothelial cells can modulate VSMCs contractility through Ca^{2+} -dependent release of vasodilators and by conducting Ca^{2+} -dependent membrane hyperpolarisation through gap-junctions (Garland, Hiley et al. 2011, Jackson 2021). For example, increase in intracellular free calcium concentration ($[\text{Ca}^{2+}]_i$) or inositol-3-phosphate (IP_3) in VSMCs can be passed to endothelial cells through gap-junctions thereby inducing the production of Ca^{2+} -dependent vasodilators in endothelial cells (Lemmey, Garland et al. 2020). Gap-junctions are formed by the connexin (cx) family members which are highly conserved among mammals (Kumar and Gilula 1996, Bennett, Contreras et al. 2003). Connexins form a hemichannel in the plasma membrane of a cell that connects to a hemichannel in the adjacent cell. Cx32, Cx37, Cx40, Cx43 are predominately expressed in endothelial cells, while Cx40, Cx43 are also present in VSMCs (Ek-Vitorin and Burt 2013). Gap-junctions play an important role in blood vessel homeostasis. For example, their alteration has been implicated in altered blood coagulation and inflammation such as in mutations in the *GJB1* gene encoding for Cx32 (Sato, Kubo et al. 2012).

Regarding regulation of VSMCs, paracrine hormones can be released locally on neighbouring cells by the tissues surrounding the vessel. These hormones, e.g. prostacyclin and thromboxane, are formed by cyclooxygenase (COX) from fatty acid and arachidonic acid residing in the plasma membrane (Rahman 2019). While COX-1 is constitutively expressed, COX-2 is expressed during inflammation (van der Donk, Tsai et al. 2002). A change in metabolic rate can also affect the vascular tone. During altered metabolic state, adenosine, inorganic phosphates, carbon dioxide, potassium and hydrogen ions can accumulate in the interstitial fluid, all these factors can stimulate VSMC tone. The uptake or removal of these metabolites by the circulating blood can therefore influence the smooth muscle cell contractility (Wolin 1991).

Overall, Ca^{2+} influx through the plasma membrane and $[\text{Ca}^{2+}]_i$ release from intracellular stores such as the sarcoplasmic reticulum (SR), are the major sources of $[\text{Ca}^{2+}]_i$ increase leading to depolarisation and smooth muscle constriction (Jackson 2020). Figure 1.1.2 shows a schematic illustration of the major stimuli and signalling pathways in vascular smooth muscle cells. VSMC contractile properties acutely depends on cytosolic $[\text{Ca}^{2+}]_i$ levels and they possess a range of mechanisms that tightly control $[\text{Ca}^{2+}]_i$. These mechanism include control of Ca^{2+} entry from the extracellular space, Ca^{2+} release from intracellular stores and extrusion to remove cytoplasmic Ca^{2+} (Amberg and Navedo 2013).

1.1.2.1 Calcium entry/removal mechanisms

In mammalian cells, $[\text{Ca}^{2+}]_i$ increase in the cytosol is achieved *via* (i) Ca^{2+} entry from the extracellular space or (ii) Ca^{2+} release from intracellular stores. Ca^{2+} entry from the extracellular space involves several plasma membrane resident ion channels such as voltage-sensitive calcium channels, non-selective cation channels and store operated calcium channels (SOCCs), described in greater detail in section 2.1.2 (Jackson and Blair 1998). Ca^{2+} release in the cytosol from intracellular stores is tightly regulated by IP_3 receptors (IP_3Rs), ryanodine receptors (RyRs) and nicotinic acid adenine dinucleotide phosphate (NAADP)-gated receptors (Galione and Churchill 2002). RyRs are big proteins (>500 kDa) formed by four subunits (Liu, Zhang et al. 2015, Van Petegem 2015, Zalk, Clarke et al. 2015). RyRs are activated when $[\text{Ca}^{2+}]_i$ increases from 300 nM up to 10 μM . However, they are inhibited by $[\text{Ca}^{2+}]_i > 10 \mu\text{M}$ (Tykocki, Boerman et al. 2017). IP_3Rs are homotetramers (>310 kDa) with one IP_3 binding site per monomer (Foskett, White et al. 2007). They are activated both by IP_3 binding or by sensing low $[\text{Ca}^{2+}]_i$ (<300 nM), while they are inhibited by high $[\text{Ca}^{2+}]_i$ (>10 μM) (Taylor 2002). When active, IP_3R induces Ca^{2+} release from the endoplasmic reticulum (ER) which results in the positive feedback known as Ca^{2+} -induced calcium-release (CICR), where elevation in $[\text{Ca}^{2+}]_i$ stimulates more release of Ca^{2+} from the ER *via* IP_3R and RyRs (Deanfield, Halcox et al. 2007). IP_3R and RyRs serve as a positive-feedback mechanism where they

induce peaks of $[Ca^{2+}]_i$ release, also known as Ca^{2+} sparks (Curtis, Tumelty et al. 2004, Balasubramanian, Ahmed et al. 2007, Kur, Bankhead et al. 2013). It also has been shown that IP_3R and $RyRs$ mediate the release of Ca^{2+} from the Golgi complex and acidic granules (Pinton, Pozzan et al. 1998, Patel and Docampo 2010, Yoo 2010). In fact, the Golgi complex was shown to have similar luminal $[Ca^{2+}]_i$ to the ER, with concentrations ranging from 300 μM to 1.4 mM in Hela cells (Pinton, Pozzan et al. 1998). Endosomes are acidic granules forming at the plasma membrane. Even though they are expected to have high luminal $[Ca^{2+}]_i$ resembling the $[Ca^{2+}]_e$ (~ 1 mM), it was shown that the endosomal luminal $[Ca^{2+}]_i$ falls to ~ 3 μM within 20 minutes from formation (Gerasimenko, Tepikin et al. 1998, Patel and Docampo 2010). Nevertheless, the luminal $[Ca^{2+}]_i$ in the endosomes is still an order of magnitude higher than $[Ca^{2+}]_i$, thus, endosomes are considered as Ca^{2+} stores enabling local release of Ca^{2+} (Patel and Docampo 2010). Similarly, lysosomes are also considered as acidic granules and Ca^{2+} stores. It was found, in macrophages and fibroblasts, that the low lysosomal pH ($\sim 4-5$) corresponds to luminal $[Ca^{2+}]_i$ of ~ 500 μM which is comparable to ER $[Ca^{2+}]_i$ (Miyawaki, Llopis et al. 1997, Christensen, Myers et al. 2002, Lloyd-Evans, Morgan et al. 2008). Non-selective cation channels are present in the lysosomal membrane to enable Ca^{2+} release in the cytosol once activated. For example, agonists such as endothelin-1 can result in NAADP production, which activates the lysosomal-resident two-pore channel (TPC) contributing to $[Ca^{2+}]_i$ elevation (Ruas, Rietdorf et al. 2010). TRPM2 channels, activated by cytosolic ADP-ribose, and TRPML1 channels, activated by $PI(3,5)P_2$, are also present on lysosomal membranes and contribute to $[Ca^{2+}]_i$ elevation (Venkatachalam and Montell 2007, Dong, Shen et al. 2010). TRPV2 channels, sensitive to heat, have been found in early lysosomes where they are also shown to have a role in $[Ca^{2+}]_i$ mobilisation (Wainszelbaum, Proctor et al. 2006, Saito, Hanson et al. 2007).

There are several mechanisms that maintain low $[Ca^{2+}]_i$ ($< \sim 30$ nM) during resting conditions and to prevent cellular damage and toxicity that would result in apoptosis and cell death in case $[Ca^{2+}]_i$ was maintained elevated for long period of time (Hill-Eubanks, Werner et al.

2011). The tone of a VSMC is directly dependent on $[Ca^{2+}]_i$, thus Ca^{2+} -extrusion mechanisms enable muscle relaxation. Plasma membrane resident transporters such as plasma membrane Ca^{2+} ATPase (PMCA) and Na^+/Ca^{2+} exchanger (NCX) are two mechanisms responsible for extruding Ca^{2+} from the cytosol into the extracellular space against its concentration gradient (Van Baelen, Dode et al. 2004, Brini and Carafoli 2011). PMCA was first discovered in erythrocytes, where it was shown that Ca^{2+} was pumped against the concentration gradient *via* ATP (Dunham and Glynn 1961). PMCA was later identified as a 140 kDa protein present in all mammalian plasma membranes (Enyedi, Vorherr et al. 1989). Calmodulin and acid phospholipids were shown to be activators of PMCA (Enyedi, Vorherr et al. 1989). The NCX exchanger can pump either Na^+ or Ca^{2+} depending on the electrochemical gradient. There are three isoforms in the NCX family 1-3, with NCX1 being highly expressed in VSMCs (Blaustein and Lederer 1999). In VSMCs, following application of agonists that induce CICR, replacement of extracellular Na^+ with Li^+ blocked NCX inducing accumulation of $[Ca^{2+}]_i$ (Zheng and Wang 2007). Cytosolic Ca^{2+} can also be sequestered in intracellular organelles. The sarco(endo)plasmic reticulum Ca^{2+} -ATPases (SERCA) sequesters calcium in the SR *via* ATP to lower $[Ca^{2+}]_i$ for relaxation and to store calcium for muscle contraction. SERCA is a pump of 110 kDa and its activity is regulated by small proteins such as phospholamban (PB) (Periasamy and Kalyanasundaram 2007). When unphosphorylated, PB was shown to act as an inhibitor of SERCA, while upon adrenergic activation, PB phosphorylation leads to SERCA activation (MacLennan, Asahi et al. 2003).

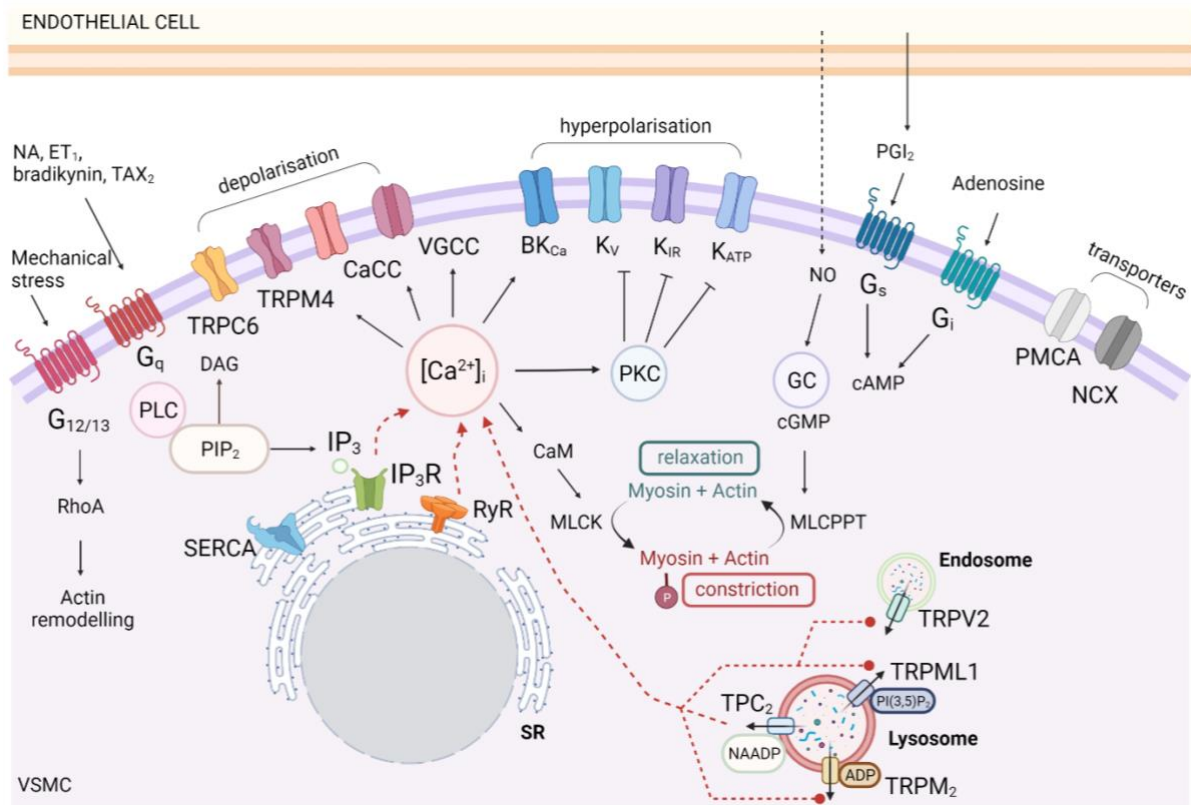


Figure 1.1.2 Ion channels and signalling pathways in VSMCs.

Schematic illustration of major ion channels and signalling pathways regulating the vascular tone of blood vessels in a smooth muscle cell. Black arrows indicate activation. Black capped lines show inhibition or deactivation. Also shown are the agents responsible for receptor binding initiating the respective intracellular signalling cascades. Adapted from (Jackson 2020).

1.2 Ion channels and membrane potential regulation in VSMCs

Cellular membranes constitute dielectric material that separates two conducting solutions (the extracellular fluid and the cytoplasm). The presence of ion channels and transporters allows selective ion passage through the plasma membrane. Ions are unequally distributed on the two sides of the membrane due to the presence of active transport mechanisms and as a consequence of the 'Donnan effect' produced by the overall net negative charge of intracellular proteins (Hille 2001). In the hypothetical case of a membrane solely permeable to one ion species, the membrane potential would rapidly reach a stable equilibrium point at which the ion fluxes due to the concentration and electrical gradient equate. This equilibrium potential is described by the Nernst equation:

$$E_{ion} = \frac{RT}{zF} \ln \frac{[X]_o}{[X]_i} \quad \text{Equation 7}$$

where E_{ion} is the electrochemical potential for an ion X, R is the universal gas constant (8.31 Jmol⁻¹/k⁻¹), F the Faraday's constant (96485 C.mol⁻¹), T the temperature in Kelvin (room temperature 294 K), z the valence of the ion in question, $[X]_o$ and $[X]_i$ the outside and inside ion-concentration of the cell respectively (Hille 2001). In a living cell, the membrane potential (V_m) is influenced by both the intracellular and extracellular ionic composition and the membrane permeability to each ion species. The Goldman-Hodkin-Katz equation (GHK) (Goldman 1943) takes these factors into consideration as:

$$V_m = \frac{RT}{F} \ln \left(\frac{p_K[K^+]_o + p_{Na}[Na^+]_o + p_{Cl}[Cl^-]_i}{p_K[K^+]_i + p_{Na}[Na^+]_i + p_{Cl}[Cl^-]_o} \right) \quad \text{Equation 8}$$

where V_m is the membrane potential in volts, p_{ion} is the relative permeability of the ion (Table 1) for VSMCs, R is the gas constant, T is the temperature in Kelvin and F is the Faraday's constant. Since cell membranes of most mammalian cells are predominantly permeable to K⁺, for most cell types the V_m is close to the reversal potential for K⁺ (E_K) (i.e. between -70 to -90

mV). The resting V_m of VSMCs, however, is maintained between -40 and -60 mV (Nelson, Cheng et al. 1995); this range is more depolarised than E_K , suggesting that other conductances are also open at resting state, contributing to a resting V_m in VSMCs that is more depolarised than the V_m of other cell types (Hirst and Edwards 1989, Thorneloe, Meredith et al. 2005). Table 1 illustrates the physiological E_{ion} in VSMCs. In VSMCs, intracellular Cl^- concentration ($[Cl^-]_i$) is higher than other cells types such as some neuron or skeletal muscle (Matchkov, Secher Dam et al. 2013, Bulley and Jaggar 2014, Hübner, Schroeder et al. 2015). The transporters HCO_3^-/Cl^- and the $Na^+-K^+-2Cl^-$ are responsible for accumulating $[Cl^-]_i$ (Matchkov, Aalkjaer et al. 2005).

Ion	$[ion]_i$ (mM)	$[ion]_e$ (mM)	E_{ion} (mV)
K⁺	165	5	-89
Na⁺	9	137	69
Cl⁻	54	134	-23
Ca²⁺	0.0001	1.2	124

Table 1 VSMC ion concentrations.

$[ion]_i$: intracellular ion concentration, $[ion]_e$: extracellular ionic concentration, E_{ion} : Nernst equilibrium potential. Ionic concentrations are reproduced from (Herring 2018). VSMC is measured in a relaxed state and it is assumed $[Ca^{2+}]_i$ is in a free, unbound state.

1.3 Ion channels and transporters in smooth muscle cells

According to their ion selectivity, channels can be grouped into K^+ , Na^+ , Ca^{2+} , and Cl^- channels. Furthermore, ion channels can be sub-divided according to their regulatory mechanisms (e.g. voltage-dependent or Ca^{2+} activated) or to other biophysical properties (e.g. outward or inward rectification).

1.3.1 K^+ channels

VSMCs express high density of large-conductance voltage- and Ca^{2+} -activated K^+ channels (BK_{Ca}) (Neylon 2002). BK_{Ca} are activated by membrane depolarisation and an increase in $[Ca^{2+}]_i$ (Jackson 2020). These channels are formed by a tetramer of $K_{Ca1.1}$ α -subunits with seven transmembrane domains and large conductance (200 pS) (Tykocki, Boerman et al. 2017). BK_{Ca} channels provide a negative-feedback mechanism where their activation prevents excessive excitation (vasospasm) of VSMCs (Tykocki, Boerman et al. 2017). These channels are inactive under resting condition as they need high $[Ca^{2+}]_i$ threshold ($> 3 \mu M$) to open (Jackson and Blair 1998). This high $[Ca^{2+}]_i$ is reached by the Ca^{2+} sparks released by ryanodine receptors in the SR (Nelson, Cheng et al. 1995). Pharmacological blockage of ryanodine receptors induces the same effect as directly blocking BK_{Ca} (Jackson 2021). Tetraethyl ammonium (TEA) and iberiotoxin were shown to block BK_{Ca} inducing vasoconstriction (Jackson 2020). Endothelium-derived vasodilators, such as NO and cGMP-protein kinase G (PKG), can also activate BK_{Ca} and induce vasodilation (Jackson 2021). It is also known that BK_{Ca} expression is increased in hypertension as a mechanism of negative feedback in response to increased vasoconstriction (Tykocki, Boerman et al. 2017). Thus, it can be inferred that both voltage-gated K^+ channels (K_v) and BK_{Ca} play an important role in the negative-feedback regulation of vascular tone.

Inwardly-rectifying K^+ (K_{ir}) channels get their name based on the fact that they conduct more current at negative than at positive voltages (Quayle, Bonev et al. 1994). This asymmetrical

conductance property is due to the channel pore being blocked by intracellular polyamines and Mg^{2+} at depolarised voltages (Matsuda 1988, Lopatin, Makhina et al. 1994, Shyng, Sha et al. 1996). In the vascular system, these channels are particularly expressed in small resistance arteries and arterioles, with predominance of the $K_{ir2.1}$ isoform (Longden and Nelson 2015). As K_v and BK_{Ca} channels, when K_{ir} channels open they favour hyperpolarisation amplifying the cAMP pathways of vasodilators (Jackson 2005, Longden and Nelson 2015, Sonkusare, Dalsgaard et al. 2016).

K_v channels are gated open by membrane depolarisation (Kuang, Purhonen et al. 2015). Blockers of K_v channels enhances VSMC contraction upon stimulation of vasoconstrictors such as phenylephrine (PE) and angiotensin II (Clément-Chomienne, Walsh et al. 1996, Mistry and Garland 1999). This is because an increase in $[Ca^{2+}]_i$ was shown to inhibit K_v7 channels by binding calmodulin (Alaimo and Villarroel 2018). The compound 4-amino pyridine (4-AP) was shown to block K_v channels in a calcium-dependent way (Tammaro, Smith et al. 2005, Baeyens, Bouryi et al. 2014, Hübner, Schroeder et al. 2015). Inactivation of K_v channels contributes to membrane depolarisation which leads to vasoconstriction (Cooke, Rossitch et al. 1991, Chadha, Zunke et al. 2012). These data suggest that K_v channels have a role in maintaining hyperpolarised V_m . Elevated $[Ca^{2+}]_i$ was shown also to inhibit ATP-activated K^+ channels (K_{ATP}). These channels are independent by voltage and their activity decreases in response to intracellular ATP (Foster and Coetzee 2016, Jackson 2020). As the other K^+ channels discussed above, vasoconstrictors acting via the cAMP or PKC pathway block K_{ATP} channels (Akatsuka, Egashira et al. 1994, Rainbow, Parker et al. 2011). Moreover, K_{ATP} blockage by the specific blocker glibenclamide induces vasoconstriction (Nelson, Patlak et al. 1990, Farouque, Worthley Stephen et al. 2002, Jackson 2020). These data indicate that both K_v and K_{ATP} channels contribute to the positive-feedback mechanisms that increases VSMC constriction and hence, myogenic tone.

1.3.2 Other cation channels

Voltage-gated Ca^{2+} channels (Ca_v) channels such as L-type and T-type voltage-gated channels are essential in modulating contraction of VSMCs. Ca_v channels formed by the $\text{Ca}_v1.2$ α -subunits provide the main source of Ca^{2+} influx during VSMCs depolarisation (Tykocki, Boerman et al. 2017). Following CICR via the IP_3 pathway from intracellular stores, cell depolarisation activates Ca_v to further increase intracellular calcium levels.

Ca_v are closed in resting condition but since they are highly dependent on voltage, a depolarisation of V_m of only 3 mV induces a two-fold increase in their current (Nelson, Patlak et al. 1990). Calmodulin binds to the C-terminus of $\text{Ca}_v1.2$ channels to regulate the calcium-dependent inhibition of these channels (Shah, Chagot et al. 2006). Once intracellular Ca^{2+} stores such as the SR have been depleted, SOCCs are activated to refill the depleted stores. In response to SR Ca^{2+} depletion the SR-resident stromal-interaction molecule (STIM) proteins activate *via* oligomerisation and translocate to the plasma membrane to open Ca^{2+} release-activated Ca^{2+} modulator 1 (ORAI1) channels (Kar and Parekh 2013, Qiu and Lewis 2019). This results in Ca^{2+} influx in the cell, where it is sequestered back in intracellular calcium stores such as in the ER by SERCA. Receptor-activated cation channels are also important for VSMC contraction. For instance, the transient receptor potential cation (TRPC) channels activated by PLC-coupled receptor and the ATP-ligand gated purinergic (P2X) both facilitate intracellular Ca^{2+} entry hence modulating vascular tone (Earley and Brayden 2015).

VSMCs express several TRP family members. For example, TRPM4 is largely expressed in cerebral resistance arteries (Gonzales, Yang et al. 2014). The Ca^{2+} sensitivity of TRPM4 channels is regulated by calmodulin, rho kinase and protein kinase-C (Li, Lu et al. 2017),(Gonzales, Yang et al. 2014). Their activation results in Na^+ influx inducing depolarisation and VSMC contraction (Earley and Brayden 2015). The TRPC6 and TRPP1

are non-selective cation channels that induce depolarisation by allowing entry of both Ca^{2+} and Na^+ (Tykocki, Boerman et al. 2017).

TPCs are non-selective channels residing in the endolysosomes (Patel and Cai 2015). While some studies have shown that TPCs are Ca^{2+} -permeable and activated by NAADP (Brailoiu, Churamani et al. 2009, Brailoiu, Rahman et al. 2010, Ruas, Davis et al. 2015), other studies have indicated that these channels are Na^+ -permeable and activated by phosphatidylinositol 3,5- bisphosphate ($\text{PI}(3,5)\text{P}_2$), and/or by voltage (Boccaccio, Scholz-Starke et al. 2014, Guo, Ma et al. 2017). Some studies have also observed both mechanisms of TPC activation (Pitt, Lam et al. 2014, Ogunbayo, Duan et al. 2018). Zhang et al. showed that NAADP is not a direct ligand of the TPC channel as the LSM12 binding protein is required for activation of TPC2 by NAADP, while the JTP2 protein interacts with TPC1 (Gunaratne, Brailoiu et al. 2021, Zhang, Guan et al. 2021).

1.3.3 Cl^- channels

In VSMCs $[\text{Cl}^-]_i$ is higher than in other cell types due to the $\text{Cl}^-/\text{HCO}_3^-$ exchanger and the $\text{Na}^+/\text{K}^+/\text{Cl}^-$ co-transporter (Matchkov, Secher Dam et al. 2013). Therefore, the equilibrium potential for Cl^- is more positive than in other cells types (Bulley and Jaggar 2014, Hübner, Schroeder et al. 2015) and the $[\text{Cl}^-]_i$ concentration in VSMCs is higher than the E_{Cl} . Therefore, opening of Cl^- channels causes a depolarising Cl^- efflux, which activates Ca_v (Heinze, Seniuk et al. 2014). The rise in $[\text{Ca}^{2+}]_i$ activates myosin light chain kinase *via* calmodulin, resulting in contraction (Chipperfield and Harper 2000). Four main families of Cl^- channels are expressed in VSMC: the cystic fibrosis transmembrane conductance regulator (CFTR), bestrophins, volume-activated Cl^- channels (CICs) and CaCCs. Several studies have showed that in different vascular beds such as aorta, portal veins and pulmonary arteries, G_q coupled receptor (G_qPCR) agonists as noradrenaline, endothelin and histamine induce Cl^- currents (Van Renterghem and Lazdunski 1993). These data support a role of Cl^- channels in

modulating VSMCs vasoconstriction. This was confirmed by demonstrations that non-selective Cl⁻ channel blockers, such as 4,4'-diisothiocyanatostilbene-2,2'-disulphonic acid (DIDS), hyperpolarised rat cerebral arteries (Nelson, Conway et al. 1997). Moreover, lowering extracellular Cl⁻ or substituting it with Br⁻ and NO₃⁻, which are more permeant anions than Cl⁻, potentiated constriction in rat cerebral arteries (Sayet, Neuilly et al. 1993).

CFTR is a cAMP-activated Cl⁻ channel mainly expressed in epithelial cells (Riordan, Rommens et al. 1989). It was shown that in rat intrapulmonary arteries CFTR activation by agonists induced vasorelaxation of aortic rings independent from endothelial cells (Cook, Rector et al. 2016). Moreover, vasoconstrictors induced aortic contraction more in CFTR^{-/-} mice than in CFTR^{+/+} mice (Robert, Norez et al. 2005). However, a precise role of CFTR in VSMCs remains unknown since CFTR channels have not been directly measured in VSMCs by electrophysiology.

Bestrophins are a four-family cGMP-dependent Cl⁻ channels. Bestrophin-3 mRNA and protein are mainly expressed in VSMCs, with bestrophin-1 and -2 weakly expressed (Matchkov, Larsen et al. 2008). It was shown that bestrophin-3 knockdown reduced cGMP-dependent Cl⁻ current activated by Ca²⁺ in rat mesenteric arteries (Matchkov, Larsen et al. 2008). Moreover, studies showed that bestrophin 3-knockdown reduced vasomotion and cell viability (Lee, Chakraborty et al. 2012, Dam, Boedtkjer et al. 2014).

Among CICs family members, CIC-3 is predominantly expressed in VSMCs (Hume, Wang et al. 2010, Bulley and Jaggar 2014). This channel is particularly important to regulate vascular cell proliferation (Eggermont, Trouet et al. 2001). It was demonstrated that Cl⁻ movements is essential to compensate cell swelling during cell proliferation (Stutzin and Hoffmann 2006).

CaCCs are abundantly expressed in VSMCs and are activated by a combination of depolarising V_m and increase in [Ca²⁺]_i (Large and Wang 1996). Upon activation, CaCCs promote Cl⁻ extrusion from the cell, thus membrane depolarisation and vasoconstriction

(Nelson, Cheng et al. 1995, Large and Wang 1996, Hartzell, Putzier et al. 2005, Leblanc, Ledoux et al. 2005, Pedemonte and Galletta 2014). This work of thesis is centred on the CaCCs coded by the TMEM16A gene. The molecular physiology and pharmacology of these channels is described in detail in section 4.1.

1.4 The biochemistry of the plasma membrane

The plasma membrane has the crucial role in providing a physical separation and signalling between the intracellular and extracellular compartments of a cell. Internal membranes compartmentalize intracellular organelles and regulate communication between them (Habibi, Emamian et al. 2014). Biomembranes are generally formed by lipids, proteins and carbohydrates. However, they are dynamically regulated and heterogeneous in order to modulate various cellular processes. For example, the flux of ions across the cell membrane is specifically maintained according to the membrane selective permeability (Ek-Vitorin and Burt 2013, Shinoda 2016). By regulating the transport of ions between the inside and outside of the cell, membranes enable an ion gradient that allows cell signalling (Uings and Farrow 2000). Moreover, specific functions of biomembranes are associated with specific morphology (Heald and Cohen-Fix 2014). For instance, tight junctions in the blood brain barrier and the epithelial cells are essential to prevent leakage of molecules or ions between tissues (Giepmans and van Ijzendoorn 2009). Because of all of the properties mentioned above, biomembranes are pivotal in the maintenance of cellular homeostasis.

The first evidence of an osmotic barrier separating the inside and outside of a cell, came by observing a monolayer of lipids forming at the air-water interface, with the hydrophilic polar head groups point to the liquid phase while the hydrophobic backbones repelled the water by facing to the air phase (Langmuir 1917). The plasma membrane was later identified as a lipid bilayer when it was discovered that the extract of lipids from human erythrocytes was 2-fold of the cell surface (Gorter and Grendel 1925). The model of “fluid mosaic” was proposed in 1972

by Singer and Nicolson, whom considered that proteins are completely or partially inserted in the lipid bilayer and can dynamically diffuse through it (Singer and Nicolson 1972). The word mosaic represents the heterogeneity of the lipid bilayer composition, being highly diverse in terms of thickness and lipid/protein ratio (Feigenson 2006). Biomembranes are also characterised by specialised lipid domains or lipid rafts, which were first identified in the glycolipid-rich apical membrane of epithelial cells (Simons and van Meer 1988). Lipid rafts are small regions, 10-200 nm, highly heterogeneous and dynamic, enriched with sterols and sphingolipids (Pike 2006). These regions are also enriched with longer hydrocarbon chains and ceramide backbones, forming specific platforms for interaction with selected signalling molecules (Simons and Sampaio 2011). In fact, lipid rafts are populated by lipids that have the ability to act as first and second messengers in signalling cascades (van Meer, Voelker et al. 2008).

The diversity of lipids present in the cell membranes (Figure 1.4.1) can be divided in categories based on their structural and chemical properties (Lydic and Goo 2018). The most abundant membrane lipids are phospholipids, formed by a polar head group and two hydrophobic hydrocarbon tails, which are usually fatty acids ranging in length from 14 to 24 carbons. One tail is usually unsaturated, with one or more *cis*-double bond, while the other is saturated. The presence of a double bond created a kink in the tail. Hence, different phospholipid composition of membranes can affect how the lipid pack one against the other, influencing the overall fluidity of the membrane.

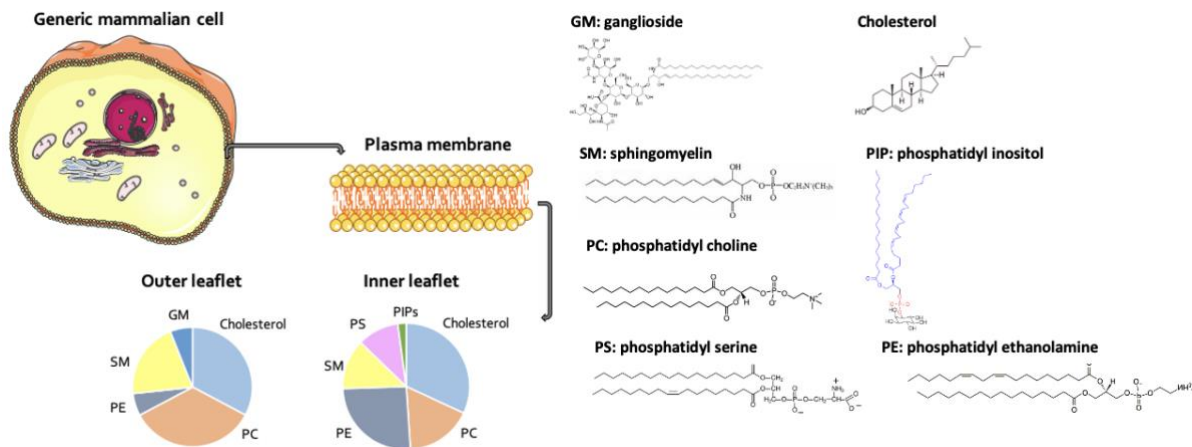


Figure 1.4.1 Lipid composition of the plasma membrane.

The bilayer lipid composition of the mammalian cell membrane differs between the intracellular and extracellular leaflet. The proportion of major lipid head-groups residing in the inner and outer leaflet of the plasma membrane are reproduced from Van Meer 2008 (van Meer, Voelker et al. 2008).

Glycerophospholipids are another main structural component of eukaryotic membranes. They have three components: a fatty acid group, glycerol and a phosphate usually present in the *sn*-3 position of the glycerol. Different classes of glycerophospholipids are distinguished by the group that is linked to the phosphate. Some examples are phosphatidylcholine (PC), phosphatidylethanolamine (PE), phosphatidylserine (PS), phosphatidylglycerol (PG) and phosphatidylinositol (PI) (van Meer 2005).

Sphingolipids (SLs) have the same components as glycerophospholipids but with ceramide as the hydrophobic group. The backbone is a sphingoid base that after acetylation forms ceramide can be linked to various head groups (Zheng, Kollmeyer et al. 2006). For example, glycosphingolipids (GSLs) have a single carbohydrate residue, glucosylceramide (GlcCer) or galactosylceramide (GalCer), while gangliosides have an oligoside containing sialic acid linked to the ceramide backbone (Kolter 2012). In mammals, SLs with a chain length of 18 carbons, such as sphingosine, are the most prevalent backbones.

Sterols are the major class of non-polar lipids in biomembranes (van Meer, Voelker et al. 2008). In mammals, cholesterol is the predominant sterol (40% of the plasma membrane) and highly regulates membrane fluidity (Ayuyan and Cohen 2018). It also influences the organisation of other lipids such as in lipid rafts and lipid-anchored membrane proteins (Silvius 2003, Grouleff, Irudayam et al. 2015). The lipid distribution across the inner and outer leaflet of biomembranes is asymmetrical (van Meer and de Kroon 2011). For example, SLMs are mainly present in the extracellular face of the plasma membrane, while PS and PE are predominantly located in the cytosolic leaflet.

Lipid distribution is also distinct within cellular membranes (van Meer and de Kroon 2011). For instance, the plasma membrane is enriched in SLMs and cholesterol (Brown and London 1998), the acidic compartments are abundant in negatively charged bis(monoacylglycerol)phosphate (Kolter and Sandhoff 2010) and the inner mitochondrial membranes are highly distributed with cardiolipin (Brown and London 1998). Ratio between proteins and phospholipids is also variable across biological membranes. In the plasma membrane there is a ratio of 1 protein per 25 phospholipids while in the mitochondrial internal membrane there is an average of 1 protein per 15 lipids (Casares, Escribá et al. 2019). This is because the mitochondria are specialised in energy processing. The myelin enclosing nerve cells is another example of specialised composition of the cell membrane according to its function. Myelin is used as electrical insulator, in these cells there is a ratio of 1 protein for 70 lipid molecules (William K. Purves 2004).

Lipids are synthesised in the ER and Golgi complex and transported by vesicular transport to the plasma membrane (De Matteis and Luini 2008), where they have diverse biological roles such as modulators of signal transduction (Lingwood 2011). Lipids can also undergo endocytosis and can be recycled in early endosomes to the Golgi complex after re-glycosylation or degraded in the lysosomes (Daniotti and Iglesias-Bartolomé 2011).

1.4.1 The endocytic system

Cells can internalise lipids, ligands and membrane proteins *via* endocytosis. This dynamic process is determined by the endosomal pathways and contributes to the plasma membrane composition which in turn influences cellular homeostasis (Grant and Donaldson 2009). The mechanism of endocytosis can be clathrin dependent (CDE) or clathrin independent (CDI). In CDE, adaptor proteins recognise specific cytoplasmic domains allowing the transport of cargo into the cell through clathrin-coated vesicles. CDI includes numerous forms of endocytosis such as transport of GSLs, phagocytosis and macropinocytosis (Mayor and Pagano 2007). This latter mechanism is highly reliant on lipid rafts. For instance, fluorescent GSLs analogues cluster in membrane microdomains prior to internalization (Singh, Puri et al. 2003, Sharma, Brown et al. 2004).

Following either CDE or CDI, endocytosed material is delivered to early endosomes where the cargo is sorted either back to the plasma membrane or targeted to the lysosome for degradation (Jovic, Sharma et al. 2010). Early endosomes, once formed at the plasma membrane, are vesicular compartments located in the cell periphery with slightly acidic pH of 6, which can allow dissociation of receptors from their ligands (Gruenberg 2001, Jovic, Sharma et al. 2010). For example, following CDE of low-density lipoproteins (LDL), lysosomal acid lipase A (LipA) hydrolyses cholesteryl esters from LDL producing unesterified cholesterol (UC). The latter is then extruded from the lysosomal via the lysosomal transport proteins Niemann-Pick type C 2 (NPC2) and NPC1 (Figure 1.4.2). This mechanism allows the recycling of the LDL-receptor (LDL-R) to the plasma membrane (Goldstein, Anderson et al. 1979).

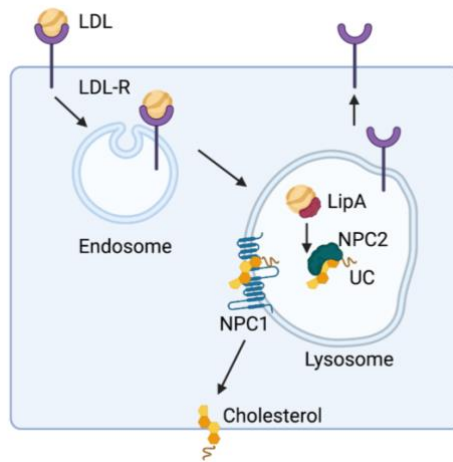


Figure 1.4.2 Lysosome mediation of cholesterol delivery to the plasma membrane.

Diagrammatic representation of the lipid transport of LDL cholesterol from the lysosome (Goldstein, Anderson et al. 1979). LDL-R is endocytosed in the endosome. Upon endosome maturation, LDLs are broken down by lysosomal acidic lipase (LipA) to release unesterified cholesterol (UC). NPC2 delivers cholesterol to the transmembrane protein NPC1, which allows cholesterol sorting to different cell compartments, including the plasma membrane via membrane contact sites. LDL-R is recycled to the plasma membrane.

1.4.2 The lysosome

Lysosomes were first discovered in 1955 by Christian de Duve when he detected hydrolytic activity in biochemical fractions (de Duve 1983). Later studies identified lysosomes as membrane-bound organelles specialising in the breakdown and recycling of intracellular macromolecules (Klumperman and Raposo 2014). The degradative function of the lysosome is driven by up to 60 hydrolytic enzymes including lipases, proteases and nucleases contained in the endo-lysosomal lumen (Sagné, Agulhon et al. 2001, Rong, McPhee et al. 2011, Liu, Zhou et al. 2012). The acidic pH of the lysosome allows optimal activity of the hydrolyses mentioned above (Bright, Davis et al. 2016). The low pH (4.5-5.5) is maintained by the H⁺-ATPase pump and by a counter flux of other ions such as Cl⁻, Na⁺ and K⁺ (Mindell 2012, Ishida, Nayak et al. 2013). Overtime early endosomes accumulates ligands and mature into late endosomes which have a pH of 5 and move along microtubules to reach the perinucleus (Dunn and Maxfield 1992). Ca²⁺ release from the late endosomes is necessary for fusion of these organelles with lysosomes (Luzio, Bright et al. 2007)

During endosome maturation, the lysosome lysosomal lumen is gradually acidified to enable fusion with other intracellular vesicles such as the late phagosome and the autophagosome (Johnson, Ostrowski et al. 2016). In fact, the lysosome is the terminal compartment of multiple endocytic pathways including endocytosis, phagocytosis and autophagy (Figure 1.4.3) (Di Fiore and von Zastrow 2014). However, lysosomes are not simply an endpoint of the cell's endocytic system, rather they are found in diverse trafficking routes sorting and recycling intracellular material via a microtubule-based system (Burkhardt, Echeverri et al. 1997, Harada, Takei et al. 1998). Moreover, there are lines of evidence showing that in response to a rise in $[Ca^{2+}]_i$, lysosomes can fuse with the plasma membrane to repair areas of damage to the plasma membrane (Rodríguez, Webster et al. 1997). This was shown by lysosomal protein markers such as Lamp1 appearing on the plasma membrane of fibroblasts at the site of mechanical disruption (Bakker, Webster et al. 1997). In fact, it is now known that the lysosome plays key roles in a variety of cellular processes such as cell signalling, repair and apoptosis (Galione and Churchill 2002, Jaiswal, Andrews et al. 2002, Divangahi, Chen et al. 2009).

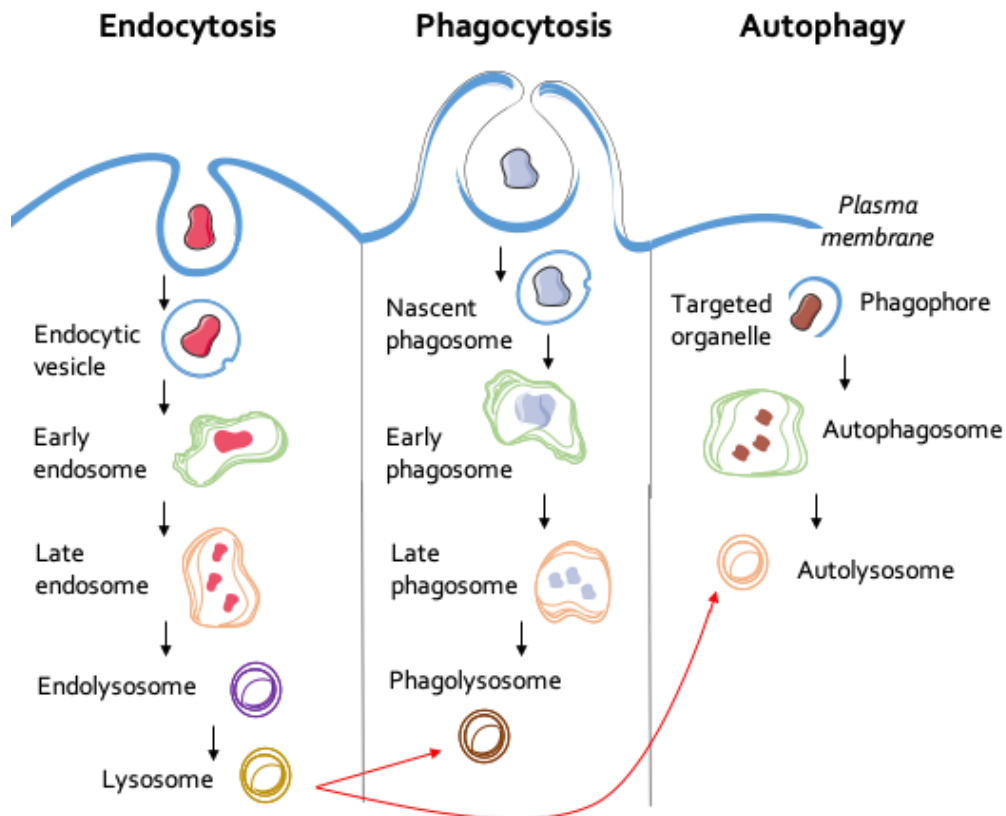


Figure 1.4.3 The role of the lysosome in endocytosis, phagocytosis, and autophagy.

Diagrammatic representation of the importance of the lysosome in regulating endocytosis, phagocytosis, and autophagy. In endocytosis, endocytic vesicles mature into lysosomes. Similarly, in phagocytosis and autophagy, the lysosome is fusing with either phagolysosome or autophagosomes to degrade the endocytic material.

The lysosomal lipid-transport proteins NPC1 and NPC2 coordinate the export of unesterified cholesterol out of the lysosome (Infante, Abi-Mosleh et al. 2008). NPC2 is a protein present in the lysosomal lumen. This soluble protein harbours a cholesterol-binding pocket lined with hydrophobic residues that are buried in a pocket; in contrast, hydroxyl groups are exposed to the lumen (Li, Wang et al. 2016). Thus, NPC2 can bind cholesterol in the hydrophobic pocket and deliver it to the NPC1 membrane-embedded protein. NPC1 is a protein of the lysosomal membrane that has a luminal N-terminal domain with a N-terminal sterol-sensing domain which is thought to bind cholesterol (Infante, Abi-Mosleh et al. 2008). The crystal structure of NPC1 shows that this protein has an opposite orientation of the sterol hydrophobic pocket to NPC2, supporting a coordinated transfer of cholesterol from the hydrophobic pocket of NPC2 to the one in the N-terminal domain of NPC1 (Li, Wang et al. 2016). Moreover, the lysosomal

proteins Lamp1 and Lamp2 were shown to bind cholesterol with high affinity and specificity to the luminal domain 1 which is also capable of interacting with NPC1 and NPC2 (Li, Wang et al. 2016, Marques and Saftig 2019). Once cholesterol and sphingolipids have been transferred to the cytosolic leaflet of the lysosome limiting membrane by NPC1, they are rapidly transported to cellular membranes such as the ER, Golgi, peroxisomes and the plasma membrane through tethering contact sites (Jin, Strunk et al. 2015, Hoglinger, Burgoyne et al. 2019, Marques and Saftig 2019).

1.5 NPC gene/protein defects

The NPC1 gene is located on chromosome 18q11 (Carstea, Polymeropoulos et al. 1993) and encodes a 13-transmembrane domain protein of 1278 amino acid (Carstea, Morris et al. 1997) which resides in the membranes of late endosomes and lysosomes (Ioannou 2005). NPC1 has been proposed as the only mammalian resistance-nodulation cell-division (RND) permease transporter (Pentchev, Comly et al. 1985, Tseng, Gratwick et al. 1999, Scott and Ioannou 2004). Davies et al showed that NPC1 can transport acriflavine, a known RND permease substrate (Davies, Chen et al. 2000). This was further supported when it was demonstrated that the yeast orthologue of NPC1, *ncr1*, could compensate for NPC1 deficiency when expressed in mammalian patient-derived cells (Malathi, Higaki et al. 2004). As RND permeases function as transmembrane efflux pumps, it was proposed that NPC1 could aid the transport of various lipids out of the late endosomes and lysosomes (Lloyd-Evans and Platt 2010). Moreover, *ncr1* is expressed on the yeast vacuole which is functionally equivalent to the eukaryotic lysosome (Patel and Cai 2015).

The NPC1 protein has three luminal domains: a N-terminal domain, a middle luminal domain and a C-terminal domain (CTD) which is cysteine-rich (Scott and Ioannou 2004). The transmembrane domains TM3-7 form the sterol-sensing domain which is highly conserved (Kuwabara and Labouesse 2002). It was shown that the small molecule U18666A can block

cholesterol export and that a point mutation in the NPC1 SSD can prevent binding of U18666A to NPC1 (Ohgami, Ko et al. 2004, Lu, Liang et al. 2015). The recent NPC1 single-particle electron cryomicroscopy (cryo-EM) structure revealed for the first time the clearly defined CTD and showed that mutagenesis of the NPC1 CTD blocks cholesterol transport from the late endosomes to the ER (Li, Lu et al. 2017). Mutations in either NPC1 or NPC2 results in Niemann-Pick disease type C (NPC), which is an autosomal recessive inherited neurodegenerative lysosomal storage disorder. More than 400 mutations have been identified in NPC patients (Park, O'Brien et al. 2003, Vanier 2010) of which 45% are distributed in the CTD of NPC1 (Scott and Ioannou 2004). The most common NPC1 mutation, I1061T, induces NPC1 misfolding resulting in protein degradation and a negligible amount of NPC1 delivered to the lysosomal membrane (Praggastis, Tortelli et al. 2015).

1.5.1 Lipid storage in NPC disease

NPC disease is characterised by lipid storage within lysosomes, such as cholesterol, and multiple sphingolipids including sphingosine, sphingomyelin and GSLs (including glucosylceramide, lactosylceramide, and monosialogangliosides GM2 and GM3) (te Vrugte, Lloyd-Evans et al. 2004, Chevallier, Chamoun et al. 2008, Lloyd-Evans, Morgan et al. 2008). This storage impairs lysosomal function resulting in a block of the endocytic pathway that impairs fusion of lysosomes and late endosomes, as well as the formation of autophagic vacuoles or phagosomes (Ko, Gordon et al. 2001, Mayran, Parton et al. 2003, Lloyd-Evans, Morgan et al. 2008). Crocker and Farber initially characterised NPC as a primary sphingomyelin storage disease (Crocker and Farber 1958). This idea was dismissed in 1984 when NPC was reclassified as a lactosylceramide (LacCer) storage disease and then in 1985 when Pentchev suggested that NPC was associated with a defect in LDL cholesterol recycling (Elleder and Smíd 1985, Pentchev, Comly et al. 1985). After the identification of the gene in 1997, sequence similarity between NPC1 and mediators of cholesterol regulation supported the hypothesis that NPC was a cholesterol storage disease. It was then reported that LDL

does not only contain cholesterol but also ceramide and GSLs (Garner, Harvey et al. 2001, Lightle, Tosheva et al. 2003). Moreover, variants of NPC disease show no storage of LDL-derived cholesterol, while still showing sphingolipid storage (Sun, Marks et al. 2001). More importantly, addition of sphingosine to healthy cells was showed to induce NPC lipid storage whereas addition of free cholesterol could not (Roff, Goldin et al. 1991).

In 2008, Lloyd et al reported that in NPC disease altered cellular lipid trafficking starts with sphingosine storage in the late endosomes and lysosomes, followed by defective endocytic trafficking and secondary storage of lipids such as cholesterol and GSLs (Lloyd-Evans, Morgan et al. 2008). Initial evidence of the key role of sphingosine in NPC diseases indicated that a 12-fold sphingosine increased was observed in liver and spleen of NPC patients and a 4-fold increase in the brain (te Vrugte, Lloyd-Evans et al. 2004). Following sphingosine elevation in NPC cells, this lipid reduces late endosomal and lysosomal Ca^{2+} levels resulting in secondary lipid storage and impairment of vesicular fusion/trafficking (Pryor, Mullock et al. 2000, Lloyd-Evans, Morgan et al. 2008, Lloyd-Evans and Platt 2010). More recently, it has been shown that NPC1 functions as a tethering protein between the lysosomes and the ER to allow cholesterol egress (Hoglinger, Burgoyne et al. 2019). In fact, in NPC1-null cells and in cells treated with U18666A, the membrane contact sites (MCS) between lysosomes and the ER were significantly reduced and resulted in cholesterol accumulation (Hoglinger, Burgoyne et al. 2019). In contrast, by artificially expressing the MCS protein ORLP1, the contact sites and cholesterol accumulation were both rescued (Hoglinger, Burgoyne et al. 2019). Therefore, NPC1 is not only important for transporting cholesterol but also for regulating tethering between intracellular organelles.

1.5.2 Therapeutics for NPC disease

NPC affects 1 in 120, 000 living births (Vanier 2010, Hendriks, Anheim et al. 2017). This disease manifests with high heterogeneity with variable age of onset and different rates of progression (Yerushalmi, Sokol et al. 2002, Wassif, Cross et al. 2016). NPC patients often

present with initial liver disease followed by neurological signs including ataxia and dementia (Vanier 2010). Main pathological features of NPC include Purkinje cell loss in the cerebellum, cerebral microvascular and neuronal excitability alterations (Cendelin 2016, Winstone, Stellitano et al. 2017). Additionally, there are some reports of vascular impairment, such as alteration of coronary circulation (Patterson, Clayton et al. 2017). Some patients also present with coagulation and platelet changes such as thrombocytopenia, anaemia and petechial rash (Spiegel, Raas-Rothschild et al. 2009, Chen, Colaco et al. 2020). Furthermore, associations between NPC1 polymorphism and cardiac disease have been identified (Wraith, Guffon et al. 2009).

Currently there is no cure for NPC disease and therapeutic options are limited. *N*-butyldeoxynojirimycin (miglustat) is the only approved therapy for NPC (Lyseng-Williamson 2014) while β CD, arimoclomol and gene therapy are under investigation (Hastings, Vieira et al. 2019).

Miglustat reduces GSLs storage by inhibiting glucosylceramide synthase and it was originally developed for Gaucher disease, which is characterised by primary defect in GSLs metabolism (Vella 1996, Cox, Lachmann et al. 2000). Miglustat has been approved for NPC pathology worldwide (apart in the USA) and early treatment slows disease onset as well as progression (Patterson, Vecchio et al. 2007). Patterson et al. have recently showed long-term survival data showing that miglustat delays disease progression and extends life span by more than 10 years (Patterson, Garver et al. 2020).

β CD was first used as a delivery system for allopregnanolone in NPC mice. This steroid was solubilised in 20% β CD improving mice lifespan and neuropathology (Griffin, Gong et al. 2004). It was then discovered that treatment with β CD alone as vehicle was responsible for the majority of improvements seen in NPC mice (Davidson, Ali et al. 2009). Intra-cisternal injection of β CD in feline models of NPC showed delay in cerebellar degeneration and in Purkinje cell loss while reducing lipid storage and increasing life span (Hastings, Vieira et al.

2019). β CD is a cyclic oligosaccharide of seven glucopyranose units, exposing hydrophilic residues while internalising hydrophobic ones. In the formation of β CD-lipid complexes, β CD can enhance the solubility of lipophilic compounds such as cholesterol. β CD can induce lysosomal exocytosis by damaging the plasma membrane and releasing storage materials entrapped in the endocytic system (Chen, Li et al. 2010). Even though β CD does not cross the blood-brain barrier (BBB), it is proposed that low concentrations of the compound are enough to change intracellular junctions and altering membrane structures, as well as enhancing solubilisation of lipids in the brain endothelial cells (Vecsernyés, Fenyvesi et al. 2014, Coisne, Hallier-Vanuxeem et al. 2016). Several studies are now demonstrating that β CD can reduce systemic and neurologic manifestations of NPC in patients (Hastings, Vieira et al. 2019).

1.6 Lipid modulation of ion channels

Lipids are essential components of cellular membranes where ion channels reside. Over the last decade several lines of evidence demonstrated that lipids can act as major modulators of ion channel activity. In this section, I will provide an overview of the main classes of lipids that can interfere with ion channel activity. For example, cholesterol is a predominant component of the plasma membrane regulating cell viability, growth and proliferation. Another important class of lipids are phosphoinositides, which are less abundant in membranes but direct many signalling pathways. Moreover, sphingolipids such as ceramide and sphingosine are also signalling lipids involved in several cellular functions and modulating some ion channel activity. Overall, lipids can modulate ion channels by direct interaction, by altering the physical properties of membranes or by facilitating the interaction of the channels with auxiliary proteins or other lipid complexes (Rosenhouse-Dantsker 2019).

1.6.1 Cholesterol

Unesterified cholesterol is mainly found at the plasma membrane (Davis and Poznansky 1987, Lange 1991). Its steroid rings are embedded in the membrane parallel to the hydrocarbon chains of the phospholipids while its hydroxyl group is exposed to the intracellular aqueous component (Yeagle 1985). Cholesterol was shown to commonly decrease channel activity and its open probability as seen for K^+ channels such as K_{IR} , K_V and BK_{Ca} , as well as CaCCs, Na^+ and Ca^{2+} channels. For example, for K_{IR} channels, the single point mutation L1222I is enough to abolish channels sensitivity to cholesterol (Rosenhouse-Dantsker, Leal-Pinto et al. 2010). For BK_{Ca} channels, cholesterol depletion with methyl- β CD increased single-channel activity (Tajima, Itokazu et al. 2011). For CaCC channels, it was shown that methyl- β CD complexed with cholesterol increases TMEM16A current rundown (De Jesus-Perez, Cruz-Rangel et al. 2018).

In contrast, cholesterol is essential for activation of other ion channels. For example, incubation of lipid bilayers with reconstituted epithelial Na^+ channels (eNaC) methyl- β CD alone reduced eNaC current (Shlyonsky, Mies et al. 2003). Similarly, incubation of TRP1-expressing HepG cells with β CD prevented carbachol-induced activation of TRP1 (Lockwich, Liu et al. 2000)

1.6.2 Phosphoinositides

Among phosphoinositides, the most abundant at the plasma membrane is PIP_2 and is a source of several second messengers such as IP_3 and DAG (Plaster, Tawil et al. 2001). PIP_2 levels depend on cellular metabolism since it can be hydrolysed, phosphorylated at the D-3 hydroxyl inositol group to form $PI(3,4,5)P_3$ or dephosphorylated to remove the phosphate in either position D-4 or D-5 of the inositol group. Its synthesis is regulated by phosphatidylinositol 4-kinase (PI4-K) and phosphatidylinositol 4-phosphate 5-kinase (PIP5K). Conversely to

cholesterol, PIP₂ generally increases channel activity and open probability like for K_{IR}, K_V, CaCCs, Na⁺, TRP and Ca²⁺ channels (Hille 2001). Molecular dynamics simulations have shown how PIP₂ opens K_{IR} channels by facilitating the conformational movement of the CTD upward (Li, Lü et al. 2015). In KCNQ2 channels, PIP₂ binds to the S4-S5 linker in the open configuration of the channel which is crucial for the increase in voltage sensitivity and current amplitude (Zhang, Zhou et al. 2013). For TRP channels, a chimera where the CTD of TRPV1 replaced the CTD of TRPM8 was employed to study the role of PIP₂ binding and demonstrating that the CTD of TRPV1 is required for PIP₂ sensitivity (Brauchi, Orta et al. 2007) For CaCC channels, Ta et al. showed that TMEM16A and TMEM16B are respectively activated and inactivated by diC8-PIP₂ (Ta, Acheson et al. 2017). Moreover, recent studies have identified multiple PIP₂ binding residues located in the TM3-5 of the TMEM16A channel (Le, Jia et al. 2019).

In fewer cases PIP₂ inhibits channel densities such as for intracellular Ca²⁺ release channels I(1,4,5)P₃ receptors and cyclic nucleotide gated channels (Hille 2001, Zhainazarov, Spehr et al. 2004). PIP₂-channel interactions have been shown to be mainly electrostatic with negatively charged phosphate groups of the phosphate head interacting with positively charged amino acids of the channel such as arginines, lysines and histidines (Rosenhouse-Dantsker 2019). It is also known that a cross-talk between cholesterol and PIP₂ levels can modulate several ion channels. For example, high cholesterol levels can down-regulate PIP₂ interaction with the Mg²⁺-inhibitory cation (MIC) and KCNQ channels (Chun, Shin et al. 2010).

1.6.3 Sphingolipids

The sphingolipid ceramide is generated by sphingomyelin hydrolysis or via ceramide synthases during different cellular processes including cellular stress, ischaemia, apoptosis and senescence (Hannun 1996). Similarly to cholesterol, ceramide increases the rigidity of cell membranes and inhibits a variety of ion channels such as K_{ir}, K_v and CFTR (Wu, Lo et al.

2001, Bock, Szabó et al. 2003, Ramu, Xu et al. 2007). Sphingosine-1-phosphate (S1P) is another sphingolipid involved in important cellular functions such as angiogenesis, cell migration, cell survival and maintenance of vascular tone (Hla 2003, Spiegel and Milstien 2003, Hla 2004, Saba and Hla 2004). S1P was shown to activate TRPC in ECs and VSMCs (Crousillac, Colonna et al. 2009, Formigli, Sassoli et al. 2009). Furthermore, S1P activates K_{ir} , BK_{Ca} and Cl^- channels (Wang, Carbone et al. 2002, Yin and Watsky 2005).

1.7 The lipid-sensitive TMEM16A Ca^{2+} -activated Cl^- channel

In the 1980's, endogenous $CaCC$ current was recorded for the first time in *Xenopus laevis* oocyte and salamander photoreceptors (Miledi 1982) (Miledi 1982, Barish 1983). This current was characterised by outward rectification in response to increase in $[Ca^{2+}]_i$ and depolarising voltage (Kuruma, Hirayama et al. 2000). The molecular identity of this channel remained elusive until 2008 when three groups independently identified the *TMEM16A* gene to encode a $CaCC$ (Caputo, Caci et al. 2008, Schroeder, Cheng et al. 2008, Yang, Cho et al. 2008). At low $[Ca^{2+}]_i$, $CaCC$ current was observed to be slowly activated at positive voltages, while at negative voltages the current was reversibly deactivated (Caputo, Caci et al. 2008, Schroeder, Cheng et al. 2008, Yang, Cho et al. 2008). In contrast, in the presence of high $[Ca^{2+}]_i$, $CaCC$ current was activated in a broader range of V_m including at hyperpolarised V_m (Yang et al., 2008). Yang et al used bioinformatics approaches followed by functional validation of the cloned *TMEM16A* gene as $CaCC$ (Yang, Cho et al. 2008). Schroeder et al. used an oocyte model from *Ambystoma mexicanum*, in which $CaCC$ s were not present, to express an isolated clone of *TMEM16A* from *Xenopus* oocyte (Schroeder, Cheng et al. 2008). In this way, *TMEM16A* expression produced current-voltage (I/V) relationships that resembled endogenous I_{CaCC} currents (Schroeder, Cheng et al. 2008). At that time, it was also known that interleukin-4 (IL-4) increased I_{CaCC} in human bronchial epithelial cell (Galiotta, Pagesy et al. 2002). Caputo et al. based his work on this latter notion and discovered that *TMEM16A* expression was increased seven-fold upon IL-4 treatment (Caputo, Caci et al. 2008).

Additionally, uridine 5'-triphosphate (UTP) and the Ca^{2+} ionophore ionomycin produced I_{CaCC} in cells transfected with *TMEM16A* (Caputo, Caci et al. 2008). Moreover, I_{CaCC} could be blocked by the CaCC inhibitor niflumic acid (NFA) (Caputo, Caci et al. 2008). Later studies used siRNA or genetic deletion of the *TMEM16A* gene to confirm that *TMEM16A* expression is required to produce native CaCCs in several human and animal models (Flores, Cid et al. 2009, Huang, Rock et al. 2009, Manoury, Tamuleviciute et al. 2010, Scudieri, Sondo et al. 2012, Cho, Lee et al. 2020). We now know that *TMEM16A* is expressed in many cells types such as VSMCs, interstitial cells of Cajal, olfactory neurons, pericytes, nociceptive and somatosensory neurons (Heinze, Seniuk et al. 2014, Fedigan, Bradley et al. 2017, Lin, Lv et al. 2018, Chen, Tan et al. 2019, Shah, Carver et al. 2020).

1.7.1 *TMEM16x* family

The mammalian *TMEM16x* family comprises ten members identified with the letter A to J (not including I). These ten paralogs share high sequence homology while forming a functionally diverse group of proteins. *TMEM16x* proteins may (i) form Ca^{2+} -activated Cl^- channels (CaCCs), (*TMEM16A* and B) (Duran and Hartzell 2011, Kunzelmann, Tian et al. 2011, Scudieri, Sondo et al. 2012, Yu, Whitlock et al. 2015); (ii) function as lipid scramblases, which facilitate bidirectional movement of lipids across the cell membranes, and may also possess non-selective ion channel activity (*TMEM16D*, E, F, K and J) or (iii) have additional cellular roles (*TMEM16C*, G, H) (Kunzelmann, Tian et al. 2011).

The *TMEM16A* and *TMEM16B* CaCCs share some electrophysiological properties, including comparable degrees of selectivity and permeability to a range of anions, and sensitivity to intracellular Ca^{2+} (Duran and Hartzell 2011, Kunzelmann, Tian et al. 2011, Scudieri, Sondo et al. 2012, Yu, Whitlock et al. 2015). *TMEM16A* and B channels also share some pharmacological properties. For example they are modulated in a complex manner by anthracene-9-carboxylic acid (A9C) and are inhibited by other commonly used Cl^- channel blockers such as DIDS and NFA to a similar extent (Garner, Harvey et al. 2001). In contrast,

the drug Ani9 was shown to selectively inhibit TMEM16A, with no significant effect on TMEM16B (Seo, Lee et al. 2016). TMEM16A is expressed in epithelial cells, where it contributes to secretion of transepithelial fluid and in contractile tissues, where it facilitates pacemaker activity as in interstitial cells of Cajal or contractile wave activity in gastrointestinal smooth muscle cells (Schroeder, Cheng et al. 2008, Hong, Lee et al. 2019). TMEM16A is also expressed in the brain, where it controls bradykinin-induced nociception and microvascular circulation (Brown and Passmore 2010, Suzuki, Suzuki et al. 2021). In contrast, TMEM16B is mainly expressed in olfactory and photoreceptors sensory neurons (Sagheddu, Boccaccio et al. 2010, Billig, Pál et al. 2011, Dibattista, Amjad et al. 2012, Pifferi, Cenedese et al. 2012).

TMEM16C to TMEM16G and TMEM16J are Ca²⁺-dependent phospholipid scramblases (Suzuki, Fujii et al. 2013, Gyobu, Miyata et al. 2016). While the TMEM16x family members described above are plasma membrane-resident channels, TMEM16H, TMEM16J and TMEM16K are found in intracellular membranes (Tian, Schreiber et al. 2012, Bushell, Pike et al. 2019). TMEM16F functions as a phospholipid-scramblase and non-specific ion channel (Suzuki, Umeda et al. 2010, Brunner, Lim et al. 2014, Yu, Whitlock et al. 2015). Figure 1.7.1 illustrates the difference in the channel structure between the scramblases and ion channels of the TMEM16x family. Suzuki et al. showed that TMEM16F can scramble a variety of phospholipids such as PS, PI, and PE (Suzuki, Umeda et al. 2010). For example, Toshihiro et al. showed that TMEM16F is required for exposure of PS, which activates platelets during blood coagulation (Fujii, Sakata et al. 2015). Point mutations in TMEM16F are associated with Scott Syndrome, a bleeding disorder caused by defective phospholipid scrambling in platelets (Brooks, Catalfamo et al. 2015). The Ca²⁺-sensitivity of TMEM16F was demonstrated to be significantly lower than for TMEM16A-B (EC₅₀ between 10-100 μM vs 1.3 and 1.9 μM) and with much longer time-dependence *I/V* relationships (Adomaviciene, Smith et al. 2013). TMEM16F non-specific ion current is suggested to coincide with its scramblase activity (Scudieri, Caci et al. 2015, Yu, Whitlock et al. 2015). The physiological function of TMEM16F current remains uncertain as Cl⁻ is not required for scrambling activity (Yu, Whitlock et al.

2015). In fact, it was shown that Cl⁻ channel inhibitors or substitution of extracellular Cl⁻ with other anions does not alter TMEM16F scramblase properties (Kmit, van Kruchten et al. 2013).

TMEM16K is an ER-resident lipid scramblase with non-specific ion channel activity (Bushell, Pike et al. 2019). The activity of this channel is dependent on Ca²⁺ and on short chain lipids. The ER membrane has symmetrical lipid distribution, which does not occur at the plasma membrane. Since many lipids are synthesised on the cytoplasmic side of the ER, scramblases play an important role in the formation of the ER membrane symmetrical lipid distribution. TMEM16K has been associated with several cellular phenomena, including spindle formation, Ca²⁺ signalling, volume regulation and apoptosis (Kramer and Hawley 2003, Wanitchakool, Ousingsawat et al. 2017). The fact that TMEM16K truncations and missense variants lead to autosomal recessive spinocerebellar ataxia type 10 (SCAR10), suggest incorrect lipid distributions in ER and other membranes in the pathophysiology of this disease (Vermeer, Hoischen et al. 2010, Balreira, Boczonadi et al. 2014).

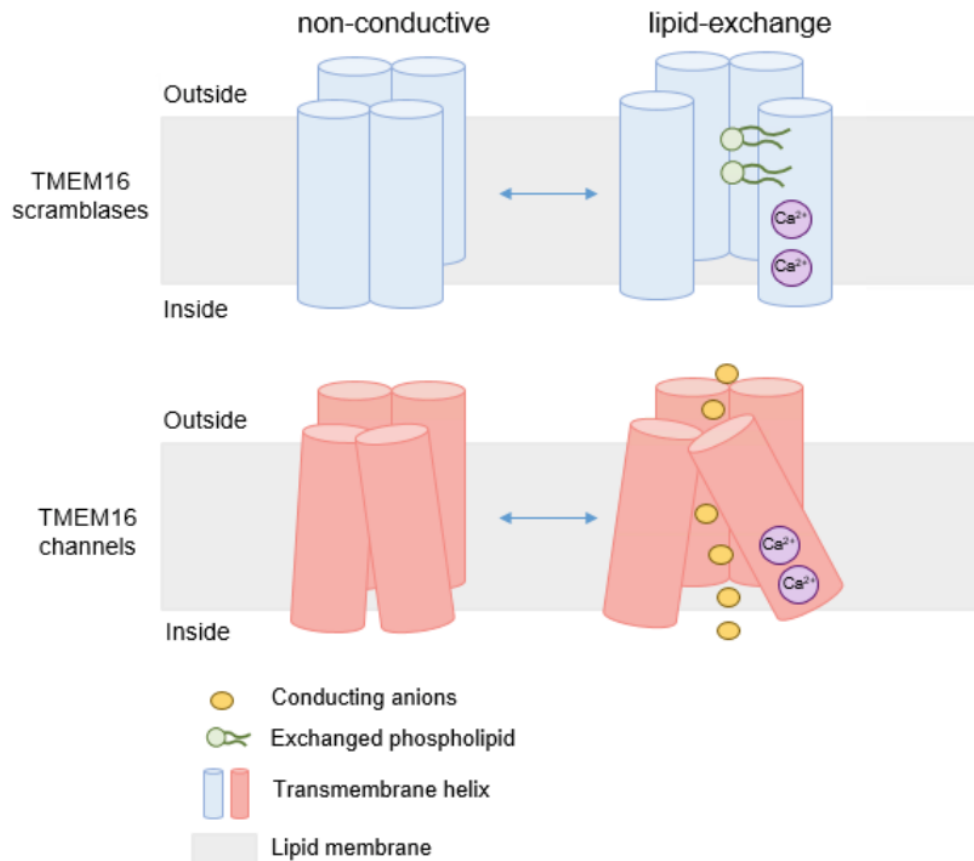


Figure 1.7.1 TMEM16x family: scramblases and ion channels.

Diagrammatic representation of the TMEM16x family members. Scramblases have a pore directly exposed to the lipid bilayer allowing lipid translocation from one side of the membrane to the other. In contrast, the pore of TMEM16 channels is partly shielded from lipids and allows only conductance of ions.

1.7.2 TMEM16A structure

TMEM16A has four splice variants, a-d, which results from different insertion or deletion of exons (Ferrera, Caputo et al. 2009, Ferrera, Caputo et al. 2010). As the other TMEM16x family members, TMEM16A is formed by ten transmembrane domains (TMDs) with intracellular N and C-terminal (Yang, Cho et al. 2008, Milenkovic, Brockmann et al. 2010). TMEM16A forms a homodimer with two pores (Fallah, Römer et al. 2011, Sheridan, Worthington et al. 2011) that are independently activated (Jeng, Aggarwal et al. 2016, Lim, Lam et al. 2016). Dimerisation of TMEM16A subunits is suggested to be irreversible as it is not affected by Ca²⁺

fluctuations or by disruption of actin filaments (Fallah, Römer et al. 2011, Sheridan, Worthington et al. 2011). The residues forming the dimerisation domain in the N-terminal region of TMEM16A are highly conserved among the other TMEM16x family members (Tien, Lee et al. 2013). In 2014 Brunner et al. obtained the X-ray structure of TMEM16A from the fungal homologue *Nectria haematococca* TMEM16 (nhTMEM16) (Brunner, Lim et al. 2014). More recently, in 2017 two groups independently identified the structure of mouse TMEM16A (mTMEM16A) *via* cryo-EM (Dang, Feng et al. 2017, Paulino, Kalienkova et al. 2017). They showed that TMEM16A is indeed formed by ten α -helices embedded in the plasma membrane with cytosolic N- and C-terminal (Dang, Feng et al. 2017, Paulino, Kalienkova et al. 2017).

The ion permeation pathway is formed by helices TM4-TM6 harbouring conserved Ca^{2+} binding residues (Brunner, Lim et al. 2014, Dang, Feng et al. 2017, Paulino, Kalienkova et al. 2017). These residues were identified through alanine mutagenesis studies as E654, E702, E705, E734 and D738 (Tien, Lee et al. 2013). These acidic residues form a negatively charged barrier to Cl^- flux. Upon binding of Ca^{2+} , this barrier is relieved through a conformational change in which the sixth TM domain opens the ion permeation pathway of TMEM16A (Paulino, Kalienkova et al. 2017, Peters, Gilchrist et al. 2018). Figure 1.7.2 illustrates the cryo-EM structure of TMEM16A and its Ca^{2+} binding sites.

Recently, Dinsdale et al. identified an outer pore region by investigating the biphasic effect of the small molecule anthracene-9-carboxylic acid (A9C) on TMEM16A (Dinsdale, Pipatpolkai et al. 2021). This work demonstrated that $[\text{Ca}^{2+}]_i$ induces a conformational change in the outer pore of TMEM16A, where the residues V539 and I636 shrink (Dinsdale, Pipatpolkai et al. 2021, Pifferi and Menini 2021). This indicates that $[\text{Ca}^{2+}]_i$ is essential to obtain a wider opening of the pore. The TMEM16A channel pore is partially lined with lipids (Dang, Feng et al. 2017, Paulino, Kalienkova et al. 2017). This is in accordance with the ancestral evolution of TMEM16A from lipid scramblases of the TMEM16x family (Whitlock and Hartzell 2017). Unlike other ion channels in which the ion permeation pathway is completely shielded from proteins,

a section of the TMEM16A pore is lining in proximity with the plasmalemmal lipids (Whitlock and Hartzell 2017).

TMEM16A is selectively permeable to large anions $\text{SCN}^- > \text{I}^- > \text{Br}^- > \text{Cl}^- > \text{F}^-$ (Schroeder, Cheng et al. 2008, Yang, Cho et al. 2008, Sagheddu, Boccaccio et al. 2010, Adomaviciene, Smith et al. 2013). The conductance of TMEM16A was reported to be 3-8 pS according to the expression system (Yang, Cho et al. 2008, Adomaviciene, Smith et al. 2013, Ta, Acheson et al. 2017).

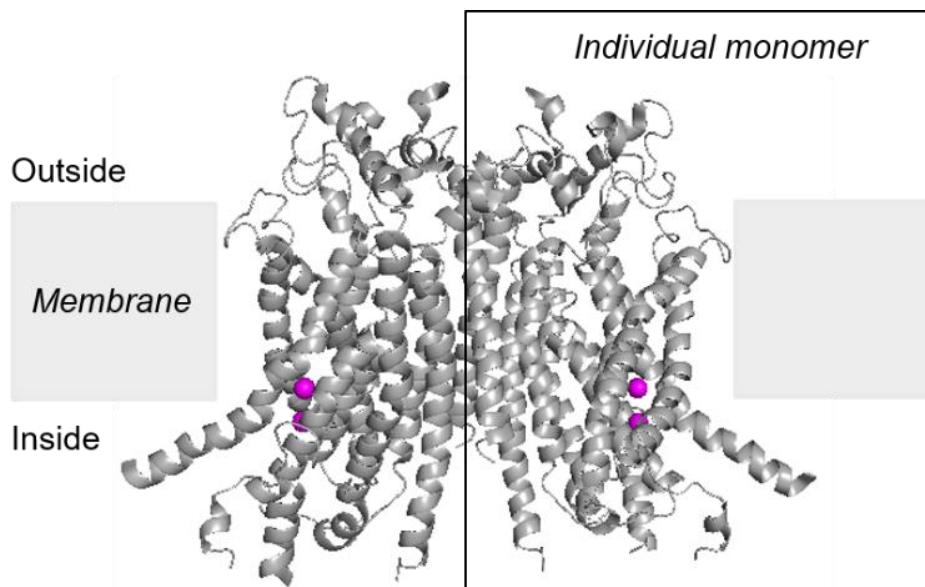


Figure 1.7.2 TMEM16A structure

Cryo-EM structure of the TMEM16A channel (Paulino, Kalienkova et al. 2017), formed by two subunits which can be activated independently by two calcium ions (illustrated in pink).

1.7.3 TMEM16A biophysical properties

The TMEM16A channel presents an outwardly rectifying *I/V* curve, as opening of the channel is favoured at depolarising membrane potentials (Kuruma and Hartzell 1999). TMEM16A currents are sensitive to voltage and Ca^{2+} (Caputo, Caci et al. 2008, Schroeder, Cheng et al. 2008). TMEM16A is gated open by $[\text{Ca}^{2+}]_i < 100 \text{ nM}$ and $[\text{Ca}^{2+}]_i$ regulates the extent of TMEM16A outward rectification (Ferrera, Caputo et al. 2010, Adomaviciene, Smith et al.

2013). TMEM16A current is voltage and time-dependent when $[Ca^{2+}]_i < 1 \mu M$, which results in a steep outward rectifying I/V relationship (Ferrera, Caputo et al. 2010). Instead, when $[Ca^{2+}]_i$ increases to $> 1 \mu M$ voltage and time-dependence are reduced, producing a more linear I/V curve (Ferrera, Caputo et al. 2010). The possibility that TMEM16A is regulated by calmodulin has been studied in depth in the literature. Several lines of evidence indicated that TMEM16A Ca^{2+} -activation is independent by calmodulin. For example, in patch-clamping experiments, application of WT calmodulin or a mutant form of calmodulin did not affect TMEM16A current density (Vocke, Dauner et al. 2013, Yu, Zhu et al. 2014). Moreover, purified human TMEM16A (hTMEM16A) in reconstituted proteoliposomes elicited TMEM16A current in the absence of calmodulin (Terashima, Picollo et al. 2013).

Different groups showed that TMEM16A can be activated in the absence of Ca^{2+} by a strong membrane depolarisation of 200 mV (Xiao, Yu et al. 2011, Contreras-Vite, Cruz-Rangel et al. 2016, Cruz-Rangel, De Jesus-Perez et al. 2017). Zhang et al. showed that the synergy between Ca^{2+} and voltage in activating TMEM16A is due to Ca^{2+} binding reducing the energy barrier required to gate open the channel at a given voltage (Zhang, Chen et al. 2014). It has also been proposed that activated TMEM16A currents can be fitted with a double exponential, suggesting that at least two states of Ca^{2+} binding are required for channel activation (Zhang, Chen et al. 2014).

1.8 TMEM16A role in vascular smooth muscle contraction

Several lines of evidence showed that TMEM16A is expressed in various vascular beds and plays a pivotal role in agonist-induced VSMC contraction (Gritli-Linde, Vaziri Sani et al. 2009, Davis, Forrest et al. 2010, Manoury, Tamuleviciute et al. 2010, Thomas-Gatewood, Neeb et al. 2011, Wang, Yang et al. 2012). As discussed above, VSMCs accumulate high $[Cl^-]_i$, therefore TMEM16A activation enables Cl^- extrusion favouring membrane depolarization and vasoconstriction.

CaCC currents were identified for the first time in the 1980s by several groups (Bader, Bertrand et al. 1982, Miledi 1982, Wang, Fermini et al. 1995), while the molecular identify of the currents was later resolved (Caputo, Caci et al. 2008, Schroeder, Cheng et al. 2008, Yang, Cho et al. 2008). It was then found in VSMCs that TMEM16A activation leads to opening of L-type Ca_v channels, enhancing Ca^{2+} influx hence leading cell contraction (Manoury, Tamuleviciute et al. 2010). Manoury et al. showed that gene silencing with short interfering RNA (siRNA) targeting TMEM16A in cultured pulmonary artery VSMCs dramatically reduced CaCC current, providing the first published evidence that TMEM16A forms CaCCs in VMSCs (Manoury, Tamuleviciute et al. 2010). Subsequent work showed that antibody blocking the TMEM16A pore significantly reduced TMEM16A-mediated current in cerebral artery (Thomas-Gatewood, Neeb et al. 2011, Wang, Yang et al. 2012). In mouse aorta, it was demonstrated that the TMEM16A inhibitor tannic acid reduced phenylephrine-induce contractions (Namkung, Thiagarajah et al. 2010). Similarly, in mesenteric rat arteries, TMEM16A down-regulation reduced agonist-induced contraction and vasomotion (Dam, Boedtkjer et al. 2014). Moreover, in airway VSMCs chronic inflammation induces increased TMEM16A expression along with enhanced VSMC contractility (Zhang, Li et al. 2013).

These data support the role of TMEM16A in mediating VSMC induced vasoconstriction. Figure 1.8.1 illustrates the signalling pathway involved in VSMC constriction in response to TMEM16A activation. Upon binding of an agonist such as NA to the G_q PCR, activation of PLC cleaves the second messenger PIP_2 in DAG and IP_3 . Subsequently, IP_3 binds to the IP_3R and stimulates release of $[Ca^{2+}]_i$ from the SR. Increase in cytosolic $[Ca^{2+}]_i$ released from intracellular stores, is enough to activate the calcium-sensitive TMEM16A. The electrochemical gradient for Cl^- in a smooth muscle cell, is such that TMEM16A opening results in diffusion of Cl^- out of the cell and membrane depolarisation. Voltage-gated calcium channels (Ca_v) are then activated by membrane depolarisation and their opening results in influx of calcium. Increase of $[Ca^{2+}]_i$ activated calmodulin, which induces phosphorylation of myosin light chain via myosin light kinase. Myosin light chain phosphorylation then allows

interaction with actin and thus, contraction of the VSMC. Hence, TMEM16A is required for amplifying the initial increase in $[Ca^{2+}]_i$ by inducing depolarisation. Heinze et al. showed the TMEM16A tamoxifen-induced knock-out results in a significant reduction of aortic contractility in mouse in response to angiotensin II or U46619 (Heinze, Seniuk et al. 2014).

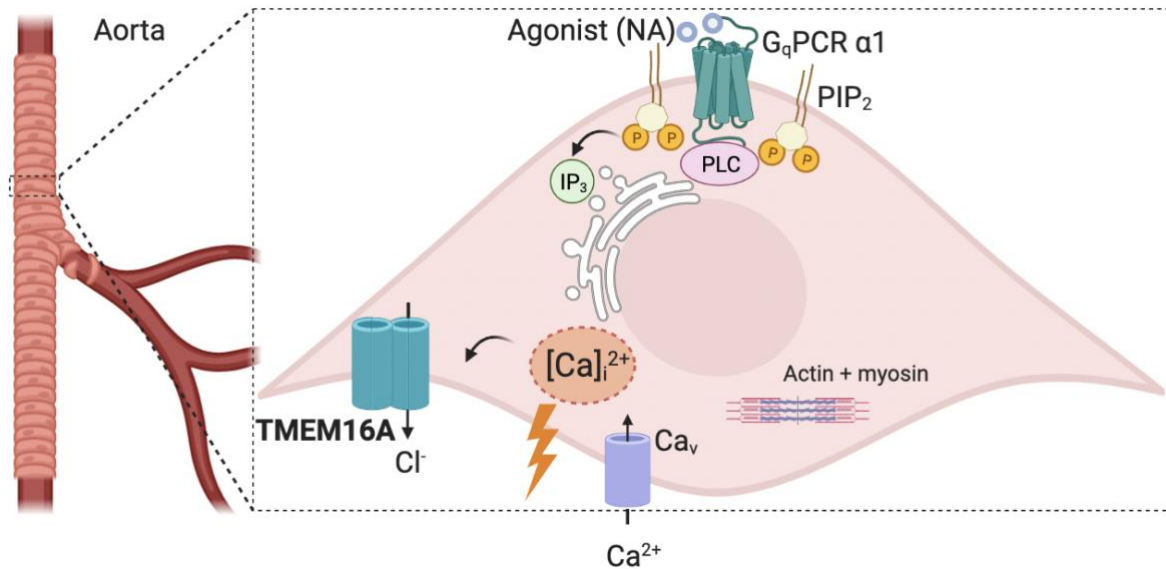


Figure 1.8.1 Role of TMEM16A in VSMC vasoconstriction.

Schematic illustration of the signalling pathway involved in TMEM16A-mediated constriction of smooth muscle cells in the aorta. In brief, upon activation of G_qPCR by an agonist as NA, PLC cleaves PIP₂ and its product IP₃ induces release of $[Ca^{2+}]_i$ from the SR. $[Ca^{2+}]_i$ increase activates TMEM16A and Cl⁻ efflux results in cell depolarisation. This in turn stimulates Ca_v to open and calcium influx further increases $[Ca^{2+}]_i$. Contraction of VSMC occurs by interaction of actin and myosin chains.

1.9 TMEM16A pharmacology

Since TMEM16A identification, several Cl⁻ channel blockers have been studied to inhibit TMEM16A, such as 5-nitro-2-(phenylpropylamino)-benzoate (NPPB), DIDS and NFA (Liu, Zhang et al. 2015). However, these compounds are not specific to TMEM16A as they can also act on volume-regulated anion channels (VRAC) (Xu 1997, Greenwood and Large 1998, Matchkov 2013, Best 1997) or affect K⁺ channels (Li, Wang et al. 2014) and intracellular Ca²⁺ stores (Ni, Kuan et al. 2014).

Synthetic TMEM16A inhibitors such as 2-acylaminoalkylthiophene-3- carboxylic acid arylamides (AACTs) (Truong et al., 2017), N-((4-methoxy)-2-naphthyl)-5- nitroanthranilic acid (MONNA) (Oh et al., 2013), CaCCinh-A01 (De La Fuente et al., 2008), and T16Ainh-A01 (Namkung et al., 2011) have also been showed to inhibit VRAC activity (Seo 2016). In contrast, the small molecule TMEM16A inhibitor Ani9, has been reported to selectively inhibit TMEM16A in a potent nM range while having negligible effect on TMEM16B (Seo, Lee et al. 2016). The small molecule TMinh-23 has been shown to block ionomycin induced TMEM16A activation and to lower blood pressure in spontaneously hypertensive rats (Cil, Chen et al. 2021) (Figure 1.9.1).

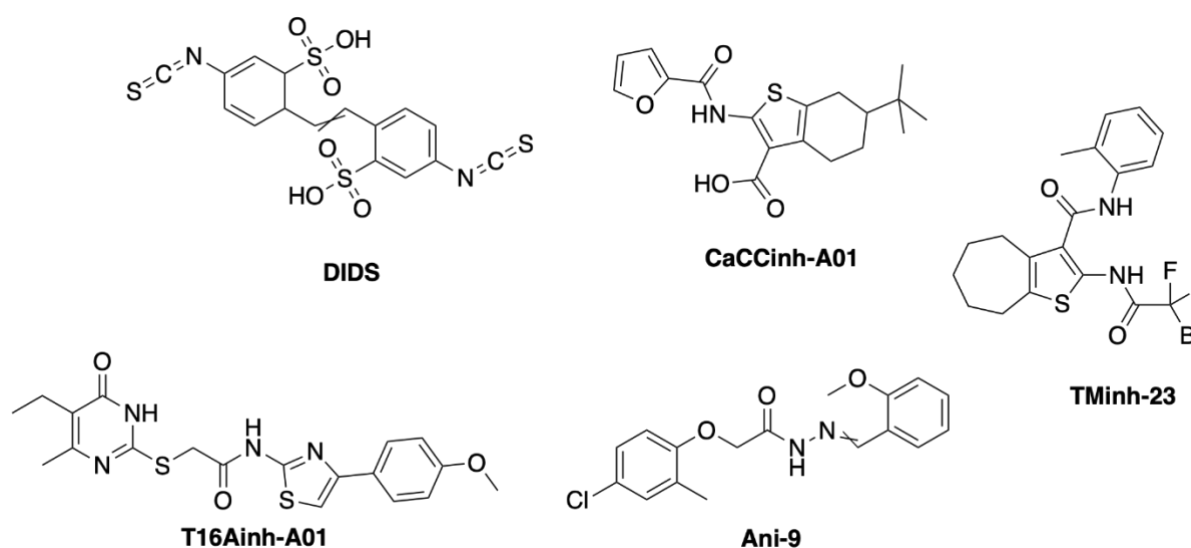


Figure 1.9.1 Synthetic TMEM16A inhibitors

Chemical structures of non-selective (DIDS and CaCCinh-A01) and selective (T16Ainh-A01, TMinh-23 and Ani-9) TMEM16A inhibitors.

Some polyphenols such as tannic and digallic acid have also been studied to inhibit TMEM16A (Namkung 2010). Among them, the natural dietary gallotannins, which is found in red wine and green tea, inhibited TMEM16A without affecting CFTR Cl⁻ channels (Namkung, Finkbeiner et al. 2010). Other dietary components inhibiting TMEM16A include dietary polyunsaturated fatty acids (PUFAs) (De Jesus-Perez, Cruz-Rangel et al. 2018), cholesterol (Sones, Davis et al. 2010) and flavonoids (Zhang, Li et al. 2017). Additionally, some compounds found in

Chinese herbal medicine can also inhibit TMEM16A. For instance, eugenol, an active ingredient of Thai herbal anti-diarrheal medicine, inhibited intestinal contractions in interstitial cells of Cajal from mouse ileum segments (Yao, Namkung et al. 2012).

1.10 Potential role for TMEM16A in vascular disease

Contraction of VSMCs within the walls of blood vessels, is a major determinant of vascular tone and blood pressure. TMEM16A is highly expressed in the aortas (Jensen, Joergensen et al. 2018) and small arteries (Dam, Boedtkjer et al. 2014), where it mediates Ca^{2+} -activated Cl^- channels. It has been postulated that this channel plays a pivotal role in the regulation of arterial blood pressure and peripheral resistance (Hübner, Schroeder et al. 2015). TMEM16A is also expressed in brain capillaries, where it regulates the blood flow to the central nervous system (CNS) and the integrity of the BBB (Liu, Zhang et al. 2019, Suzuki, Suzuki et al. 2021, Korte, Ilkan et al. 2022).

1.10.1 Hypertension

Hypertension affects more than 25% of the global population and is a risk factor for stroke, coronary heart disease, heart failure and renal failure (Hajjar, Kotchen et al. 2006, Elliott 2007, Cipolla, Liebeskind et al. 2018). There is an unmet need for hypertensive drugs, as the current hypertensive drugs may have low efficacy in significant proportions of hypertensive patients and may lead to side effects (Persell 2011, Sim, Bhandari et al. 2013, Lamirault, Artifoni et al. 2020). Several studies have pinned TMEM16A as a potential target to reduce blood pressure (Wang, Li et al. 2015, Askew Page, Dalsgaard et al. 2019). Downregulation of TMEM16A activity reduced vasoconstriction in response to NA and vasopressin in rat mesenteric arteries (Davis, Forrest et al. 2010, Dam, Boedtkjer et al. 2014). Heinze et al. showed that in constitutive TMEM16A-knockout mice, the mean arterial blood pressure was decreased (Heinze, Seniuk et al. 2014). TMEM16A inhibitors have also been used to study the effect of these small molecules on blood pressure. For example, T16A(inh)-A01 was used

to relax human and mice blood vessels (Davis, Shi et al. 2013). Cil et al. showed that the TMEM16A-inhibitor TMinh-23 decreased blood pressure in mesenteric arteries of spontaneously hypertensive rats (Cil, Chen et al. 2021). Moreover, in idiopathic pulmonary arterial hypertension, TMEM16A was strongly upregulated in small pulmonary arteries and in pulmonary artery smooth muscle cells (Papp, Nagaraj et al. 2019).

1.10.2 Microcirculation in the brain

Pericytes are contractile cells found in microvessels of small diameters such as the arterioles, venules and capillaries (Armulik, Abramsson et al. 2005). They were first described in the late 19th century and early identified as responsible for the structural and functional properties of local blood flow in the brain (Eberth 1871, Rouget 1873). Even though the brain accounts only of 2% of the adult human body weight, it receives 20% of cardiac blood flow to the CNS (Willie, Tzeng et al. 2014). In the CNS, blood vessels are classified according to their size in arterioles, capillaries and venules (Attwell, Mishra et al. 2016). The arterioles originate from large arteries penetrating into the cortex and running in the brain parenchyma into smaller arterioles and then into capillaries as their diameter decreases (Yamazaki and Kanekiyo 2017). The capillaries then increase their diameter again and separate into post-capillary venules, which join with others into larger veins (El-Bouri and Payne 2016). TMEM16A is expressed in VSMCs and pericytes which share markers such as neuron-gial antigen 2 (NG2), platelet derived growth factor receptor beta (PDGFR β) or vimentin (Smyth, Rustenhoven et al. 2018).

Pericytes play a pivotal role in maintaining the structure and stability of the vascular network. Cerebral flow is finely tuned by neuronal activity in a process known as neurovascular coupling (NVC) where capillary diameter changes with neuronal activity (Peppiatt, Howarth et al. 2006, Hall, Reynell et al. 2014, Kisler, Nelson et al. 2017, Wardlaw, Benveniste et al. 2020). NVC involves pericytes, endothelial cells, VSMCs, astrocytes and neurons (Abbott, Patabendige et al. 2010, Attwell, Buchan et al. 2010, Kisler, Nelson et al. 2017). Pericytes induce constriction of capillaries by responding to agonists such as endothelin-1 (ET-1), thromboxane A2 and

angiotensin II (Dodge, Hechtman et al. 1991). In contrast, they induce capillary vasodilation in response to other factors such as prostacyclin (Dodge, Hechtman et al. 1991). Individual pericytes are present on capillaries, which are closely located to neurons. In fact, capillaries are positioned ~ 8.4 μm of distance from neurons while ~ 70 μm from arterioles (Bergers and Song 2005). This tight regulation helps pericytes to tune the diameter of capillaries to increase or reduce local blood flow and energy supply to neurons. Figure 1.10.1 illustrates pericytes organisation around capillaries in the CNS.

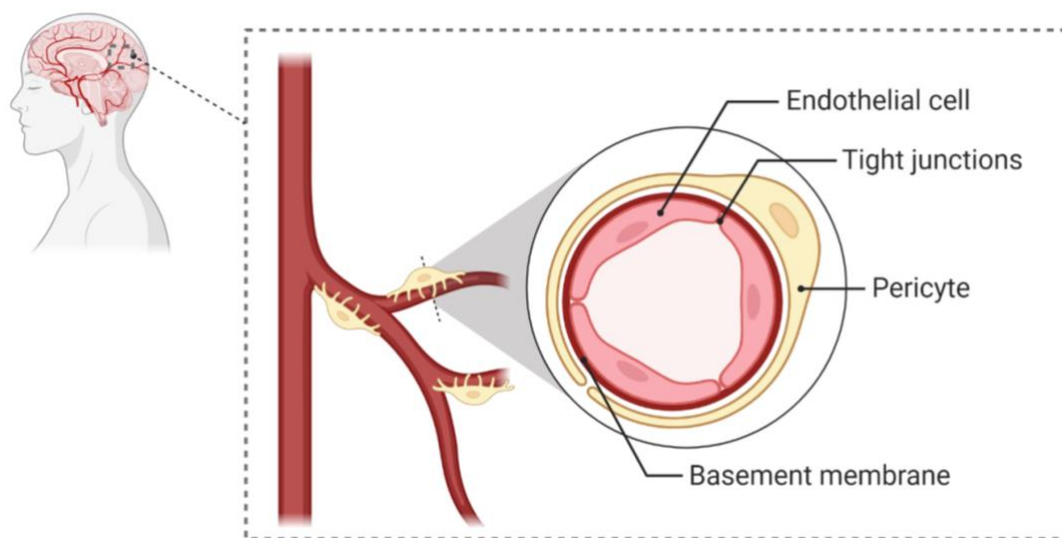


Figure 1.10.1 Pericytes surrounding capillaries in the brain.

Diagrammatic representation of pericytes positioned on the capillaries in the brain. Pericytes are characterised by long extensions that enables them to surround the capillary diameter. In this way, they can regulate the vasoconstriction and dilation of the vessel in response to neurotransmitter-stimulation.

In the CNS, the BBB forms a semipermeable barrier where tight junctions and adherents' junctions control movements of circulating ions, molecules and materials between the blood and the brain (Luissint, Artus et al. 2012, Daneman and Prat 2015). Pericytes play a crucial role in maintain the BBB as they control tight junctions and alignment with endothelial cells (Bergers and Song 2005).

Pericytes are also pivotal in the generation of new blood vessels or angiogenesis. During this process, pericytes are recruited from the bone marrow and brain parenchyma in response to the secretion of PDGFR β from endothelial cells (Rajantie, Ilmonen et al. 2004, Gaengel, Genové et al. 2009). On the other hand, pericytes control the stabilisation of endothelial cells by releasing factors such as transforming growth factor beta (TGF β), angiopoietin 1 (Angpt1) and vascular endothelial growth factor (VEGF) (Durham, Surks et al. 2014, Teichert, Milde et al. 2017, Blocki, Beyer et al. 2018).

In pathological conditions such as ischaemic stroke and vascular dementia, pericytes die readily in rigor constricting the capillaries in a no-reflow phenomenon (Yemisci, Gursoy-Ozdemir et al. 2009). During ischaemia, hypoxia reduces levels of intracellular ATP, which increases [Ca²⁺]_i as it prevents Ca²⁺ cellular extrusion as PMCA requires ATP for its function (Arnould, Michiels et al. 1992, Peters, Tijssen et al. 1998). Pericytes death in rigor around capillaries results in long-lasting reduction in the diameter of capillaries results in decrease of cerebral blood flow, breakdown of the BBB, neuronal damage and cell death (Kloner, King et al. 2018). Pericytes death can further increase neuronal damage because *via* receptor-mediated endocytosis or phagocytosis, pericytes uptake neurotoxic products (i.e. immunoglobins, fibrin and albumin) which can enter a breached BBB (Armulik, Genové et al. 2010, Bell, Winkler et al. 2010, Schultz, Byman et al. 2017). Moreover, in vascular dementia, pericytes degeneration leads to vessel instability and demyelination (Bell, Winkler et al. 2010). Pericytes can clear amyloid- β (A β) deposition through the LDL-R mediated pathway (Ma, Zhao et al. 2018). It was shown that pericytes loss aggravates A β deposition in transgenic mice (Sagare, Bell et al. 2013) and that A β can constrict human capillaries (Nortley, Korte et al. 2019). These data show that pericytes function and properties are fundamental to maintain cerebral homeostasis.

1.11 Hypothesis and aims

TMEM16A Ca^{2+} -activated Cl^- channel are a key depolarising force in VSMCs (Matchkov, Aalkjaer et al. 2005, Manoury, Tamuleviciute et al. 2010, Bulley and Jaggar 2014, Hübner, Schroeder et al. 2015). TMEM16A has a pore with some degree of exposure to the surrounding plasmalemmal lipids; this may confer lipid sensitivity to the channel (Whitlock and Hartzell 2017). Mutations in *NPC1* lead to NPC, a disorder associated with impaired lipid homeostasis, which causes neurodegeneration and vascular impairment (Platt 2018). In this thesis it is hypothesised that the TMEM16A channel is modulated by lipid and thus indirectly controlled by the activity of NPC1. It is further hypothesised that this modulation will constitute a means of control of VSMCs and pericytes tone, which abundantly express TMEM16A and that pharmacological modulation of the channel can counteract its control by NPC1. The specific aims are:

- To define the electrophysiological and pharmacological properties of TMEM16A and TMEM16x paralogues expressed in VSMCs.
- To examine if cellular inhibition of the lysosomal protein NPC1 can alter TMEM16A activity and to elucidate the underlying mechanism.
- To establish if TMEM16A modulation by NPC1 occurs in isolate rodent arteries and capillaries, where TMEM16A is highly expressed.

Chapter 2

Methods

2.1 Chemicals and reagents

Unless stated otherwise, chemicals were purchased from Sigma-Aldrich, UK. Primers were purchased from IDT Technologies (Belgium). Sequencing was performed by GATC Biotech, Germany. The compounds AUT11813, AUT11814 and AUT11817 were manufactured by Autifony Therapeutics.

2.2 Animals

All animal care and experimental protocols were in accordance with the UK Home Office regulations (Guidance on the Operation of Animals, Scientific Procedures Act, 1986). The use of transgenic mice was approved by the University Ethics Committee. Animal studies were reported in compliance with the ARRIVE guidelines (Kilkenny, Browne et al. 2010, McGrath and Lilley 2015). BALBc/NPC1^{nlh} and their respective wild-type (WT) controls (*Npc1*^{+/+}) were bred as heterozygotes to generate homozygous null (*Npc1*^{-/-}) (Pentchev, Gal et al. 1980). Mice were housed under non-sterile conditions, with food and water available *ad libitum*. Since *Npc1* deficiency affects both genders similarly (Morris, Bhuvaneshwaran et al. 1982), mice of either sex were selected randomly on the day of the experiment. Adult mice aged 8-8.6 weeks were used in this study.

2.3 Cell preparation

2.3.1 Cell lines

Chinese Hamster Ovary (CHO) and Human embryonic kidney 293T (HEK-293T) were used for heterologous expression studies. These cell lines are used widely as heterologous expression systems because for their low expression of endogenous Cl⁻ channels (Adomaviciene, Smith et al. 2013, Ta, Acheson et al. 2017). The HEK-293T cells are engineered to express the Simian Virus 40 (SV40), which is a large T-antigen that increases the transfection efficiency and viral replication (Lin, Boone et al. 2014). CHO cells were WT or containing a deletion for the *Npc1* locus (*Npc1*^{-/-}) (Dahl, Reed et al. 1992, Millard, Srivastava et al. 2000, Higaki, Ninomiya et al. 2001). Gene trap mutagenesis was used to delete the *Npc1* locus as described in the literature (Higaki, Ninomiya et al. 2001). Gene trap mutagenesis is based on the integration of a reporter gene lacking a promoter into the genome and its expression from a tagged endogenous promoter (Friedrich and Soriano 1991). In brief, a CHO cell line expressing the murine ecotropic virus receptor was incubated with a supernatant containing gene trap retroviruses (Higaki, Ninomiya et al. 2001). Infected cells were selected by isolating G418-resistant colonies by colony-lifting and expanded in nonselective medium (Higaki, Ninomiya et al. 2001). The insertion site of the trap vector was determined by PCR analysis using a primer specific for the trap vector as previously described (Zambrowicz, Imamoto et al. 1997).

2.3.2 Cell culture

Cell lines used were cultured in Dulbecco's Modified Eagle's Medium F-12 (Sigma-Aldrich, UK) supplemented with 10% foetal bovine serum (Sigma-Aldrich, UK) and 0.5% gentamicin (Sigma-Aldrich, UK). Cells were cultured in a humidified incubator with 5% CO₂ at 37°C. Cells were grown in T25 flasks (Corning, UK), passaged when reaching 70-80% confluency, and media was replaced every 2-3 days. Cells were washed with 5 ml of phosphate buffered saline solution (PBS) (Thermo Fisher Scientific, UK) at room temperature, followed by incubation with trypsin (Sigma-Aldrich, UK) for 1 minute at 37°C. Cell media (4 ml) was then added to the detached cells in order to deactivate trypsin. Cells were then centrifuged at 2000 rpm for 3 min. Cells were then counted using a hemacytometer and plated on continuation flasks. ~ 50,000 cells were plated in 35 mm Petri dishes (Corning, UK) and cultured for 24 hours before transfection.

2.3.3 Cell transfection

Cells were transiently transfected with 0.3-1 µg vectorial DNA for expression of TMEM16 channels and 0.2 µg of CD8 construct using Fugene HD (Promega, UK) transfection reagent. In some experiments, the TMEM16A channel was co-transfected with 1 µg of α 1 receptor or with 1 µg of PH-PLC δ . The Fugene HD reagent is a lipid-based transfection. This mechanism of transfection comprises of DNA contained in a monolayer of lipids to be taken up into cells *via* endocytosis (Jacobsen, Calvin et al. 2004). DNA and transfection reagent were combined in 50 µl of culture medium. The transfection reagent (1.5 µl) was used for every 1 µg of total DNA. The mix containing culture medium, DNA and transfection reagent was added to cells plated 24 hours previously. Cells were used ~12–48 h after transfection. For patch-clamp recordings, cells were washed with extracellular solution and transfected cells were identified by adding 1.2 µl Dynabeads anti-CD8 antibody-coated beads (Invitrogen, UK). This process

allows antibody-coated beads to bind to cells expressing the CD8 membrane antigen which should be presumably expressed along the co-transfected DNA construct of interest (Jurman, Boland et al. 1994).

2.3.4 Native smooth muscle cells isolation

Wild-type or *Npc1*^{-/-} Balb/c mice were sacrificed by cervical dislocation according to the UK Home Office guidelines. The heart and lungs were removed and the thoracic aorta was isolated and placed in ice-cold physiological salt solution (PSS), Table 2. The thoracic aorta was then mechanically cleaned from connective tissue and perivascular fat in ice-cold PSS by using forceps and scissors under a stereo-microscope (Leica, zoom 2000). The cleaned aorta was laterally cut into three sections and then opened longitudinally in order to increase the surface area for enzymatic digestion. Artery sections were then washed with ice-cold PSS and followed by dissociation medium (DM), Table 3.

Pieces of aorta were then placed for 1 hour at 4°C in 1.5 mg/ml papain. Papain is a cysteine protease that is activated when the sulphhydryl groups are reduced. The activation of papain was achieved by adding 0.5 mg/ml of the reducing agent dithiothreitol (DTT) and incubated in a water bath at 37°C for 5 min. Aortic sections were then placed in DM enriched with 0.35 mg/ml of collagenase type I from *Clostridium histolyticum* in a water bath at 37°C for 4 min. Collagenase was used for its endopeptidase activity to digest collagen in the connective tissue around the vessel. The aortic sections were then washed twice in DM at room temperature to remove any enzymatic residue. They were then triturated using a polished glass pipette for 30-60 s to separate the aortic VSMCs from the vessel. The isolated VSMCs were stored in DM on ice and used on the same day for experiments. A drop of cell suspension was placed on a 35 mm Petri dish (Corning, UK) and left for 5 min to allow cells adhesion. After addition

of appropriate extracellular solution to the dish, cells were used for patch-clamp electrophysiology.

Table 2 Physiological salt solution (PSS)

Compounds	Concentration (mM)
NaCl	122
KCl	5
HEPES	10
KH ₂ PO ₄	0.5
NaH ₂ PO ₄	0.5
MgCl ₂	1
D-Glucose	11
CaCl ₂	1.8
pH to 7.4 with NaOH	

Table 3 Dissociation medium (DM)

Compounds	Concentration (mM)
NaCl	110
KCl	5
HEPES	10
KH ₂ PO ₄	0.5
NaH ₂ PO ₄	0.5
Taurine	10
EDTA	10
D-glucose	10
CaCl ₂	0.2
MgCl ₂	2
Phenol red	0.03
pH to 7.3 with NaOH	

2.4 Molecular Biology

2.4.1 Bacterial transformation

DNA constructs were subcloned into a vector containing a selectable marker gene, conferring resistance to an antibiotic (ampicillin or kanamycin), which allowed selection of bacteria that have taken up the vector (Table 4). A strain of *Escherichia Coli* non-infectious to humans (50 μ l), Subcloning Efficiency DH5 α Competent Cells (Invitrogen, UK), were used to transform plasmid DNA (Hanahan 1983). In brief, 100 ng of plasmid DNA was added to the DH5 α cells. The mix was then incubated on ice for 30 min and then heat-shocked at 42°C for 20 s. This process forms small pores on the bacterial membrane surface to allow the uptake of plasmid DNA into the bacterial cells. The latter were then incubated with 250 ml of a super optimal broth with catabolite repression (SOC medium) in a shaker at 3000 rpm for an hour at 37°C. Catabolite repression is a regulatory mechanism that involves rapid inhibition of the use of certain sources when a preferred source is present. This mechanism allows bacteria to quickly adapt and selectively use substrates from a mixture of different carbon sources. Bacteria were then plated on a lysogeny broth (LB) agar plate supplemented with the appropriate antibiotic (ampicillin at 100 mg/ml or kanamycin at 50 mg/ml) and incubated overnight at 37°C. Only bacteria cells that have been transformed with the DNA plasmid containing the marker gene for resistance to either ampicillin or kanamycin were able to grow on the plate. An individual colony of bacteria was inoculated into a 5 or 100 ml of LB-broth supplemented with the appropriate antibiotic and incubated in a shaker at 3000 rpm for 16 hours at 37°C in order to expand bacteria cells (mini or midi-prep). Bacterial transformation was performed next to a Bunsen Burner flame to create an aseptic environment and reduce the possibility of unspecific bacterial infection add (Green 2012).

Table 4 Plasmid DNA.

DNA construct	Vector	Antibiotic resistance	Gene number (PubMed)	Providers
TMEM16A	pcDNA3.1	Ampicillin	NM_178642.5	OriGene, USA
TMEM16B	pcDNA3.1	Ampicillin	NM_153589.2	OriGene, USA
TMEM16F	PCMV6	Kanamycin	NM_175344	OriGene, USA
TMEM16K	pcDNA3.1	Ampicillin	NM_018075	OriGene, USA
DrVSP	pIRES-EGFP	Kanamycin	NM_001025458.1	Prof. Y. Okamura, Osaka University
α 1-receptor	pcDNA3.1	Ampicillin	NM_000680	OriGene, USA
CD8	Custom Vector	Ampicillin	NM_001145873.1	Dr M. Pusch
KCNE1-CD8	pIRES-CD8	Ampicillin	NM_000219.5	G. Sandoz, Université Cote d'Azur, CNRS, INSERM, iBV, Nice, France
PH-PLC δ	pcDNA3.1	Ampicillin	NM_006225.4	Addgene, USA

2.4.2 DNA extraction and purification

Plasmid DNA was extracted and purified using either QIAprep Spin Miniprep kit (Qiagen, UK) or HiSpeed Plasmid Midi Kit (Qiagen, UK). The procedure was performed as per manufacturer's instruction. Briefly, bacteria cells were pelleted *via* centrifugation and resuspended in solution containing alkaline detergents to lyse the cells. Lysed cells were then pelleted *via* centrifugation and the lysate containing DNA was neutralised and absorbed onto a silica membrane. Ethanol was used to wash the membrane, then eluted with a buffer containing Tris and EDTA to solubilise DNA. The Tris deprotonates and solubilises the DNA, while the EDTA inhibits nucleases preventing DNA degradation. DNA concentration and purity were measured using a Nanodrop 2000c spectrophotometer (Thermo Scientific, UK). The DNA concentration was measured with a spectrophotometer (Nanadrop 2000cTM, Thermo Scientific). The ratio of optical density measured at 260 nm wavelength over that measured at

280 nm or 230 nm wavelength indicates purity of the DNA (Lucena-Aguilar, Sánchez-López et al. 2016).

2.4.3 Site directed mutagenesis and primer design

Primers were designed using Primer3web (version 4.0.0, Whitehead Institute and Howard Hughes Medical Institute, <http://primer3.sourceforge.net/>) and sequences aligned using the Basic Local Alignment Search Tool (BLAST®, NCBI). Primers used to construct mutant TMEM16A channels are described below, Table 5. A Quikchange® Lightning Site-directed Mutagenesis kit (Agilent Technologies, UK) was used for single point mutagenesis (Figure 2.4.1). The mutagenesis reaction was performed as detailed in the manufacturer's instructions. In brief, 5 µl 10x reaction buffer, 1.25 µl (125 ng) of each primer, 1 µl dNTP mix, 1.5 µl QuikSolution reagent, 1 µl Quikchange® Lightning enzyme and ddH₂O to a total volume of 50 µl were added to 10-100 ng mTMEM16A DNA. The PCR reaction protocol was; 95°C for 2 min, 95°C for 20 s, 60°C for 10 s, 68°C for 3 min (based on a plasmid size of 5.4 kbp, 30 s/kb of plasmid length) and a final extension step of 68°C for 5 min. The temperature cycling allowed the primers to anneal to the DNA template and extend the length of the new DNA constructs with the desired mutation. Dpn I (2 µl) restriction enzyme was added to each amplification reaction and incubated at 37 °C for 5 min with gentle shaking. The Dpn I enzyme digests parental, nonmutated, supercoiled DNA. Mutant DNA was amplified by transforming into XL10-Gold® ultracompetent cells (Qiagen, UK). XL10-Gold® ultracompetent cells have a high transformation efficiency phenotype (average efficiency $\geq 5 \times 10^9$ transformants/µg of supercoiled DNA). Also, 2 µl β-mercaptoethanol was added to 45 µl XL-10-Gold® ultracompetent cells and incubated on ice for 2 min. The β-mercaptoethanol provides conditions which increases the efficiency of transformation. To ensure the single-point mutation had been successful mutant DNA was sequenced.

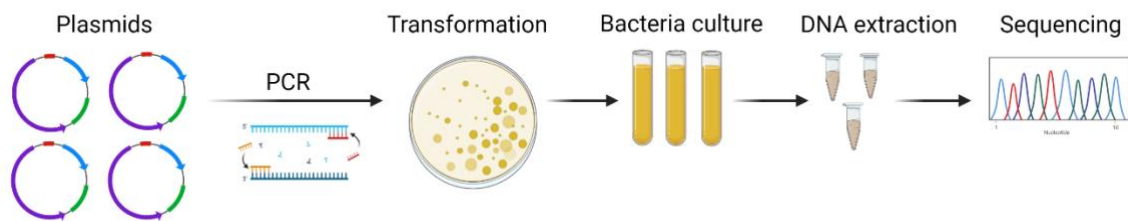


Figure 2.4.1 Single point site directed mutagenesis

Diagrammatic representation of the steps for insertion of a single point mutation into template DNA (plasmids) using PCR with forward and reverse primers complementary to the sequence of interest. The DNA is then transformed into DH5 α cells and grown overnight to expand individual bacterial colonies. The DNA is then extracted and purified using Qiaprep Spin Miniprep kit (Qiagen, UK), and sent for Sanger sequencing.

Table 5 Primers designed to constitute mutant TMEM16A channels

DNA	Forward primer (5'-3')	Reverse primer
R482A	CTGACCTGGAGGGACGCATTCCCAGCCTATTC	GAAATAGGCTGGGAATGCGTCCCTCCAGGTCAG
R575A	GAAGAGCTTTGAGGAGGCGCTAACCTTCAAGGC	GCCTTGAAGGTTAGCGCCTCCTCAAAGCTCTTC
Q645A	GGCAAGCAGCTAATCGCCAACAATCTCTTCGAG	CTCGAAGAGATTGTTGGCGATTAGCTGCTTGCC
I637A	TGTATCCAGCTGAGCGCCATTATGCATGGGCAAG	CTTGCCCAGCATAATGGCGCTCAGCTGGATACA

2.5 Patch-clamp electrophysiology

Patch-clamp electrophysiology is a technique that allows to measure the electrical properties of cell membranes through the use of microelectrodes (Hamill, Marty et al. 1981). The approach enable either voltage clamp or current clamp across the cell membrane. The experiments described in this thesis have been performed in the voltage clamp to enable assessment of membrane current to any give imposed voltages. Furthermore, different configurations can be adopted such as whole-cell and inside out configuration (used in this thesis, and detailed below).

The cell can be considered equivalent to an electrical circuit where the cell membrane is acting as an insulator separating two conductors (intracellular and extracellular solutions with defined electrolyte composition). In this way, the cell can store charges as a capacitor when a given voltage is clamped across the membrane. The amount of charge stored is dependent on the surface area, thus the size of the cell is estimated based on the measured capacitance. In fact, the capacitance is proportional to the surface area, with large cells having larger capacitance. The relationship between capacitance (C) and charge (Q) can be described as:

$$C = \frac{\Delta Q}{\Delta V} \quad \text{Equation 9}$$

where ΔV is the change in voltage. In the cell, the flux of ions generating ionic current (I_i) is controlled by ion channels which act as variable resistors (R). Upon channel opening, voltage flows across the membrane (capacitor) as in a circuit. This generates a capacitive current (I_c) dependent on the change in voltage per s ($\Delta V/\Delta t$):

$$I_c = C \frac{\Delta V}{\Delta t} \quad \text{Equation 10}$$

The total current (I_T) in a circuit is given by the contribution of I_i and I_c (Figure 2.5.1). It follows that:

$$I_T = I_i + C \frac{\Delta v}{\Delta t} \quad \text{Equation 11}$$

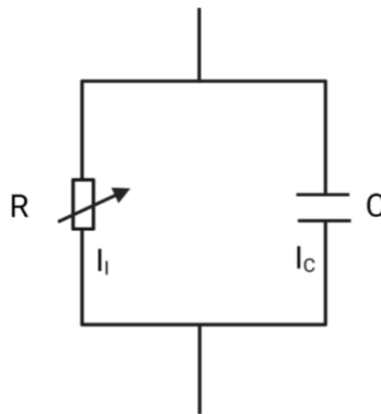


Figure 2.5.1 The cell membrane as a model of an electrical circuit.

C is the membrane capacitance; R is the electrical resistance of the membrane; I_c and I_i are the capacitive and the ionic currents, respectively.

Applying a voltage pulse to the cell causes the cell membrane to become temporarily charged, and a transient cell capacitance current is observed. The change in membrane potential always takes place after a delay as a result of the cell's capacitance. After this brief charging period, a steady state is reached ($\Delta V/\Delta t = 0$), the capacitor current becomes zero and the total current is only made up of the ionic current. Thus, the current flowing across the membrane is proportional only to the conductance, i.e. the number of open ion channels. Due to the voltage-dependent nature of ion channels, the voltage-clamp technique allows for a direct measurement of ionic currents by controlling the voltage, thus the opening and closing of

voltage-gated ion channels. However, since I_c is a transient current only visible at the start of a voltage step, the overall current flowing across the membrane is proportional only to the I_i .

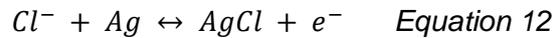
In this thesis the patch-clamp experiments were carried out in the out in whole-cell and inside-out configuration during voltage clamp mode. The membrane V_m was held at a desired value by constantly injecting a compensatory current (Molleman 2008). The amplitude of this current changes as a function of alterations in the resistance of the membrane, such as those due to changes in ion channel gating.

2.5.1 Patch-clamp experimental set up

An Olympus IX51 inverted microscope (Olympus, UK) and micromanipulator (Scientifica, UK) were positioned on an anti-vibration air table (Newport, USA) and surrounded by a Faraday cage to provide mechanical stability and electrical shielding (Molleman 2008). Optimal electrical shielding was obtained by connecting the individual items of the set-up to a single ground point, avoiding current loops between the instruments (Molleman 2008). GePulse software (<http://users.ge.ibf.cnr.it/pusch/programs-mik.htm>) with an analogue-to-digital and digital-to-analogue (AD/DA) converter (USB-6221, National Instruments, UK). All currents were low-pass filtered at 2-5 kHz and sampled at 10 kHz (unless otherwise stated). The signal is filtered using a low-pass anti-aliasing filter to “clean” it from white noise. Whole-cell capacitance and in-series resistance were compensated by ~70% during voltage clamp, using the Axon amplifier in-built compensation circuits.

Pipettes were pulled daily from borosilicate glass capillaries using a two-stage vertical puller (Narishege, UK) and had resistances between 2 and 3.5 M Ω in the working solutions. The bath solution was grounded through an Ag–AgCl reference electrode. An AgCl electrode was also used for the pipette electrode and connected to a head stage. The AgCl electrodes consist of a silver wire (0.01 mm diameter) that has an outer coat of AgCl. The ionic current

from the cell is converted to an electrical current within the metal wire according to the following reaction:



which occurs at the interface between the liquid and the metal. This reaction is reversible, minimising the solid-liquid junction potential induced by redox reaction (electron transfer) between the metal electrodes and the salt solutions (Hamill, Marty et al. 1981). Experiments were conducted at 20-22°C (room temperature). Liquid junction potential was calculated and subtracted offline (Neher 1992).

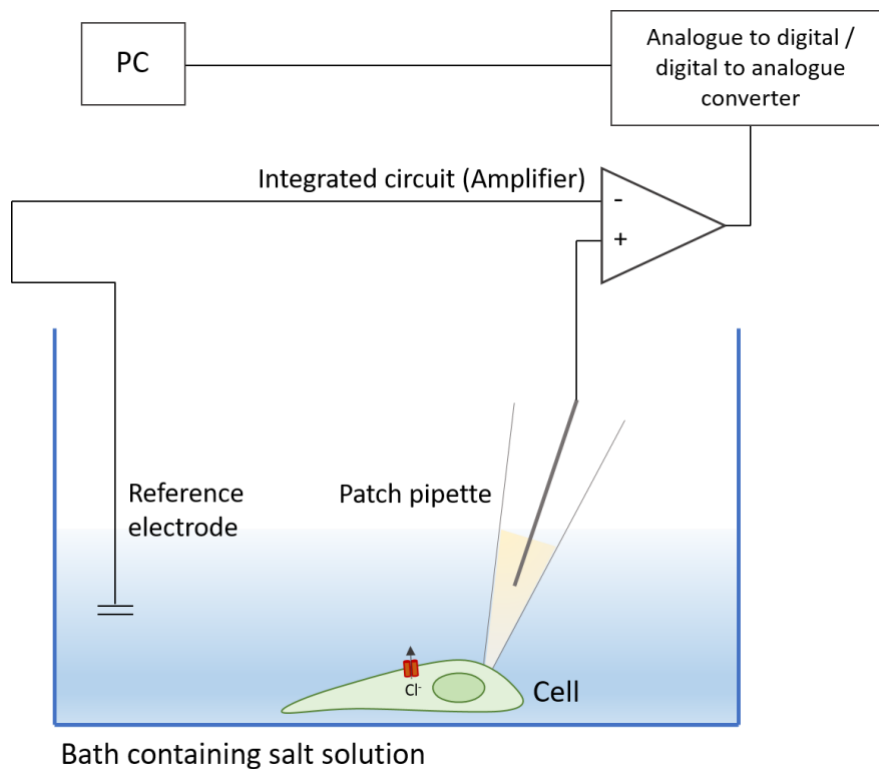


Figure 2.5.2 Diagrammatic representation of the whole-cell patch clamp experimental set up.

In the whole-cell configuration circuit, the patch pipette is attached to the cell to diffuse the solution from the pipette into the cell. Once the solution of the pipette is in contact with the cell, current is injected using the electrode present in the pipette to clamp membrane potential. The reference electrode present in the bath records changes in membrane potential in response to ion channel activity. The signal is then amplified by the integrated circuit and converted by the analogue to digital/digital to analogue converter on to the computer (PC).

2.5.2 Patch-clamp configurations

To establish whole-cell and inside-out patch-clamp configurations, the tip of the pipette is first gently pressed on the cell membrane and suction is applied to obtain a high resistance (>1 G Ω) seal. The whole-cell patch-clamp configuration can be achieved following the formation of the G Ω seal, when additional suction is applied to rupture the membrane and enable the pipette solution to come in contact with the cell interior. Whole-cell patch-clamp configuration allows recording of the overall activity of all the open ion channels on the cell membrane. As soon as the whole-cell configuration was obtained, cells were lifted and held at 0 mV for 3 min, prior to commencement of the experiment. This facilitated the intracellular solution in patch-pipette to enter the cell and fully equilibrate with the intracellular environment.

To obtain the inside-out configuration, the patch of the cell membrane that is in contact with the tip of the pipette was excised after formation of the G Ω seal, by pulling the pipette diagonally away from the membrane. In this way, the cytosolic side of the cell membrane was exposed to the bath solution while the extracellular side was facing the pipette solution. The inside-out configuration was used to study the effect of modulators applied to the intracellular side of the membrane.

In the whole-cell configuration, capacitance is present as the cell membrane can store charge and act as a capacitor. The series resistance refers to the sum of the access resistance and pipette resistance in series with the membrane capacitor (Molleman 2008). Membrane resistance and cell capacitance need to be overcome to control the V_m and therefore needs to be compensated. Because larger cell membranes can store more charge, the cell capacitance also reflects the size of the cell. To compare currents from cells of different sizes, the current (expressed in pA) was normalised for cell capacitance (expressed in pF) and thus, the current density data is given as pA/pF.

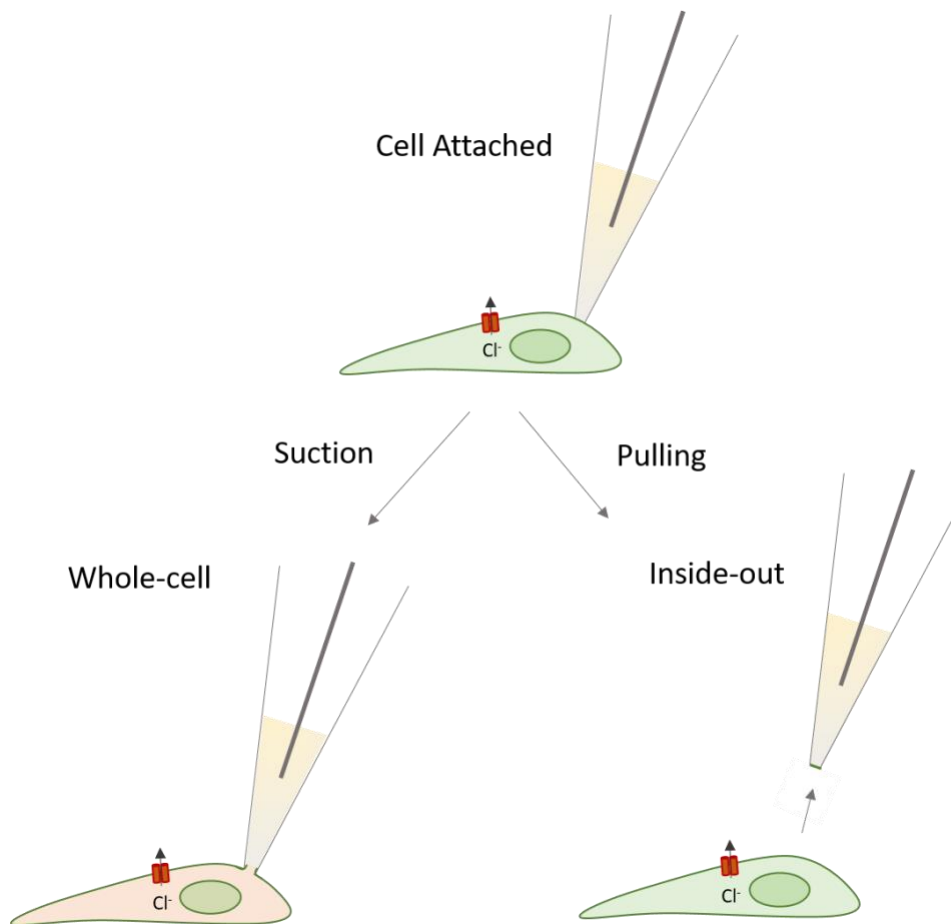


Figure 2.5.3 Diagrammatic representation of recording configurations in patch-clamp electrophysiology.

Schematic illustration of the configurations whole-cell and inside-out patch clamp configurations used in this thesis. In the whole-cell mode, the solution present in the pipette is in contact with the intracellular solution. In the inside-out mode, the pipette tip is used to pull part of the cellular membrane so that the intracellular side is exposed.

2.5.3 Perfusion system

Some experiments required the cell or excised patch to be exposed to various modulators. The exchange of solutions was achieved by using a gravity-driven local perfusion system consisting of eight tubes of 1.2 mm diameter. The perfusion system was then lowered into the bath solution, and the cell or excised patch attached to the tip of the patch pipette moved in front of a tube. The change of solution was achieved via manually moving the tubes.

2.5.4 Stimulation protocols

2.5.4.1 Current *versus* voltage relationship (IV-Ramp)

IV-Ramp protocol consisted of gradual changes in V_m from -100 mV and + 100 mV obtained during a 1 s intervals. Ramps were elicited every 1 s from a holding a holding potential of 0 mV.

2.5.4.2 Current *versus* voltage relationships (IV-CaCC)

IV-CaCC protocol consisted of 1s steps ranging from -100 mV to + 100 mV in 20 mV increments wach followed by a step of -60 mV. Pulses were elicited every 2 s from a holding potential of 0 mV. The peak current was measured at each potential, divided by the cell capacitance (C_m) and plotted *versus* V_m .

2.5.4.3 Current *versus* ligand relationship (IV-Steps)

IV-Steps protocol consisted of 1.5 s steps from 0 to + 70 mV for 1.5 s followed by -70 mV step for 1 s before returning to 0 mV. The steady-state current measured at increasing concentration of the ligand was normalised for the current measured in the absence of the ligand (I/I_0) and plotted *versus* the ligand concentration. The dose-response curve was fitted with the Hill equation where K_d is the apparent dissociation constant and h is the Hill coefficient:

$$\frac{I}{I_{\text{ligand}}} = \frac{1}{1 + \left(\frac{[\text{ligand}]}{K_d}\right)^h} \quad \text{Equation 13}$$

2.5.4.4 Current versus ligand relationship (IV-Tail)

IV-Tail protocol consisted of 1 s steps from -100 to +140 mV in 40 mV increments (test pulse). Each test pulse was preceded every 2 s by a pre-pulse of +70 mV with a holding potential of 0 mV. Steady-state currents were measured at the end of the test pulse and normalised to the pre-test pulse at +70 mV.

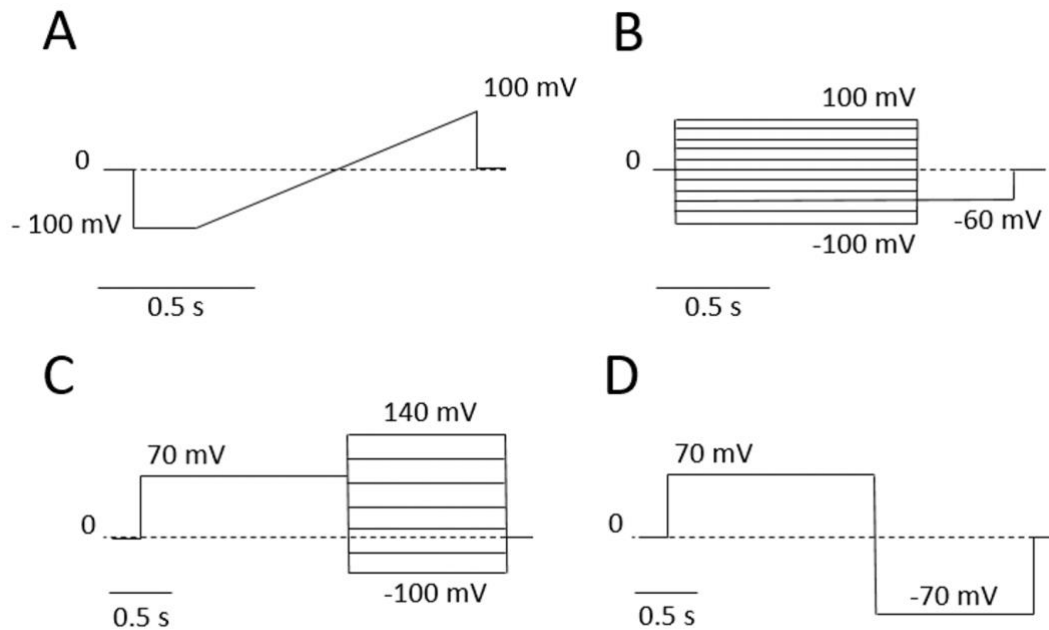


Figure 2.5.4 Voltage stimulation protocols for patch-clamp electrophysiology recordings.

(A) IV-Ramp voltage protocol, (B) IV-CaCC voltage protocol, (C) IV-Tail protocol and (D) IV-Steps protocol. Dashed lines indicate 0 mV.

2.5.5 Solutions for electrophysiology

Electrophysiological solutions were designed to isolate the I_{CaCC} elicited by the TMEM16A and TMEM16B channels. In order to prevent K^+ currents, Cs^+ was used to replace K^+ . Free intracellular Ca^{2+} ($[Ca^{2+}]_i$) was controlled by EGTA or HEDTA. These two different chelators have different affinities for Ca^{2+} and were used to obtain different concentrations of $[Ca^{2+}]_i$ (McGuigan and Stumpff 2013). The individual compositions of intracellular and extracellular

solutions are reported in Table 6, Table 7 and Table 8. The concentration of free $[Ca^{2+}]_i$ in intracellular solution was calculated using Patcher's Power tool (Dr Mendez and Dr Wurriehausen, Max-Planck Institute).

Table 6 Extracellular solution for measurement of I_{CaCC} (ECS)

Compounds	Concentration (mM)
NaCl	150
D-mannitol	10
D-glucose	10
HEPES	10
MgCl ₂	1
pH to 7.4 with NaOH	

Table 7 Intracellular solution for measurement of I_{CaCC} (ICS)

Compounds	Concentration (mM)
CsCl	130
EDTA or HEDTA	10
HEPES	10
CaCl ₂	See Table 8
MgCl ₂	1
pH to 7.3 with NaOH	

Table 8 Ca^{2+} for intracellular solution for measurement of I_{CaCC}

Free $[Ca^{2+}]_i$ (μM)	Concentration (mM)	Chelator
0	-	EGTA
0.056	4.5	EGTA
0.103	6	EGTA
0.206	7.5	EGTA
0.274	8	EGTA
0.605	2.1	HEDTA
1.04	3.1	HEDTA
2.27	4.8	HEDTA
12.46	7.8	HEDTA
78.07	9	HEDTA

Table 9 Low EGTA intracellular solution for measurement of I_{CaCC}

Compounds	Concentration (mM)
CsCl	130
EGTA	1.5
HEPES	10
CaCl ₂	1
MgCl ₂	1
pH to 7.3 with NaOH	

2.5.6 Noise analysis

In the macroscopic steady state current, there is a population of individual channels opening and closing in random order. In this way, the mean current level fluctuates creating noise. Noise analysis is a method that allows to identify the single channel conductance (i), the open probability (P_o) of a channel and the numbers on channels (N) in a cell. These values can be determined by assessing the mean and variance of the steady state current (Hille 2001).

For non-stationary noise analysis, a voltage step protocol of 3 s at 70 mV was applied repeatedly every 2 s to allow each steps to start in the same condition (Heinemann and Conti 1992, Tammaro and Ashcroft 2007). The mean current recorded at the start of each step ($I(t)$) was calculated as the sum of the currents elicited by each step at a time point derived by the number of steps

$$I(t) = \frac{1}{n} \sum_{k=1}^n I_k(t) \quad \text{Equation 14}$$

Where $I(t)$ is the mean current at the time t when each step starts, n is the number of steps, k is the step at time t , and $I_k(t)$ is the current amplitude elicited by the step at time t .

The variance at time t is the sum of squared difference between $I_k(t)$ and $I(t)$ divided by the number of steps

$$\sigma I(t) = \frac{1}{n} \sum_{k=1}^n (I_k(t) - I(t))^2 \quad \text{Equation 15}$$

The macroscopic current (I) can be determined through a number of identical and independent channels (N) by this product:

$$I = iNP_o \quad \text{Equation 16}$$

And the variance (σ^2) is:

$$\sigma^2 = Ni_2P_o(1-P_o) \quad \text{Equation 17}$$

where $(1-P_o)$ is the probability of the channels being closed. By combining the equations, values of I and σ^2 can be calculated using this equation:

$$\sigma^2 = iN - \frac{1}{N} \quad \text{Equation 18}$$

The values of I and σ^2 were calculated by equation 18. Background variance and current at 0 mV were subtracted. σ^2 versus I relationship was fitted with equation 18 which gives an estimation of i and N . Substitution of these values into equation 17 will result in P_o .

2.6 Wire myography

Myography from *myo* meaning muscle in Latin, can be used to measure or “graph” the isometric tension of isolated blood vessels. Isometric derives from Greek referring to equal “iso” and measuring “metria”. Myography involves two wires passing through the lumen of the vessel and connected to jaws that can be separated to induce a stretch in the artery ring (Mulvany and Halpern 1977). The tension is detected by a piezoelectric force transducer attached to one of the jaws (Figure 2.6.1). Piezoelectricity, derived from Greek “piezo” meaning squeeze or press and “electron” referring to an ancient source of electric charge, is the ability to generate electricity in response to applied pressure (Marino, Genchi et al. 2017).

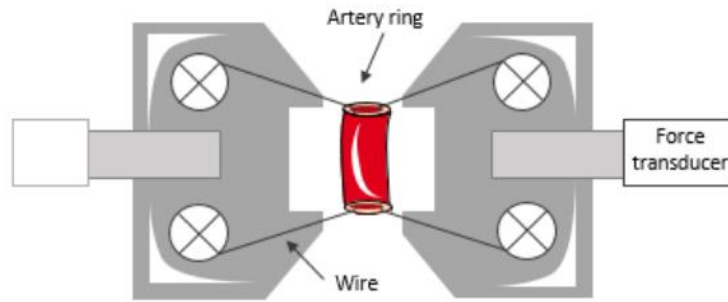


Figure 2.6.1 Diagrammatic representation of the wire myography set up

Schematic illustration of the set up for wire myography. The aortic or mesenteric ring is depicted in red, with two wires lined on each vessel wall. One arm of the myograph is connected to the force transducer to read changes in force as mN, while the other arm is a micrometre which enables to mechanically stretch the ring.

2.6.1 Wire myography experimental setup

The thoracic aorta was dissected immediately after cervical dislocation of control or *Npc1^{-/-}* mice. It was then cleaned from all perivascular fat and connective tissue in ice-cold PSS. For the mesenteric artery, the entire mesenteric bed was dissected and placed in ice-cold PSS. Third-order branches of the superior mesenteric artery were then dissected and cleaned from all perivascular fat and connective tissue in ice-cold PSS. The aorta or mesenteric artery was then cut in 2 mm length rings. The aorta or mesenteric artery rings were mounted on the jaws of the wire myograph 410A system (Danish Myo Technology, Denmark) using a 40 μm or 25 μm gold-plated tungsten wire (Goodfellow, UK), respectively. One of the myograph jaws was connected to a micrometer that allowed manual adjustment of the distance between the two jaws. This allowed to control basal artery stretch. The other jaw was connected to a force transducer measuring the tension produced by the artery ring in response to stretch. The myograph chamber was split in two independent chambers of 5 ml which were maintained at 37°C.

2.6.2 Normalisation theory

The magnitude of contraction and sensitivity of a vessel to agonists varies depending on the extent of stretch applied to that vessel. It is therefore necessary to apply an equal amount of stretch to all vessels regardless of vessel length, animal sex or genotype so that vessel responses can be accurately compared with each other (Mulvany and Halpern 1977). The aim of the normalisation procedure was to identify the micro-meter reading, i.e. distance between the jaws, necessary to produce the internal circumference (IntCir) that the vessel would have if relaxed under 90 % of 100 mmHg transmural pressure (Mulvany and Halpern 1977), this was termed the IntCir₁₀₀.

Mesenteric arteries were set to an IntCir that would achieve a transmural pressure of 70 mmHg (IntCir₇₀) as mesenteric vascular bed experiences less pressure than the aorta. In order to normalise the amount of stretch applied to the vessel segments to the appropriate IntCir, a computer program was written with by Dr Paolo Tammaro and Dr Hannah Garnet which implemented the algorithm determined by Mulvany and Halpern (Mulvany and Halpern 1977) into the IGOR (Wavemetrics, USA) platform. This programme was termed the normalisation procedure script. The normalisation procedure script is underpinned by the LaPlace law:

$$T = P_i \times \frac{IntCir}{2\pi} \quad \text{Equation 19}$$

Where P_i is the effective pressure for each vessel segment and T is the tension as force (in mN) divided by the vessel length x2 (in mm). The P_i is an estimate of the pressure needed to stretch the vessel to the measured IntCir₁₀₀.

2.6.3 Normalisation procedure

To acclimatise the artery rings to the wire myograph, ice-cold PSS was replaced with PSS warmed to 37 °C immediately after mounting and vessels left to stabilise for ~30 min. The stretch of the vessel was then increased step-wise by increasing the distance between the myograph jaws in 100 µm or 50 µm increments for the aorta or mesenteric artery, respectively. The normalisation procedure script takes the jaw measurement and tension values at each step as inputs, alongside the vessel length and wire thickness to calculate the jaw measurement that must be applied to create the desired transmural pressure, which is at 90 % of measured IntCir_{100} for the aorta. The normalisation procedure was designed by Dr Paolo Tamaro in WaveMetrics, USA. The program calculates the internal circumference of the vessel over the range of measurements in response to mechanical stretch. These values were plotted *versus* the tension and fitted with an exponential curve. For aortic rings, the internal circumference was set at 100 mmHg and for mesenteric arteries at 70 mmHg. The program then uses these values and the thickness of the wire 40 µm and 25 µm respectively for aortic and mesenteric rings, to calculate the desired transmural pressure.

2.6.4 Wire myography experimental design

Isometric tension measurements were recorded using an AD/DA converter (USB-6221, National Instruments, UK) and Chart v5 (Strathclyde University, UK) software. All experiments were performed at 37 °C. Functional viability of vessels was assessed after normalisation by ensuring the contractile response to KCl (55 mM) remained consistent over three repeats. Each KCl treatment lasted 6 min in length. Between additions vessel tension was relaxed back to baseline by washing with PSS pre-warmed to 37 °C. All data was normalised to percentage change from maximum PE-induced constriction to allow for variation in overall contractile force.

2.6.5 Wire myography solutions

Isolated aortic or mesenteric rings were dissected, stored on ice, and studied in PSS using wire myography, Table 10. Vessels were pre-constricted with PSS in which the K^+ concentration had been raised to 50 mM by equimolar substitution of NaCl with KCl (High K^+ PSS) (Table 11). The contractile response is presented as relative to the K^+ PSS (50 mM) re-tone. In experiments where the contribution of chloride channels was studied, low $[Cl^-]_o$ PSS was used. In these experiments $[NaCl]$ was reduced in PSS and replaced with equimolar Na-methanesulfonate (Na-MES), Table 12. This was used to maintain the $[Na^+]$ without affecting the permeability of TMEM16A as MES is impermeant. For the K^+ dose response experiments, K-MES was used to increase the $[K^+]$ (Table 13).

Table 10 Physiological salt solution (PSS)

Compounds	Concentration (mM)
NaCl	122
KCl	5
HEPES	10
KH_2PO_4	0.5
Na_2PO_4	0.5
$MgCl_2$	1
D-Glucose	11
$CaCl_2$	1.8
pH to 7.4 with NaOH	

Table 11 High K^+ physiological salt solution (PSS)

Compounds	Concentration (mM)
NaCl	72
KCl	55
HEPES	10
KH_2PO_4	0.5
NaH_2PO_4	0.5
$MgCl_2$	1
D-Glucose	11
$CaCl_2$	1.8
pH to 7.4 with NaOH	

Table 12 Low Cl physiological salt solution (PSS)

Compounds	Concentration (mM)
NaCl	22
KCl	5
HEPES	10
KH ₂ PO ₄	0.5
NaH ₂ PO ₄	0.5
MgCl ₂	1
D-Glucose	11
CaCl ₂	1.8
Na-MES	100
pH to 7.4 with NaOH	

Table 13 K-MES physiological salt solution (PSS)

Compounds	Concentration (mM)
NaCl	22
KCl	1
HEPES	10
KH ₂ PO ₄	0.5
Na ₂ PO ₄	0.5
MgCl ₂	1
D-Glucose	11
CaCl ₂	1.8
K-MES	See Table 14
pH to 7.4 with NaOH	

Table 14 K-MES MES physiological salt solution (PSS) for variable K-MES concentrations

K-MES (mM)	Concentration (mM)
1	0
10	9
30	29
70	69
100	99
Mannitol was added to obtain 285.4 mOsm	

2.6.6 [PE]-tension relationship analysis

Contractility of aortic rings was measured in response to increasing doses of PE. Dose response data was based on cumulative additions of the drug (diluted in PSS) to the bath solution. TMEM16A modulators, such as Ani9, were pre-incubated with the aortic rings for 25 min prior to adding the first dose of PE. Data was normalised to the third KCl (50 mM) contractile response to allow for variation in overall contractile force. Each KCl (50 mM) treatment lasted for 6 min, after which the vessel was washed with PSS until the tension relaxed back to baseline. The tension *versus* [PE] relationship was collected for each set of experiments and fitted to the Hill Equation as following:

$$T = \frac{T_{max}}{1 + \left(\frac{[PE]}{EC_{50}}\right)^h} \quad \text{Equation 20}$$

where the T_{max} is the maximal force reached, [PE] is the concentration of phenylephrine, EC_{50} is the effective concentration producing 50% of the maximal response and h is the Hill coefficient.

2.7 Cortical slices preparation

Cortical slices (300 μ m-thick) were prepared for immunostaining and cell death experiments on a Leica VT1200S vibratome in ice-cold, oxygenated (95% O₂/5% CO₂) slicing solution (Hall, Reynell et al. 2014). The slicing solution is described in Table 15.

The slices were incubated at 37°C in the slicing solution (20 min), and then transferred into a modified solution at room temperature in which the N-methyl-D-glucamine chloride, MgCl₂, CaCl₂ and Na ascorbate were replaced by (in mM) 92 NaCl, 1 MgCl₂ 2 CaCl₂ and 1 Na-ascorbate. Experiments involving cortical slices were performed within 3-4 hrs of sacrificing mice.

Table 15 Slicing solution for cortical slices

Compounds	Concentration (mM)
N-methyl-D-glucamine Cl	93
KCl	2.5
NaHCO ₃	3
MgCl ₂	10
NaH ₂ PO ₄	1.2
D-Glucose	25
CaCl ₂	0.5
HEPES	20
Na-ascorbate	5
Na-pyruvate	3
Kynurenic acid	1
pH to 7.4 with NaOH	

2.8 Imaging

2.8.1 Immunocytochemistry & Immunocytochemistry

Immunofluorescence staining was carried out using the (i) CHO WT, (ii) CHO *Npc1*^{-/-}, and (iii) HEK-293T cell lines. Cells were plated at a density of approximately 10,000 cells/cm² on glass coverslips and were allowed to grow for ~24 hrs prior to staining. Before fixation, cells were washed three times with cold PBS (Gibco, UK) and fixed in 4% paraformaldehyde in PBS for 20 min. After fixation, cells were washed twice with cold PBS. For staining of intracellular components, cells were permeabilised with 0.2% (v/v) Triton-X-100 (Merck, UK) in PBS for 5 min. Following this, cells were washed with cold PBS and then blocked with 1% bovine albumin serum (BSA) in PBS for 30 min at room temperature. Coverslips were then incubated in PBS containing 1% BSA with the primary antibodies (Table 16) for 1 h at room temperature. Coverslips were then washed three times with PBS and stained with appropriate secondary antibodies for 1 h at room temperature. Following this, coverslips were washed three times with PBS and then nuclei were stained with 4',6-diamidino-2-phenylindole (DAPI) in PBS for

5 min at room temperature. Coverslips were then washed three times with double distilled water before being mounted onto microscope slides using a drop of Vectashield mounting medium (Vector Laboratories, USA) and sealed with generic nail varnish. The microscope slides were stored in the dark at 4 °C until imaged.

Table 16 Antibodies and dyes used for live and fixed staining

Antibodies or Dyes	Origin
Anti-KDEL	Ab12223
Anti-LAMP1	Ab25245
Anti-HA	H6908
Ani-NPC1	Sc-271335
Anti-NG2	AB5320
Anti-IB4	I32450
Anti-ANO10	HPA051569
Anti-16A	Ab53212
Anti-Ano6	HPA038958
Anti-TMEM16B	Ab91573
Anti-PIP ₂	Sc-53412
Anti-PI	81845
Filipin	F9765
Dil	D3911

2.8.2 Live Imaging

Stable cell lines were grown on sterile glass petri dishes. Before imaging, cells were transfected with 800 ng of a genetic encoded probe for PIP₂, PH-PLC δ . After 16-24h from transfection, cells were washed twice for 5 min with ECS at room temperature. Cells were then incubated with the plasma membrane marker Dil (1:100) for 5 min at 37 °C. Before imaging, cells were then washed twice for 5 min with ECS at room temperature to get rid of excessive dye. Cells were excited with a 405 nm laser at room temperature.

2.8.3 Calcium imaging

Cells were washed with recording media and incubated with 1 μ M of Fluo-4 (F14201) at room temperature for 30 min in the dark. After the incubation, cells were washed with the recording medium (Table 17) and were then excited with a 470 nm laser. Images were acquired at room temperature. Changes in Fluo-4 fluorescence were measured by drawing regions of interest (ROIs) over the soma of cells in FIJI and by normalizing each intensity value to the baseline average (F/F_0).

Table 17 Calcium imaging recording medium

Compounds	Concentration (mM)
KCl	5
NaCl	140
D-Glucose	10
NaH ₂ PO ₄	1
MgCl ₂	1
CaCl ₂	2
Ascorbate	1
pH to 7.4 with NaOH	

2.8.4 Cortical slice capillary pericyte imaging

Acute cerebral cortical slices were perfused at a rate of 5 ml/min with heated (~34 °C) artificial cerebrospinal fluid (aCSF) solution described in Table 18. The aCSF was gassed with 20% O₂, 5% CO₂, 75% N₂. The oxygen- and glucose- deprived (OGD) aCSF solution was obtained by replacing glucose with 7 mM sucrose and by equilibrating the solution with 5% CO₂ and 95% N₂. Endothelin-1 (ET-1) was applied following a 5-min baseline.

For ischaemia pericyte death experiments, cortical slices were prepared from Sprague Dawley rats as described above (Section 2.7). Slices were transferred into conical flasks under OGD or control (aCSF) conditions in the absence or presence of Ani9. The solutions were

supplemented with 7.5 μ M of the necrosis marker propidium iodide and kept in the dark for the entire duration of the experiment. After the 1 hr incubation, the slices were swiftly washed 3 times (using the above incubation solutions in the absence of propidium iodide, prior to transfer to 12-well plates for fixation in 4% paraformaldehyde for 1 hr on a rocking shaker. Following 3 washes in PBS, slices were incubated in 10 μ g/ml IB4 in blocking buffer (10% (vol/vol) horse serum, 0.3% (vol/vol) Triton X-100, 1.5% (wt/vol) glycine and 1% (wt/vol) bovine serum albumin in PBS) overnight at 4°C on a shaker. Slices were then washed 3 times in PBS before incubation with the nuclear stain DAPI in PBS on a shaker at room temperature for 1 hr. Following 3 washes in PBS, slices were mounted on microscope slides in ProLong™ Glass Antifade Mountant before imaging.

Table 18 Artificial cerebrospinal fluid (aCSF) solution

Compounds	Concentration (mM)
KCl	2.5
NaCl	124
D-Glucose	10
HEPES	10
MgCl ₂	1
CaCl ₂	2
pH to 7.4 with NaOH	

2.9 Imaging analysis

Imaging analysis was performed by the LSM510 META confocal laser scanning system (Zeiss, UK) connected to an inverted AxioVert 200 microscope with a \times 63 objective (Zeiss, UK), controlled by Zen 2012 (Blue edition) software (Zeiss, UK)

ImageJ was used to analyse images collected. Co-localisation studies were performed with a 60x oil-immersion objective. Co-localisation was assessed by quantitatively determining the Manders' overlap coefficient (MOC) and Pearson's correlation coefficient (PCC) using Fiji

software with the Coloc2 plugin (Costes, Daelemans et al. 2004, Dunn, Kamocka et al. 2011). Two different MOCs were obtained (M1 and M2), which quantify the independent contributions of two selected channels to the pixels of interest. MOCs represents the fractions of a marker present in the other. PCCs were also calculated as a measure of pixel-by-pixel cross-correlation coefficients. MOC and PCC values range from 0 (no correlation) to 1 (complete overlap).

For analysis of pericytes in brain slices, Z-stacks (xyz dimensions 292 μm x 292 μm x 10 μm) were used with a 20x objective at 1 μm z-step size in layer IV starting at a depth of 20-30 μm from the surface of the slice to exclude cells damaged by slicing. Pericytes were identified as being embedded in the IB4-labeled capillary basement membrane with a bump-on-a-log morphology. The fraction of dead pericytes was obtained by dividing the number of propidium iodide -containing pericytes by the total number of pericytes counted using the Cell Counter plugin in FIJI. Imaging was performed in 2-4 slices and 3-4 regions per slice for each animal.

2.10 Data & statistical analysis

Electrophysiological data was analysed using ANA (Dr M. Pusch, CNR, Italy) or IGOR (Wavemetrics, USA). Myography data was analysed using IGOR. ImageJ (National Institutes of Health, USA) and Graph-Pad Prism 9 (GraphPad Software Inc., CA, USA) were used for analysis of imaging data. D'Agostino-Pearson omnibus test was used to assess the normality of data. For non-normally distributed data, a non-parametric statistical analysis was performed using the Mann-Whitney U Test (comparing 2 groups, unpaired), the Wilcoxon test with continuity correction (comparing 2 groups, paired) or the Kruskal-Wallis test with Dunn's post hoc test (comparing > 2 groups). For normally distributed data, two-tailed Student's t-test (comparing 2 groups) or one-way ANOVA (comparing > 2 groups). To reduce the probability of a false positive or Type I Error, Bonferroni's *post-hoc* test was used for statistical analysis as appropriate. Data are presented as mean \pm SEM alongside the number of experiments (n) and number of animals (N), where appropriate. Differences were considered significant if $p <$

0.05 and all tests were 2-tailed. Graphs were plotted using IGOR (Wavemetrics, USA) and images were finalized with CorelDraw (X8, Corel Corporation). BioRender.com and Microsoft Power Point were used for creating diagrammatic representations.

2.10.1 Experimental design

This project involved the use of mice for cell and tissue studies. The use of human samples was not possible due to low availability of samples from patients with NPC disease. The use of freshly isolated VSMCs from arteries was necessary as cultured cells may have remodelled expression of the various ion channels. Rodents (mice or rats) were used because they represent a well-established model for cardiovascular physiology, thus enabling comparison of my results with those already published in the literature. Rodents share physiological and biochemical properties with humans; thus, the observations made using this model provides insight into human physiology and biochemistry.

2.10.2 Randomisation

Randomisation was carried out as effectively as possible throughout this thesis. In experiments involving transfection, transfected cells were identified using anti-CD8 beads, and then selected at random for patch-clamp electrophysiology. Patch-clamp electrophysiology experiments using native cells also relied on cells being selected at random. For myography experiments, the thoracic aorta was dissected and then freshly isolated aortic rings were chosen at random for experimentation. In experiments using two or more different treatments, randomisation was achieved by changing the order of application of the agents. For electrophysiological experiments, each cell was obtained from a petri dish containing cells that were independently passaged and transfected. Thus, recording obtained from individual cells were considered as independent observations. Furthermore, automated analysis procedures for an objective method of analysis (e.g. count of vesicles number per cell, measurements of current amplitude or capillary diameter), were used for each group when possible. The

methods of analysis were established during study design and prior to the execution of the experiments.

2.10.3 Operator blinding

Blinding is a useful approach in the collection and analysis of data that could involve a bias in the collection of data, or a degree of qualitative interpretation of the results. Objective methods of analysis, such as automated analysis procedures were used for each experiment type, with methods of analysis devised prior to execution of the experiment. Myography experiments could not be blinded as for most experiments both myography chambers contained aortic rings obtained from either wild-type or mutant mice were obtained from a colony managed by the operator. Mice were randomly assigned to treatment groups and the drugs coded and the staff blinded to treatment. Automated analysis of tension at selected time points ensured no user bias during data analysis occurred. Objective methods of analysis, such as automated analysis procedures (e.g. curve fitting) built in the Igor analysis platform (Wavemetrics, USA), were used for each group. This overall approach removed the possibility that differential assessment of experimental results could potentially result in bias during the study.

2.11 Contribution to work

Unless otherwise state, all experiments in this thesis were designed by Lara Scofano and Dr Paolo Tammaro. Experiments were executed and analysed by Lara Scofano. Dr Kathryn Acheson contributed to the collection data for figure 4.1.2. Dr Rumaita Al Hosni contributed to the collection of data for figure 4.2.1 and 5.3.2. Dr Zeki Ilkan contributed to the collection of data for figure 5.3.3. I also would like to thank Zuzanna Borawska, whom I supervised during her final year undergraduate project, for her contribution to figure 4.3.4.

Chapter 3

TMEM16A characterisation

3.1 Functional and cellular properties of TMEM16 channels

This project began by investigating the TMEM16A current (I_{CaCC}) in a heterologous expression system (HEK-293T cells). Specifically, the Ca^{2+} and V_m sensitivity of the channel and response to pharmacological modulators were studied and compared with that of other TMEM16x members (TMEM16B, TMEM16F and TMEM16K) that are also expressed in VSMCs, as outlined in greater detail in the Introduction (Section 1.3.3) (Davis et al., 2010; Manoury, Tamuleviciute, & Tammara, 2010). This characterisation enabled comparison of cloned TMEM16A mediated currents with I_{CaCC} measured in isolated aortic VSMCs (described in Chapter 5, Section 5.1.1).

The pharmacological agents used were (i) Ani9 (Seo, Lee et al. 2016), (ii) a series of novel blockers developed by Autifony Therapeutics (AUT11813 and AUT11814), and (iii) a small molecule activator provided by Autifony Therapeutics (AUT11817). This chapter provides a detailed characterisation of the function and pharmacological properties of the TMEM16A channel, and thus enabled me to identify the appropriate experimental conditions for the recording of I_{CaCC} in heterologous systems (Chapter 4) and in freshly isolated VSMCs and native systems (Chapter 5).

3.2 Electrophysiological profile of TMEM16A

Whole-cell TMEM16A currents were recorded from transfected HEK-293T cells with an intracellular pipette solution containing 0, 100, 300 or 600 nM free $[Ca^{2+}]_i$ (Figure 3.2.1). To examine whether the endogenous Cl^- current are elicited in HEK-293T cells, mock-transfected HEK-293T cells were whole-cell patch-clamped and stimulated with the “IV-CaCC” protocol. Figure 3.1 shows that currents elicited in the absence of $[Ca^{2+}]_i$ were comparable to the currents recorded from mock-transfected cells over membrane potentials ranging from -100 to +100 mV. When $[Ca^{2+}]_i$ was raised to 100 nM, I_{CaCC} was still negligible. This can be explained by the variety of Ca^{2+} sensitivity reported in different TMEM16A splice variants in the literature (Ni, Kuan et al. 2014), ranging from <100 nM (Yang, Cho et al. 2008) to > 2 μ M (Tien, Peters et al. 2014). In the presence of 300 nM $[Ca^{2+}]_i$, large outward and inward I_{CaCC} were observed in response to depolarising and hyperpolarising voltages, respectively. The instantaneous I_{CaCC} elicited in response to each voltage step increment in the “IV-CaCC” protocol, relaxed towards a time-dependent plateau that was reached at the new steady-state. The current amplitude was larger at positive V_m than at negative V_m of the same magnitude, indicating outward rectification in accordance with what has been observed in native I_{CaCC} (Hartzell, Yu et al. 2009, Davis, Forrest et al. 2010). At +100 mV cells expressing TMEM16A elicited an I_{CaCC} of 312.0 ± 08.1 pA/pF when dialysed with 300 nM free $[Ca^{2+}]_i$ and 601.2 ± 12.2 pA/pF when the intracellular pipette solution was increased to 600 nM free $[Ca^{2+}]_i$. The “IV-CaCC” stimulation also revealed the voltage dependency of TMEM16A-mediated I_{CaCC} . In fact, in the presence of 300 nM free $[Ca^{2+}]_i$, the I_{CaCC} was -15.06 ± 4.0 pA/pF at -60 mV and 316.0 ± 38.5 pA/pF at +100 mV. Overall, these data show the strong Ca^{2+} and V_m dependency of TMEM16A-mediated I_{CaCC} .

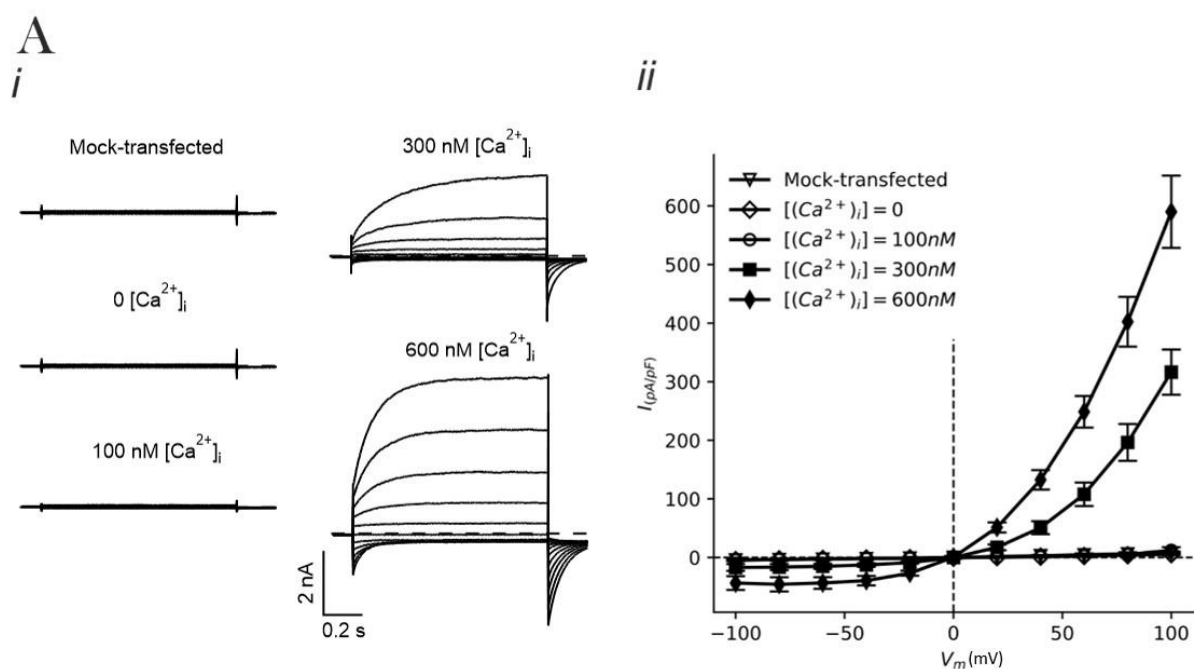


Figure 3.2.1 TMEM16A IV-relationship

(A) i) Whole-cell currents recorded from a mock-transfected HEK-293T cell or HEK-293T cell expressing TMEM16A dialysed with 0, 100, 300 or 600 nM $[Ca^{2+}]_i$ as indicated. Dashed horizontal line represents the zero-current level. Voltage protocol “IV-CaCC” is described in the Methods (Figure 2.5.4); ii) mean activating whole-cell current versus V_m relationships measured at the end of the 1 s voltage pulse from -100 to +100 mV in 20 mV increments in mock-transfected HEK-293T cells (n=6) or TMEM16A-expressing HEK-293T cells dialysed with 100 (n=8), 300 (n=9) or 600 nM (n=6) $[Ca^{2+}]_i$.

To identify the range of $[Ca^{2+}]_i$ in which TMEM16A channels are activated, $[Ca^{2+}]_i$ sensitivity was studied with the inside-out patch clamp configuration in CHO or HEK-293T cells. (Figure 3.2.2). The Ca^{2+} sensitivity of CHO cells expressing TMEM16A was compared to the one in HEK-293T cells. This is because a genetic cell line of CHO cells (knock-out for *Npc1* gene locus) was used in Chapter 4 to study TMEM16A modulation by NPC1 inhibition. In both cell lines, patches were excised from TMEM16A-transfected HEK-293T or CHO cells and held at +70 mV prior to exposure to solutions with various $[Ca^{2+}]_i$. The current was normalised to the average current elicited at the two highest $[Ca^{2+}]_i$ of 12 and 78 μM (I_{max}). I/I_{max} was plotted against $[Ca^{2+}]_i$ and fitted with the Hill equation (Equation 13). The EC_{50} was $0.7 \pm 0.1 \mu M$ in HEK-293T cells (n=15) and $0.8 \pm 0.0 \mu M$ in

CHO cells (n=7). The Hill coefficient was 1.63 ± 0.06 in HEK-293T cells (n=15) and 1.94 ± 0.27 μM in CHO cells (n=7). No significant difference was observed in the EC_{50} and Hill coefficient values between HEK-293T cells and CHO cells (Table 19).

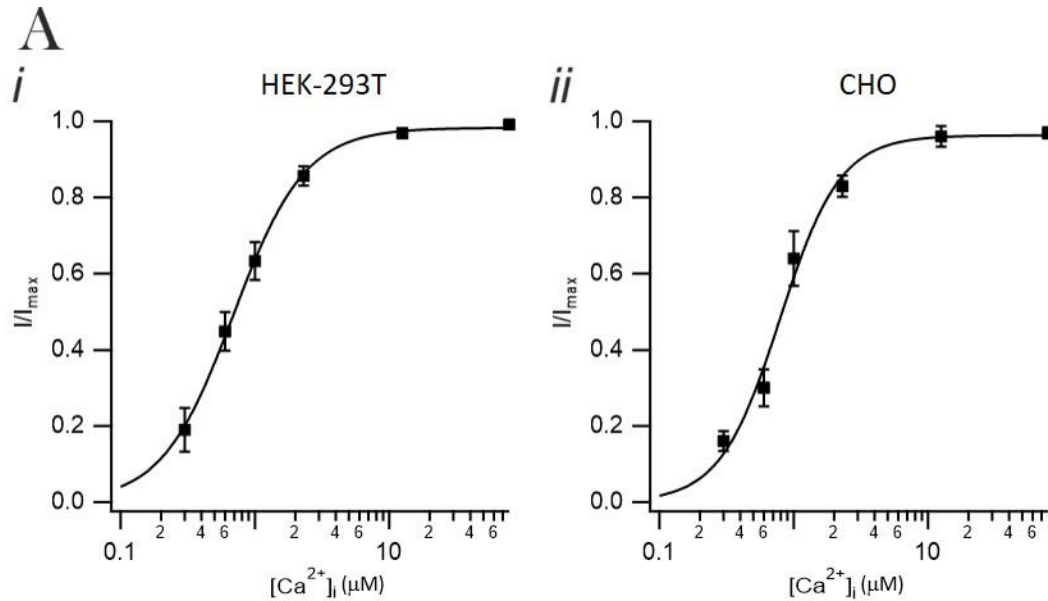


Figure 3.2.2 *TMEM16A* calcium-sensitivity.

TMEM16A currents were recorded at +70 mV from inside-out patches excised from i) HEK-293T cells (n=15) and ii) CHO cells (n=7). Mean current versus $[Ca^{2+}]_i$ relationship normalised to the current recorded in the two highest $[Ca^{2+}]_i$ was fitted using the Hill equation.

Cell lines	EC_{50} (μM)	max	h	N
HEK-293T	0.68 ± 0.01	0.98 ± 0.01	1.63 ± 0.06	15
CHO	0.78 ± 0.06	0.96 ± 0.03	1.94 ± 0.27	7

Table 19 Hill-fit parameters (EC_{50} , max and h) (Eq. 13) for HEK-293T and CHO cells.

Current versus $[Ca^{2+}]_i$ relationships obtained in HEK-293T and CHO cells.

3.3 Other TMEM16x family members expressed in the vasculature

3.3.1 Electrophysiological profile and cellular expression of TMEM16B

The next set of experiments aimed to characterise the current mediated by the other TMEM16x members (TMEM16B, TMEM16F and TMEM16K) for which expression in VSMCs has been reported (Davis, Forrest et al. 2010, Manoury, Tamuleviciute et al. 2010). TMEM16B was expressed in HEK-293T cells and the whole-cell I_{CaCC} was recorded in response to the “IV-CaCC” protocol. TMEM16B currents are less sensitive to $[Ca^{2+}]_i$ than TMEM16A currents (Adomaviciene, Smith, Garnett, & Tamaro, 2013). Thus, TMEM16B currents were measured in the presence of 600 nM $[Ca^{2+}]_i$ to obtain a degree of Ca^{2+} -dependent activation comparable to that observed for TMEM16A currents in 300 nM $[Ca^{2+}]_i$ (Adomaviciene, Smith et al. 2013). At +100 mV TMEM16A currents were 122 ± 6.0 pA/pF while TMEM16B currents were 62 ± 7.6 pA/pF. Both currents had a strong outwardly rectifying IV-relationship. To compare the activation kinetics of the I_{CaCC} recorded from cells expressing TMEM16A or TMEM16B, the activation time constant, $\tau_{1/2}$, was calculated at 60, 80 and 100 mV. The $\tau_{1/2}$ was calculated as the time taken to reach the half-maximal current. In cells expressing TMEM16A, $\tau_{1/2}$ increased with V_m resulting in a $\tau_{1/2}$ of 96.4 ± 1.4 pA/pF at +60 mV and 111.2 ± 2.5 pA/pF at +100 mV. In cells expressing TMEM16B, $\tau_{1/2}$ was ~ 2-fold faster than for TMEM16A channels (Figure 3.3.1).

To assess the subcellular localisation of TMEM16A and TMEM16B, HEK-293T cells expressing TMEM16A were fixed and stained with either the TMEM16A or TMEM16B antibody as described in more detail in the Method (Section 2.8.1). Nuclei were stained with DAPI. In accordance with the literature (Schreiber, Ousingsawat et al. 2020), I found that both the TMEM16A and TMEM16B channels were abundantly expressed at the plasma membrane (Figure 3.3.1).

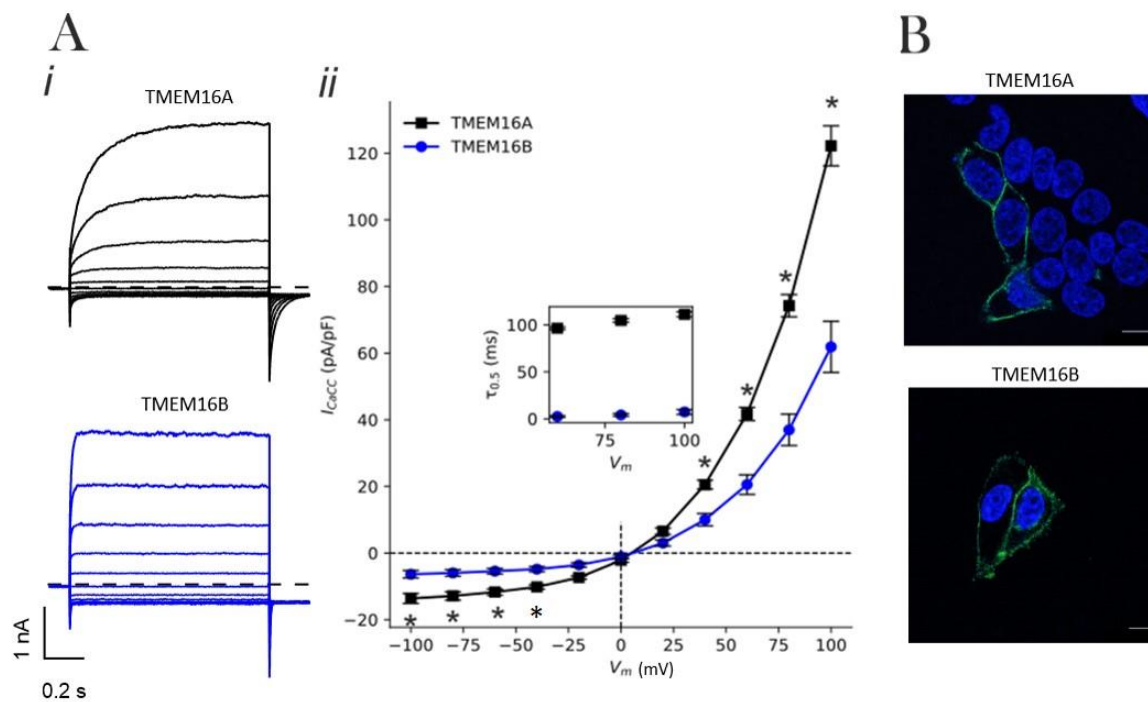


Figure 3.3.1 Properties of TMEM16A and TMEM16B IV-relationships.

(A) i) Whole-cell currents recorded from a TMEM16A or TMEM16B expressing HEK-293T cells, as indicated. $[Ca^{2+}]_i$ was 300 nM for TMEM16A and 600 nM for TMEM16B. Dashed horizontal line represents the zero-current level. Voltage protocol “IV-CaCC” is described in the Methods (Figure 2.5.4); ii) mean activating whole-cell current versus V_m relationships measured at the end of the 1 s voltage pulse from -100 to +100 mV in 20 mV increments in TMEM16A ($n=7$) or TMEM16B ($n=6$) transfected HEK-293T cells. Inset in (ii) shows mean $\tau_{1/2}$ of current activation for TMEM16A and TMEM16B, measured in the presence of 300 and 600 nM $[Ca^{2+}]_i$ respectively and at various membrane potentials ($n=7-8$). * indicates $p \leq 0.05$, unpaired t -test. (B) Representative confocal images of HEK-293T cells expressing TMEM16A or TMEM16B (green) and DAPI (blue). Scale bar = 10 μm .

3.3.2 Electrophysiological profile and cellular expression of TMEM16F

In addition to the TMEM16A and TMEM16B CaCC channels, the TMEM16x family includes the scramblase TMEM16F (Hartzell, Yu et al. 2009, Pedemonte and Galiotta 2014). The Cl⁻ TMEM16F current amplitude gradually increases from the point where whole cell configuration is established (Acheson, 2016; Hartzell, Yu, Xiao, Chien & Qu, 2009; Pedemonte & Galiotta, 2014). TMEM16F is reported to have very low affinity to [Ca²⁺]_i compared to TMEM16A and TMEM16B, thus it was studied in the presence of 78 μM [Ca²⁺]_i as previously established (Grubb, Poulsen et al. 2013, Scudieri, Caci et al. 2015). The “IV-CaCC” protocol was run every 2 minutes after achieving whole-cell (defined as t=0 minutes) in HEK-293T cells transiently expressing TMEM16F. TMEM16F current increased over time from the establishment of the whole-cell configuration, with full development of an outward-rectifying current at 10 minutes (Figure 3.4). From 6 minutes since the beginning of the experiments, large outward membrane currents were generated in response to depolarising voltages and large tail currents were observed when returning to hyperpolarising voltages in accordance with previous reports (Scudieri, Caci et al. 2015). At +100 mV, the TMEM16F increased from 31.4 ± 7.5 pA/pF at t=2, to 81.5 ± 7.9 pA/pF at t=6 and to 158.8 ± 17.6 pA/pF at t=10 (Figure 3.3.2). To assess subcellular localisation of TMEM16F compared to TMEM16A and TMEM16B-expressing HEK-293T cells, I performed immunofluorescence experiments in TMEM16F-expressing HEK-293T cells (Figure 3.3.2). I found that TMEM16F was distributed mainly at the plasma membrane, similarly to the TMEM16A and TMEM16B channels described above (Figure 3.3.1) and in line with to the literature (Scudieri, Caci et al. 2015).

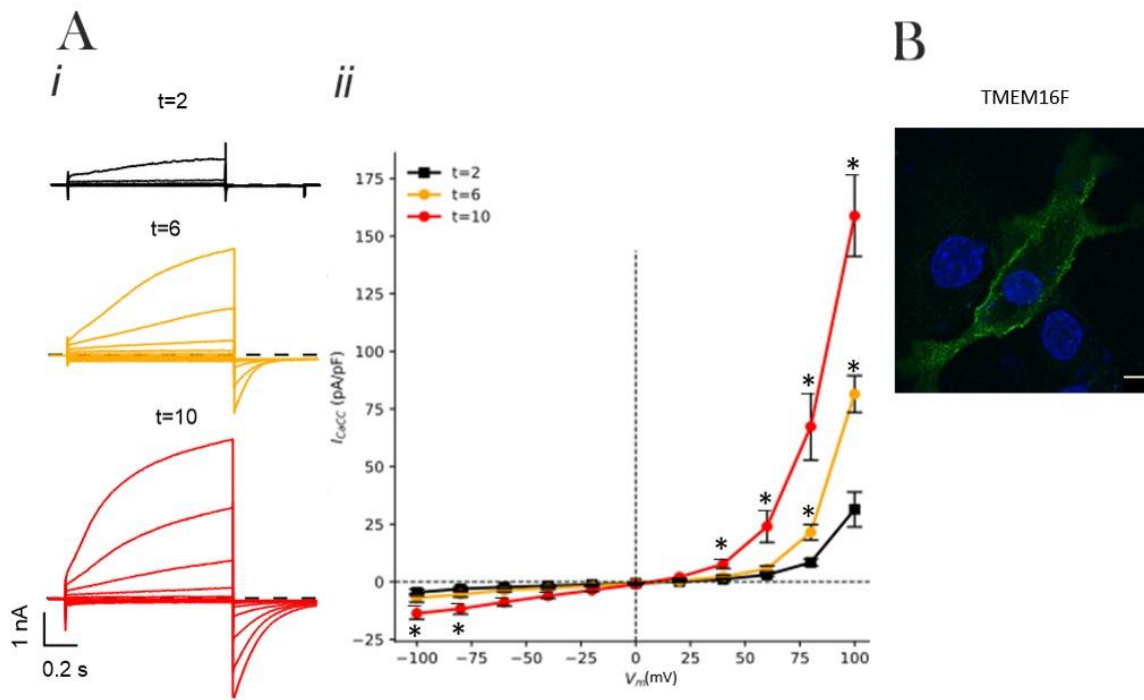


Figure 3.3.2 TMEM16F time-dependent current.

(A) i) Whole-cell currents recorded from a mock-transfected HEK-293T cell or HEK-293T cell expressing TMEM16F dialysed with $78 \mu\text{M} [\text{Ca}^{2+}]_i$ as indicated. Dashed horizontal line represents the zero-current level. Voltage protocol “IV-CaCC” is described in the Methods (Figure 2.5.4); ii) mean activating whole-cell current versus V_m relationships measured at the end of the 1 s voltage pulse from -100 to +100 mV in 20 mV increments in TMEM16F-expressing HEK-293T cells reordered at t=2 (n=11), t=6 (n=7) and t=10 (n=9). * indicates $p \leq 0.05$, unpaired t-test. (B) Representative confocal images of HEK-293T cells expressing TMEM16F and DAPI (blue). Scale bar = 10 μm .

3.3.3 Electrophysiological profile and cellular expression of TMEM16K

Among the ten members of the TMEM16x family, the electrophysiological properties and cellular localisation of TMEM16K was recently published by our group (Bushell, Pike et al. 2019). We first tested if TMEM16K could function at the plasma membrane as a CaCC like TMEM16A, TMEM16B and TMEM16F. Whole-cell currents were measured in the presence of either 300 nM or 78 μ M of $[Ca^{2+}]_i$. These $[Ca^{2+}]_i$ were selected as they are sufficient to elicit I_{CaCC} in cells expressing TMEM16A, TMEM16B or TMEM16F, respectively. However, the presence of 300 nM or 78 μ M of $[Ca^{2+}]_i$ did not activate any current in TMEM16K-expressing HEK-293T cells. In fact, similar currents were recorded in TMEM16K and mock-transfected cells. At +100 mV, the recorded I_{CaCC} in the presence of 300 nM $[Ca^{2+}]_i$ was 4.0 ± 0.6 pA/pF in cells expressing TMEM16K and 274.2 ± 33.9 pA/pF in TMEM16A-transfected cells. This suggested that TMEM16K does not form Ca^{2+} -activated channels at the plasma membrane. In high $[Ca^{2+}]_i$ of 78 μ M, the recorded I_{CaCC} was 28.1 ± 3.1 pA/pF in cells expressing TMEM16K and 135.2 ± 19.4 pA/pF in TMEM16F-transfected cells. The absence of membrane current, led us to hypothesise that TMEM16K is localised intracellularly. Thus, I next studied TMEM16K cellular localisation using immunocytochemistry. In accordance with the patch-clamp experiments, I observed no TMEM16K localisation at the plasma membrane. Endogenous TMEM16K was stained with TMEM16K antibody in human bone osteosarcoma epithelial (U2OS) cells (Figure 3.3.3). These cells were also stained with the ER marker KDEL and nuclei marker DAPI. The correlation coefficients (Pearson's, M1 and M2), described more in details in the Method section (2.9), were measured to assess the overlap of TMEM16K with the ER marker. Figure 3.3.3 shows that the correlations coefficients were 0.70 ± 0.0 , 0.79 ± 0.0 and 0.81 ± 0.0 for Pearson's, M1 and M2, respectively. These data indicate that TMEM16K is subcellularly localised in the ER.

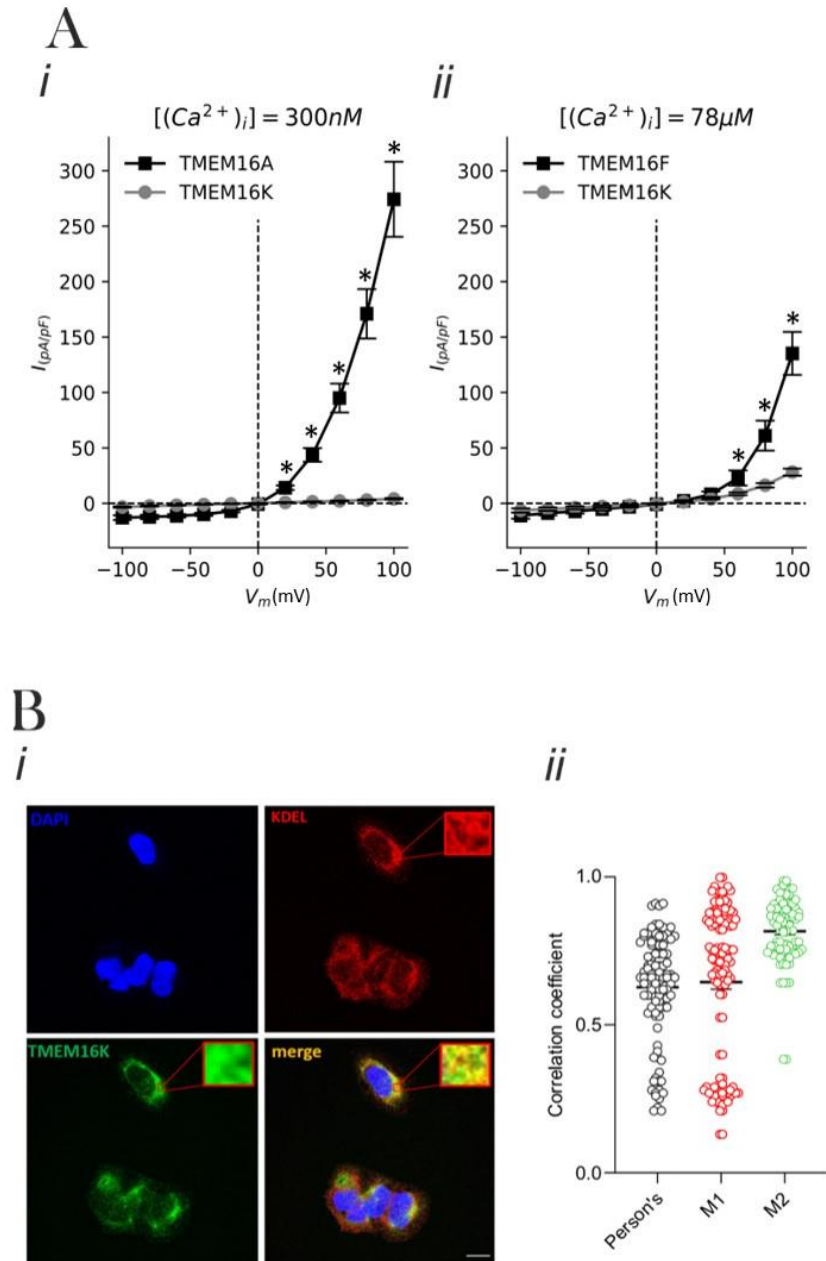


Figure 3.3.3 TMEM16K is an intracellular channel localised at the ER.

(A) *i*) Whole-cell current versus voltage relationships for HEK-293T cells expressing TMEM16A ($n = 13$) or TMEM16K ($n = 13$). $[Ca^{2+}]_i$ was $0.3 \mu M$; *ii*) Whole-cell current versus voltage relationships for HEK-293T cells expressing TMEM16F ($n = 17$) or TMEM16K ($n = 11$). $[Ca^{2+}]_i$ was $78 \mu M$. Dashed horizontal line represents the zero-current level. Voltage protocol “IV-CaCC” is described in the Methods (Figure 2.5.4) (B) *i*) Representative confocal images of U2OS cells stained using antibodies to endogenous TMEM16K (green), the ER resident protein signature KDEL (red), along with DAPI staining of nuclei and the merge. Insets show the degree of colocalisation of TMEM16A and KDEL (yellow). Scale bars = $10 \mu m$; *ii*) Quantitative analysis of TMEM16K and KDEL co-localisation in U2OS cells ($n=23-48$).

3.4 Pharmacology of TMEM16A channels

3.4.1 Ani9 is a selective TMEM16A inhibitor

Ani9 has been identified by Seo et al. as a potent inhibitor of TMEM16A, with an IC_{50} of 106 nM in Fischer rat thyroid cells stably expressing human TMEM16A (Seo, Lee et al. 2016). Here, we tested Ani9 in heterologously expressed TMEM16A channels in HEK-293T cells, since no previous reports of the potency of Ani9 in this cell system have been published to date. TMEM16A currents were recorded in response to the “IV-tail” protocol described in details in Methods (Section 2.5.4.4). TMEM16A currents were measured at the end of the test pulse, and normalised to the pre-pulse. Figure 3.4.1 shows that 2 μ M of Ani9 in the presence of 300 nM $[Ca^{2+}]_i$, was able to produce a near full block of the elicited TMEM16A current. Ani9 blocked the TMEM16A current at all the V_m tested. Moreover, the potency of Ani9 in the presence of high $[Ca^{2+}]_i$ was studied (n=6). Figure 3.4.1 shows that in the presence of high $[Ca^{2+}]_i$ (1 μ M), 3 μ M of Ani9 blocked the TMEM16A current less potently than in the presence of 300 nM $[Ca^{2+}]_i$, leaving a residual, unblocked, TMEM16A current of ~8 fold (n=6). These data indicates that the potency of Ani9 on the TMEM16A channel is Ca^{2+} -dependent.

The effect of Ani9 on the closely related family member TMEM16B was also studied in the HEK-293T expression system. Whole-cell TMEM16B currents were elicited in response to the “IV-tail” protocol in the presence of 600 nM $[Ca^{2+}]_i$. TMEM16B currents were measured at the end of the test pulse, and normalised to the pre-pulse measure in the absence of Ani9. There was no significance difference between TMEM16B current in the presence or absence of 3 μ M of Ani9 (n=4) (Figure 3.4.2). Therefore, it was confirmed in line with Seo et al. that Ani9 has no effect on TMEM16B (Seo et al. 2016).

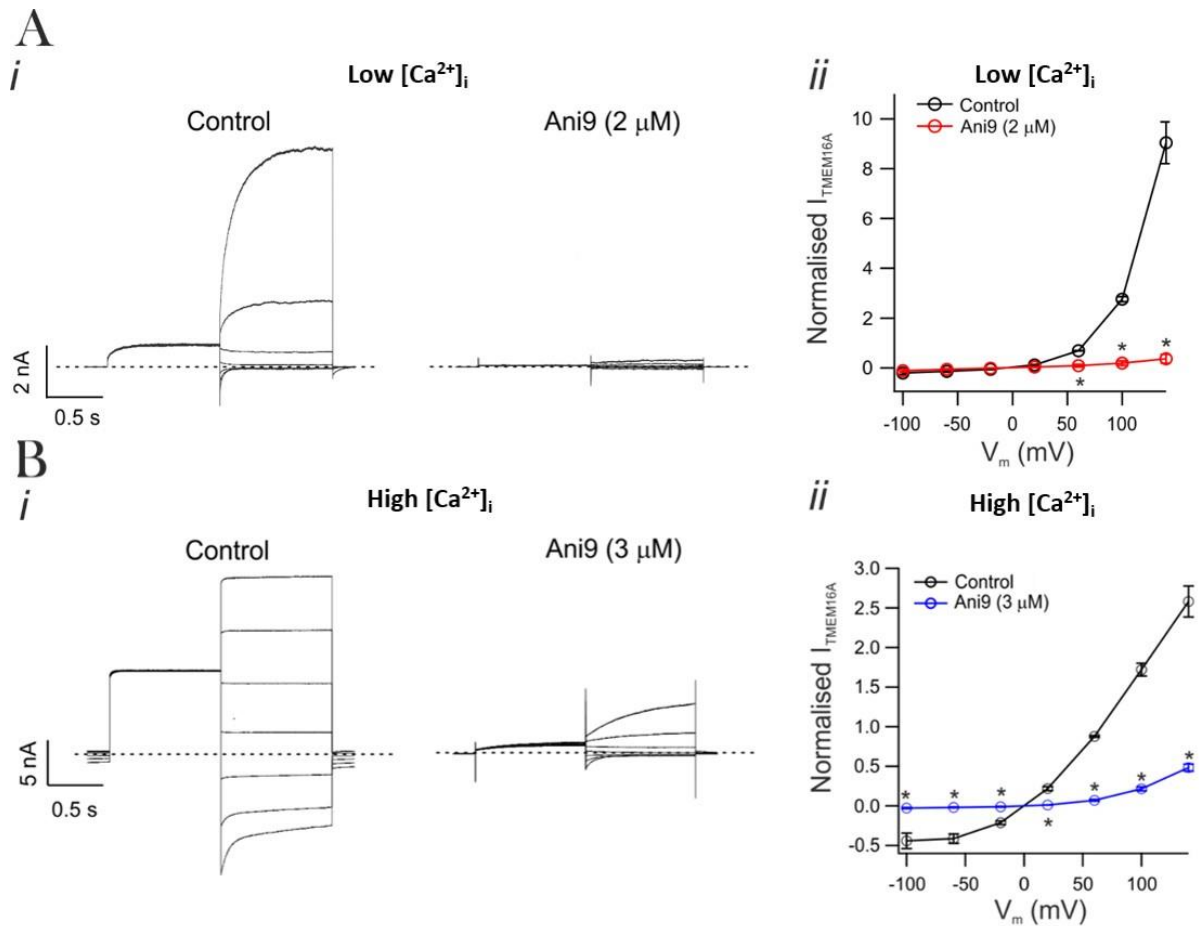


Figure 3.4.1 Effect of Ani9 on cloned TMEM16A currents

(A) *i*) Whole-cell currents recorded from a HEK-293T cell expressing TMEM16A dialysed with low $[Ca^{2+}]_i$ (300 nM) in the presence or absence of Ani9 (2 μM), as indicated. Dashed horizontal line represents the zero-current level. Voltage protocol “IV-tail” is described in the Methods (Figure 2.5.4); *ii*) mean activating whole-cell current versus V_m relationships measured at the end of test pulses from -100 mV to +140 mV and normalised to the end of the 1 s pre-pulse at +70 in TMEM16A-expressing HEK-293T cells reordered recorded in the presence or absence of Ani9 (3 μM) ($n=6$). (B) Whole-cell currents recorded from a HEK-293T cell expressing TMEM16A dialysed with high $[Ca^{2+}]_i$ (1 μM) in the presence or absence of Ani9 (3 μM), as indicated; *ii*) mean activating whole-cell current versus V_m relationships measured in TMEM16A-expressing HEK-293T cells reordered recorded in the presence or absence of Ani9 (3 μM) ($n=6$). * indicates $p \leq 0.05$, paired t-test.

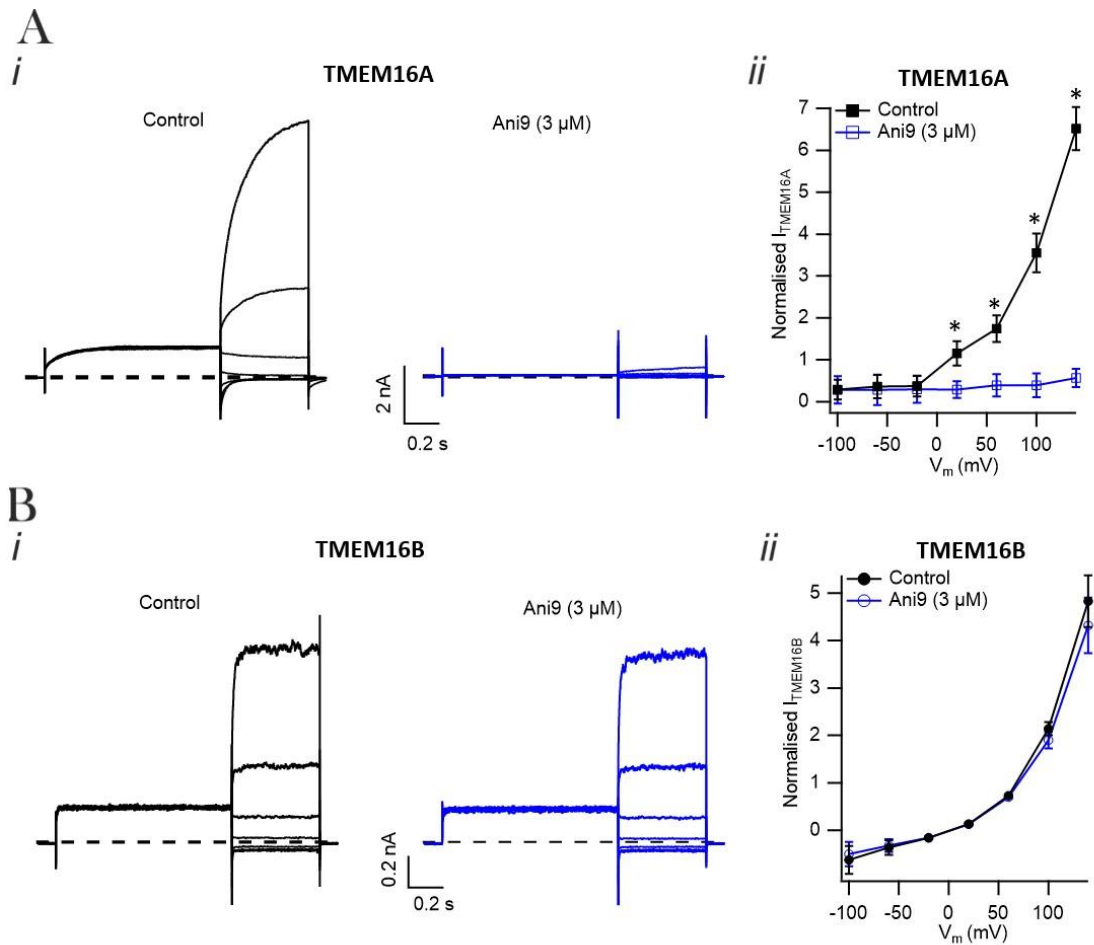


Figure 3.4.2 Effect of Ani9 on cloned TMEM16B currents

(A) *i*) Whole-cell currents recorded from a HEK-293T cell expressing TMEM16A dialysed with 300 nM $[Ca^{2+}]_i$ in the presence or absence of Ani9 (3 μ M), as indicated; *ii*) mean activating whole-cell current versus V_m relationships measured in TMEM16A-expressing HEK-293T cells reordered recorded in the presence or absence of Ani9 (3 μ M) ($n=4$). Dashed horizontal line represents the zero-current level. Voltage protocol “IV-tail” is described in the Methods (Figure 2.5.4); (B) Whole-cell currents recorded from a HEK-293T cell expressing TMEM16B dialysed with 600 nM $[Ca^{2+}]_i$ in the presence or absence of Ani9 (3 μ M), as indicated; *ii*) mean activating whole-cell current versus V_m relationships measured in TMEM16B-expressing HEK-293T cells reordered recorded in the presence or absence of Ani9 (3 μ M) ($n=4$). * indicates $p \leq 0.05$, paired *t*-test.

3.4.2 AUT11813 and AUT11814 as TMEM16A inhibitors

Ani9 was confirmed to be a potent and selective inhibitor of TMEM16A (Figure 3.6 and Figure 3.7). In order to identify novel inhibitors of the TMEM16A currents, the effects of AUT11813 and AUT11814 were tested in heterologous TMEM16A system. Unpublished work from our lab showed that Ani9 is subjected to high first pass metabolism and may have poor BBB permeability. Thus, Ani9 may not be suitable for possible future *in vivo* studies. As part of my pharmacological characterisation, I have studied new compounds (AUT11813 and AUT11814) with improved pharmacokinetic characteristics. These compounds have been provided by Autifony Therapeutics. While the structure of these compounds was not made available to me because currently protected by intellectual patent rights, these new compounds may provide a valuable resource for possible future *in vivo* studies. Thus, I have characterised these compounds as part of my project.

The TMEM16A-mediated I_{CaCC} was studied using the whole-cell configuration of the patch-clamping technique. TMEM16A-transfected HEK-293T cells were perfused with increasing concentrations from 0.3 to 10 μM of AUT11813 or AUT11814 compounds. Following the application of the compounds, cell was washed by perfusing with ECS between each concentration to allow the current to return to baseline levels. At the end of the experiment, the cell was perfused with high concentration of Ani9 (3 μM) in order to subtract cell leakage. Both compounds blocked the TMEM16A currents in HEK-293T cells (Figure 3.4.3). Their effects were tested in response to increasing concentrations from 0.3 to 10 μM . The IC_{50} were $1.4 \pm 0.6 \mu\text{M}$ and $0.8 \pm 0.2 \mu\text{M}$ for AUT11813 and AUT11814, respectively (Table 20). In response to the maximal concentration of 10 μM , the maximum inhibition was $70 \pm 0.0 \%$ (n=8) for AUT11813 and $99 \pm 0.0 \%$ (n=3) for AUT11814.

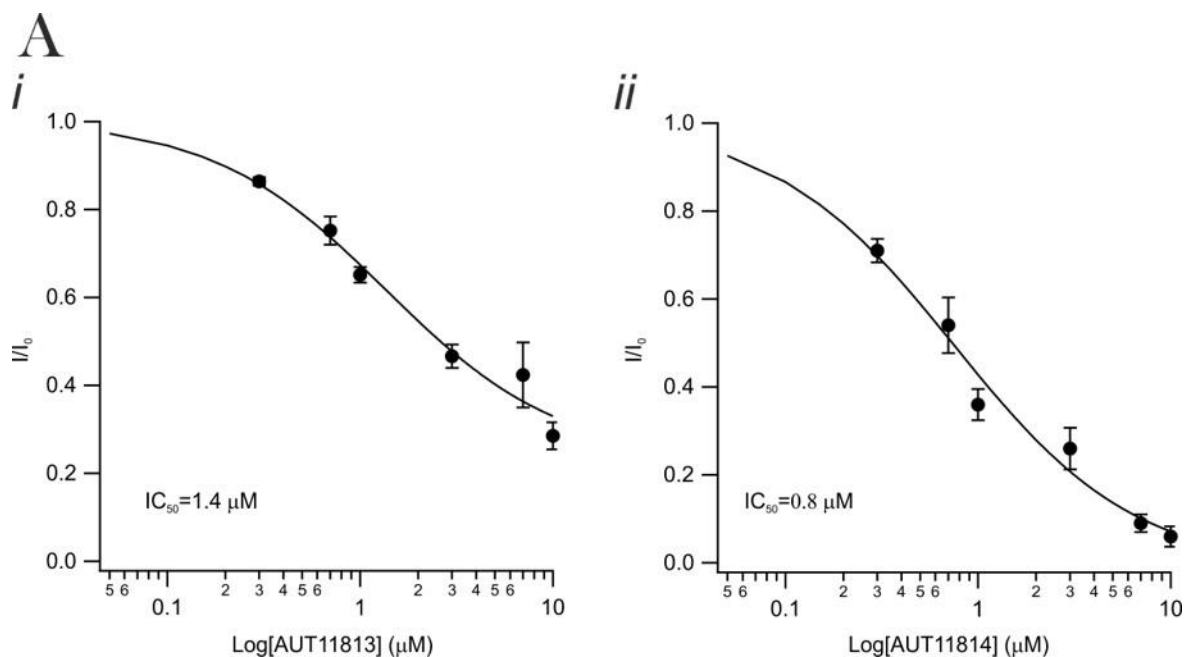


Figure 3.4.3 The effects of AUT11813 and AUT11814 on whole-cell TMEM16A currents

(A) i) Inside-out patch currents measured in response to 1 s +70 mV step followed by -70 mV from a HEK-293T cell expressing TMEM16A dialysed with 300 nM $[\text{Ca}^{2+}]_i$ and perfused with AUT11813 ($n=8-15$); ii) Inside-out patch currents measured in response to 1 s +70 mV step followed by -70 mV from a HEK-293T cell expressing TMEM16A dialysed with 300 nM $[\text{Ca}^{2+}]_i$ and perfused with AUT11814 ($n=3-10$). Data was fitted with the Hill equation (Equation 13).

HEK-293T	IC_{50} (μM)	max	h	N
AUT11813	1.35 ± 0.68	1.00 ± 0.04	0.96 ± 0.34	8-15
AUT11814	0.78 ± 0.24	0.98 ± 0.03	0.92 ± 0.29	3-10

Table 20 Hill-fit parameters (IC_{50} , max and h) (Eq. 13) for HEK-293T cells expressing TMEM16A.

Mean current versus $[\text{AUT11813}]$ and $[\text{AUT11814}]$ relationships obtained in inside-out patches excised from TMEM16A-expressing HEK-293T cells.

3.5 TMEM16A functional role in the vasculature

3.5.1 TMEM16A-mediated mouse aortic contractility

As described in more details in the Introduction, TMEM16A channels are important components of agonist-induced vasoconstriction (Pedemonte and Galletta 2014). To quantify the contribution of TMEM16A to agonist-induced contraction in isolated rodent artery rings, the isometric force generated by rodent aortic arteries rings was investigated *via* wire-myography. PE, an agonist of the α_1 G_q coupled receptor, was used to activate the IP₃-pathway leading to [Ca²⁺]_i increase and activation of TMEM16A. Aortic rings were exposed to increasing concentrations of PE (Figure 3.5.1). The tension *versus* [PE] relationship was fitted with the Hill equation (Equation 13).

To determine the contribution of TMEM16A to PE-induced contraction, aortic rings were incubated with the selective TMEM16A inhibitor Ani9 (3 μ M). Ani9 inhibited 49 % of the contraction induced in response to the maximal PE concentration (10 μ M). The contribution of VGCCs was also studied as Cl⁻ efflux upon TMEM16A activation depolarises the membrane to allow activation of this family of channels, described more in details in the Introduction (Section 1.8). Thus, we were interested in studying the residual TMEM16A activity by comparing inhibition of PE-induced contraction between the TMEM16A blocker Ani9 (Seo, Lee et al. 2016) and nifedipine, a VGCC blocker (Shen, Jiang et al. 2000, Zhang, Berra-Romani et al. 2007). Aortic rings were incubated with nifedipine (10 nM) prior to the application of PE. Fig 3.5.1 shows that nifedipine inhibited 65 % of the contraction induced in response to the maximal PE concentration (10 μ M).

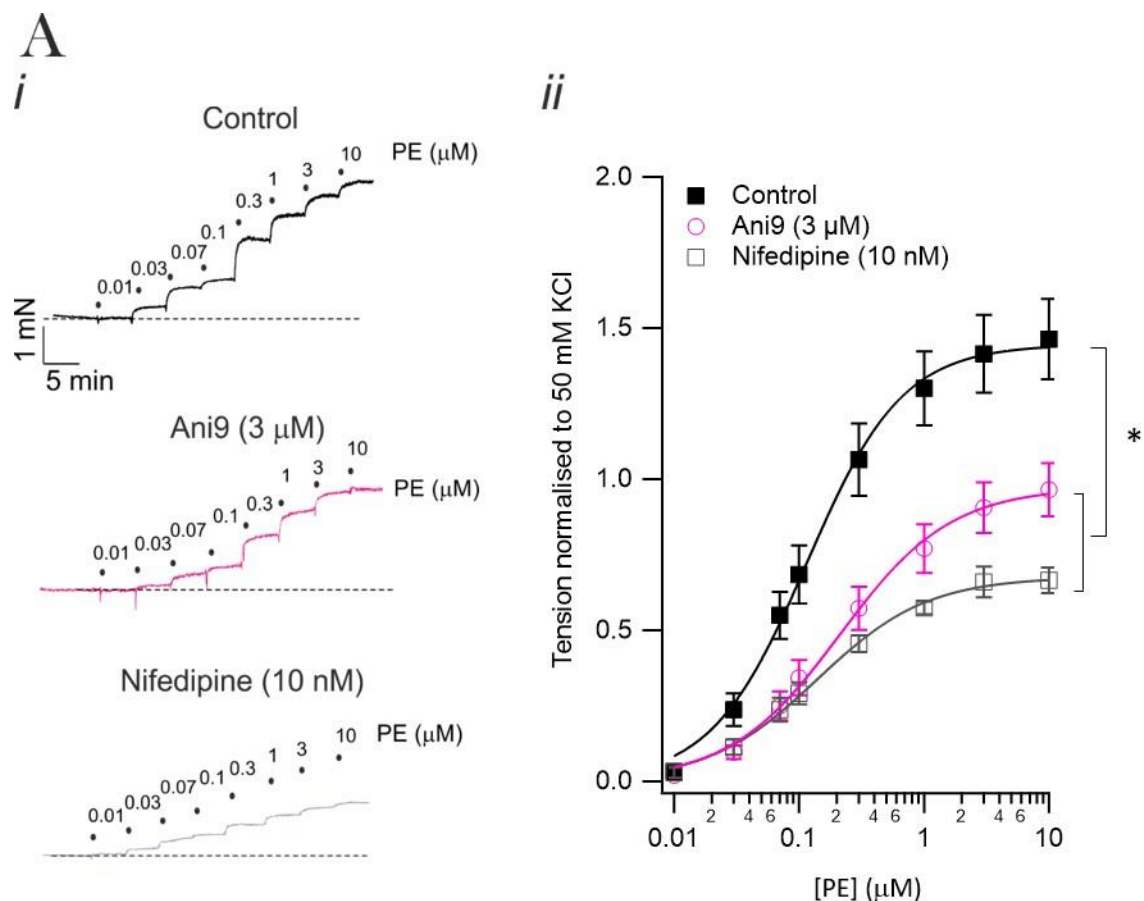


Figure 3.5.1 The effect of Ani9 on phenylephrine-induced contraction in mouse arteries.

(A) i) Isometric aortic ring tension induced by cumulative addition of phenylephrine (PE) in the range 0.01 – 10 μM in untreated mouse aortic rings (control) or in the presence of 3 μM Ani9 or nifedipine (10 nM). Dotted line represents baseline tension; ii) change in isometric tension versus [PE] relationship of mouse aortic rings in control (N=9), in the presence of 3 μM Ani9 (N=7) or in the presence of nifedipine (10 nM) (N=5). Tension was normalised to 50 mM KCl and fitted with the Hill equation (Equation 13). * indicates $p \leq 0.05$, paired t-test.

Aortas	EC ₅₀ (μM)	max	h	N
Control	0.12 \pm 0.00	0.98 \pm 0.01	1.28 \pm 0.07	9
Ani9	0.21 \pm 0.02 *	0.77 \pm 0.02	0.97 \pm 0.07	7
Nifedipine	0.14 \pm 0.01	0.67 \pm 0.01	0.98 \pm 0.06	5

Table 21 Hill-fit parameters (EC₅₀, max and h) (Eq. 13) for mouse aortic rings.

Mean tension versus [PE] relationships obtained in mouse aortic rings. * indicates $p \leq 0.05$, unpaired t-test.

3.5.2 TMEM16A-mediated rat aortic contractility

Selective TMEM16A activators are not well known in the literature. Hence, I next investigated the AUT11817 compound which has been developed as a potential activator of the TMEM16A channel. AUT11817 (300 nM) did not induce any aortic constriction in the absence of an agonist (Figure 3.5.2). In contrast, AUT11817 enhanced the PE-induced constriction of rat aortic rings in response to increasing concentrations of PE. In response to the maximal PE concentration (1 μ M), AUT11817 induced 40 ± 0.1 % increase in the PE-induced contraction compared to untreated aortic rings (control) (Figure 3.5.2).

I have shown that Ani9 is a suitable tool compound to selectively and potently block TMEM16A (Section 3.4.1). In order to study other pharmacological TMEM16A inhibitors, I investigated the effect of the TMEM16A inhibitors AUT11814 and Ani9 on the PE-induced constriction of rat aortic rings. AUT11814 and Ani9 induced a similar block of 90 ± 0.1 % and of 94 ± 0.1 % respectively on the contraction induced in response to the maximal PE concentration (1 μ M) (Figure 3.5.2).

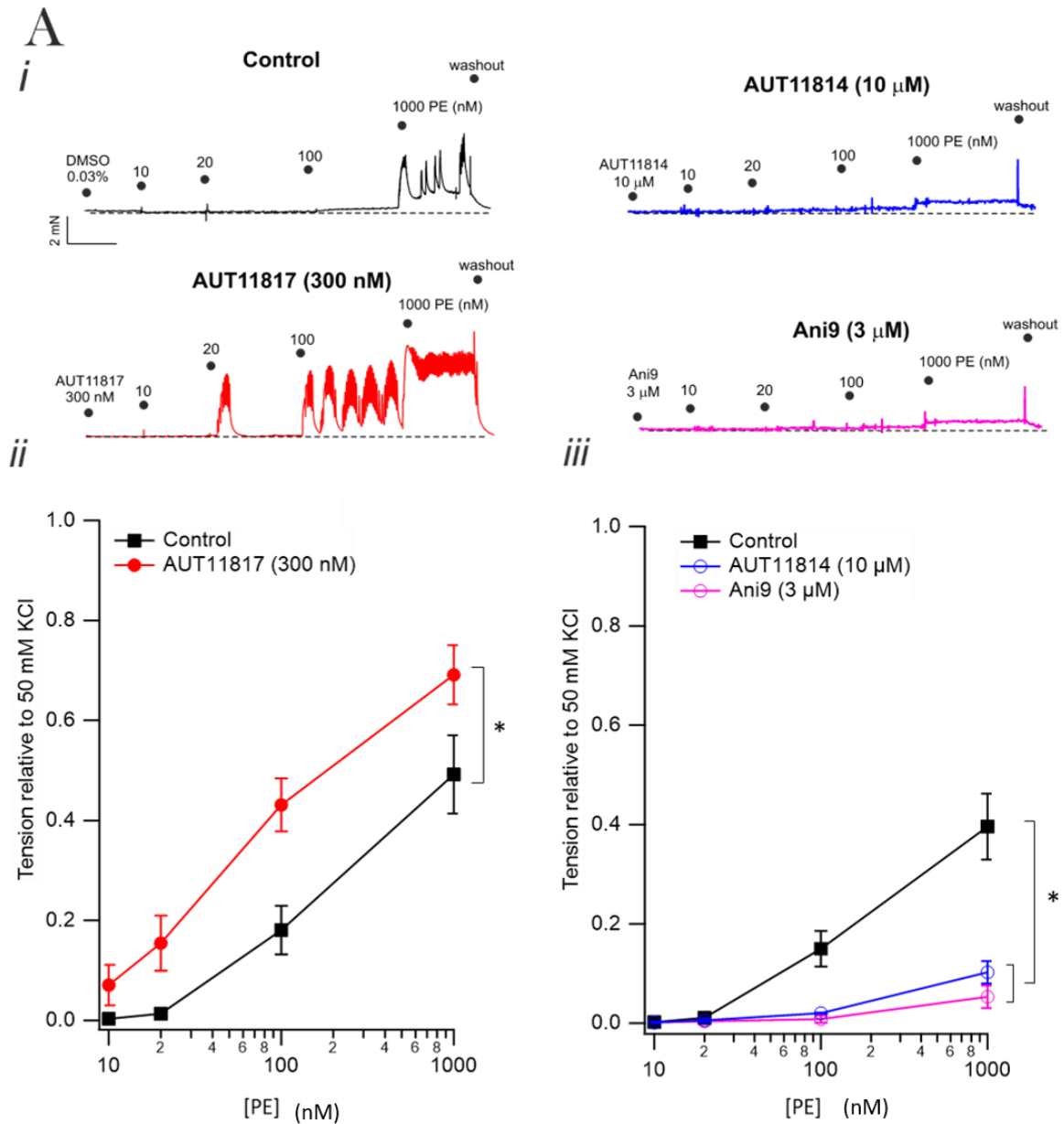


Figure 3.5.2 The effect of AUT11817, AUT11814 and Ani9 on phenylephrine-induced contraction in rat arteries.

(A) i) Isometric aortic ring tension induced by cumulative addition of phenylephrine (PE) in the range 10 – 1000 nM in untreated rings (control) or in the presence of AUT11817 (300 nM), AUT11814 (10 μM) or Ani9 (3 μM). Dotted line represents baseline tension; ii) change in isometric tension versus [PE] relationship of mouse aortic rings in control (N=3), in the presence of 300 nM AUT11817 (N=7), 10 μM AUT11814 (N=4) or 3 μM Ani9 (N=3). Tension was normalised to 50 mM KCl and fitted with the Hill equation (Equation 13). * indicates $p \leq 0.05$, paired t-test.

3.6 Discussion

This chapter has outlined the key electrophysiological properties and cellular localisation of cloned TMEM16A, TMEM16B and TMEM16F in an heterologous system. The role of TMEM16K was also explored and was found to localise in the ER (Bushell, Pike et al. 2019). The extent by which TMEM16A contributes to agonist-induced contraction in rodent aortic rings was assessed. The pharmacology of the TMEM16A channels was explored with a focus on small molecules such as the potent and selective TMEM16A-blocker Ani9 (Seo, Lee et al. 2016) and some compounds currently under development (Autifony Therapeutics). These small molecules were assessed in heterologous systems as well as in isolated vessels. AUT11814 potently inhibited I_{CaCC} in heterologous system and also the agonist-induced contraction in aortic rings. AUT11817 significantly potentiated the agonist-induced contraction in aortic rings.

3.6.1 Properties of cloned TMEM16A-mediated currents and other TMEM16x family members

The features of the TMEM16A and TMEM16x family members were studied in this chapter. While the electrophysiological features of the TMEM16x have been previously reported (Scudieri, Caci et al. 2015, Pifferi 2017, Bushell, Pike et al. 2019, Dinsdale, Pipatpolkai et al. 2021), there is no published systematic study in which these channels have been studied and compared in the same expression system and in equivalent recording conditions (including stimulation protocols and electrophysiological solutions). The work presented in this chapter remedy this deficit and enabled me to identify the appropriate experimental conditions to study TMEM16A channels in heterologously and native systems for the rest of the work conducted as part of my DPhil project .

Cloned TMEM16A channels expressed in HEK-293T cells produced a distinctive outwardly rectifying current characterised by large currents at positive V_m and small currents at negative

V_m . Ca^{2+} was essential for activation of TMEM16A channels, as the I_{CaCC} elicited in the presence of 0 nM $[Ca^{2+}]_i$ was equivalent to that recorded in mock-transfected HEK-293T cells. Moreover, increasing the $[Ca^{2+}]_i$ from 300 nM to 600 nM, resulted in a significant increase in the I_{CaCC} -mediated TMEM16A current. These data are consistent with that present in the literature describing TMEM16A in heterologous systems (Caputo, Caci et al. 2008, Yang, Cho et al. 2008, Adomaviciene, Smith et al. 2013, Heinze, Seniuk et al. 2014). The I_{CaCC} -mediated TMEM16A current response was also studied in inside-out patches in HEK-293T and CHO cell lines. In both cellular model, increasing doses of $[Ca^{2+}]_i$ induced an increment in I_{CaCC} -mediated TMEM16A at +70 mV.

Among the TMEM16x family members, only TMEM16B-transfected cells elicited I_{CaCC} at low $[Ca^{2+}]_i$. This is in accordance with the literature indicating that even if TMEM16A and TMEM16B share similar biophysical properties, TMEM16A channels are activated by 300-600 nM $[Ca^{2+}]_i$ while TMEM16B is activated by 800-1000 nM $[Ca^{2+}]_i$ (Ferrera, Caputo et al. 2009, Pifferi, Dibattista et al. 2009, Adomaviciene, Smith et al. 2013). Activation and deactivation kinetics are also very different between TMEM16A and TMEM16B channels. Figure 3.4.1 shows that in accordance with the literature, the difference in time constant between these two channel family members is more than 10-fold (Caputo, Caci et al. 2008, Pifferi, Dibattista et al. 2009). This is also reflected in the single channel conductance which is known to be around 1 pS for TMEM16B, while up to 3-5 pS for TMEM16A (Pifferi 2009, Adomaviciene 2013). In native tissues, TMEM16B expression has been reported to be minimal in smooth muscle (Davis, Forrest et al. 2010). In fact, it is reported in the literature that TMEM16B mainly functions as CaCC in photoreceptors and olfactory neurons (Li, He et al. 2019, Wang, Simms et al. 2019).

As described in more details in the introduction (Section 1.7.1) TMEM16F is functionally and structurally divergent from TMEM16A and TMEM16B due to its lipid scramblase properties. In this chapter, TMEM16F-induced current was studied in the presence of 78 μM $[Ca^{2+}]_i$. Figure

3.3.2 showed that TMEM16F produced I_{CaCC} after 3 minutes in the presence of high $[Ca^{2+}]_i$. Thus, under physiological condition, it is unlikely that TMEM16F can contribute to native I_{CaCC} in VSMCs either under resting conditions, where $[Ca^{2+}]_i \sim 300-400$ nM or under excitation where $[Ca^{2+}]_i \sim 1$ μ M (Hill-Eubanks 2011). Moreover, since TMEM16F current develops slowly over the duration of several minutes, it is unlikely that the fast Ca^{2+} sparks can activate the channel (Jaggar, Porter et al. 2000). In fact, it has been proposed in the literature that TMEM16F works mainly as a scramblase and that its current is equal to the ionic leak associated with phospholipid translocation (Gyobu, Ishihara et al. 2017, Ye, Han et al. 2018).

TMEM16K currents were similar to endogenous currents in mock-transfected cells, excluding the possibility that TMEM16K can elicit I_{CaCC} at the plasma membrane. The immunocytochemistry data showed that TMEM16K is located in the ER. In fact, we reported that TMEM16K is a ER-resident lipid scramblase with non-specific ion channel activity (Bushell, Pike et al. 2019). Scramblases play an important role in the ER to maintain the symmetrical distribution of membrane lipids. Unlike the plasma membrane, where lipids are asymmetrically arranged, most of the lipids produced in the cytoplasmic side of the ER, have to be transported by scramblases, like TMEM16K, in the inner side of the ER membrane to maintain lipid symmetry. More recently, TMEM16K has also been reported to form contact sites between the ER and the endosomes (Petkovic, Oses-Prieto et al. 2020).

Overall, these data indicate a primary role of TMEM16A among the TMEM16x family members, to elicit I_{CaCC} in an heterologous system. Since this project is focussed on studying I_{CaCC} , the properties of TMEM16A are studied more in depth in this thesis. The scramblase properties of TMEM16F and TMEM16K could be investigated in a different project.

3.6.2 Action of the TMEM16A-inhibitors in heterologous system

To date, Ani9 has been identified as a TMEM16A inhibitor with a potent IC_{50} (Seo et al). In this thesis, the selectivity and potency of Ani9 was confirmed by showing that Ani9 potently and specifically inhibits TMEM16A over TMEM16B (Figure 3.3.1). Moreover, since the modulatory effect of Ani9 has not been characterised in depth in the literature, I also studied Ani9 inhibition on TMEM16A in condition of high $[Ca^{2+}]_i$ (1 μ M). This experiment revealed that Ani9 left a residual, unblocked, TMEM16A current in condition of high $[Ca^{2+}]_i$ at positive and negative V_m (Figure 3.4.1). Therefore, this data suggests that Ani9 action on TMEM16A is modulated by $[Ca^{2+}]_i$. Previous studies from our group (unpublished data) have shown that Ani9 has off targets such as TMEM16F and also that it crosses the BBB in limited amounts. Therefore, this thesis looked at the effect of other pharmacological compounds based on Ani9 structure, as potential alternative candidates to be studied *in vivo* to block the TMEM16A channel. I constructed a dose response for the compounds AUT11813 and AUT1184 in TMEM16A-transfected HEK-293T cells (Figure 3.3.2). While both compounds inhibited TMEM16A current, AUT11814 showed a more similar IC_{50} to Ani9 and thus could be studied further in the future to be a potential target for *in vivo* TMEM16A inhibition.

3.6.3 Features of TMEM16A-mediated vessel contraction in the aorta

The role of TMEM16A in inducing agonist-mediated contraction in the aorta was studied both in mice and rat tissues. In both animal models, TMEM16A has shown to play a major role in regulating this mechanism. In fact, Cil et al. and Heinze et al. independently showed that pharmacological or tamoxifen-induced inhibition of TMEM16A, respectively, abolishes agonist-induced aortic contractility (Heinze, Seniuk et al. 2014, Cil, Chen et al. 2021). Incubation of aortas with Ani9 resulted in a dramatic inhibition of agonist-induced contraction. Nifedipine, a blocker of L-type gated $[Ca^{2+}]_i$ channels was used to fully block agonist-induced contraction (Sun, Xia et al. 2012, Danielsson, Perez-Zoghbi et al. 2015). The application of nifedipine revealed that the residual contribution of L-type gated $[Ca^{2+}]_i$ channels in the agonist-

induced contraction is minimal, while most of the response could be inhibited by the TMEM16A-specific inhibitor Ani9. The inhibition of aortic agonist-induced contraction by Ani9 was also studied in rat tissues. Figure 3.5.1 and 3.5.2 show that Ani9 blocked aortic agonist-induced contraction in rat tissues to a similar extent as in mouse tissues. From my studies in heterologous system, I found that AUT11814 is a potent TMEM16A-inhibitor. Thus, I studied the effect of AUT11814 in aortic rings. I found that AUT11814 blocked agonist-induced contraction similar to Ani9 treatment. This indicates that AUT11814 could be studied as a physiological TMEM16A blocker. The recently identified TMEM16A-inhibitor TMinh-23 (Cil, Chen et al. 2021) showed a similar block in agonist-induced contraction compared to AUT11814 treatment.

Regarding activators of TMEM16A channels in native tissues, there is a lack of potent and selective compounds shown in the literature. Some compounds, such as E_{act} and F_{act} , have been shown to activate TMEM16A currents indirectly by increasing TMEM16A current in the absence of $[Ca^{2+}]_i$ (Namkung, Phuan et al. 2011, Genovese, Borrelli et al. 2019). This effect was explained by activation of TRP4V and thus, increase of $[Ca^{2+}]_i$ to activate TMEM16A (Genovese, Borrelli et al. 2019). Thus, I studied the effects of AUT11817 in the absence of the PE agonist as well as in response to increasing concentrations of PE (Figure 3.5.2). I showed that in the absence of extracellular stimulus from agonist (0 μ M PE), application of AUT11817 to aortic rings does not alter contraction. In contrast, AUT11817 application during aortic stimulation from 10 nM PE to 1 μ M PE induced an increase in contraction. These data indicates that physiologically, AUT11817 can increase agonist-induced contraction only upon TMEM16A activation by an agonist.

Overall, this chapter has shown that the TMEM16A and TMEM16x functional and cellular properties can be studied in heterologous and native systems according to the literature. I showed that Ani9 can be used as a pharmacological tool to block TMEM16A current both in

cellular models and in tissues. Moreover, I identified AUT11814 and AUT11817 as potential candidates for blocking and activating TMEM16A channels, respectively.

Chapter 4

Control of TMEM16A activity by the lysosomal NPC1 protein

4.1 NPC1 modulation of TMEM16A channel properties

As described in more details in the Introduction (Section 1.7.1), there are ten protein members within the e mammalian TMEM16 family: TMEM16A-K, excluding I (Pedemonte and Galiotta 2014, Falzone, Malvezzi et al. 2018). The majority of the TMEM16 family members function as lipid scramblases, translocating lipids across membranes and also acting as non-selective ion channels (Yang, Kim et al. 2012, Malvezzi, Chalal et al. 2013, Lee, Khelashvili et al. 2018, Lee, Watanabe et al. 2020). While the TMEM16K and TMEM16H have lower sequence homology from the rest of the family, the remaining paralogs have similar homology (Pedemonte and Galiotta 2014, Falzone, Malvezzi et al. 2018). TMEM16A and TMEM16B have strong anion selectivity over cations (Yang, Cho et al. 2008, Pifferi, Dibattista et al. 2009, Lim, Lam et al. 2016, Jiang, Yu et al. 2017). Most ion channels types (e.g. K⁺ or Na⁺ channels) have a pore composed of series of α -helical domain arranged to form a proteinaceous water filled pore (Hille 2001). In contrast, TMEM16A has a pore with large sections directly exposed to the lipids of the plasma membrane (Whitlock and Hartzell 2017). The cryo-EM structures of the TMEM16A channel (Dang, Feng et al. 2017, Paulino, Kalienkova et al. 2017) show that the pore assumes an hourglass shape that is largely shielded from the membrane, but a detachment of TM4 and TM6 creates a funnel-shaped vestibule that has regions directly exposed to the cytoplasm and the lipid bilayer. The vicinity of plasmalemmal lipids to the ion permeation pathway suggests that TMEM16A-mediated currents can be directly influenced by lipids. In accord with this proposition, is the notion that the channel is controlled by a range of lipids including PIP₂ (Ta, Acheson et al. 2017, Le, Jia et al. 2019, Hawn, Akin et al. 2021, Jia and Chen 2021) and omega-3 dietary fatty acids (De Jesus-Perez, Cruz-Rangel et al. 2018, Leon-Aparicio, Sánchez-Solano et al. 2022).

The central hypothesis of my project (Introduction, Section 1.11) is that the structural features of the pore of the TMEM16A channel confer the channel the capacity to response to changes in the lipid composition of the plasma membrane (Falzone, Malvezzi et al. 2018, Kalienkova,

Clerico Mosina et al. 2021); thus the TMEM16A channel could serve as a lipid sensor to couple changes in lipid homeostasis to changes in cell electrical activity. The focus of this chapter are the plasma membrane changes that occur as a consequence of loss-of-function of the NPC1 protein. As outlined in greater detail in the Introduction (Sections 1.4.2), the lysosomal NPC1 protein is a key mediator of intracellular lipid trafficking (Infante, Abi-Mosleh et al. 2008). Mutations of NPC1 lead to the NPC disease, a fatal disorder associated with impaired cellular lipid homeostasis, which causes neurodegeneration and vascular impairment (Louwette, Regal et al. 2013, Benussi, Cotelli et al. 2019). Loss of NPC1 activity causes a block of intracellular lipid transport, inducing extensive lipid accumulation in the lysosomes and late endosomes, as well as reduced lipid transport to intracellular membranes (Wojtanik and Liscum 2003). The key results presented in this chapter indicate that changes in plasma membrane composition by NPC1 are a powerful cellular mean to control the activity of the TMEM16A channels.

4.1.1 NPC1 inhibition impairs cholesterol distribution

In order to study the effect of NPC1 inhibition on intracellular lipid distribution, the naturally fluorescent antibiotic filipin was used to detect unesterified cholesterol (Vivas, Tiscione et al. 2019). Two distinct cellular models of loss-of-NPC1 function were used: *i*) HEK-293T cells treated with the specific NPC1 inhibitor U18666A (5 μ M, 24h) (Lu, Liang et al. 2015) and *ii*) CHO M12 cells in which the *Npc1* gene was deleted, termed CHO-*Npc1*^{-/-} (Millard, Srivastava et al. 2000). After U18666A treatment in HEK-293T or in CHO-*Npc1*^{-/-} cells, filipin staining was visible as intracellular inclusions (vesicles) in the endolysosomes (Figure 4.1.1) There was a ~ 2-fold increase in the number of vesicles *per* cell when NPC1 was inhibited pharmacologically or *via* gene deletion (Figure 4.1.1). Treatment of these two cell lines with β CD prevented cholesterol accumulation (Coisne, Tilloy et al. 2016, Megías-Vericat, Company-Albir et al. 2018). Cells that were maintained in the culture medium supplement with β CD (250 μ M) for 24 hours showed reduced number of cholesterol-filled vesicles *per* cell to a level similar to that observed in untreated cells (Figure 4.1.1). In addition, the number of

cholesterol-filled vesicles *per* cell did not differ from control cells or cells in which *Npc1* was re-introduced *via* stable viral expression. Thus, pharmacological inhibition of NPC1 or deletion of the *Npc1* gene induced cholesterol accumulation in cell lines (which is an hallmark of NPC1 dysfunction) and this change was prevented by treatment with β CD or by re-introduction of the *Npc1* coding region (Lloyd-Evans, Morgan et al. 2008, Megías-Vericat, Company-Albir et al. 2018, Tiscione, Vivas et al. 2019, Vivas, Tiscione et al. 2019).

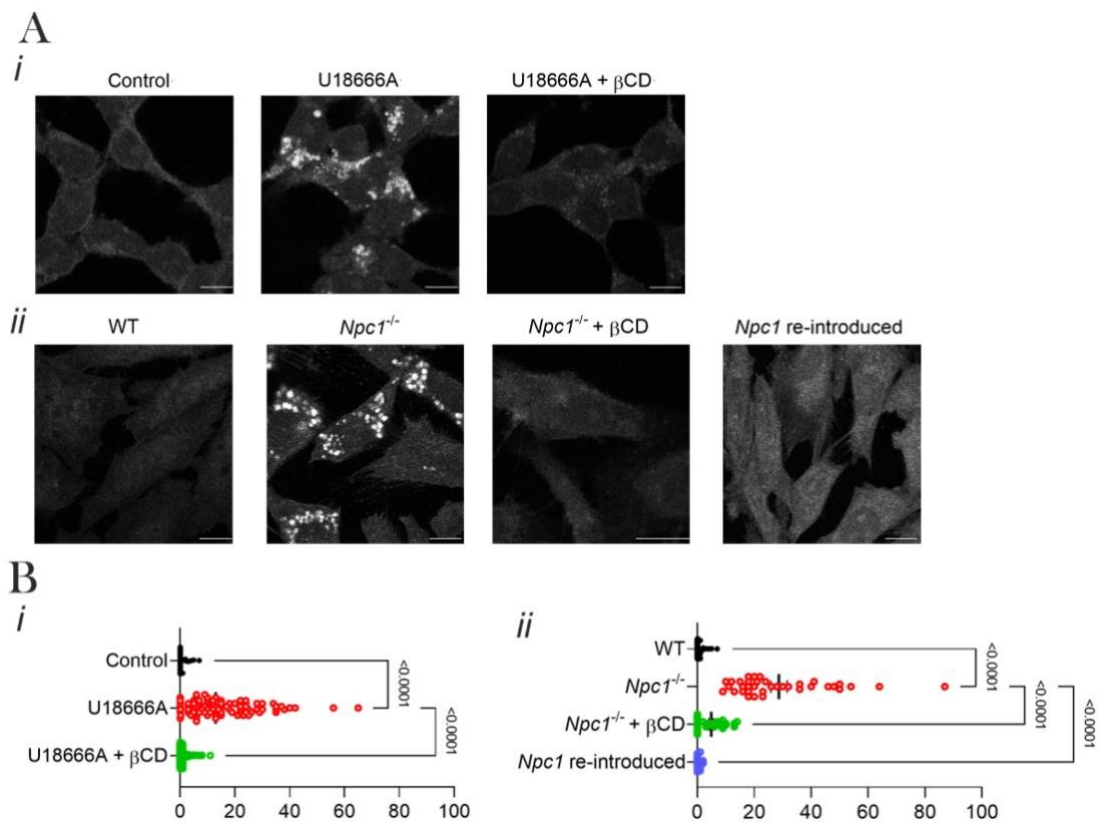


Figure 4.1.1 NPC1 inhibition or *Npc1* gene deletion impairs intracellular lipid homeostasis.

(A) Representative confocal images of HEK-293T (i) and CHO-*Npc1*^{-/-} (ii) cells stained with the cholesterol marker filipin. (B) i) Number of vesicles per cell in HEK-293T cells exposed to vehicle (n=42), 5 μ M U18666A (n=83) and U18666A in the presence of 250 μ M β CD (n=129); ii) Number of vesicles per cell in WT CHO cells (n=68), CHO-*Npc1*^{-/-} (n=36), CHO-*Npc1*^{-/-} cells exposed either to 250 μ M β CD (n=35) or in *Npc1*^{-/-} cells where *Npc1* was re-introduced (n=39). Unpaired t-test. Scale bar = 10 μ m

4.1.2 Pharmacological NPC1 inhibition or genetic *Npc1* deletion enhances TMEM16A currents

The next set of experiment aimed to investigate the consequence of lipid redistribution described above on the electrophysiological properties of heterologous TMEM16A channels. In either HEK-293T treated with U18666A or CHO-*Npc1*^{-/-} cells transfected with TMEM16A, the magnitude of the whole-cell current was assessed. NPC1 inhibition with U18666A (5 μ M, 24 h) enhanced heterologous TMEM16A current density in HEK-293T cells by ~2 fold. At +100 mV, TMEM16A current increased from 100.2 \pm 16.0 pA/pF (n=18) in control cells to 234.0 \pm 39.5 pA/pF (n=21) in cells exposed to U18666A ($p=0.005$) (Figure 4.1.2). Figure 4.1.2 shows that CHO-*Npc1*^{-/-} cells, the heterologous TMEM16A current density was also increased. For example, at +100 mV, TMEM16A current was activated of ~ 3-fold from 236.4 \pm 62.5 pA/pF in WT cells (n=15) to 636.7 \pm 65.4 pA/pF in *Npc1*^{-/-} cells (n=15) ($p=0.02$) (Figure 4.1.2). In NPC1 inhibition with U18666A or in *Npc1* deletion, the E_{rev} was not significantly affected being ~0 in each case (very close to the expected equilibrium potential for Cl⁻ (E_{Cl}) in our recordings conditions). The increases in TMEM16A current amplitude described above may be due to underlying changes in channel gating, which may manifest in changes in current kinetics. Thus, the kinetic of the TMEM16A current before and after NPC1 inhibition was assed and expressed as the time required for the current to reach half maximal amplitude ($\tau_{1/2}$) at a given V_m during the IV-CaCC protocol (see Methods, Chapter 3, section 2.5.4.2). NPC1 inhibition resulted in a reduction of $\tau_{1/2}$ by about 2-fold. At +100 mV, in untreated HEK-293T cells $\tau_{1/2}$ was 111.2 \pm 4.0 ms (n=14) and in cells treated with U18666A $\tau_{1/2}$ was 60.4 \pm 3.2 ms (n=15) ($p<0.05$) (Fig. 4.1.2). In WT cells, at +100 mV, $\tau_{1/2}$ was 145.0 \pm 10.1 ms (n=14) and 70.2 \pm 6.5 ms (n=12) in CHO-*Npc1*^{-/-} cells ($p<0.05$) (Fig 4.1.2).

TMEM16A shares ~70% sequence homology with TMEM16B channel, and ~20% with TMEM16F channel and scramblase (Suzuki, Fujii et al. 2013, Falzone, Malvezzi et al. 2018). The next set of experiments aimed at gaining insight into whether NPC1 selectively controls TMEM16A or can also affect other members of the TMEM16A family. Thus, I studied the effect of NPC1 inhibition on the TMEM16B Cl⁻ current, as well as on the TMEM16F non-selective

cation current, using the whole-cell configuration of the patch-clamp technique. HEK-293T cells expressing either TMEM16B or TMEM16F (Figure 4.1.3) were incubated overnight with U18666A (5 μ M). In the presence of 600 nM of $[Ca^{2+}]_i$, NPC1 inhibition had no effect on whole-cell TMEM16B currents (Fig. 4.1.3). At +100 mV TMEM16B current was 122.2 ± 20.0 pA/pF (n=15) in control HEK-293T cells and 132.0 ± 26.4 pA/pF (n=12) in cells where NPC1 was inhibited ($p > 0.05$). As described in Chapter 3 (Section 1.7.1), TMEM16F is far less sensitive to $[Ca^{2+}]_i$ than TMEM16A, therefore I studied TMEM16F current in the presence of 78 μ M of $[Ca^{2+}]_i$. At +100 mV, TMEM16F current was 116.4 ± 2 pA/pF (n=11) in control cells and 106.3 ± 37.5 pA/pF (n=7) in U18666A-treated cells ($p > 0.05$). These results indicate that NPC1 loss of function affects TMEM16A and not the closely-related members of the same family.

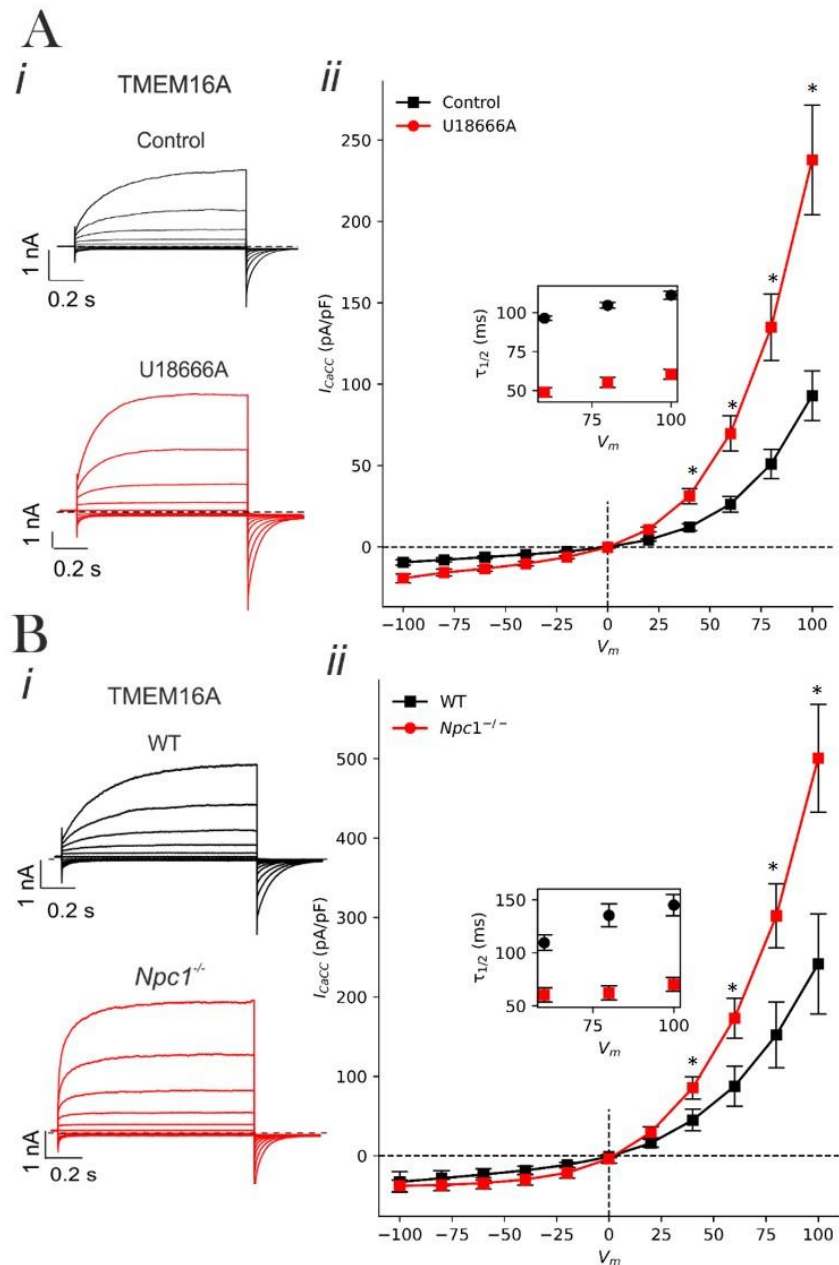


Figure 4.1.2 TMEM16A current is enhanced during NPC1 inhibition

(A) *i*) Whole-cell currents recorded from a TMEM16A expressing HEK-293T cell in the presence or absence of U18666A (5 μ M), as indicated. The cell was dialysed with 300 nM $[Ca^{2+}]_i$; *ii*) mean whole-cell current versus V_m relationships measured at the end of the 1 s voltage pulse from - 100 to + 100 mV in 20 mV increments in the absence ($n=18$) or presence ($n=21$) of U18666A. Inset in (*ii*) shows mean $\tau_{1/2}$ of current activation for TMEM16A expressing HEK-293T cell in the presence ($n=14$) or absence of U18666A ($n=15$), as indicated. (B) *i*) Whole-cell currents recorded from a TMEM16A expressing WT or $Npc1^{-/-}$ CHO cells, as indicated. The cell was dialysed with 300 nM $[Ca^{2+}]_i$; *ii*) mean whole-cell current versus V_m relationships measured at the end of the 1 s voltage pulse from - 100 to + 100 mV in 20 mV increments in WT ($n=14$) or $Npc1^{-/-}$ ($n=12$) cells. Inset in (*ii*) shows mean $\tau_{1/2}$ of current activation in WT CHO cells ($n=68$), CHO- $Npc1^{-/-}$ ($n=36$). Dashed horizontal line represents the zero-current level. Voltage protocol "IV-CaCC" is described in the Methods (Figure 2.5.4), * indicates $p \leq 0.05$, unpaired t-test.

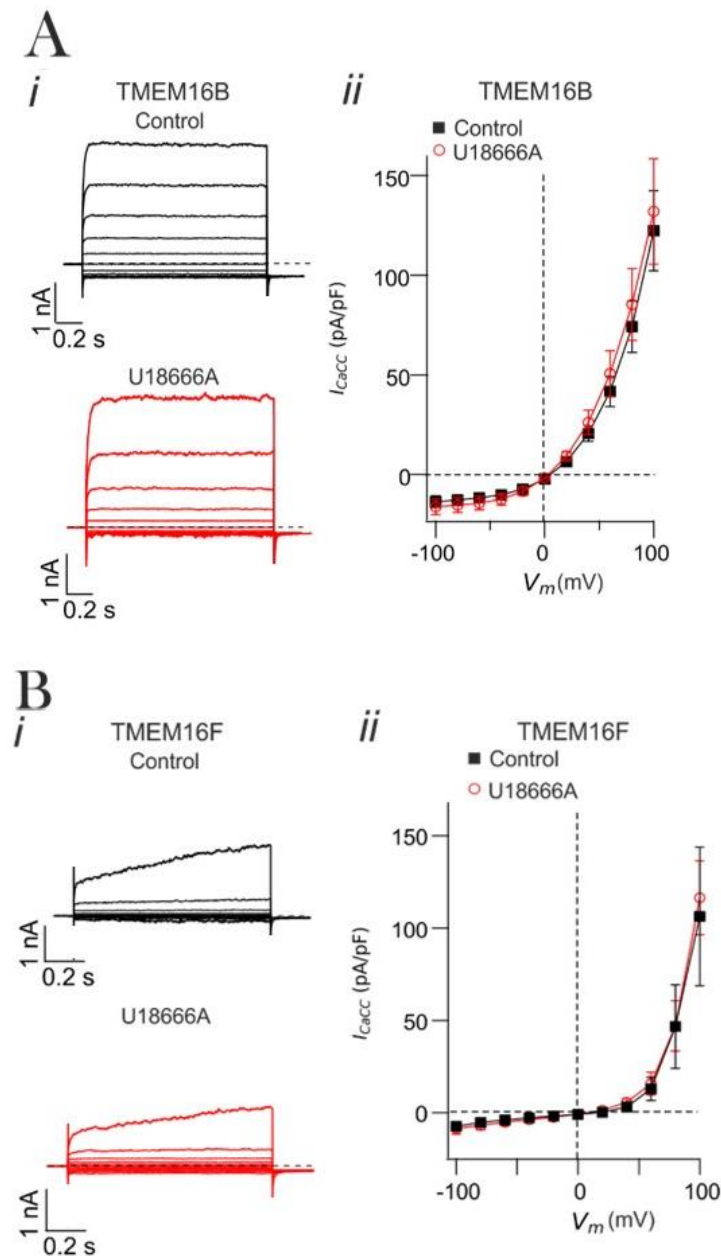


Figure 4.1.3 TMEM16B and TMEM16F activity during NPC1 inhibition

(A) *i*) Whole-cell currents recorded from a TMEM16B expressing HEK-293T cell, as indicated. The cell was dialysed with 600 nM $[Ca^{2+}]_i$; *ii*) mean whole-cell current versus V_m relationships measured at the end of the 1 s voltage pulse from - 100 to + 100 mV in 20 mV increments in the absence ($n=15$) or presence ($n=12$) of U18666A. (B) *i*) Whole-cell currents recorded from a TMEM16F expressing HEK-293T cell, as indicated. The cell was dialysed with 78 μM $[Ca^{2+}]_i$; *ii*) mean whole-cell current versus V_m relationships measured at the end of the 1 s voltage pulse from - 100 to + 100 mV in 20 mV increments in the absence ($n=10$) or presence ($n=7$) of U18666A. Dashed horizontal line represents the zero-current level. Voltage protocol “IV-CaCC” is described in the Methods (Figure 2.5.4), * indicates $p \leq 0.05$, unpaired *t*-test.

Based on the premise that TMEM16A activity is enhanced by NPC1 loss-of-function, I investigated whether the underlying mechanism is an alteration of the intracellular distribution of the TMEM16A and NPC1 protein following NPC1 inhibition. After U18666A treatment, the overall intracellular distribution of TMEM16A and NPC1 was assessed in HEK-293T cells. The colocalisation between TMEM16A and NPC1 assessed before and after NPC1 inhibition with U18666A (Figure 4.1.4). Mander's correlation coefficient (M1) was 0.4 ± 0.0 (n=60) in control cells and 0.4 ± 0.0 (n=61) in the presence of U18666A ($p > 0.05$) (Figure 4.1.4). The intracellular distribution of TMEM16B and TMEM16F was also studied before and after NPC1 inhibition with U18666A. The colocalisation of either TMEM16F or TMEM16B with NPC1 was not affected by U18666A treatment (Figure 4.1.4). These results suggest that there is partial overlap of cellular localisation between TMEM16x (TMEM16A, TMEM16B or TMEM16F) and NPC1. However, their cellular distribution was not affected by NPC1 inhibition excluding the possibility that large rearrangement of TMEM16 proteins and NPC1 distribution are required for modulation of TMEM16A currents by NPC1.

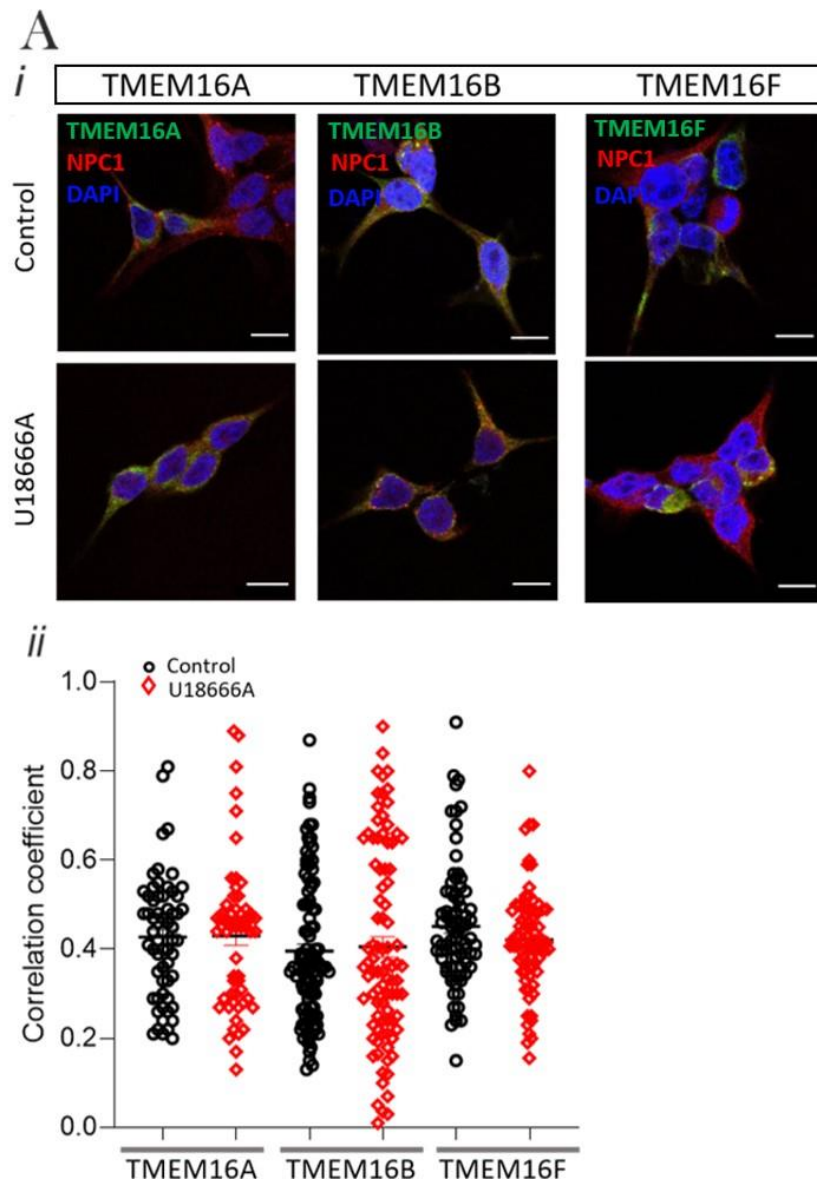


Figure 4.1.4 NPC1 co-localisation with cloned TMEM16A, TMEM16B and TMEM16F channels.

(A) i) Representative confocal images of HEK-293T cells expressing TMEM16A. TMEM16A, TMEM16B or TMEM16F (red), DAPI (blue) and the degree of TMEM16A and NPC1 overlap is shown (yellow). Scale bar = 10 μ m; ii) Mander's correlation coefficient ($M1$) determined for the overlap of TMEM16A, TMEM16B and TMEM16F with NPC1 in the absence or presence of 5 μ M U18666A ($n=60-100$).

4.1.3 Treatment with β CD or NPC1 re-introduction rescues TMEM16A activation

The data presented above shows that the altered lipid distribution in HEK-293T treated with U18666A or in CHO-*Npc1*^{-/-} cells can be rescued by overnight incubation with β CD (Figure 4.1.5). Thus, the next experiment aimed at studying if β CD treatment can alter TMEM16A current density. Following NPC1 inhibition in HEK-293T cells *via* U18666A incubation, cells were treated with β CD (250 μ M; 24h) and the effect of whole-cell current density was assessed. Under these conditions, the current density was indistinguishable from that obtained in the absence of β CD; similarly, current density in CHO-*Npc1*^{-/-} cells treated with β CD was also similar to control CHO cells (Figure 4.1.5). The data suggests that β CD prevents the TMEM16A current activation caused by inactivation of NPC1 function. This idea was tested further by *Npc1* re-introduction into CHO-*Npc1*^{-/-} cells *via* stable viral infection. I observed that TMEM16A current density recorded from *Npc1*^{-/-} cells expressing *Npc1* did not differ from the one recorded in WT cells (Figure 4.1.5).

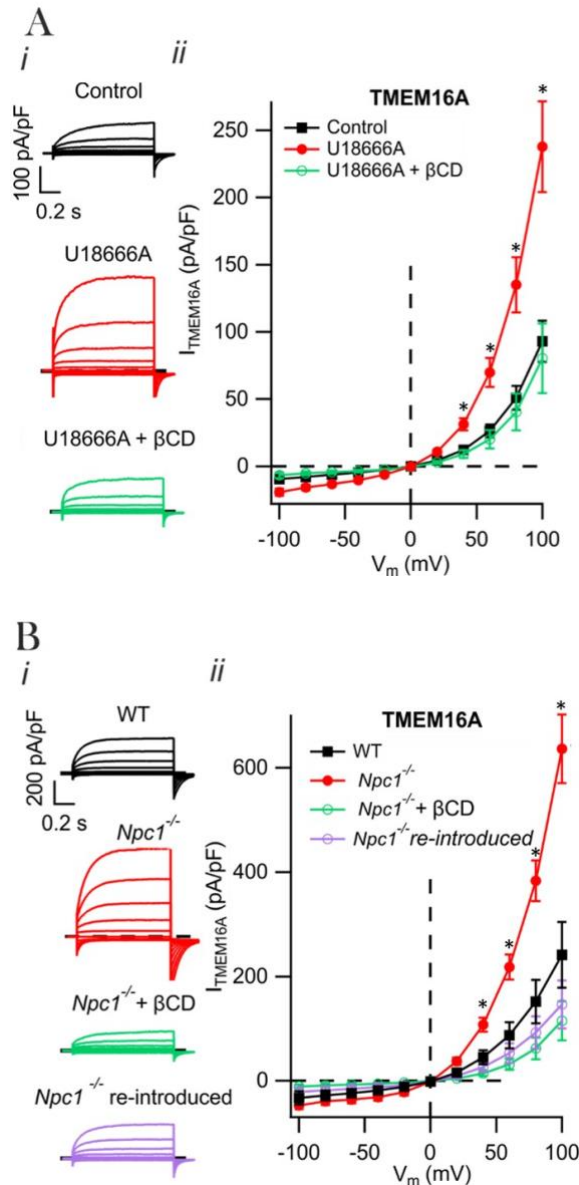


Figure 4.1.5 TMEM16A activation by NPC1 is rescued by β CD treatment or NPC1 re-introduction.

(A) *i*) Whole-cell currents recorded from a TMEM16A expressing HEK-293T cell dialysed with 300 nM $[Ca^{2+}]_i$ in the absence or presence of 5 μ M U18666A alone or with 250 μ M β CD, as indicated; *ii*) mean whole-cell current versus V_m relationships measured at the end of the 1 s voltage pulse from -100 to +100 mV in 20 mV increments in the absence ($n=16$) or presence ($n=18$) of U18666A alone or with 250 μ M β CD ($n=8$). (B) *i*) Whole-cell currents recorded from a WT and $Npc1^{-/-}$ cells in the presence or absence of 250 μ M β CD or $Npc1^{-/-}$ cells where $Npc1$ was re-introduced, as indicated; *ii*) mean whole-cell current versus V_m relationships measured in the WT ($n=15$), $Npc1^{-/-}$ cells ($n=15$), $Npc1^{-/-}$ cells treated with 250 μ M β CD ($n=12$) or $Npc1^{-/-}$ cells where $Npc1$ was re-introduced ($n=12$). Dashed horizontal line represents the zero-current level. Voltage protocol “IV-CaCC” is described in the Methods (Figure 2.5.4.); * indicates $p \leq 0.05$, unpaired *t*-test.

4.1.4 TMEM16A response to $\alpha 1$ adrenergic-receptors is modulated by NPC1

The experiments described above used fixed $[Ca^{2+}]_i$ in the pipette solution achieved *via* a controlled degree of $[Ca^{2+}]_i$ buffering with an appropriate concentration of EGTA (see Methods Section 2.5.5). However, as described in the Introduction (Section 1.8), *in vivo* TMEM16A is activated by a dynamic change in Ca^{2+} in response to G_q PCR activation. To examine whether TMEM16A channel activation by a G_q PCR, is also subjected to modulation by NPC1, the $\alpha 1$ -R was co-expressed with TMEM16A in HEK-293T cells. Whole-cell currents were assessed in the presence or absence of U18666A (control). PE was used to activate the $\alpha 1$ -R. In control conditions, following perfusion of the cell with a solution supplemented with PE, the whole-cell current amplitude increased substantially reaching a peak after ~ 3 s of exposure to PE (Figure 4.1.6). For example, at +95 mV, the TMEM16A current increase was of 3.5 ± 0.8 fold ($n=14$) as a result of exposure to PE ($1 \mu M$) (Figure 4.1.6). In the presence of U18666A, the PE-mediated current increase was enhanced further (Figure 4.1.6); at +95 mV the TMEM16A current increase in the presence of U18666A was of 12.4 ± 3.0 fold ($n=13$) (Figure 4.1.6).

To examine whether the larger TMEM16A current increase involved recruitment of an endogenous current during $\alpha 1$ receptor activation in HEK-293T cells, the specific TMEM16A inhibitor Ani9 ($3 \mu M$) was used. After PE perfusion, Ani9 was added in the presence of PE in cells co-transfected with TMEM16A and the $\alpha 1$ receptor that were exposed to U18666A ($5 \mu M$) for 24h or left untreated (control). In both conditions, Ani9 blocked TMEM16A activation by PE. These data show that NPC1 inhibition enhanced the agonist-induced TMEM16A activation.

To evaluate whether NPC1 inhibition interferes with the function of the $\alpha 1$ receptor, Ca^{2+} release was assessed in cells co-transfected with TMEM16A and the $\alpha 1$ receptor that were exposed to U18666A (5 μM) for 24h or left untreated (control). When PE (10 μM) was applied to HEK-293T cells expressing the $\alpha 1$ -adrenoceptor, an increase in the Fluo-4-AM signal was observed in control cells or cells treated with U18666A. (Figure 4.1.6). There was no difference in the F/F_0 in cells treated with U18666A compared to control. Therefore, the TMEM16A PE-mediated activation during NPC1 inhibition was not dependent on TMEM16A activation by $[\text{Ca}^{2+}]_i$.

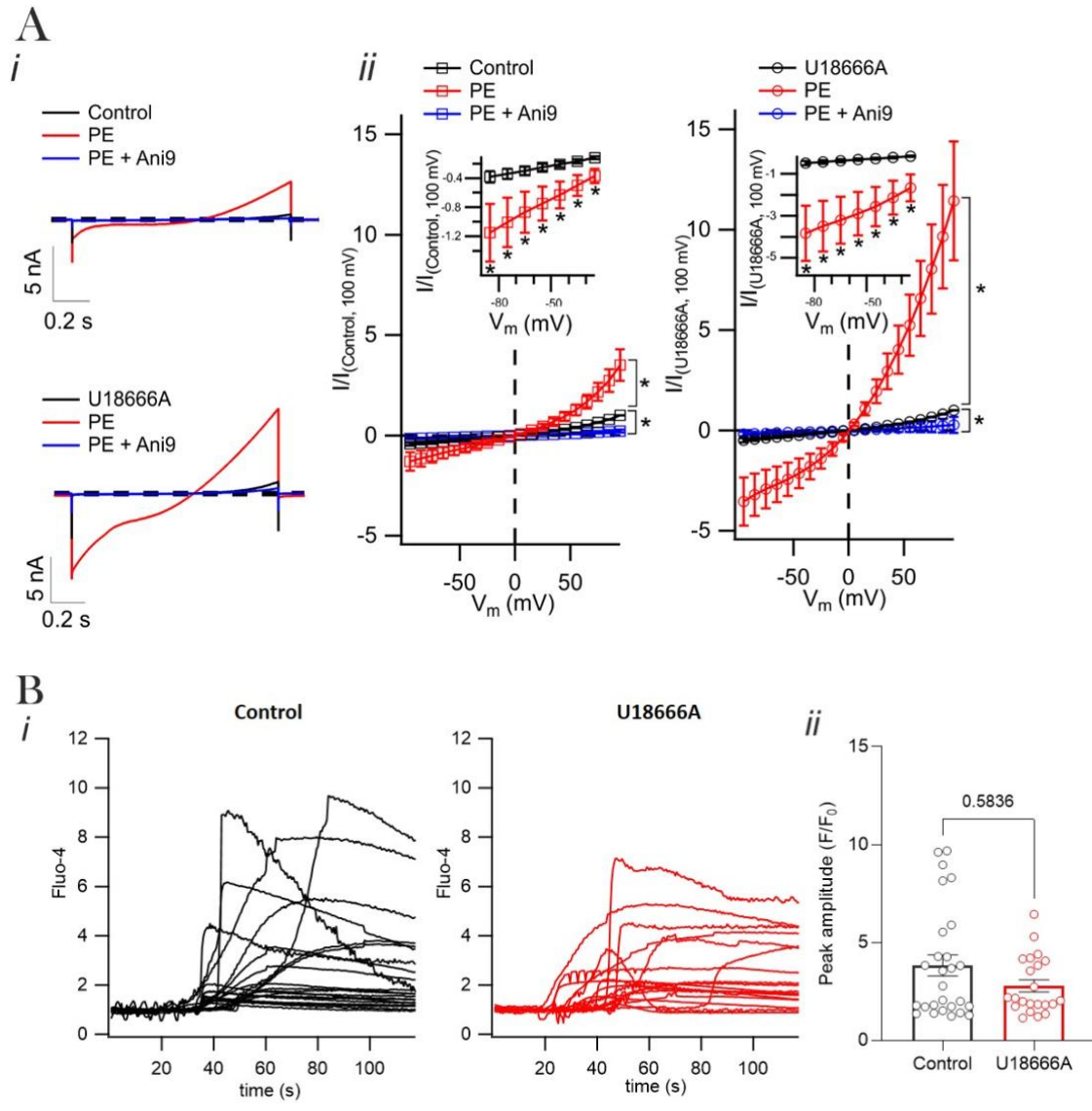


Figure 4.1.6 Activation of TMEM16A current by α_1 -adrenergic receptor activation is enhanced upon NPC1 inhibition

(A) *i*) Whole-cell currents recorded from HEK-293T cells co-expressing TMEM16A and the α_1 adrenergic receptor in the presence or absence of U18666A (5 μM) and Ani9 (3 μM) as indicated. Voltage protocol “IV-Ramp” is described in the Methods (Figure 2.5.4) and intracellular solutions contained low intracellular EGTA. PE (1 μM , red) and Ani9 (3 μM , blue) were added as indicated in control cells or in cells treated U18666A; *ii*) mean whole-cell current versus V_m relationships recorded in control cells in the absence ($n=13$) or presence ($n=13$) of PE alone or with Ani9 ($n=5$); *iii*) mean whole-cell current versus V_m relationships recorded in cells treated with U18666A in the absence ($n=11$) or presence ($n=11$) of 1 μM PE alone or with Ani9 ($n=5$). * indicates $p \leq 0.05$, paired *t*-test. (B) *i*) Individual traces for Fluo-4-AM fluorescence ratios elicited in response to 10 μM PE in the presence ($n=18$) or absence ($n=19$) of μM U18666A; *ii*) mean fluorescence Fluo-4-AM peak F/F_0 from control cells ($n=30$) or cells treated with 5 μM U18666A ($n=27$) in response to 10 μM PE. * indicates $p \leq 0.05$, unpaired *t*-test.

4.1.5 TMEM16A gating is affected during NPC1 inhibition

As described in more details in the Method (Section 2.5.6), the amplitude of the whole-cell TMEM16A current (I) is given by the product of the number of channels in the membrane (N), the channel open probability (P_o), and the single-channel current (i) as $I = NP_o i$ (Eq. 16). We argued that the increase in TMEM16A current during NPC1 inhibition described above, should involve modulation of one or more of these parameters. Thus, I utilised non stationary noise analysis to simultaneously assess changes in N , i and P_o of TMEM16A channels in the absence and presence of NPC1 inhibition. In these experiments, cells with comparable current density of 70.63 ± 10.1 pA/pF ($n=10$, control) and 94.2 ± 16.2 pA/pF ($n=10$, U18666A), were used to ensure comparable levels of signal to background noise in the two conditions. The analysis revealed that P_o was increased during cell treatment with U18666A (5 μ M, 24h), while the single channel conductance was unchanged and consequently the number of channels *per* pF (channel density) was slightly reduced to give rise to current densities of similar amplitude before and after NPC1 inhibition.

It was argued that if NPC1 inhibition affects TMEM16A gating (i.e. increase in P_o), mutant forms of the TMEM16A channel in which the transmembrane helix 6 (TM6) gate is biased in the open state may not be susceptible to this modulation. Thus, I studied the effects of U18666A (5 μ M, 24h) on TMEM16A mutant channels where the TM6 steric gate is constitutively open, even in the absence of $[Ca^{2+}]_i$. These mutant channels have isoleucine 637 or glutamine 645 substituted with an alanine and were termed TMEM16A-I637A and TMEM16A-Q645A, respectively. Figure 4.1.7 demonstrates that the TMEM16A-I637A and TMEM16A-Q645A current densities were not affected by NPC1 inhibition at all V_m tested. Thus, removal of the main TMEM16A gating component abolished the U18666A-mediated current increase suggesting that NPC1 inhibition may interfere with that gating of the TM6 of TMEM16A.

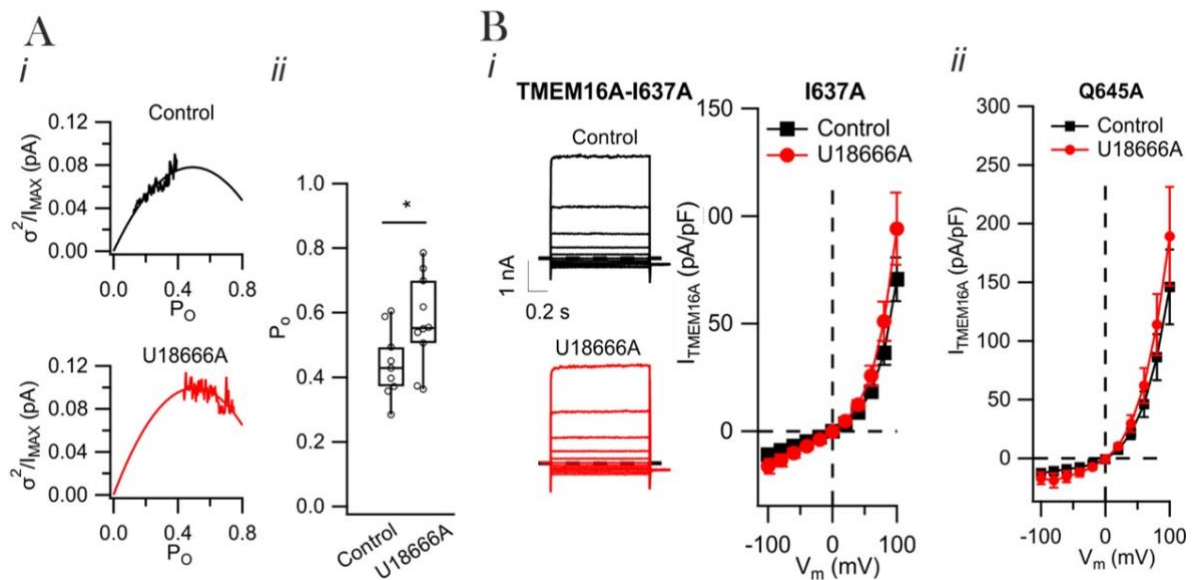


Figure 4.1.7 TMEM16A channel gating is modulated by NPC1 inhibition

(A) i) Whole-cell stationary noise analysis recorded from TMEM16A expressing HEK-293T cells in the absence and presence of U18666A (5 μ M). $[Ca^{2+}]_i$ was 600 nM and V_m was +70 mV. The parabolic line is the best simultaneous fit of the data using Equation 17; ii) mean P_o obtained from stationary noise analysis in cells exposed to vehicle ($n=10$) or U18666A ($n=10$). (B) i) Whole-cell currents recorded from TMEM16A-I637A expressing HEK-293T cells in the presence of 0 $[Ca^{2+}]_i$. Mean whole-cell current versus V_m relationships measured at the end of the 1 s voltage pulse from -100 to +100 mV in 20 mV increments in the absence ($n=10$) or presence ($n=14$) of 5 μ M U18666A; ii) mean whole-cell current versus V_m relationships measured in TMEM16A-Q645A transfected HEK-293T cells in the absence ($n=12$) or presence ($n=8$) of 5 μ M U18666A. Dashed horizontal line represents the zero-current level. Voltage protocol “IV-CaCC” is described in the Methods (Figure 2.5.4.) * indicates $p \leq 0.05$, unpaired *t*-test.

4.2 Sphingosine does not affect in TMEM16A activation by NPC1

To address the mechanism underlying the change in TMEM16A gating during NPC1 inhibition, we investigated if the primary lipid stored in the NPC pathogenic cascade could affect TMEM16A activity. Sphingosine is the first lipid stored in the endosolysosomes after treatment with U18666A (Lloyd-Evans, Morgan et al. 2008). Thus, I asked if sphingosine could be responsible for activating TMEM16A during NPC1 inhibition. I investigated the direct effect of sphingosine on TMEM16 by exposing inside-out patches excised from TMEM16A expressing HEK-293T cells to increasing doses of sphingosine. In these experiments, V_m was kept constant at +70mV and $[Ca^{2+}]_i$ was 600 nM, in order to induce half-maximal TMEM16A activation (Ta, Acheson et al. 2017). I found that TMEM16A activity was not altered by sphingosine concentrations ranging from 0.1 to 10 μ M (Figure 4.2.1). This result indicates that sphingosine may not be primarily involved in the regulation of the TMEM16A channel by NPC1.

In order to study if sphingosine metabolism could modulate TMEM16A current, we incubated cells with either the ceramidase inhibitor, ceranib (0.4 μ M), or the sphingosine kinase 1 inhibitor, PF-543 (0.1 μ M) (Figure 4.2.1). With either treatment, in whole-cell patch-clamps where $[Ca^{2+}]_i$ was 300 nM, TMEM16A current was unchanged in the presence or absence of either ceranib or PF-543 (Figure 4.2.1). These results further exclude a direct modulation of TMEM16A by sphingosine when NPC1 is inhibited.

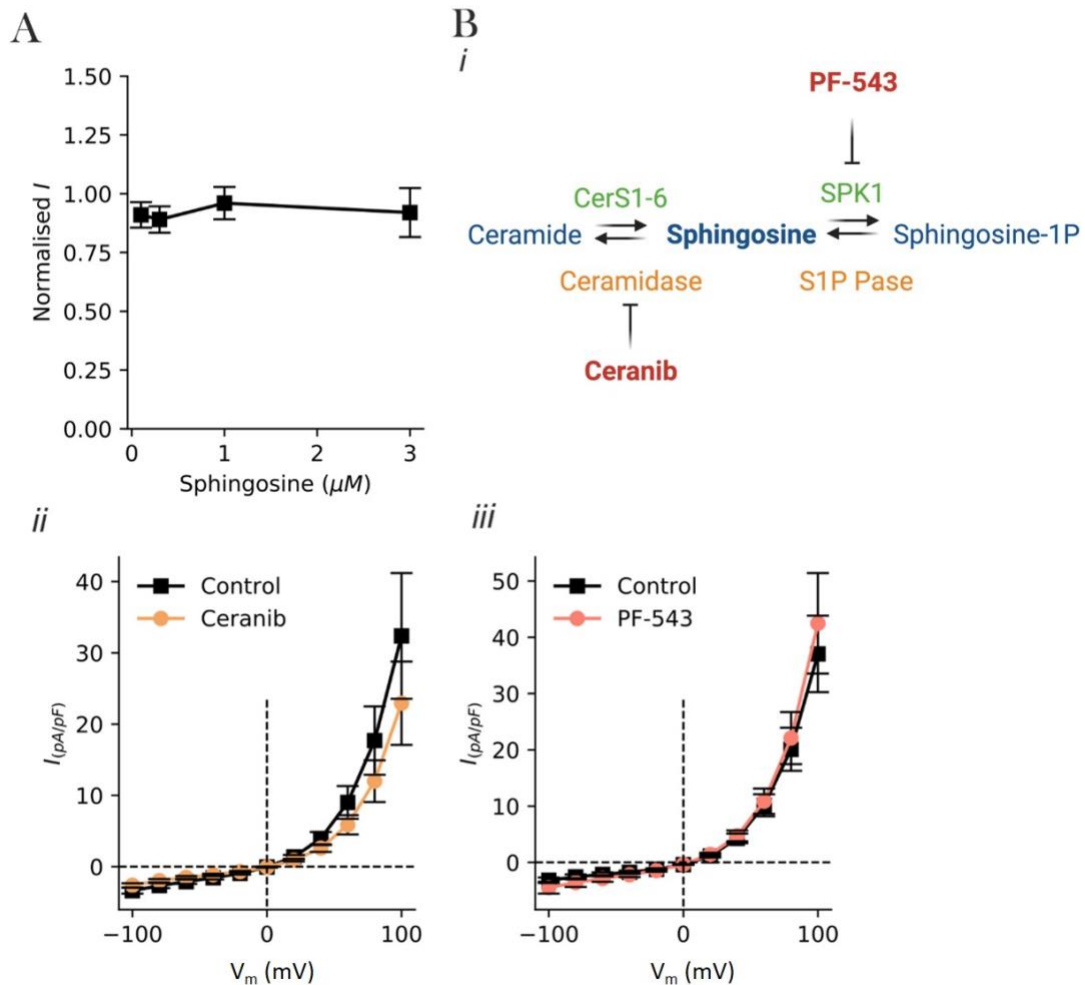


Figure 4.2.1 Spingosine secondary effect on TMEM16A activation.

(A) TMEM16A currents recorded in inside-out patches excised from HEK-293T cells to [spingosine] (μM), as indicated. The voltage was maintained at +70 mV for the whole duration of the recordings. Mean current versus [spingosine] relationship measured at +70 mV and normalised to the current measured in the highest [spingosine] concentration ($n=5-6$). (B) *i*) Diagrammatic illustrations of the pathways involving ceranib and PF-543; ceramidase synthase (CerS1-6), sphingosine kinase 1 (SPK1), sphingosine 1 phosphatase (S1P); *ii*) whole-cell currents were recorded in TMEM16A-transfected HEK-293T cells with the “IV-CaCC” protocol in the presence of $0.3 \mu\text{M}$ $[\text{Ca}^{2+}]_i$; mean whole-cell current versus V_m relationships recorded in the absence ($n=12$) or presence ($n=13$) of $0.4 \mu\text{M}$ ceranib; *iii*) mean whole-cell current versus V_m relationships recorded in the absence ($n=17$) or presence ($n=18$) of $0.1 \mu\text{M}$ PF-543. Dashed horizontal line represents the zero-current level. Voltage protocol “IV-CaCC” is described in the Methods (Figure 2.5.4.)

4.3 The action of NPC1 on the TMEM16A channel involves PIP₂

Based on the notion that sphingosine is not the primary lipid responsible for directly activating TMEM16A current during NPC1 inhibition, I then examined if the potent TMEM16A activator PIP₂ might be involved in this mechanism. We argued that changes in PIP₂ levels might underlie the change in current density since (i) TMEM16A is highly sensitive to PIP₂ (Ta, Acheson et al. 2017), (ii) PIP₂ cellular distribution is dynamically regulated by the lysosomes (Ebner, Koch et al. 2019) and (iii) PIP₂ plasmalemmal levels are altered when NPC1 is inhibited (Vivas, Tiscione et al. 2019).

To ensure that the heterologous model used in this project was suitable to study the direct modulation of PIP₂ on the TMEM16A channel, the water soluble PIP₂ analogue diC8-PIP₂ was tested. Inside-out patches were excised from HEK-293T cells expressing TMEM16A and perfused with diC8-PIP₂. The V_m was kept constant at +70 mV and $[Ca^{2+}]_i$ was 600 nM. When the excised patch was perfused with increasing doses of diC8-PIP₂ in a range from 0.3 to 100 µg/mL, TMEM16A current increased up to ~ 2 fold when the patch was perfused with 100 µg/mL (n=10) (Figure 4.3.1). The inside-out patch clamp configuration allowed me to assess the direct effect of exogenous diC8-PIP₂ on the TMEM16A channel independent from intracellular components.

The *danio rerio* voltage phosphatase (DrVSP) was used to deplete PIP₂ from the plasma membrane. This was to establish the conditions to obtain plasma membrane depletion of PIP₂ as previously shown (Ta, Acheson et al. 2017). DrVSP is a protein localised at the plasma membrane, which when activated by depolarizing voltages depletes membrane-localised PIP₂ content (Okamura et al. 2009). In cells co-expressing TMEM16A and DrVSP, the TMEM16A current was reduced after DrVSP activation at +100 mV (Figure 4.3.1). Additionally, I co-transfected HEK-293T cells with TMEM16A and the mutant DrVSP where the PIP₂

dephosphorylating domain was rendered inactive by cysteine replacement in position 302 with a serine (DrVSP (C302S)) to inactivate the phosphatase activity (Imai et al. 2012). In HEK-293T cells co-expressing TMEM16A and DrVSP(C302S), the elicited current was unaffected by the depolarising step from -100 mV to +100 mV (Figure 4.3.1). These results indicate that PIP₂ is a potent activator of the TMEM16A channel in accordance with the literature (Ta, Acheson et al. 2017).

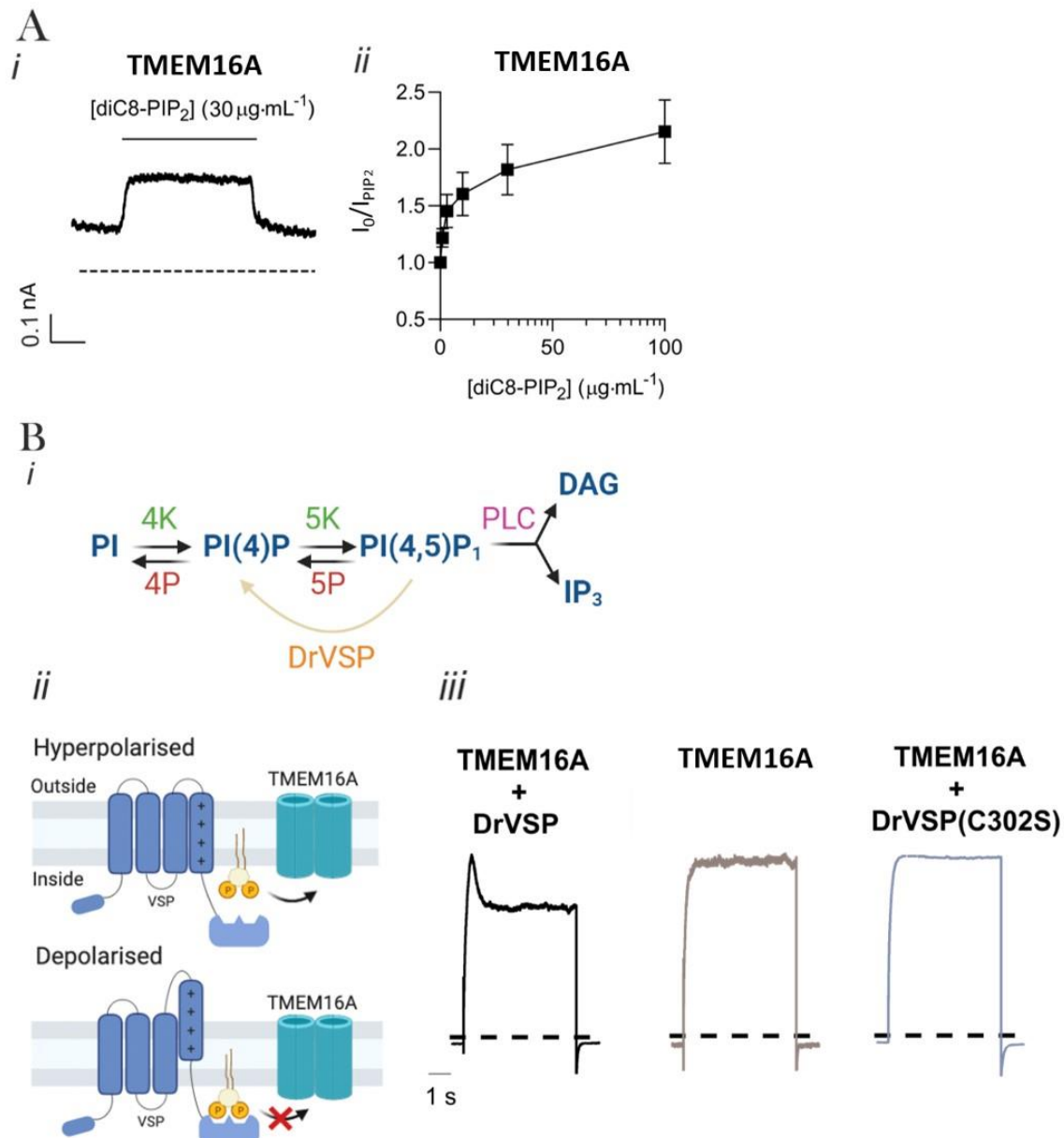


Figure 4.3.1 TMEM16A current is activated by diC8-PIP₂ and reduced by PIP₂ depletion

(A) *i*) Inside-out current recorded from TMEM16A-expressing HEK-293T excised patches. diC8-PIP₂ (30 μg/mL) was applied to the intracellular side of the patch, as indicated by the horizontal bar. V_m was maintained at +70 mV for the duration of the recordings in the presence of 600 nM [Ca²⁺]_i. Dashed lines represent zero-current levels; *ii*) mean current versus [diC8-PIP₂] relationships expressed relative to the current measured in the absence of diC8-PIP₂ ($n=10$). (B) *i*) Diagrammatic representation of the pathway involved in PIP₂ depletion by DrVSP; *ii*) diagrammatic representation of the mechanism of PIP₂ dephosphorylation by DrVSP. At hyperpolarised V_m the catalytic domain of DrVSP does not interact with PIP₂, upon depolarisation, PIP₂ hydrolysis occurs; *iii*) effects of DrVSP or DrVSP(C302S) on the kinetics of TMEM16A. Currents were recorded in the presence of 0.3 μM [Ca²⁺]_i in response to the ‘IV-Step’ protocol described in Method (Section 2.5.4.3).

4.3.1 DrVSP-mediated PIP₂ depletion prevents NPC1 modulation of TMEM16A

The experiment illustrated above confirmed that PIP₂ is a potent activator of the TMEM16A current. It was then investigated whether the increased in TMEM16A-current induced by NPC1 inhibition (Section 4.1.2) could be mediated by PIP₂. In order to do so, I co-transfected HEK-293T cells with TMEM16A and DrVSP. Whole-cell TMEM16A current was studied in response to PIP₂ depletion in HEK-293T cells in the presence or absence (control) of U18666A. As shows in the diagrammatic illustration of the stimulation protocol (Figure 4.3.2) a pre-pulse from -100 mV to +100 mV was used to activate DrVSP to deplete plasmalemmal PIP₂ (Figure 4.3.2). The pre-pulse then enabled the study of whole-cell TMEM16A currents in the absence of PIP₂. I observed that TMEM16A steady-state current upon PIP₂ depletion was unchanged in the presence or absence of U18666A in HEK-293T cells (Figure 4.3.2). At +100 mV TMEM16A current after PIP₂ depletion was 26.9 ± 4.5 pA/pF in control cells and 22.1 ± 5.2 pA/pF in cells treated with U18666A ($p > 0.05$) (Figure 4.3.2).

I then co-transfected HEK-293T cells with TMEM16A and the mutant DrVSP(C302S). In these cells, the TMEM16A current density was potentiated by inhibition of NPC1 with U1866A, reinforcing the hypothesis that PIP₂ is required for NPC1-mediated activation of TMEM16A channels (Figure 4.3.2).

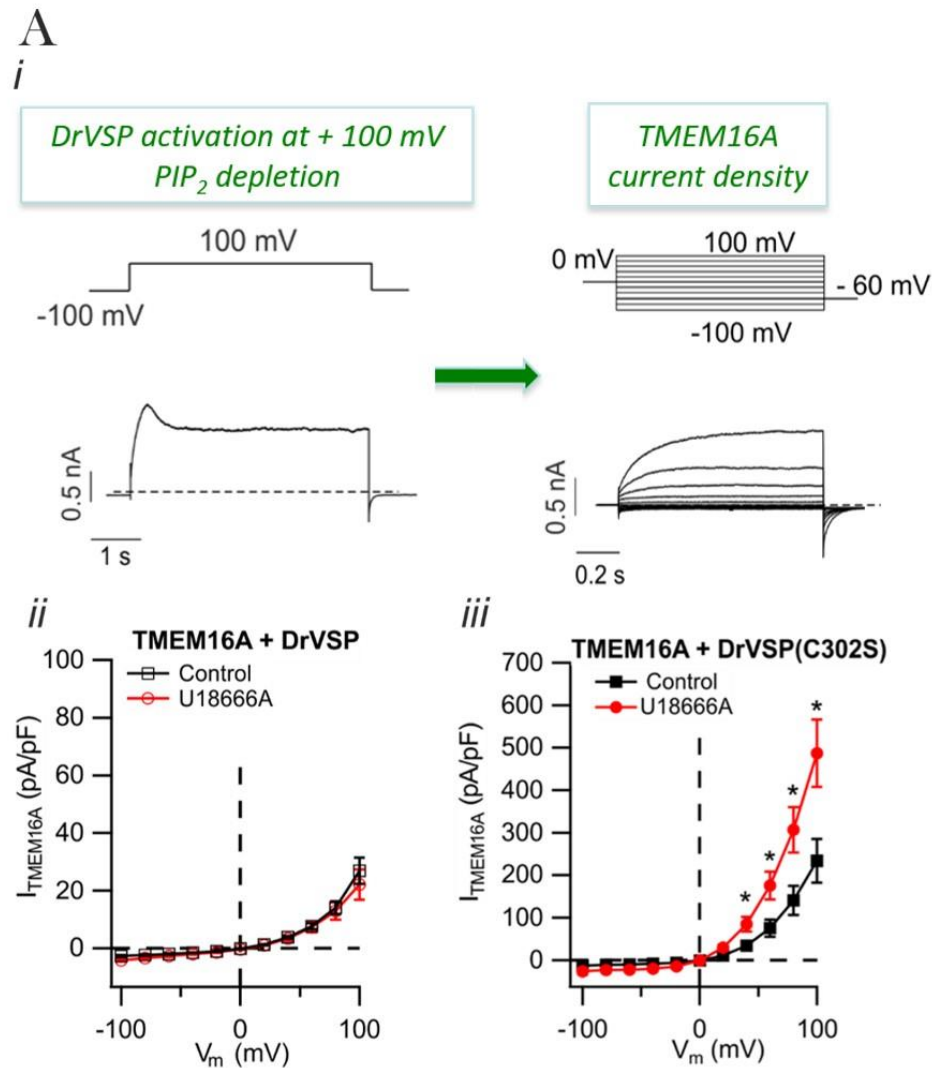


Figure 4.3.2 PIP₂ depletion by DrVSP abolishes NPC1 activation of TMEM16A current

(A) *i*) Protocol steps for activation of DrVSP with a pre-pulse of +100 mV followed by the IV-CaCC protocol for assessing TMEM16A current density; *ii*) mean whole-cell current versus V_m relationships recorded in the absence ($n=13$) or presence ($n=13$) of U18666A from HEK-293T cells co-expressing TMEM16A and DrVSP; *iii*) mean whole-cell current versus V_m relationships recorded in the absence ($n=10$) or presence ($n=9$) of U18666A from HEK-293T cells co-expressing TMEM16A and DrVSP(C302S). Dotted black and red lines indicate TMEM16A current recorded from control and U18666A-treated cells. Currents were recorded in the presence of $0.3 \mu\text{M} [\text{Ca}^{2+}]_i$ in response to the 'IV-CaCC' protocol described in Method (Section 2.5.4.2). * indicates $p \leq 0.05$, unpaired *t*-test.

4.3.2 Scavenging PIP₂ with neomycin prevents NPC1 modulation of TMEM16A

The effect of neomycin, which binds with high affinity to PIP₂ thus effectively preventing its action on the channel (Suh and Hille 2007, Xie, John et al. 2008), was also tested. The intracellular pipette solution was supplemented with neomycin (1 mM) during whole-cell recordings in HEK-293T cells transfected with TMEM16A. I observed that in the presence of neomycin there was no difference in TMEM16A steady-state current in the presence or absence of the NPC1 inhibitor U18666A. For example, at +100 mV, with neomycin in the intracellular pipette solution, TMEM16A current was 43.8±8.9 pA/pF in control cells and 41.0±9.7 pA/pF in cells treated with U18666A ($p>0.05$) (Figure 4.3.3).

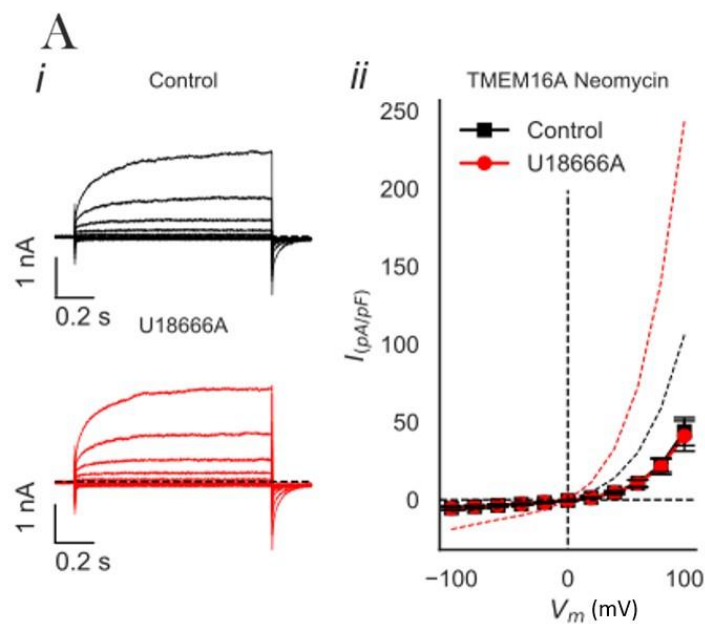


Figure 4.3.3 Neomycin sequesters PIP₂ blocking TMEM16A current activation by NPC1

(A) i) Whole-cell currents recorded from a HEK-293T cell expressing TMEM16A dialysed with 300 nM [Ca²⁺]_i in the absence or presence of U18666A alone or with neomycin (1 mM); ii) mean whole-cell current versus V_m relationships measured at the end of the 1 s voltage pulse from -100 to +100 mV in 20 mV increments in the absence ($n=8$) or presence ($n=11$). Dotted black and red lines indicate TMEM16A current recorded from control and U18666A-treated cells in the absence of neomycin (Figure 2.5.4.2). Currents were recorded in the presence of 0.3 μ M [Ca²⁺]_i in response to the 'IV-CaCC' protocol described in Method (Section 2.5.4.2). Unpaired t -test.

4.3.3 A PIP₂-insensitive TMEM16A mutant channel is also insensitive to NPC1

To further confirm that PIP₂ is involved in the modulation of TMEM16A by NPC1, I mutated a key residue proposed in the binding sites of TMEM16A to PIP₂ (Le, Jia et al. 2019). I mutated the basic residues R482 essential for maintaining the open state of TMEM16A by PIP₂ to an alanine (R482A) (Le, Jia et al. 2019). I then confirmed that the TMEM16A-R482A mutant channel is insensitive PIP₂. This experiment was conducted by co-transfecting HEK-293T cells with the TMEM16A-R482A mutant channel and DrVSP. I showed that the whole-cell TMEM16A-R482A current was not altered by activation of DrVSP and PIP₂ depletion (Figure 4.3.4). In the presence or absence of the NPC1 inhibitor U18666A, the TMEM16A current recorded from WT TMEM16A channels was not different from the one recorded in cells expressing the TMEM16A-R482A mutant channel (Figure 4.3.4). For example, in the TMEM16A-R482A mutant channel, at +100 mV, the current recorded was 87.8±18.6 pA/pF (n=21) in control cells and 69.2±18.4 pA/pF (n=20) in cells treated with the U18666A ($p>0.05$) (Figure 4.3.4).

To further understand how PIP₂ can modulate TMEM16A current during NPC1 inhibition, I reduced PIP₂ degradation by inhibiting PLC with edelfosine (10 μM, 30 min) (Suenami, Iino et al. 2018). It was hypothesised that PLC inhibition by edelfosine would raise plasmalemmal PIP₂ levels, hence activating TMEM16A current. In HEK-293T cells expressing WT TMEM16A channels, edelfosine application enhanced TMEM16A current to a similar extent of NPC1 inhibition (2-fold) (Figure 4.3.5). In contrast, in cells expressing the PIP₂-insensitive TMEM16A(R482A) channels, edelfosine treatment did not alter the TMEM16A current properties (Figure 4.3.5). These data further support that PIP₂ is a major modulator of TMEM16A-NPC1 regulation.

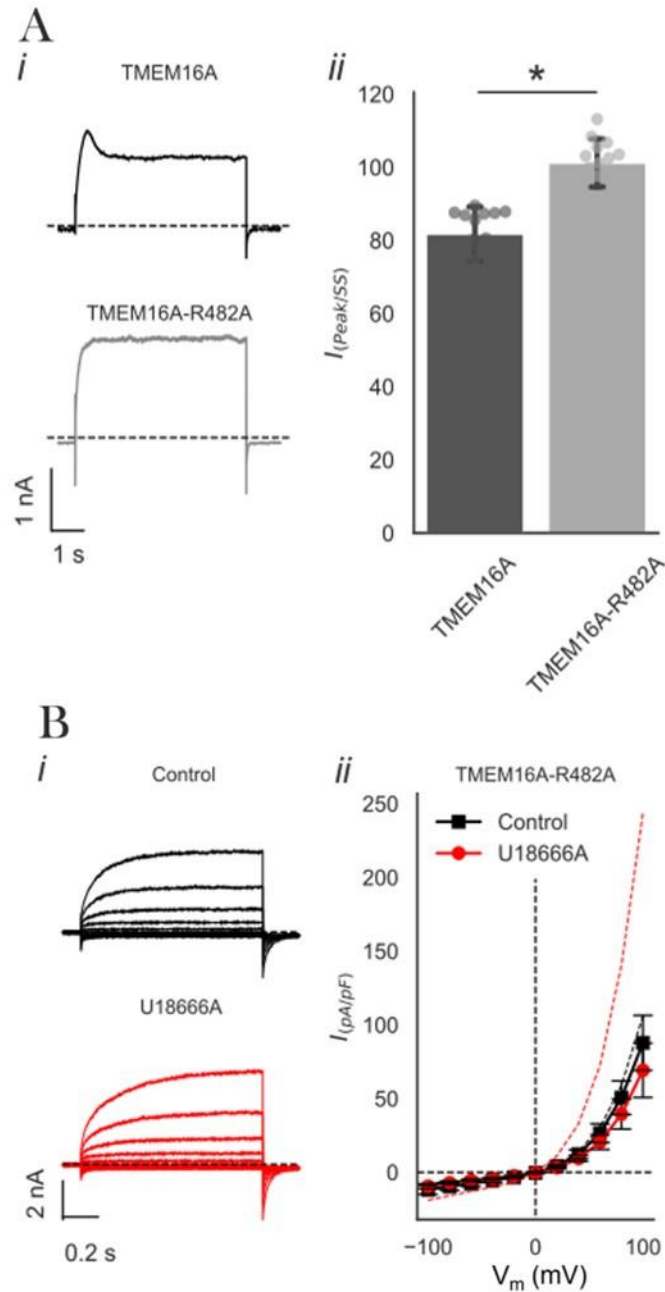


Figure 4.3.4 TMEM16A-R482A mutant channel is not modulated by NPC1 inhibition

(A) *i*) Whole-cell currents recorded from HEK-293T cells expressing TMEM16A or TMEM16A-R482A in response to the “IV-steps” voltage protocol; *ii*) mean TMEM16A ($n=13$) or TMEM16A-R482A ($n=13$) normalised current. Peak currents were normalised to the steady-state current. (B) *i*) Whole-cell currents recorded from HEK-293T cells expressing TMEM16A-R482A in the presence or absence of 5 U18666A; *ii*) mean whole-cell current versus V_m relationships recorded in the absence ($n=21$) or presence ($n=20$) of U18666A from HEK-293T cells expressing TMEM16A-R482A. Dotted black and red lines indicate WT TMEM16A current recorded from control and U18666A-treated cells. Currents were recorded in the presence of $0.3 \mu\text{M} [\text{Ca}^{2+}]_i$ in response to the ‘IV-CaCC’ protocol described in Method (Section 2.5.4.2). * indicates $p \leq 0.05$, unpaired t -test.

A
i

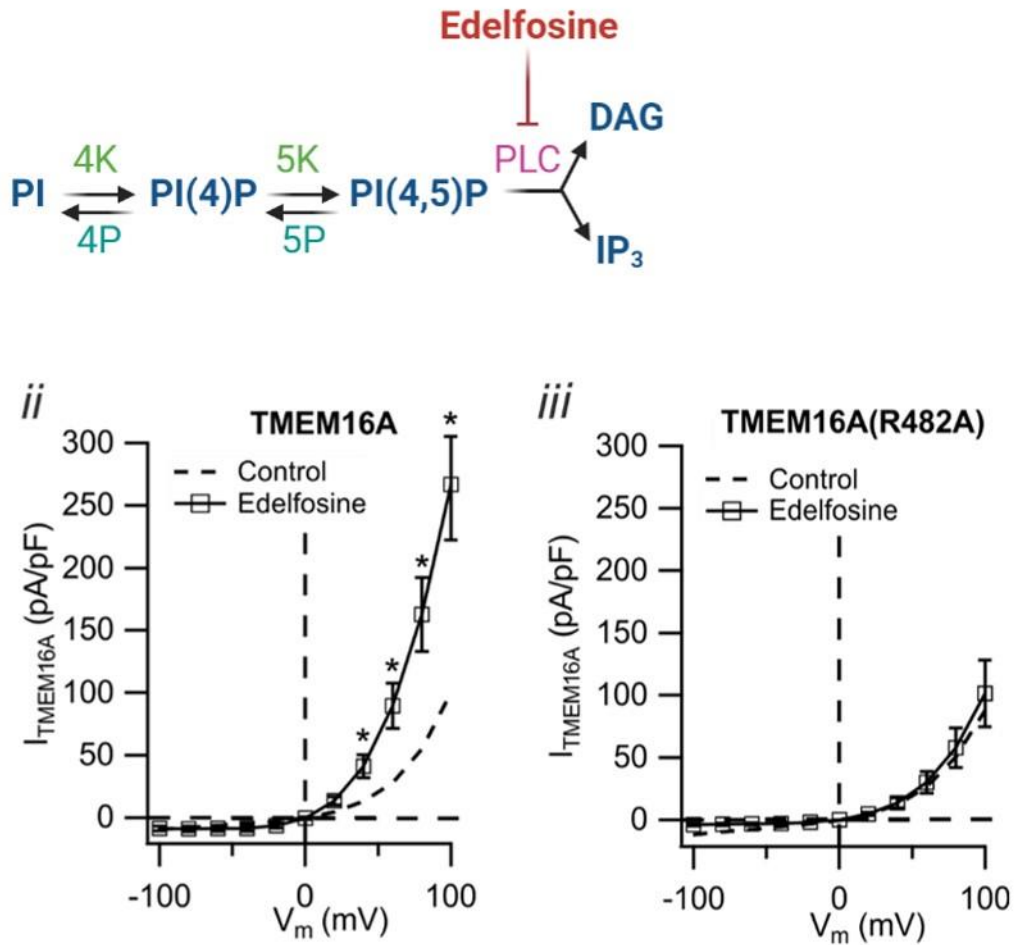


Figure 4.3.5 Block of PLC with edelfosine enhances TMEM16A currents

(A) i) Diagrammatic representation of edelfosine mechanism of action; ii) mean whole-cell current versus V_m relationships recorded in the presence of 10 μM edelfosine from HEK-293T cells expressing TMEM16A ($n=6$); iii) mean whole-cell current versus V_m relationships recorded in the presence of 10 μM edelfosine from HEK-293T cells expressing TMEM16A(R482A) ($n=9$). Currents were recorded in the presence of 0.3 μM $[\text{Ca}^{2+}]_i$ in response to the 'IV-CaCC' protocol described in Method (Section 2.5.4.2). * indicates $p \leq 0.05$, unpaired t -test.

4.3.4 Plasmalemmal PIP₂ level is increased during NPC1 inhibition

To elucidate the role of PIP₂ in TMEM16A regulation by NPC1, I investigated if the distribution of PIP₂ at the plasma membrane, is altered during NPC1 inhibition. I labelled PIP₂ by transfecting HEK-293T cells with a cyan fluorescent protein (CFP) fused to the pleckstrin homology (PH) domain of PLC δ 1 that specifically binds to PIP₂ (Tuzi, Uekama et al. 2003, van Leeuwen, Vermeer et al. 2007). The plasma membrane was stained by using a lipophilic membrane stain (Dil) that is weakly fluorescent until incorporated into membranes (Yektaeian, Mehrabani et al. 2019). I observed that PIP₂ overlap with the plasma membrane increased in the presence of the NPC1 inhibitor U18666A. Specifically, the mean Mander's coefficient (M1) increased from 0.54 ± 0.0 in control cells to 0.64 ± 0.01 (n=68) in the presence of U18666A (n=68) (p=0.0006) (Figure 4.3.6).

Since I showed that β CD can rescue both cholesterol accumulation in the endocytic system and TMEM16A activation, I then tested if β CD acts by correcting PIP₂ at the plasma membrane. In HEK-293T cells incubated with β CD (250 μ M, 48h), the M1 coefficient was similar to control cells. This indicates that the molecular mechanism of TMEM16A activation upon NPC1 inhibition is relying on more PIP₂ distributed at the plasma membrane.

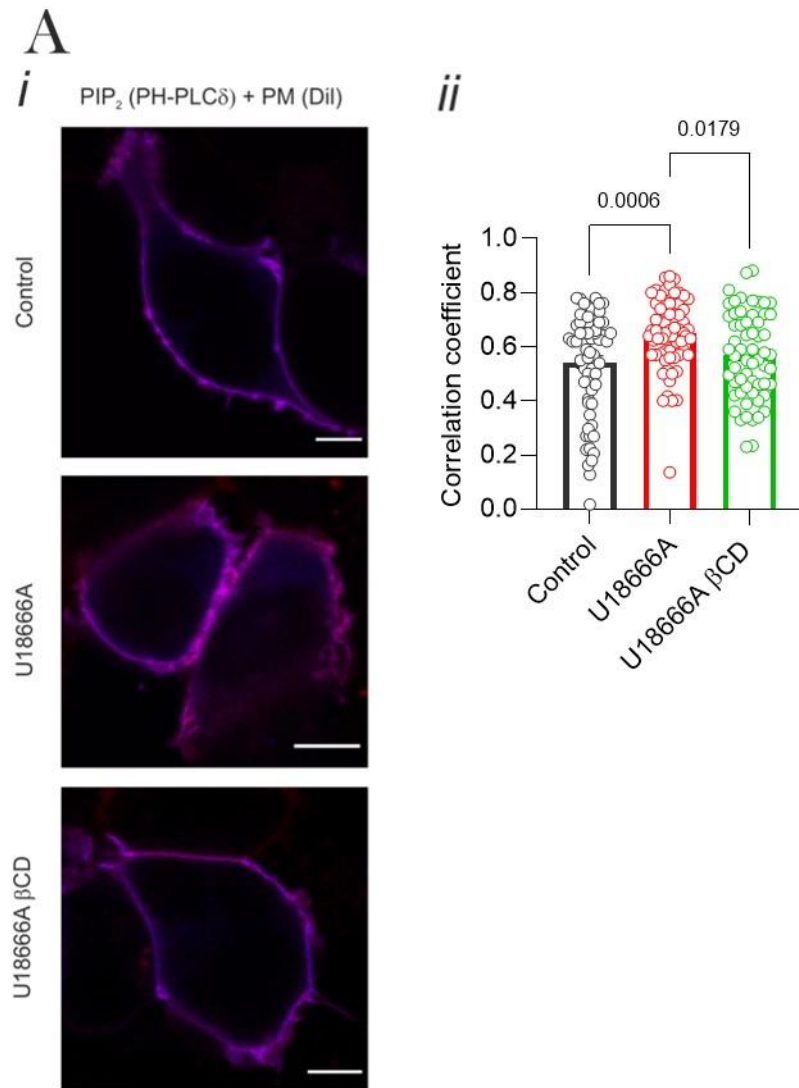


Figure 4.3.6 PIP₂ cellular distribution is increased at the plasma membrane during NPC1 inhibition

(A) *i*) Live HEK-293T cells transfected with the PIP₂ sensor PH-PLC δ (blue) and stained with the plasma membrane (PM) marker Dil (red). In the merged panel the degree of PIP₂ and PM overlap is shown (pink). Scale bar is 10 μ m; *ii*) Mean correlation coefficient between PH-PLC δ and Dil signal for cells in the presence or absence of U18666A ($n=59-69$). Unpaired *t*-test.

4.4 TMEM16A modulation by NPC1 is not affected by the KCNE1 auxiliary subunit

The potassium voltage-gated channel subfamily E member 1 (KCNE1) protein, is a component of the K_v7 potassium channels. KCNE1 has recently been shown to also combine with and modulate the function of the TMEM16A channel (Prado et al. 2021). The association of KCNE1 with TMEM16A was demonstrated both in recombinant overexpression and in native cells (Ávalos Prado, Häfner et al. 2021). In K_v channels, KCNE1 forms part of cholesterol and PIP_2 binding sites (Coyan, Abderemane-Ali et al. 2014, Dvir, Strulovich et al. 2014). Thus, I explored the possibility that KCNE1 also participates to the lipid sensitivity of the TMEM16A channel. Co-expression of KCNE1 and TMEM16A in HEK-293T cells led to a ~ 4.5 fold increase in TMEM16A current density, consistent with the notion that KCNE1 has an activation effect on TMEM16A (Prado et al. 2021) (Figure 4.4.1). Incubation of these co-transfected cells with U18666A (5 μ M, 24 h) lead to a further ~2 fold increase on the current, comparable to that seen in the absence of KCNE1, thus indicating that KCNE1 is not involved in the NPC1-induced activation of the TMEM16A channel (Figure 4.4.1).

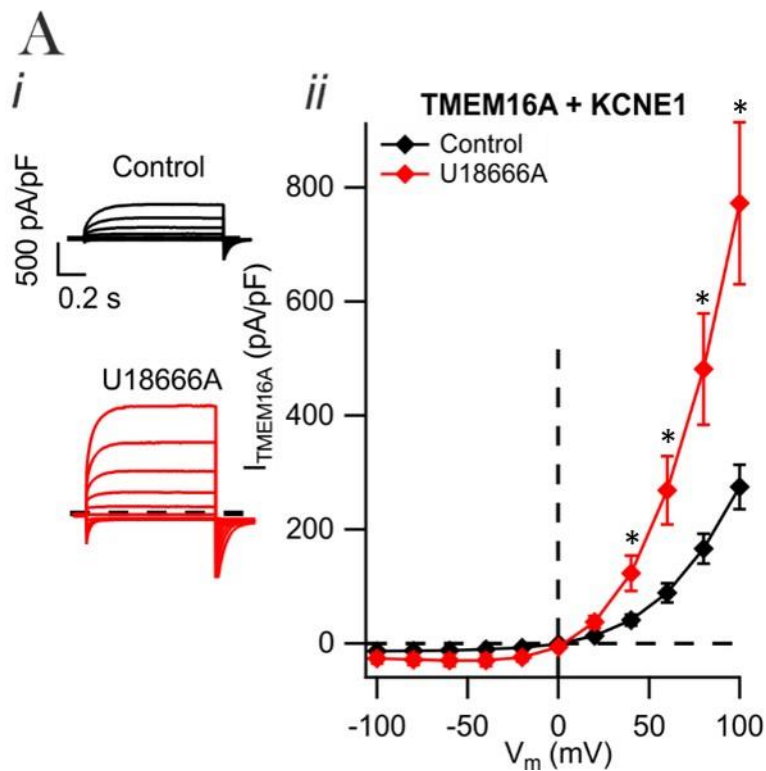


Figure 4.4.1 The TMEM16A auxiliary subunit KCNE1 does not regulate the channel modulation by NPC1.

(A) i) Whole-cell currents recorded from a HEK-293T cell expressing TMEM16A-KCNE1 dialysed with 300 nM $[Ca^{2+}]_i$ in the absence or presence of U18666A. Dashed horizontal line represents the zero-current level. Voltage protocol “IV-CaCC” is described in the Methods (Section 2.5.4.2); ii) mean whole-cell current versus V_m relationships measured at the end of the 1 s voltage pulse from -100 to +100 mV in 20 mV increments in the absence ($n=6$) or presence ($n=10$) of U18666A * indicates. $p \leq 0.05$, unpaired t-test

4.5 Discussion

The TMEM16A channel pore was shown to be partially accessed by plasmalemmal lipids (Paulino, Kalienkova et al. 2017) and modulated by a variety of lipids such as PIP₂ and DHA (De Jesus-Perez, Cruz-Rangel et al. 2018). The NPC1 lysosomal protein is a pivotal regulator of lipid trafficking (Davies, Chen et al. 2000) and mutations in this protein cause a genetic lysosomal disorder associated with impaired lipid homeostasis, NPC (Carstea, Morris et al. 1997). This chapter demonstrates that the TMEM16A-mediated currents recorded from cells where NPC1 is not functional are significantly enhanced compared to control cells with normal NPC1 activity.

Cells where NPC1 was pharmacologically inhibited or genetically deleted were identified as suitable models of altered lipid homeostasis as reported in the literature (Du, Lukmantara et al. 2017, Vivas, Tiscione et al. 2019). NPC1 inhibition was found to increase TMEM16A currents specifically, as it had no effect on the two other TMEM16 family members TMEM16B and TMEM16F. The cellular distribution of TMEM16A and the other two family members was found to not be altered during NPC1 inhibition. TMEM16A modulation by NPC1 was abolished by treating cells with β CD, a drug in clinical trials for NPC disease (Coisne, Tilloy et al. 2016), or by genetic re-introduction of the NPC1 protein. A direct role of sphingosine to activate TMEM16A was excluded, as exogenous sphingosine application or interference with sphingosine metabolism pathways did not produce any effect on TMEM16A activity. TMEM16A modulation by NPC1 occurred in response to α 1 adrenergic receptor stimulation, indicating that endogenous modulators of TMEM16A can activate the channel during NPC1 inhibition. PIP₂ was shown to be a major regulator of TMEM16A activation by NPC1. I also demonstrate that NPC1 inhibition can increase PIP₂ levels which can be rescued by β CD, an agent that modulates membrane-cholesterol levels, which are affected upon NPC1 inhibition (Taglieri, Delfin et al. 2013, Chun and Chung 2020). Moreover, expression of the TMEM16A

auxiliary subunit KCNE1 (Ávalos Prado, Häfner et al. 2021) did not alter TMEM16A modulation by NPC1. Overall, the main findings of this chapter were that TMEM16A activity is enhanced by NPC1 inhibition by increased levels of plasmalemmal PIP₂ and thus, affecting the channel response to PIP₂.

4.5.1 TMEM16A current is activated by NPC1 inhibition

It is widely accepted that loss of function in the NPC1 lysosomal protein causes impaired lipid homeostasis by inducing a block in the endolysosomal lipid trafficking (Platt 2018). This results in accumulation of unesterified cholesterol, which appears as intracellular lipid inclusions (Cenedella 2009). I demonstrated that NPC1 inhibition with the specific NPC1 inhibitor U18666A (Lu, Liang et al. 2015) or genetic deletion of the *Npc1* locus (Carstea, Morris et al. 1997) resulted in accumulation of filipin-stained vesicles compared to control cells with normal NPC1 activity. In both cell models of NPC1 inhibition, I found that TMEM16A current in the whole-cell mode of patch-clamp recordings was significantly increased. I demonstrated that among some members of the TMEM16 family (TMEM16B and TMEM16F) this effect is specific to TMEM16A. It was recently reported that in the OSC19 cell line model of human squamous cell carcinoma overexpressing TMEM16A, lysosomal number and acidic vesicles are increased together with an increase in their area and perimeter (Vyas, Gomez-Casal et al. 2022). This data is in accordance with our discovery that TMEM16A is enhanced during NPC1 inhibition, where lysosomes are also enlarged and accumulating in number due to impairment in endolysosomal fusion and trafficking (Lloyd-Evans, Morgan et al. 2008).

4.5.2 TME161A activation by NPC1 inhibition can be corrected by β CD and *Npc1* re-introduction

In accordance with data in the literature reporting that treatment with β CD can normalise cholesterol levels in cells where NPC1 is inhibited (Peake and Vance 2012, Swaroop, Thorne et al. 2012), I showed that filipin-staining in β CD treated cells is corrected to control levels. To further investigate if NPC1 is responsible for TMEM16A activation, I used a cell line model

where NPC1 was reintroduced *via* stable viral expression. I found that re-introduction of NPC1 normalised TMEM16A current to control levels. This suggests that NPC1 loss of function specifically activates TMEM16A and that this activation can be corrected by ameliorating NPC1 function through β CD treatment or NPC1 reintroduction.

4.5.3 TMEM16A open probability is increased during NPC1 inhibition

From non-stationary noise analysis studies I found that pharmacological NPC1 inhibition increased TMEM16A P_o without affecting single channel conductance. Consistent with the notion that the TM6 forms the pore of the TMEM16A channel (Peters et al. 2018), I studied two mutant TMEM16A channels in the TM6. There was no difference in the current recorded from cells expressing either the TMEM16A mutant channels I637A or Q645A during NPC1 inhibition. These channels were open in the absence of $[Ca^{2+}]_i$ as substitutions of isoleucine for an alanine in position 637 (I637A) or glutamine for an alanine in position 645 (Q645A) renders the channel constitutively open (Peters, Gilchrist et al. 2018).

4.5.4 Effect of α 1 adrenergic receptor stimulation during NPC1 inhibition

As described in Chapter 1, TMEM16A can be activated by an increase in $[Ca^{2+}]_i$ induced by G_q coupled signalling. I used PE as a synthetic analogue of NA, which binds to the G_q α 1 adrenergic receptor to induce the IP_3 pathway and subsequent increase in $[Ca^{2+}]_i$. In cells co-expressing TMEM16A and the α 1 adrenergic receptor, TMEM16A current was enhanced significantly more when NPC1 was inhibited compared to control cells. The TMEM16A inhibitor Ani9 reduced the PE-induced activation during NPC1 inhibition. One potential mechanism to explain the increase in PE-induced TMEM16A activation by NPC1 is based on an increase $[Ca^{2+}]_i$ upon NPC1 inhibition. It is known in published work that NPC disease is characterised by defective calcium signalling from the intracellular stores (Lloyd-Evans and Platt 2010,

Tiscione, Vivas et al. 2019). In this chapter I show that the overall $[Ca^{2+}]_i$ is not altered during NPC1 loss of function in accordance with other work (Lloyd-Evans and Platt 2010, Vitner, Platt et al. 2010, Tiscione, Vivas et al. 2019).

4.5.5 PIP₂ is a potent mediator of the TMEM16A channel regulation by NPC1

Recent studies identified PIP₂ as a potent activator of TMEM16A (Ta, Acheson et al. 2017). Here, I showed that indeed PIP₂ modulates TMEM16A by increasing its current density. Moreover, I found that PIP₂ is a major regulator of the TMEM16A modulation by NPC1 as *i*) scavenging endogenous PIP₂ with neomycin prevented NPC1 modulation by NPC1; *ii*) depletion of plasmalemmal PIP₂ with a voltage-sensitive phosphatase abolished TMEM16A activation during NPC1 inhibition and *iii*) the PIP₂ insensitive mutant where an arginine has been replaced with an alanine in position 482 (R482A) were also insensitive to NPC1 inhibition.

4.5.6 PIP₂ activates TMEM16A during NPC1 inhibition by distributing at the plasma membrane in a cholesterol-dependent manner

I showed that PIP₂ distribution at the plasma membrane is increased upon NPC1 loss of function and that treatment with β CD reduced both PIP₂ levels at the plasma membrane and TMEM16A activation by PIP₂. This data is in accordance with studies indicating a cross-talk between cholesterol and PIP₂ levels at the plasma membrane (Kwik, Boyle et al. 2003, Chun, Shin et al. 2010). Increasing membrane cholesterol was shown to increase phospholipase-C (PLC) isoforms which are responsible for hydrolysing plasma membrane PIP₂. It was also shown that cholesterol enrichment reduces γ^{32} -P incorporation into PIP₂ by 35% (Chun, Shin et al. 2010). Moreover, the effect of cholesterol on PIP₂ levels can be prevented by incubation with PLC inhibitors (Chun, Shin et al. 2010). Another study in support of cholesterol modulation

of PIP₂ levels showed that a high-cholesterol diet increased the levels of brain PLC (Chun, Oh et al. 2013).

We hypothesise that during NPC1 inhibition, plasma membrane cholesterol is reduced as cholesterol is entrapped in the endolysosomal system (Garver, Krishnan et al. 2002, Wiegand, Chang et al. 2003) (Figure 4.1.1), leading to reduced activation of PLC and higher PIP₂ plasmalemmal levels thus activating TMEM16A current (Ta, Acheson et al. 2017, De Jesus-Perez, Cruz-Rangel et al. 2018). This hypothesis was tested by inhibiting PLC with edelfosine and showing that edelfosine increased TMEM16A current density to a similar extent of NPC1 inhibition (Figure 4.1.2). I also reported a 10% increase in plasmalemmal PIP₂ levels at the plasma membrane (Figure 4.3.6). In human platelets, the concentration of plasmalemmal PIP₂ was reported to be ~200 μM (Hartwig, Bokoch et al. 1995). Therefore, a 10% increase could account for an increment of ~20 μM in plasmalemmal PIP₂ levels. From the inside-out dose-response to PIP₂, it is possible to infer that an increment of ~20 μM in plasmalemmal PIP₂ levels would produce an increase of ~2 fold in TMEM16A current (Figure 4.3.1). This is in accordance with the increment of ~2 fold observed at +70 mV in the TMEM16A current density during NPC1 pharmacological inhibition or *Npc1* locus deletion (Figure 4.1.2). Moreover, a recent study has found that during NPC1 inhibition, the cholesterol/PI4P cycle is altered leading to increased recruitment of PI4K on Golgi and lysosomal membranes (Vyas, Gomez-Casal et al. 2022). Consequences of this altered pathway include enhanced anterograde trafficking to the plasma membrane (Vyas, Gomez-Casal et al. 2022) which could also result in increased plasmalemmal PIP₂ levels activating TMEM16A as observed in this project.

4.6 TMEM16A auxiliary subunit KCNE1 does not affect the channel response to NPC1 inhibition

It was recently discovered that KCNE1 is an auxiliary subunit of two distinct ion channels KCNQ1 (Nakajo and Kubo 2015) and TMEM16A (Ávalos Prado, Häfner et al. 2021). Thus, in this chapter I explored if NPC1 loss of function could affect KCNE1 assembly to TMEM16A and thus, TMEM16A activity. In the presence of the NPC1 inhibitor U18666A, there was no difference in the current recorded from TMEM16A-expressing cells to cells co-expressing TMEM16A and KCNE1. Thus, excluding a role of KCNE1 in the enhanced TMEM16A activity during NPC1 inhibition.

4.7 Conclusions

The data presented in this chapter suggest that TMEM16A activity is enhanced upon NPC1 inhibition. We suggest that this modulation might arise because of higher PIP₂ levels in membranes of cells where the lipid homeostasis is impaired due to loss of NPC1. We propose that TMEM16A activity could be increased in disease models where NPC1 function is lost, as in NPC disease. This discovery is in line with recently published data showing a link between lysosomal flux and TMEM16A suggesting that TMEM16A overexpression is associated with increased lysosomal number and flux (Vyas, Gomez-Casal et al. 2022). Thus, the link between TMEM16A and lysosomal function is just starting to be shed light on and could aid to a better understanding of intracellular pathways that are involved in lysosomal disorders such as NPC.

Chapter 5

Vascular over-activity in *Npc1*^{-/-} mice
relies on TMEM16A potentiation

5.1 Native TMEM16A currents in vascular smooth muscle cells are modulated by NPC1

As it was outlined in greater detail in the Introduction, the TMEM16A channel is a key depolarising force in VSMCs and in pericytes (Introduction, section 1.8 and 1.10). The channel is gated open by a rise in $[Ca^{2+}]_i$, which in VSMCs is typically initiated by agonists acting on G_q PCRs; thus TMEM16A is crucially involved in V_m depolarisation in response to locally released (e.g. noradrenaline and ATP released by sympathetic nerve terminal) or circulating (e.g. angiotensin II or thromboxane) contractile agonists (Manoury, Tamuleviciute et al. 2010, Bulley and Jaggar 2014, Matchkov, Boedtkjer et al. 2015). Having established in Chapter 4 that TMEM16A current is enhanced in a heterologous system during loss-of- NPC1 function, in this chapter the physiological relevance of the regulation of the channel by NPC1 is studied with emphasis in VSMCs where TMEM16A and NPC1 are abundantly expressed. Specifically, the work presented in this chapter aimed to: (i) assess the magnitude of the whole-cell CaCC current in freshly VSMCs isolated from *Npc1*^{-/-} mice and WT; (ii) study the contractile response of the aorta and mesenteric arteries (*Npc1*^{-/-} and WT) to the NA analogue PE using wire myography and (iii) image cerebral cortical pericytes in isolated brain slices obtained from *Npc1*^{-/-} and WT mice either during agonist stimulation or during ischaemic challenge (oxygen glucose deprivation conditions). Supported by the combined use of selective inhibitors of the TMEM16A channel and ionic substitution experiments, the data presented in this chapter demonstrate that *Npc1* deletion results in enhanced CaCC current in contractile vascular cells and hypersensitivity of these cells to contractile agonists.

5.1.1 TMEM16A current is enhanced in vascular smooth muscle cells isolated from *Npc1*^{-/-} mice

There is no published report of the electrophysiological properties of VSMCs when NPC1 is not functional. This investigation is described in this chapter and began by examining the properties of TMEM16A-mediated CaCC currents in VSMCs. These cells were obtained from thoracic aorta dissected from *Npc1*^{-/-} mice and matching WT controls using the protocol described in Methods, Section 2.3.4. The electrophysiological properties of VSMCs were studied using the whole-cell patch-clamp technique. The currents were recorded in response to the “IV-CaCC” protocol (Methods 2.5.4.2) from a holding V_m of 0 mV. In these experiments, $[Ca^{2+}]_i$ was buffered to 600 nM to enhance the endogenous CaCC current. Figure 5.1.1 shows that in cells that lack the *Npc1* gene, the CaCC current is significantly elevated at all V_m tested. This was with the exception of the current measured in response to the pulse to 0 mV because at this voltage the currents are very small given the vicinity of this V_m to the E_{Cl} (~1 mV) in our recording conditions. For example, the CaCC current increased by ~2 fold (at +100 mV) from 18.6 ± 2.8 pA/pF ($n=24$, $N=10$) in WT VSMCs to 37.5 ± 5.9 pA/pF ($n=22$, $N=9$) in *Npc1*^{-/-} VSMCs ($p=0.005$) (Figure 5.1.1). This activation of CaCC current is comparable to the activation observed for the heterologous TMEM16A current Chapter 4 (Figure 4.1.2).

Our Cs-based intracellular solution (Methods, 2.5.5) enables selective recording of Cl^- currents in VSMCs. To assess what fraction of the total Cl^- current recorded is mediated by TMEM16A, whole-cell Cl^- were also recorded in the presence of Ani9, a specific TMEM16A blocker (Seo, Lee et al. 2016). Figure 5.1.1 shows that in the presence of Ani9 (3 μ M), the CaCC current recorded in VSMCs obtained from either WT or *Npc1*^{-/-} mice was significantly reduced and reached comparable level at all V_m tested. For example, at +100 mV the whole cell current was 7.2 ± 2.7 pA/pF ($n=3$, $N=3$) and 7.0 ± 2.0 pA/pF ($n=3$, $N=3$) ($p=0.95$) for WT and *Npc1*^{-/-} in VSMCs, respectively.

Given the fact that aortic VSMCs have high input resistance of $>1\text{ G}\Omega$ (Worley, Deitmer et al. 1986), a $\sim 6\text{ pA}$ increase due to NPC1 inhibition has the potential to produce significant membrane depolarisation (estimated $\sim 6\text{ mV}$) which is sufficient to reach the activation threshold for Ca_v channel and thus trigger $[\text{Ca}^{2+}]_e$ influx and VSMCs contraction (Akaike, Kanaide et al. 1989, Aaronson and Smirnov 1996, Rorsman, Ta et al. 2018).

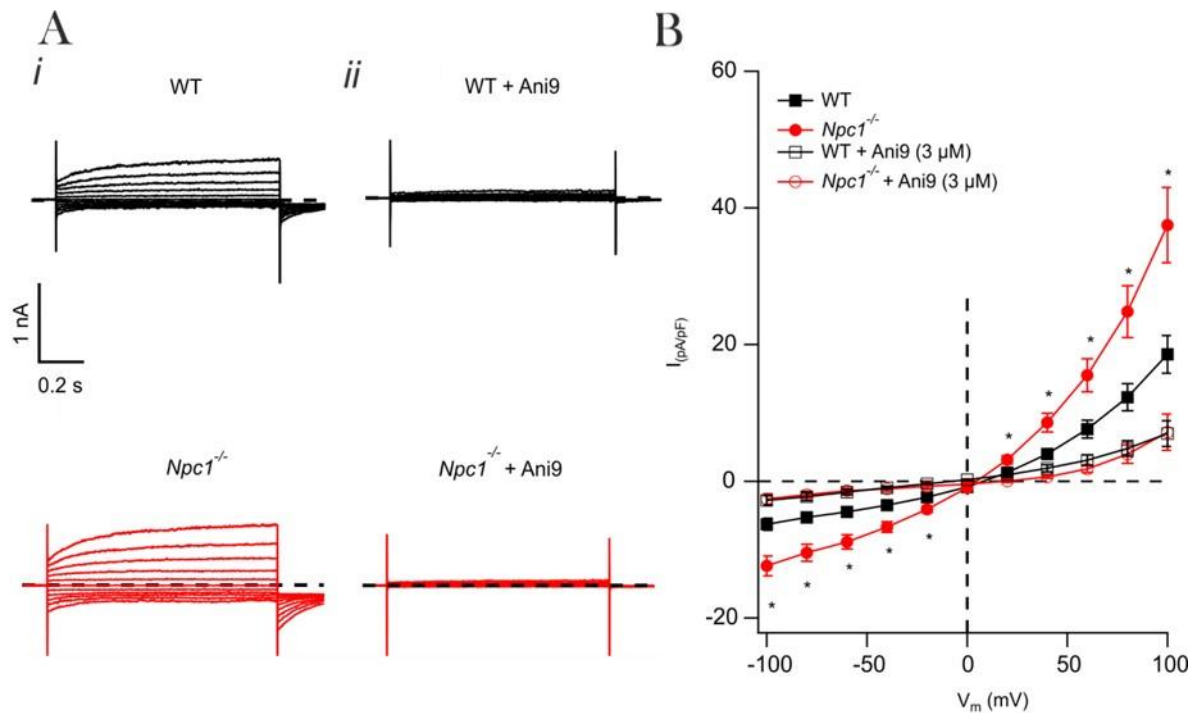


Figure 5.1.1 TMEM16A currents in VSMCs.

(A) Whole-cell currents recorded from VSMCs isolated from WT or *Npc1*^{-/-} thoracic aortas in the presence (ii) or absence of Ani (3 μM). VSMCs were dialysed with 600 nM $[\text{Ca}^{2+}]_i$. Voltage protocol “IV-CaCC” is described in the Methods (Section 2.5.4.2); (B) Mean activating whole-cell current versus V_m relationships measured at the end of the 1 s voltage pulse from -100 to +100 mV in 20 mV increments in WT ($n=22$, $N=9$) or *Npc1*^{-/-} ($n=24$, $N=10$) VSMCs and in WT ($n=3$, $N=3$) or *Npc1*^{-/-} ($n=3$, $N=3$) SMCs in the presence of Ani9 (3 μM). * indicates $p \leq 0.05$, unpaired *t*-test.

5.2 TMEM16A modulation by NPC1 impacts arterial function

Experiments in the previous section demonstrated the contribution of the TMEM16A channel in the increase of CaCC currents observed in VSMCs isolated from *Npc1*^{-/-} mice compared to WT. Since isolated VSMCs from *Npc1*^{-/-} mice show an increase of 2 fold at resting V_m , we hypothesised that *Npc1*^{-/-} aortic vessels are more sensitive to G_qPCRs activation which leads to TMEM16A activation, VSMCs depolarisation and contraction. Therefore, this section aimed to study the agonist-induced contractile properties of native *Npc1*^{-/-} vessels.

5.2.1 PE-mediated vessel contraction is increased in the vasculature of *Npc1*^{-/-} mice

To study the role of TMEM16A in arterial contraction, I performed experiments on isolated aorta and mesenteric arteries for the following reasons: (i) these arteries express functional TMEM16A channel (Figure 5.1.1) (Davis, Forrest et al. 2010, Heinze, Seniuk et al. 2014, Cil, Chen et al. 2021); (ii) the comparative analysis enables the investigation of the importance of TMEM16A in both a large conduit artery (aorta) and smaller resistance arteries (mesenteric arteries).

Isolated artery rings from WT or *Npc1*^{-/-} mice were exposed to increasing [PE] during isometric tension recording *via* a wire myograph (Methods 2.6). An increase in the vessel tension above baseline was observed as [PE] was raised to 0.03 μ M [PE]. The PE-induced tension reached a maximal level at 10 μ M [PE]. The tension measured in the presence of each [PE] was normalised to the tension evoked by KCl (50 mM).

The normalised tension was plotted *versus* [PE] and the relationship fitted using the Hill Equation (Eq. 13). The fitted curve revealed that in aortic rings isolated from *Npc1*^{-/-} mice, the plateau obtained from each [PE] was significantly increased compared to WT mice (Figure

5.2.1) as shown in Table 22. Similarly, for isolated mesenteric rings from *Npc1*^{-/-} mice, the plateau was significantly higher for [PE] in the concentration range between 1 and 10 μM (Figure 5.2.1). For aortic rings, there was a shift on the EC_{50} calculated by the fit of the [PE]-response curves from $0.15 \pm 0.01 \mu\text{M}$ in WT to $0.07 \pm 0.08 \mu\text{M}$ in *Npc1*^{-/-} mice (Table 22). For mesenteric rings, the shift in EC_{50} was even more pronounced giving a value of $1.49 \pm 0.13 \mu\text{M}$ in WT and of $0.55 \pm 0.03 \mu\text{M}$ in *Npc1*^{-/-} mice (Table 23). For both aortas and mesenteric arteries, an increase in the maximal tension was also observed (Table 22-23).

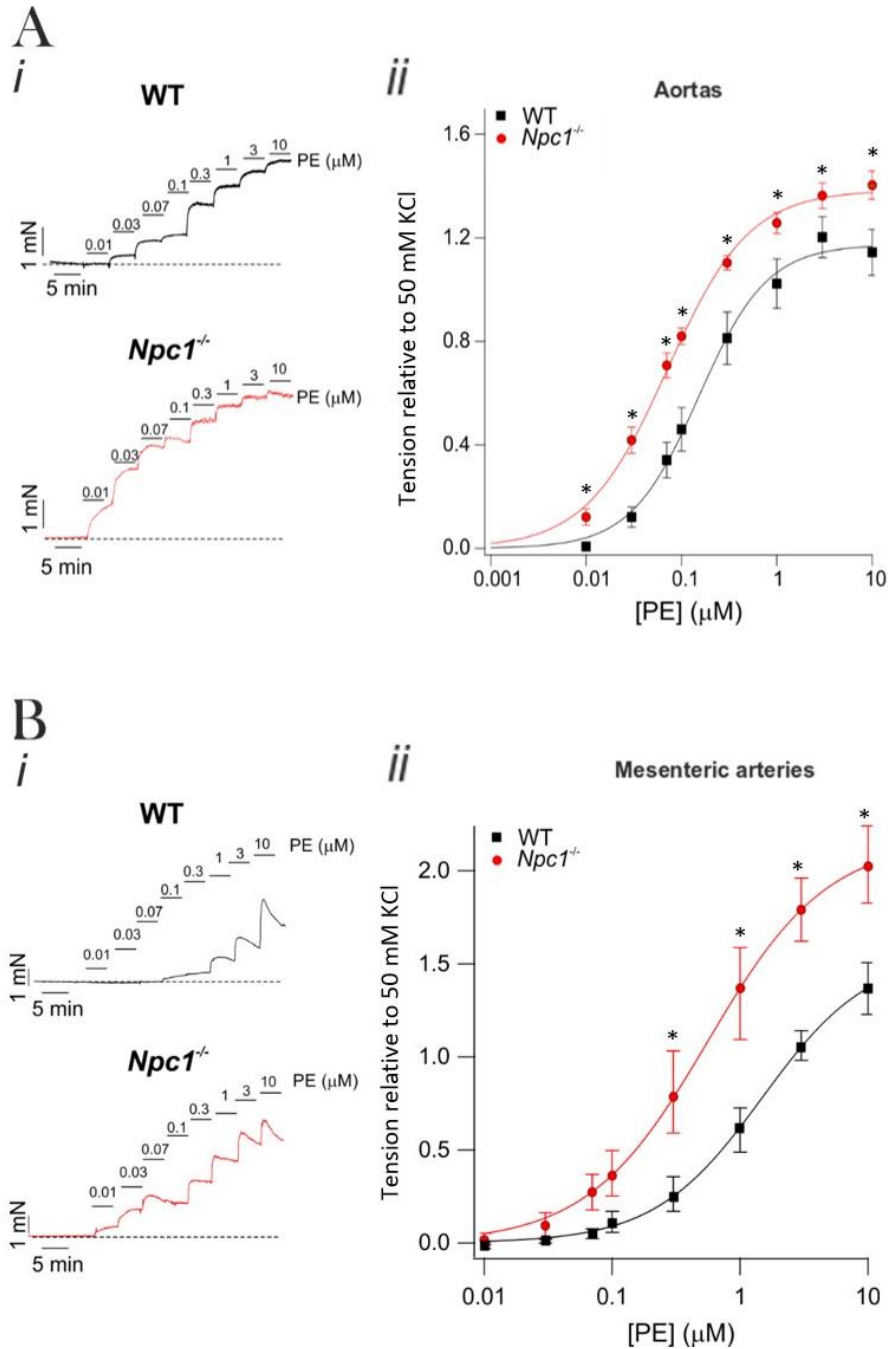


Figure 5.2.1 PE-induced contraction in isolated aortic rings and mesenteric arteries from *Npc1*^{-/-} mice

(A) i) PE-induced isometric tension in aortic rings isolated from WT and *Npc1*^{-/-} mice; ii) mean tension versus [PE] relationship of aortic rings isolated from WT (n=18, N=9) and *Npc1*^{-/-} (n=18, N=9) mice. (B) i) PE-induced isometric tension in mesenteric arteries isolated from WT and *Npc1*^{-/-} mice; ii) mean tension versus [PE] relationship of mesenteric arteries isolated from WT (n=4, N=4) and *Npc1*^{-/-} (n=5, N=5) mice. Dotted line represents baseline tension. * indicates $p \leq 0.05$, unpaired t-test.

Aortas	EC₅₀ (μM)	max	h	N
WT	0.15 ± 0.01 *	1.45 ± 0.02 *	1.16 ± 0.08	9
<i>Npc1</i> ^{-/-}	0.07 ± 0.08 *	1.88 ± 0.03 *	1.07 ± 0.0	9

Table 22 Hill-fit parameters (EC_{50} , max and h) (Eq. 13) for aortic rings.

Tension versus [PE] relationships obtained in aortic rings isolated from WT or *Npc1*^{-/-} mice. * indicates $p \leq 0.05$, unpaired t-test.

Mesenteric arteries	EC₅₀ (μM)	max	h	N
WT	1.49 ± 0.13 *	1.56 ± 0.04 *	1.03 ± 0.05	4
<i>Npc1</i> ^{-/-}	0.55 ± 0.03 *	2.12 ± 0.04 *	0.92 ± 0.03	5

Table 23 Hill-fit parameters (EC_{50} , max and h) (Eq. 13) for mesenteric rings.

Tension versus [PE] relationships obtained in mesenteric rings isolated from WT or *Npc1*^{-/-} mice. * indicates $p \leq 0.05$, unpaired t-test.

To examine whether the enhanced contractility to PE observed in *Npc1*^{-/-} mice relies on enhanced TMEM16A currents, the response of WT and *Npc1*^{-/-} rings to an increase in $[K^+]_e$ was studied. It was argued that a rise in $[K^+]_e$ will cause a depolarising shift in the V_m thus bypassing the depolarisation provided by TMEM16A (Heinze, Seniuk et al. 2014). It was anticipated that no change would therefore be observed in the response to high $[K^+]_e$ in WT and *Npc1*^{-/-} rings.

To achieve this, aortic rings were constricted by raising $[K^+]_e$ to depolarise the membrane to a more positive equilibrium potential than the E_{Cl} (Casteels, Kitamura et al. 1977, Rorsman, Ta et al. 2018). Under these conditions, L-type Ca_v are activated resulting in an increase of $[Ca^{2+}]_i$ and thus, contraction. I was able to study the contractility properties of aortic rings independent from the contribution of Cl^- channels by replacing $[Cl^-]_E$ with K-MES. This is because MES is not permeable to Cl^- channels. Therefore, I was able to study if the increased aortic constriction observed in *Npc1*^{-/-} mice was dependent on Cl^- channels. WT or *Npc1*^{-/-} aortic rings were

exposed to increasing concentration of $[K^+]_e$ (1, 10, 30, 70, 100 mM). There was no difference between the tension induced by the increasing doses of KCl in WT and *Npc1*^{-/-} mice (Figure 5.2.2, Table 24).

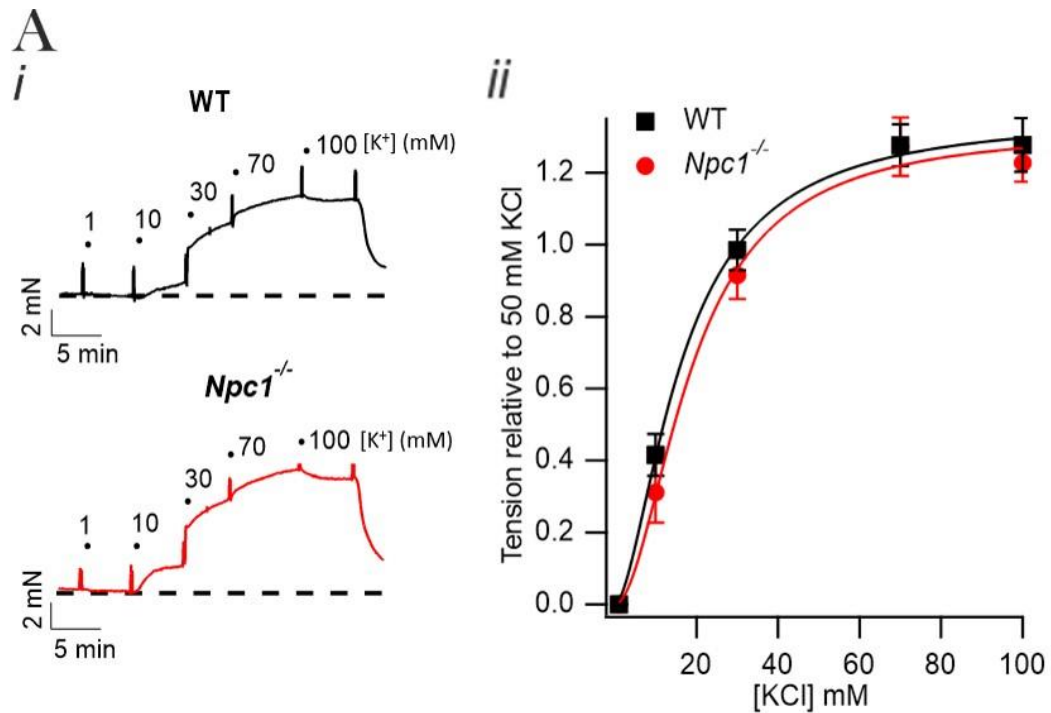


Figure 5.2.2 Structural properties of isolated aortic rings from *Npc1*^{-/-} mice

(A) i) Isometric tension recordings obtained from WT and *Npc1*^{-/-} aortic rings in response to increasing doses of K-MES; ii) Mean tension in response to KCl for aortic rings obtained from WT ($n=6$, $N=6$) and *Npc1*^{-/-} mice ($n=5$, $N=5$) mice. Unpaired *t*-test.

Aortas	EC ₅₀ (μM)	max	h	N
WT	16.48 ± 1.07	1.36 ± 0.04	1.67 ± 0.16	5
<i>Npc1</i> ^{-/-}	18.95 ± 2.04	1.32 ± 0.06	1.88 ± 0.03	5

Table 24 Hill-fit parameters (EC₅₀, max and h) (Eq. 13) for aortic rings.

Tension versus $[K^+]_e$ relationships obtained in aortic rings isolated from WT or *Npc1*^{-/-} mice. Unpaired *t*-test.

It was argued that histological changes in the arteries might have occurred as a result of *Npc1* deletion. Histological change could potentially affect smooth muscle force of contraction and/or affect vessel compliance. To assess the vessel compliance, I studied the response of aortic and mesenteric rings to stretch. Rings were mounted on the wire myograph and gradually stretched by increasing the distance between the myograph jaws in increments of 100 μm for aortic rings and 50 μm for mesenteric rings (Figure 5.2.3). No difference in vessel compliance in response to stretch was observed in either types of arteries between WT and *Npc1*^{-/-} mice.

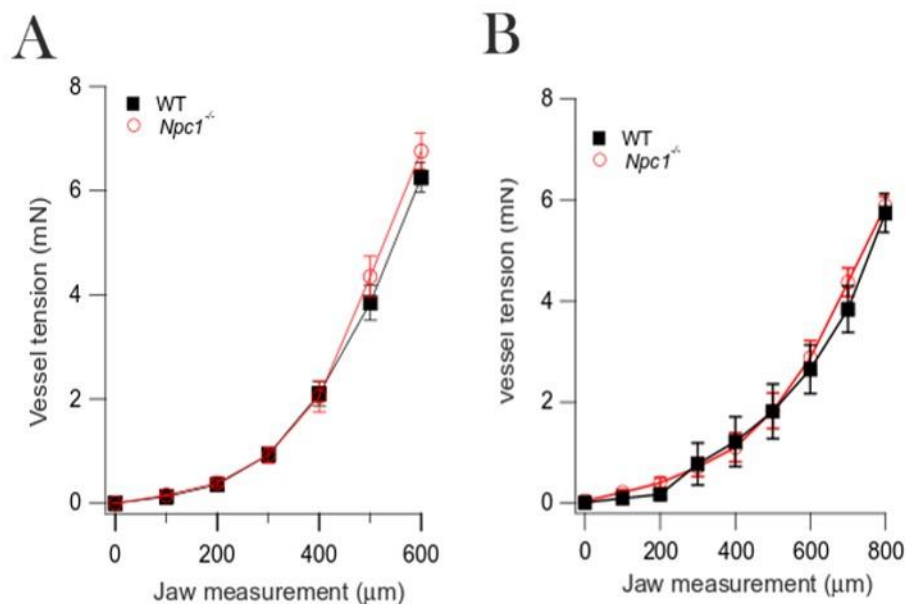


Figure 5.2.3 Structural properties of isolated aortic rings and mesenteric arteries from *Npc1*^{-/-} mice

(A) Mean tension in isometric tension in response to increasing stretch for aortic rings isolated from WT and *Npc1*^{-/-} mice ($n=18$, $N=9$); (B) Change in isometric tension in response to increasing stretch for mesenteric arteries isolated from WT and *Npc1*^{-/-} mice ($n=18$, $N=9$); Unpaired *t*-test.

5.2.2 β CD treatment of *Npc1*^{-/-} mice restores enhanced PE-mediated vessel contraction

Based on the premise that *i*) β CD is used to reduce lipid accumulation in NPC disease (Liu 2012, Tanaka, Yamada et al. 2015, Hastings, Vieira et al. 2019) and *ii*) treatment with β CD reduced the enhanced activity of TMEM16A heterologous systems (Chapter 4, section 4.1.3), the effect of β CD on the PE-induced contraction of aortic rings isolated from *Npc1*^{-/-} mice was investigated. *Npc1*^{-/-} mice were treated with β CD (4 g/kg/week) *via* intravenous injection for the five weeks preceding the experiment. Aortic ring obtained from *Npc1*^{-/-} treated with β CD were mounted of a wire myograph to study their sensitivity to PE during isometric tension recordings. An increase in the vessel tension was observed from 0.03 μ M [PE] and reached a maximal level at 10 μ M [PE]. However, there was no difference in the [PE]-evoked tension between WT mice and *Npc1*^{-/-} mice treated for 5 weeks with β CD. For example, in response to 1 μ M of PE, the isometric tension was 1.25 ± 0.12 mN and 1.24 ± 0.11 mN in WT and β CD-treated *Npc1*^{-/-} mice, respectively ($p > 0.05$) (Figure 5.2.4). Treatment with β CD did not change the EC_{50} , calculated by the Hill fit (Eq. 13) of the [PE]-response curves between WT and *Npc1*^{-/-} aortic rings. Upon β CD treatment, for WT aortic rings the EC_{50} was 0.04 ± 0.00 μ M and 0.16 ± 0.00 μ M for *Npc1*^{-/-} (Table 25). These data indicate that β CD treatment is rescuing the increased aortic contractility observed for untreated *Npc1*^{-/-} mice in response to PE and mirror the reduction in heterologous TMEM16A current that follows β CD treatment (Chapter 4, Figure 4.1.5).

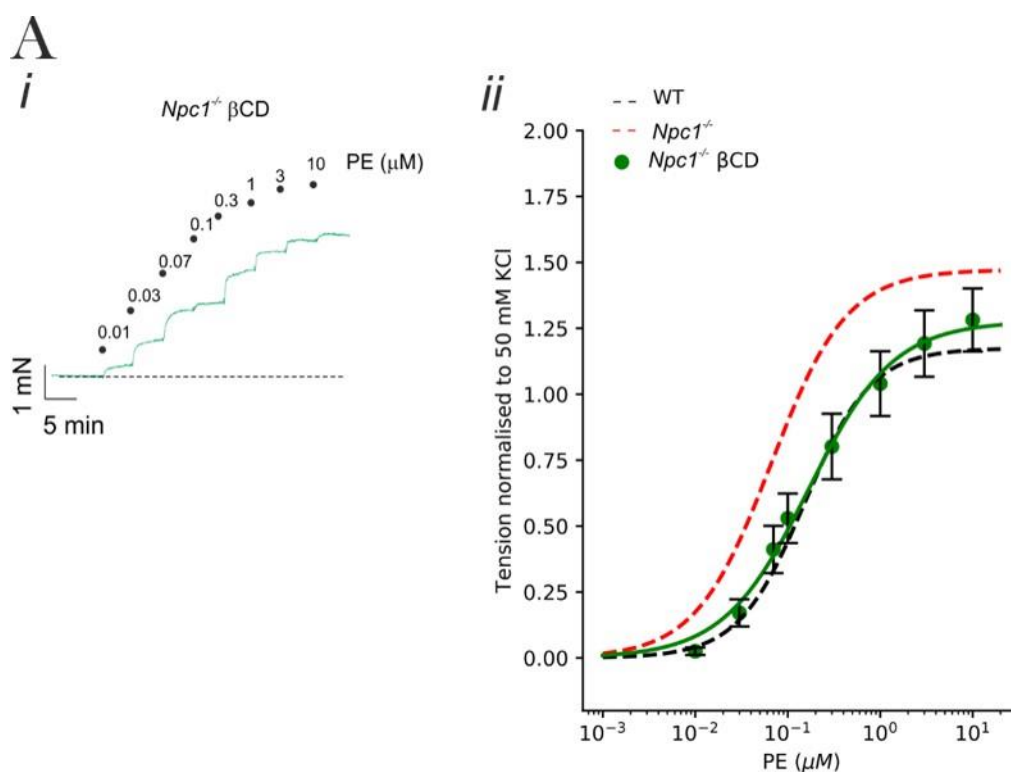


Figure 5.2.4 PE-induced contraction in aortic rings from $Npc1^{-/-}$ mice treated with β CD

(A) Mean tension versus [PE] relationship of aortic rings isolated from $Npc1^{-/-}$ mice treated with β CD. Dotted lines represent WT and $Npc1^{-/-}$ aortic rings from figure 5.3.

β CD	EC_{50} (μ M)	max	h	N
WT	0.04 ± 0.00	1.49 ± 0.02	1.02 ± 0.08	3
$Npc1^{-/-}$	0.16 ± 0.02	1.48 ± 0.04	0.95 ± 0.09	5

Table 25 Hill-fit parameters (EC_{50} , max and h) (Eq. 13) for aortic rings in mice treated with β CD.

Tension versus [PE] relationships obtained in aortic rings isolated from WT or $Npc1^{-/-}$ mice treated with β CD (4 g/kg/week) for 5 weeks. Unpaired t-test.

5.2.3 Blocking TMEM16A reduces contractility of *Npc1*^{-/-} aortas

To examine the role of TMEM16A in PE-induced contraction in WT and *Npc1*^{-/-} mice, I inhibited TMEM16A with the specific inhibitors Ani9 (Seo, Lee et al. 2016) and TMinh-23 (Cil, Chen et al. 2021) during wire myography. Aortic rings isolated from WT or *Npc1*^{-/-} mice were mounted on a wire myograph and incubated for 30 minutes with Ani9 (3 μ M) or TMinh-23 (3 μ M) before exposure to various [PE]. In the presence of Ani9 or TMinh-23, there was no change between the PE-induced contraction of aortic rings isolated from WT or *Npc1*^{-/-} mice (Figure 5.2.5). In the presence of Ani9, the EC₅₀ was 0.21 ± 0.02 in WT and 0.19 ± 0.02 in *Npc1*^{-/-} aortic rings (Table 26). Incubation of aortic rings with TMinh-23 reduced the EC₅₀ to 0.11 ± 0.0 in WT and 0.09 ± 0.0 for *Npc1*^{-/-} (Table 26-27). The maximal response to 10 μ M PE (max) was 0.97 ± 0.02 in WT and 0.92 ± 0.02 for *Npc1*^{-/-} aortic rings in the presence of Ani9, while 1.16 ± 0.03 and 1.10 ± 0.01 in the presence of TMinh-23, respectively (Table 26-27).

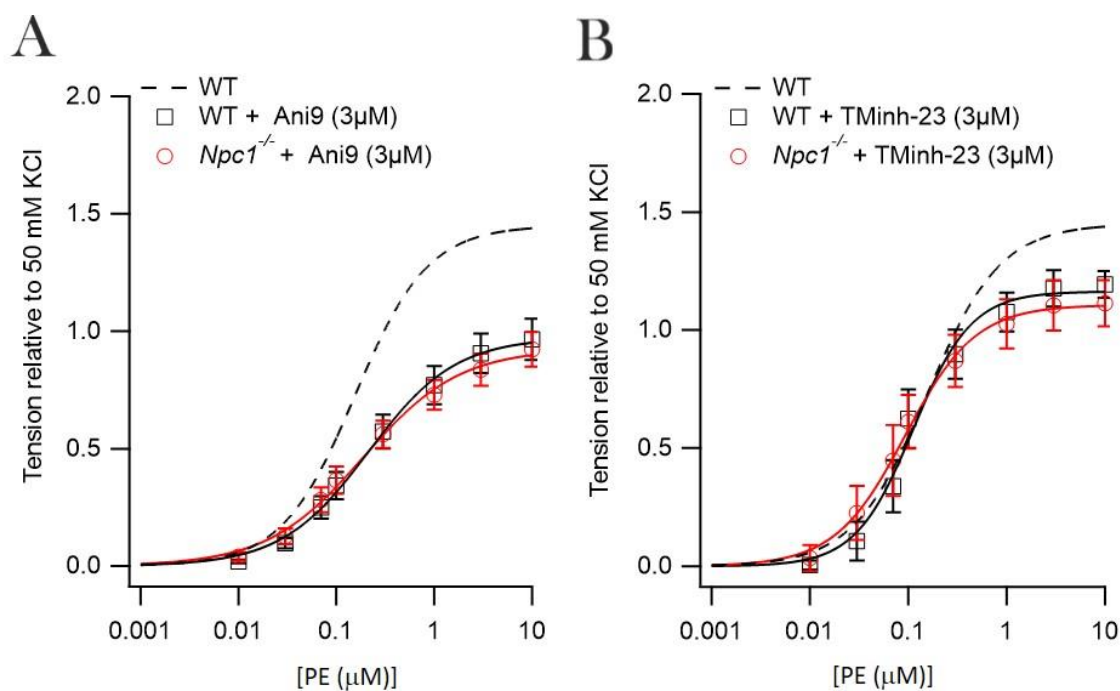


Figure 5.2.5 PE-induced contraction in $Npc1^{-/-}$ isolated aortic rings in the presence of the TMEM16A inhibitors Ani9 or TMinh-23.

(A) Mean tension versus [PE] relationship of aortic rings isolated from WT ($n=9$, $N=9$) and $Npc1^{-/-}$ ($n=9$, $N=9$) mice in the presence of Ani9 ($3 \mu\text{M}$). (B) Mean tension versus [PE] relationship of aortic rings isolated from WT ($n=4$, $N=4$) and $Npc1^{-/-}$ ($n=4$, $N=4$) mice in the presence of TMinh-23 ($3 \mu\text{M}$). $p>0.05$, unpaired t -test.

Ani9 ($3 \mu\text{M}$)	EC_{50} (μM)	max	h	N
WT	0.21 ± 0.02	0.97 ± 0.02	0.98 ± 0.07	9
$Npc1^{-/-}$	0.19 ± 0.02	0.92 ± 0.02	0.88 ± 0.07	9

Table 26 Hill-fit parameters (EC_{50} , max and h) (Eq. 13) for aortic rings in the presence of the TMEM16A inhibitor Ani9.

Tension versus [PE] relationships obtained in aortic rings isolated from WT or $Npc1^{-/-}$ mice. Rings were incubated with Ani9 ($3 \mu\text{M}$) for 30 minutes before incremental additions of [PE]. Unpaired t -test.

TMinh-23 (3 μM)	EC₅₀ (μM)	max	h	N
WT	0.11 \pm 0.0	1.16 \pm 0.03	1.47 \pm 0.2	4
<i>Npc1</i> ^{-/-}	0.09 \pm 0.0	1.10 \pm 0.01	1.21 \pm 0.08	4

Table 27 Hill-fit parameters (EC_{50} , max and h) (Eq. 13) for aortic rings in the presence of the TMEM16A inhibitor TMinh-23.

Tension versus [PE] relationships obtained in aortic rings isolated from WT or *Npc1*^{-/-} mice. Rings were incubated with TMinh-23 (3 μ M) for 30 minutes before incremental additions of [PE]. Unpaired t-test.

5.2.4 Aortas isolated from *Npc1*^{-/-} mice are more sensitive to changes in extracellular chloride

The experiments described above implicate TMEM16A in the enhanced PE-induced contractility in *Npc1*^{-/-} mice. To test this proposition further, I performed myography experiments under conditions of altered $[Cl^-]_E$. The rationale was that altering $[Cl^-]_E$ would induce a shift in transmembrane Cl^- hence increasing the magnitude of the outward Cl^- currents to depolarise V_m and induce muscle contraction. Thus, I examined the effect of lowering $[Cl^-]_E$ in aortic rings stimulated by PE with the expectation that this will cause a depolarising shift in E_{Cl} . If TMEM16A plays a primary role in the enhanced contraction observed in *Npc1*^{-/-} mice, we anticipated that lowering $[Cl^-]_E$ would have more of an effect on the tone of aortic rings isolated from *Npc1*^{-/-} mice than WT.

PE (0.03 μ M) was used for *Npc1*^{-/-} aortic rings in order to elicit the same amount of vessel constriction to WT. Contraction of the aortic rings in low $[Cl^-]_E$ were normalised to the contraction recorded in normal $[Cl^-]_E$. Low $[Cl^-]_E$ strongly enhanced contraction of aortic rings in *Npc1*^{-/-} compared to WT, indicating a role for Cl^- channels in this response. Isometric tension recordings in low $[Cl^-]_E$ showed that at an agonist concentration of 0.03 μ M PE, normalised aortic tension increased of ~1.5 fold from 2.1 \pm 0.2 in WT (n=10) to 3.14 \pm 0.4 in *Npc1*^{-/-} (n=10)

($p=0.007$) (Figure 5.2.6). These data further implicate TMEM16A in the enhanced PE-induced contractility in $Npc1^{-/-}$ mice.

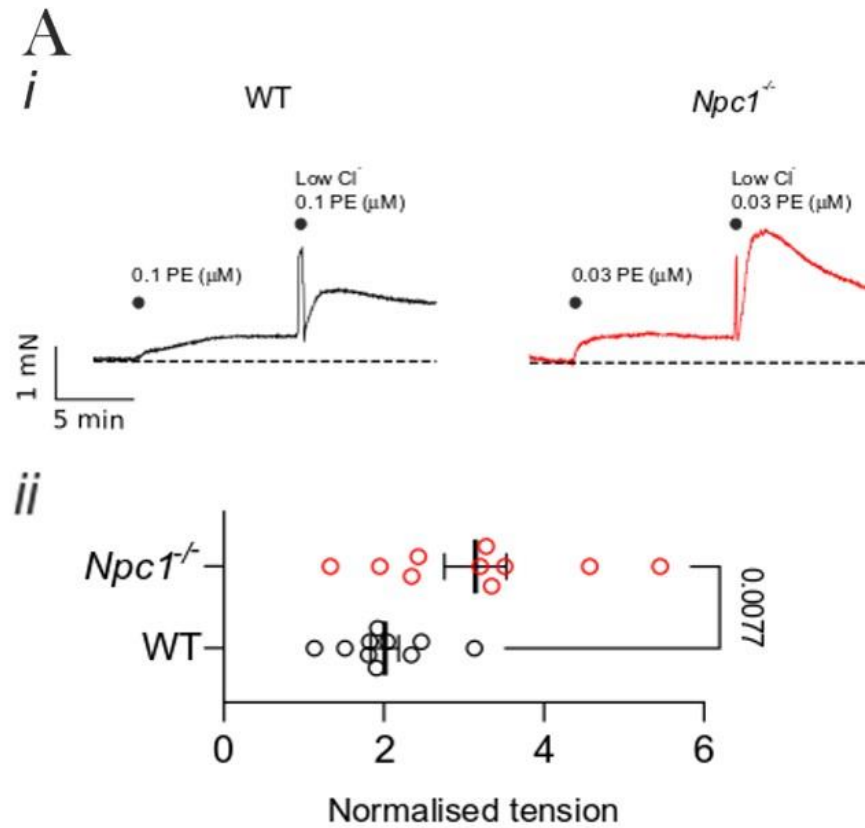


Figure 5.2.6 Extracellular Cl^- in PE-induced arterial contraction in $Npc1^{-/-}$ aortic rings

(A) *i*) Isometric tension recordings recorded from aortic rings obtained from WT or $Npc1^{-/-}$ mice. PE and low $[Cl^-]$ were applied as indicated; *ii*) mean fold change in tension induced by low $[Cl^-]$, in aortic rings obtained from WT and $Npc1^{-/-}$ mice. * indicates $p \leq 0.05$, unpaired *t*-test.

5.3 TMEM16A modulation on NPC1 affects capillary function

5.3.1 Pericytes density is decreased in brain slices of *Npc1*^{-/-} mice

Pericytes play a pivotal role in the regulation of the microvasculature in the brain as described in Chapter 1. The Tamaro lab has shown that TMEM16A is highly expressed in cerebral cortical pericytes where it controls the agonist-induced contraction around the surrounding capillary (Korte, Ilkan et al. 2022). It is also known that NPC disease is characterised by vascular dementia resulting in neuronal cell death (Sévin, Lesca et al. 2007, Lin, Liu et al. 2021). Thus, we investigated the pericytes density and distribution in brain slices of WT and *Npc1*^{-/-} mice. Brain slices of 200 µm thickness were stained for pericytes using the primary antibody NG-2 (red) and capillaries were labelled with isolectin-4 (green) (Figure 5.3.1). Isolectin-4 (IB-4) binds α-D-galactose groups in the basement membrane of capillaries (Nelson, Sagare et al. 2020). NG-2 antibodies, binding to chondroitin sulfate proteoglycan, were used to stain positive pericytes processes (Mishra, O'Farrell et al. 2014). Pericytes were identified by the presence of *i*) NG-2 red staining, *ii*) IB-4 staining of the basement membrane of capillaries and *iii*) by their specific bump-on-a-log morphology with thin processes (Mishra, O'Farrell et al. 2014, Korte, Ilkan et al. 2022). I counted the number of pericytes in each cortical slice, measured the capillary length for each slice and expressed the number of pericytes for every 100 µm capillary of length. Figure 5.3.1 shows that the mean number of pericytes *per* 100 µm capillary length reduced from 1.1±0.1 in WT (n=34, N=5) to 0.7±0.0 in *Npc1*^{-/-} (n=27, N=5) mice ($p=0.01$). There was no difference in the density of capillaries between WT and *Npc1*^{-/-} mice (Figure 5.3.1)

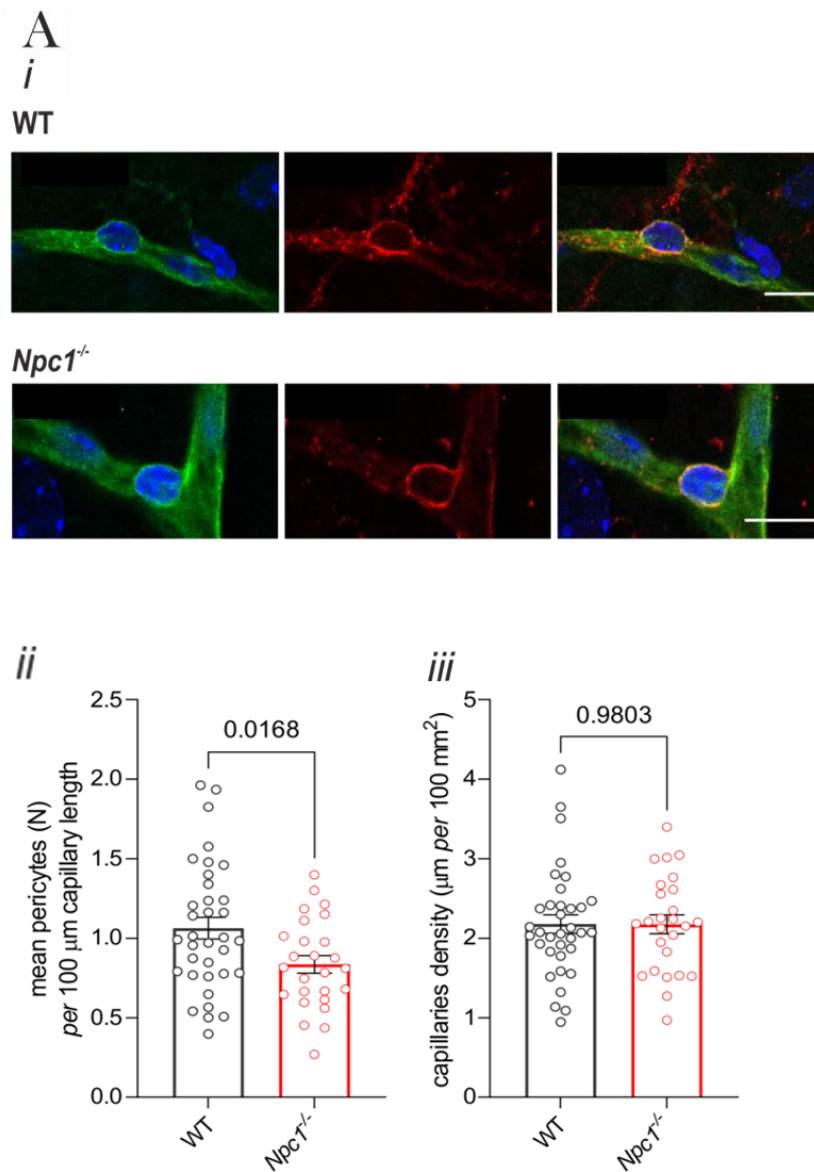


Figure 5.3.1 The distribution of pericytes in *Npc1*^{-/-} mice microvasculature

(A) *i*) Representative immunostaining of capillaries isolectin (green), pericytes NG-2 (red) and nuclei DAPI in (blue). Scale bar = 10 μm; *ii*) mean pericytes number per 100 μm capillary length in WT ($n=34$, $N=5$) and *Npc1*^{-/-} mice ($n=27$, $N=5$). $p \leq 0.05$, unpaired *t*-test; *iii*) capillary density μm per 100 mm² in WT ($n=34$, $N=5$) and *Npc1*^{-/-} mice ($n=27$, $N=5$). Unpaired *t*-test.

5.3.2 TMEM16A modulation of NPC1 increases capillary contractility properties in *Npc1*^{-/-} mice

Based on the enhanced PE-induced contractility observed in *Npc1*^{-/-} aortas and mesenteric arteries (Figure 5.2.1), we then asked if the contractility properties of brain capillaries in response to an agonist were also enhanced. Endothelin-1 (ET-1) was used as a powerful vasoconstrictor of capillaries to activate pericytes in WT and *Npc1*^{-/-} freshly isolated cerebral slices (Nortley, Korte et al. 2019, Korte, Ilkan et al. 2022). The diameter of a capillary was measured, next to the corresponding soma of a pericyte (indicated by the red arrows in Figure 5.3.2), before (baseline) and during perfusion with 10 nM ET-1 for 35 minutes. In response to ET-1 perfusion capillaries from *Npc1*^{-/-} constricted significantly more than capillaries from WT mice. Their diameter reduced by ~80% in cortical capillaries of *Npc1*^{-/-} and by ~50% in WT mice. This data indicates that the capillaries found in *Npc1*^{-/-} brain microvasculature show enhanced agonist-induced contractility compared to WT.

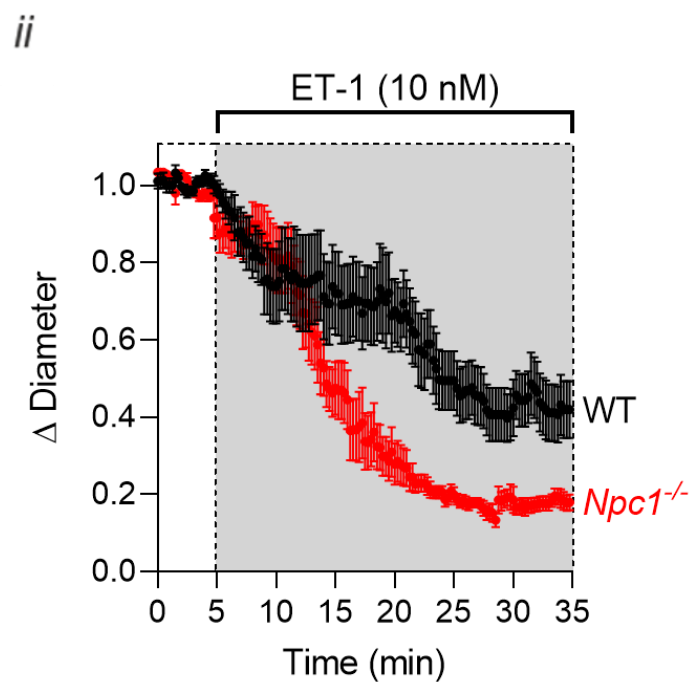
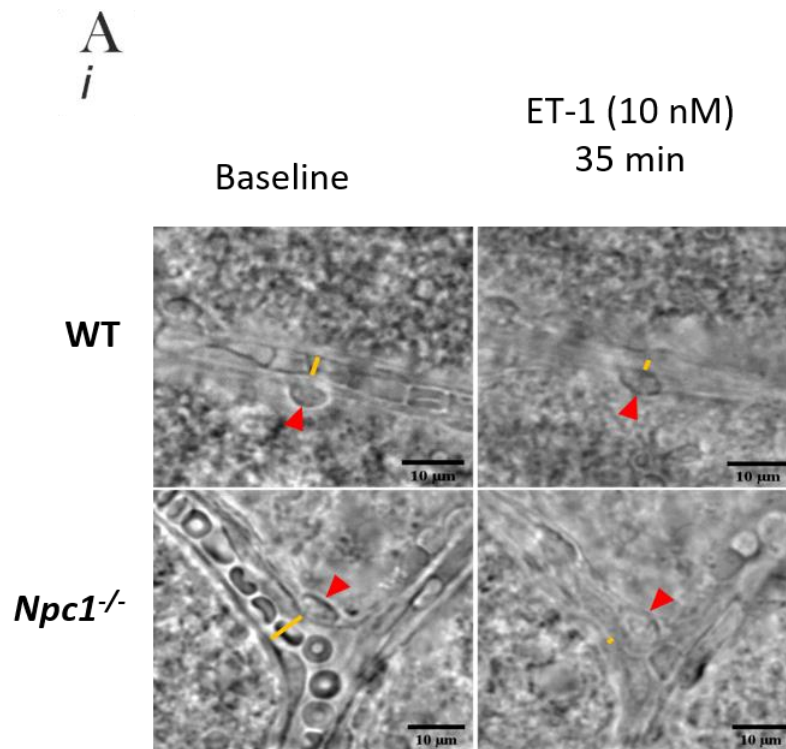


Figure 5.3.2 Capillary constriction in response to endothelin-1 in *Npc1*^{-/-} brain microvasculature

(A) *i*) Representative bright field images of cerebral capillaries from WT and *Npc1*^{-/-} mouse brain slices before and after ET-1 (10 nM) exposure. Red arrow heads indicate pericytes and yellow lines show capillary diameter. Scale bar = 10 μm; *ii*) average capillary diameter change in WT (N=7) and *Npc1*^{-/-} (N=7) mice in response to ET-1 perfusion.

5.3.3 TMEM16A modulation of NPC1 increases pericytes cell death in *Npc1*^{-/-} mice

As described in the Introduction, pericytes play a crucial role in regulating capillary function in physiology and pathophysiology (Hall, Reynell et al. 2014). For example, during ischaemia, low [ATP]_i can block the ATP-dependent Ca²⁺ pumps and thus raise [Ca²⁺]_i. We expected that this process may activate TMEM16A as recently published by our lab (Korte, Ilkan et al. 2022). Moreover, in accordance with the enhanced TMEM16A activity found in *Npc1*^{-/-} native tissues, we also expected that TMEM16A activation during ischaemia may be even more pronounced in *Npc1*^{-/-} mice. OGD was used to induce brain damage in freshly isolated cortical slices from WT and *Npc1*^{-/-} mice (Tasca, Dal-Cim et al. 2015, Ryou and Mallet 2018). Isolectin-4 was used to label the blood vessels while propidium iodide was used to stain dead cells (Hall, Reynell et al. 2014). When cerebral slices were incubated with the aCFS, there was minimal pericyte cell death which was unchanged in WT and in *Npc1*^{-/-} mice. In contrast, in OGD conditions, there was ~70% pericytes cell death in *Npc1*^{-/-} mice and ~40% in WT mice (Figure 5.3.3). The TMEM16A specific inhibitor Ani9 reduced pericytes death to the same level in WT and *Npc1*^{-/-} mice. These data indicates that in *Npc1*^{-/-} brain microvasculature, TMEM16A might mediate the enhanced OGD-induced pericyte death.

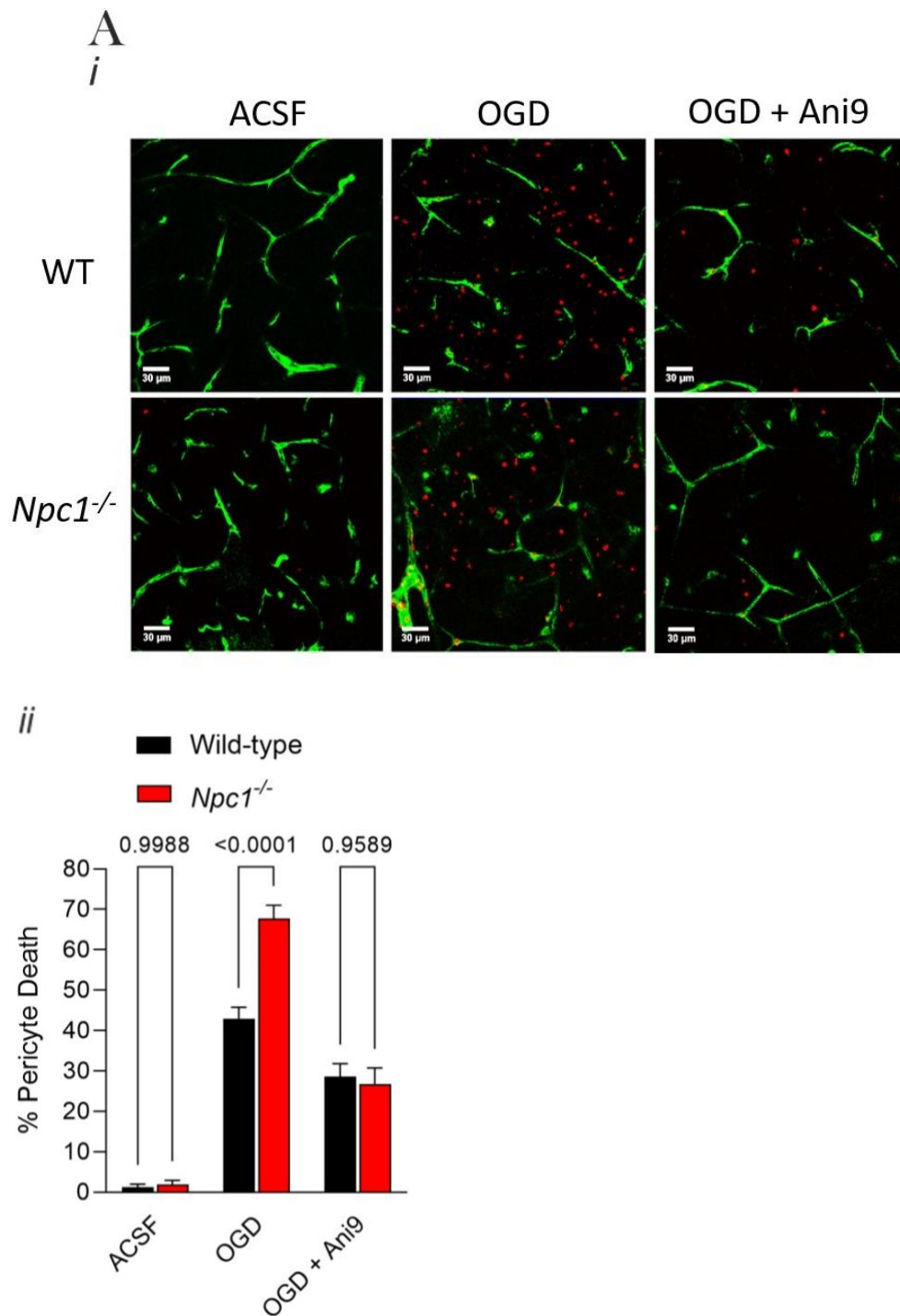


Figure 5.3.3 Pericytes cell death in *Npc1*^{-/-} brain microvasculature.

(A) *i*) Representative images from WT and *Npc1*^{-/-} mouse brain slices where green indicates isolectin-1 (capillaries) and red propidium iodide (dead cells). Scale bar = 30 μ m; *ii*) average percentage pericyte death in WT (N=4) and *Npc1*^{-/-} (N=4) brain slices under baseline (ACSF), and ischaemia (OGD) conditions with and without Ani9 (2 μ M).

5.4 Discussion

This chapter has outlined that *Npc1*^{-/-} mice have enhanced TMEM16A currents in isolated VSMCs and that this results in enhanced agonist-induced contractility in the vasculature compared to WT mice, including large conduit (aorta), resistance (mesenteric) arteries, and microvasculature (cerebral cortical capillaries). Furthermore, cortical pericytes density was reduced in *Npc1*^{-/-} mice and the extent of cell death in response to OGD was enhanced in *Npc1*^{-/-} mice. Pharmacological inhibition of the TMEM16A channel could rescue the vascular phenotype in *ex vivo* studies. These data provide insights into the mechanisms underlying vascular alterations in NPC disease.

5.4.1 Electrophysiological properties of native *Npc1*^{-/-} smooth muscle cells

Experiment involving heterologous TMEM16A expression demonstrated that TMEM16A current is enhanced during NPC1 inhibition. We therefore studied the effect of *Npc1* genetic deletion on currents of VSMCs isolated from the aorta of 8 weeks-old *Npc1*^{-/-} mice. TMEM16A current was found to be increased by ~2 fold at +100 mV and by ~1 fold at -100 mV and -80 mV. However, this increment in current is lower than seen in heterologous systems. This difference could be due to auxiliary units present in native currents that are not found in cloned channels. For example, association between the L-type $\text{Ca}_v1.4$ and TMEM16A in physiological conditions makes TMEM16A susceptible to changes in Ca^{2+} channels (Caputo, Piano et al. 2015). In heterologous system, 300 nM $[\text{Ca}^{2+}]_i$ was used while in VSMCs, while 600 nM $[\text{Ca}^{2+}]_i$ was used to enhance opening of native TMEM16A channels. Overall, this data is showing the TMEM16A current is enhanced during NPC1 inhibition not only in heterologous system, but also in cells isolated from symptomatic *Npc1*^{-/-} mice. In fact, from the 8th week of age, *Npc1*^{-/-} mice have been described to mimic visceral and neuronal human NPC1 disease phenotype (Santiago-Mujica, Flunkert et al. 2019) .

5.4.2 Agonist-mediated contractility in *Npc1*^{-/-} mice

As described in Chapter 1, TMEM16A is highly expressed and functional in the aorta and in mesenteric arteries (Furness 2017). Some studies have shown that NPC disease is associated with cardiovascular disease as altered levels of cholesterol can lead to forms of atherosclerosis, myocardial infarction and stroke (Podechard, Le Ferrec et al. 2009, Ma, Xu et al. 2010, Afzali, Nakhaee et al. 2013, Afzali, Hashemi et al. 2017, Jeong, Bae et al. 2019). Moreover, it is known that in NPC disease, altered lipid homeostasis leads to severe accumulation of foam cells deriving from macrophages and VSMCs that form lipid-laded deposits on blood vessel walls (Podechard, Le Ferrec et al. 2009, Koga and Aikawa 2012). Despite the report of cardiovascular disease in some NPC patients, there is limited understanding of the underlying mechanism. In this chapter, the response of the aorta and mesenteric artery to PE was studied in WT and *Npc1*^{-/-} mice. The response to PE was increased of ~2 fold in aortas and mesenteric arteries of *Npc1*^{-/-} compared to WT mice (Figure 5.2.1). PE was used as a synthetic analogue of NA which leads VSMCs contraction by the stimulation of the α_1 G_qPCR as outlined in Chapter 1. The enhanced response to PE in vessels isolated from *Npc1*^{-/-} mice is in accordance with the increased TMEM16A currents recorded in the heterologous system when TMEM16A was co-expressed with the α_1 adrenergic receptor and stimulated with PE during NPC1 inhibition in Chapter 4.

I also tested if the isolated vessels from *Npc1*^{-/-} mice had a different response to contraction induced by a change in $[K^+]_e$. Thus, KCl was used as a depolarising agent to reduce the electrochemical gradient for K^+ in order to induce contraction by membrane depolarisation. There was no difference in the KCl-induced contraction in both aortic and mesenteric rings isolated from *Npc1*^{-/-} or WT mice. Since the extent of contraction and sensitivity in isolated vessels depends on the stretch applied to the vessel, we also compared the tension generated to a change in stretch in *Npc1*^{-/-} or WT mice. There was no difference in the tension induced by stretch in aortic and mesenteric rings isolated from *Npc1*^{-/-} or WT mice. This data suggests

that the enhanced PE-contractility observed in *Npc1*^{-/-} native tissues is dependent on the contribution to the agonist-induced contraction rather than to the response to stretch or membrane depolarisation.

Several studies have shown that β CD-treatment reduces accumulation of cholesterol and other lipids in NPC disease (Liu 2012, Jeong, Bae et al. 2019). Here we found that the enhanced PE-induced contractility in *Npc1*^{-/-} mice was reduced to WT levels in *Npc1*^{-/-} mice treated intravenously with β CD for 5 weeks. β CD is reported to have low penetration of the blood brain barrier (Liu et al 2009) and is administered systemically to target major organs or injected in the cerebrospinal fluid (Davidson, Ali et al. 2009, Coisne, Hallier-Vanuxeem et al. 2016, Pallottini and Pfrieger 2020). This data indicates that β CD might be a suitable compound to reduce the increased agonist-mediated contractility in *Npc1*^{-/-} mice.

5.4.3 TMEM16A modulates agonist-mediated contractility in *Npc1*^{-/-} mice

In order to study if the enhanced agonist-mediated contractility in *Npc1*^{-/-} mice is regulated by TMEM16A we studied the TMEM16A current properties in VSMCs, as well as the agonist-induced contraction of aortas and mesenteric arteries.

TMEM16A current was increased in *Npc1*^{-/-} VSMCs, aortas and mesenteric arteries. The specific TMEM16A inhibitors Ani9 and TMinh-23 were used as a pharmacological tool to block TMEM16A activity in native tissues (Seo, Lee et al. 2016, Centeio, Cabrita et al. 2020, Cil, Chen et al. 2021). Incubation with TMEM16A inhibitors reduced PE-induced contraction in aortic and mesenteric *Npc1*^{-/-} arteries to the same levels recorded from WT mice.

Systolic hypertension is a vascular problem associated with NPC1 disease but the underlying mechanisms are not well understood (Afzali, Nakhaee et al. 2013, Afzali, Hashemi et al. 2017).

TMEM16A has been proposed as a determinant of systemic blood pressure (Heinze, Seniuk

et al. 2014, Askew Page, Dalsgaard et al. 2019). For example, several studies showed an increase in TMEM16A current in both conduit and resistance arteries of spontaneous hypertensive rats (Wang, Li et al. 2015, Askew Page, Dalsgaard et al. 2019). Systolic blood pressure (SBP) is influenced by factors such as ejection fraction, arterial compliance and the timing of wave reflection (Herring 2018). An increased vascular reactivity, such as that observed in isolated *Npc1*^{-/-} aortic rings, may lead to increased pulse wave velocity, and consequently higher SBP.

In this chapter I also showed that mesenteric arteries, which are known to significantly contribute to peripheral resistance (Levy, Ambrosio et al. 2001), have increased agonist-induced contraction *Npc1*^{-/-} mice. Even though blood pressure abnormalities were thought to originate from altered kidney function for more than four decades, several studies have more recently showed that primary abnormalities in the vasculature can also directly cause abnormalities of blood pressure (Mendelsohn 2005, Davis, Shi et al. 2013, Seo, Lee et al. 2016, Cil, Chen et al. 2021). Hence, the enhanced activity in aortas of *Npc1*^{-/-} mice could explain the hypertension observed in some NPC disease patients (Afzali, Nakhaee et al. 2013, Afzali, Hashemi et al. 2017).

5.5 TMEM16A modulation on NPC1 regulates brain capillaries function in *Npc1*^{-/-} mice

Within the brain, TMEM16A is functionally expressed in the microvasculature, specifically in cerebral pericytes and VSMCs surrounding arterioles and capillaries (Vanlandewijck, He et al. 2018, Zeisel, Hochgerner et al. 2018). Therefore, we examined if the enhanced vessel contractility in *Npc1*^{-/-} mice could also occur in the brain. We investigated the properties and function of pericytes in the prefrontal cortex, where pericytes are highly abundant (Persidsky, Hill et al. 2016). We show that the density of pericytes per 100 μm of capillaries was significantly reduced in *Npc1*^{-/-} mice compared to WT mice. This data indicates that altered

properties of blood vessel contractility in *Npc1*^{-/-} mice can be related to structural changes of pericytes density in the brain. Pericytes density reduction and degeneration was shown to be associated with Alzheimer disease and vascular dementia in the literature (Sagare, Bell et al. 2013, Halliday, Rege et al. 2016, Miners, Schulz et al. 2018). Moreover, some studies indicate that NPC disease shares similar pathophysiology, such as failure in cholesterol and endo-lysosomal trafficking, with Alzheimer disease where cerebrovascular dysfunction is responsible for neuronal cell death (Nixon, Wegiel et al. 2005, Roher, Debbins et al. 2012, Cruz Hernández, Bracko et al. 2019). Therefore, the reduction of pericytes density observed in *Npc1*^{-/-} cerebral slices (Figure 5.3.1), might be a significant contributing factor to the neurodegeneration observed in NPC disease.

We also showed that pericyte function is enhanced in *Npc1*^{-/-} cerebral slices leading to an increase in agonist-induced constriction. It is known that increased contractility of pericytes in the brain can lead to neurovascular uncoupling and reduced blood flow (Larivière, Thibault et al. 1993, Hibbs, Love et al. 2021). Thus, we hypothesised that the increased contractility in *Npc1*^{-/-} cerebral slices might result in increased pericytes death during pathophysiology. OGD was used to induce artificial ischaemia in brain slices of *Npc1*^{-/-} and WT mice. We observed a significant increase in pericytes cell death in *Npc1*^{-/-} mice compared to WT which was rescued by incubation with the TMEM16A inhibitor Ani9. These results implicate TMEM16A in the impaired pericyte-mediated capillary contractility observed in *Npc1*^{-/-} mice. This is very important in the regulation of brain function as impaired pericyte activity can lead to pericytes dying in rigor around capillaries reducing blood flow to the brain and thus affecting neurovascular coupling as described in the Introduction (Section 1.10.2).

5.6 Conclusions

The data presented in this chapter suggest that TMEM16A plays an important role in regulating the enhanced agonist-induced contractility in aortas, mesenteric arteries and brain

capillaries of *Npc1*^{-/-} mice. In freshly isolated VSMCs from *Npc1*^{-/-} aortas, the CaCC current recorded from patch-clamping experiments, was significantly increased compared to VSMCs isolated from WT mice. Moreover, treating *Npc1*^{-/-} VSMCs with the TMEM16A-inhibitor Ani9 prevented this activation. On a tissue level, aortic and mesenteric blood vessels showed enhanced agonist-induced contractility in *Npc1*^{-/-} mice. This regulation is dependent on Cl⁻ channels, as *i*) depolarising the membrane with high [K⁺]_e did not alter contractility in *Npc1*^{-/-} mice from WT and *ii*) lowering [Cl⁻]_e to activate Cl⁻ channel exacerbated the enhanced agonist-induced contractility in *Npc1*^{-/-} mice. The Cl⁻ channel TMEM16A plays an important role in this mechanism, as blocking the channel with the specific inhibitors Ani9 or TMinh-23 reduced enhanced agonist-induced contractility in *Npc1*^{-/-} mice to WT levels. Moreover, the data illustrated in this chapter also suggests that blood vessel contractility properties are also affected in *Npc1*^{-/-} brain, where the contractility of capillaries is tightly regulated by pericytes expressing TMEM16A. Pericytes distribution was reduced in *Npc1*^{-/-} brain while the agonist-mediated capillary constriction was increased. During artificial ischaemic conditions, more pericytes cell death was observed in *Npc1*^{-/-} and this could be rescued by application of Ani9. We therefore propose that TMEM16A activity could be targeted in NPC disease pathophysiology.

Chapter 6

Concluding Remarks

Concluding remarks

The overall objectives of this thesis were (i) to examine the possibility that TMEM16A channel senses and responds to change in plasmalemmal lipid composition determined by the lysosome, (ii) to define the role of the NPC1 protein in these effects and (iii) to advance our understanding of the pharmacology of the TMEM16A channel with the view of correcting alterations in channel function in disease of altered lipid homeostasis. This work of thesis reveals a previously unanticipated mechanism of control of the TMEM16A channel by the lysosome. The work also demonstrates that the TMEM16A channel current is enhanced during NPC1 inhibition. Physiologically, this increase results in enhanced arterial contractility in response to G_qPCR agonists. This knowledge could help in the future to design new therapies for NPC and to study other lysosomal disorders where TMEM16A function might also be altered.

The work of this thesis began with a systematic characterisation of TMEM16A and its family members TMEM16A, TMEM16B, TMEM16F and TMEM16K, which are also expressed in VSMCs (Manoury, Tamuleviciute et al. 2010). This examination involved the analysis of the electrophysiological profile and cellular localisation of these channels. We discovered that TMEM16K, unlike the other TMEM16x family members which are plasma membrane resident channels, is an intracellular channel residing in the ER (Bushell, Pike et al. 2019). The effect of Ani9, a potent and selective TMEM16A blocker, was studied and reported to be selective over TMEM16B, in accordance with the literature (Seo, Lee et al. 2016). The ability of the novel small molecules AUT11813 and AUT11814 (designed and synthesised by Autifony Therapeutics), to inhibit TMEM16A current in heterologous system was studied. Since AUT11814 showed a more potent IC₅₀ compared to AUT11813, it was then used as a tool to specifically block TMEM16A in isolated aortic rings in response to PE stimulation of the α 1-adrenergic receptors. This analysis demonstrated that both Ani9 and AUT11814 strongly inhibited mouse aortic rings constriction in response to PE treatment. In addition, since there

is limited knowledge of TMEM16A activators, the novel small molecule activator AUT11817, was used to gain further insights in the physiological role of vascular TMEM16A channels. It was found that AUT11817 strongly activated the response of rat aortic rings to PE.

A key finding of the work presented in this thesis is the novel discovery that the TMEM16A channels are activated during inhibition of the lysosomal lipid transporter protein NPC1. TMEM16A has a strong sensitivity to a variety of lipids which has been characterised by several groups (Ta, Acheson et al. 2017, De Jesus-Perez, Cruz-Rangel et al. 2018) and its pore has regions directly exposed to the plasmalemmal lipids (Whitlock and Hartzell 2016). We combined this knowledge with the notion that NPC1 regulates the transport of lipids from the lysosome to several intracellular organelles and the plasma membrane (Lloyd-Evans and Platt 2010, Hoglinger, Burgoyne et al. 2019) and thus hypothesised that a cross-talk between TMEM16A and NPC1 may occur. We discovered that TMEM16A Cl^- current is enhanced during NPC1 pharmacological inhibition or deletion of the *Npc1* locus. We showed that βCD , an investigational therapy for NPC1 disease, or genetic re-introduction of the *Npc1* locus were able to rescue TMEM16A activation by NPC1 inhibition in heterologous systems. The effect of NPC1 inhibition was also studied in response to activation of TMEM16A *via* the α 1-adrenergic receptor. It was found that PE stimulated TMEM16A Cl^- currents, that this activation was exacerbated during NPC1 inhibition and that it could be blocked by Ani9.

We then worked towards the understanding of the mechanism involved in TMEM16A potentiation by NPC1. TMEM16A gating components were studied using stationary noise analysis and the TMEM16A mutants, I637A and Q645A, where the pore of the channel is locked in its open conformation. We discovered that NPC1 inhibition increased the TMEM16A open probability and did not alter the current density of TMEM16A gating mutants. Moreover, we demonstrated that PIP_2 is required for TMEM16A activation by NPC1. This finding was cross-validated by a number of several independent experiments: (i) PIP_2 plasmalemmal

depletion by DrVSP and (ii) the PIP₂ scavenger neomycin prevented TMEM16A activation by NPC1, (iii) the PIP₂ insensitive TMEM16A channel R482A was also insensitive to NPC1 inhibition and (iv) the PLC inhibitor edelfosine induced TMEM16A activation to a similar extent to NPC1 inhibition. Using confocal microscopy, we discovered that plasmalemmal PIP₂ is increased during NPC1 inhibition and β CD can be used to rescue it. Our results indicate that TMEM16A is activated by NPC1 *via* an increase in the channel open probability which is based on increased PIP₂ plasmalemmal levels.

We also worked towards elucidating if the increased TMEM16A activity observed in heterologous system could be translated into native tissues. We observed that in VSMCs isolated from *Npc1*^{-/-} mice, TMEM16A current was increased to a similar extent as in our heterologous system and could be rescued by treatment with Ani9. In addition, we studied the response of *Npc1*^{-/-} mouse aortic and mesenteric rings to PE, and discovered that PE stimulation was increased in both vessel types. The increased aortic contractility found in *Npc1*^{-/-} aortic rings could be prevented by (i) treatment with β CD, incubation with the TMEM16A specific blockers (ii) Ani9 or (iii) TMinh-23. We discovered that the increased contractility in *Npc1*^{-/-} tissues was also present in cortical brain capillaries in response to ET₁. Moreover, it was found that *Npc1*^{-/-} cortical brain slices have a deficit in pericytes distribution compared to WT mice. In addition, during oxygen-glucose deprivation conditions, pericytes death was increased in *Npc1*^{-/-} cortical slices and this increase could be blocked by Ani9.

The work present in this thesis provides insights into the mechanisms underlying vascular impairments when NPC1 is not functional (Figure 6.1). This is in accordance with reports showing cardiovascular alterations in some NPC disease patients like narrowing and swelling of coronary arteries (Ishii, Takahashi et al. 2006, Afzali, Hashemi et al. 2017). Correcting vascular impairments in NPC disease could be particularly important at a cardiac level to improve narrowing of coronary arteries due to lipid accumulation and at a microvascular level in the brain where reduced blood flow can enhance neurodegeneration (Ishii, Takahashi et al. 2006, Jeong, Bae et al. 2019).

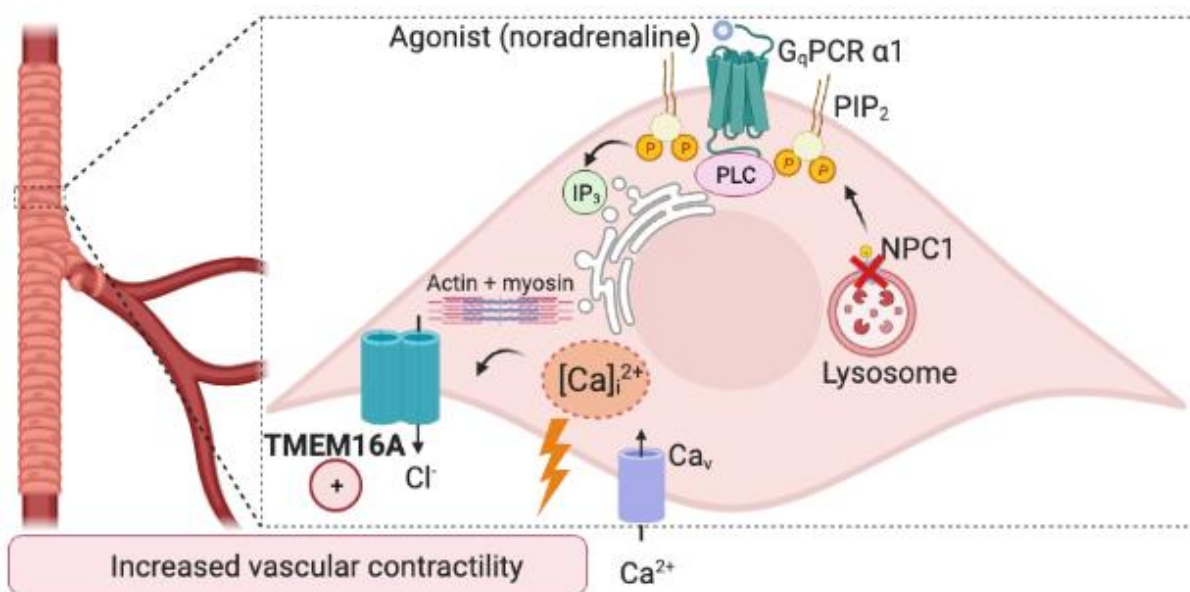


Figure 5.6.1 Proposed mechanism of TMEM16A activation and increased vascular contractility in a VSMC cell during NPC1 inhibition.

Diagrammatic summary of the key results of the study presented in this thesis. The TMEM16A channel activity is enhanced during NPC1 inhibition in a VSMC. Activation of α₁-adrenergic receptors G_qPCRs by PE initiates the IP₃ signalling pathways leading to Ca²⁺ release from the ER. The resulting activation of TMEM16A leads to Cl⁻ efflux, membrane depolarisation, Ca_v channels activation, Ca²⁺ entry and contraction. TMEM16A activation during NPC1 inhibition is based on increased open channel probability due to augmented plasmalemmal PIP₂ levels. TMEM16A activation can lead to increased vascular contractility in NPC disease models where NPC1 is not functional.

Future Directions

The work presented above shows that the mechanism underlying TMEM16A activation during NPC1 inhibition relies on PIP₂. Additional work would be required in order to elucidate this mechanism further:

- 1) The molecular mechanism responsible for altered PIP₂ levels during NPC1 inhibition is not fully defined. In this work, we have hypothesised that altered levels of cholesterol can affect intracellular PIP₂ levels and distribution. In Chapter 4, I have speculated that PLC may be involved because PLC is normally activated by cholesterol and the reduced cholesterol on the plasma membrane during NPC1 inhibition as a result may reduce the activity of PLC, potentially leading to accumulation of PIP₂. It would be important to experimentally assess the level of plasmalemmal cholesterol in cells where NPC1 was pharmacologically inhibited or genetically deleted. Exogenous addition of cholesterol in these cellular models during patch-clamp experiments could give information on how and if cholesterol is affecting TMEM16A current during NPC1 impairment. However, cholesterol is a difficult lipid to dissolve due to its high hydrophobicity and some studies have applied cholesterol complexed to β CD instead of direct application. An alternative approach could be to utilise siRNA for PLC isoforms to probe the role of PLC in cholesterol-mediated PIP₂ accumulation in the cells systems used in this project.
- 2) This work has shown that plasmalemmal PIP₂ levels are increased during NPC1 inhibition (Figure 4.3.6). However, I have also shown that upon α 1 adrenergic activation with PE, PIP₂ cleavage increases $[Ca^{2+}]_i$ levels activating TMEM16A and that this activation is enhanced in cells where NPC1 was pharmacologically inhibited (Figure 4.1.6). Additional work would be required to confirm that higher PIP₂ levels are responsible for the enhanced TMEM16A current in response to α 1-adrenergic receptor

activation observed in cells where NPC1 is inhibited. This could be studied by co-expressing TMEM16A, DrVSP and the α 1-adrenergic receptor in the presence or absence of the NPC1 inhibitor. After activation of DrVSP to deplete PIP₂ levels, followed by α 1-adrenergic receptor activation, TMEM16A currents can be studied to understand the contribution of PIP₂ during α 1-adrenergic stimulation.

Publications, Presentations, Posters and Awards

Publications

Simon R. Bushell, Ashley C. W. Pike, Maria E. Falzone, Nils J. G. Rorsman*, Chau M. Ta*, Robin A*. Corey, Thomas D. Newport*, John C. Christianson*, **Lara F. Scofano***, Chitra A. Shintre, Annamaria Tessitore, Amy Chu, Qinrui Wang, Leela Shrestha, Shubhashish M. M. Mukhopadhyay, James D. Love, Nicola A. Burgess-Brown, Rebecca Sitsapesan, Phillip J. Stansfeld, Juha T. Huiskonen, Paolo Tammaro, Alessio Accardi & Elisabeth P. Carpenter (*equal contribution): "The structural basis of lipid scrambling and inactivation in the endoplasmic reticulum scramblase TMEM16K"

Nature Communications, 2019. 10(1): p. 3956

Lara F. Scofano, Rumaitha Al-Hosni, Kathryn E. Acheson, Zuzanna Borawska, Claire Smith, Zeki Ilkan, Frances M. Platt, and Paolo Tammaro: "Lipid-mediated control of the TMEM16A Ca²⁺- gated Cl⁻ channel by the lysosomal NPC1 protein"

(Manuscript in preparation)

Kathryn Acheson, **Lara F. Scofano**, Ria Dinsdale, and Paolo Tammaro: "The TMEM16A chloride channel offers a novel therapeutic target for the omega-3 fatty acid DHA"

(Manuscript in preparation)

Presentations and Posters

Lara F. Scofano, Rumaitha Al-Hosni, Kathryn E. Acheson, Zuzanna Borawska, Claire Smith, Zeki Ilkan, Frances M. Platt, and Paolo Tammaro: "Effect of altered lipid trafficking on the modulation of vascular tone by the TMEM16A chloride channel" Poster Presentation, BHF Cre Symposium 2021

Lara F. Scofano, Kathryn E. Acheson, Claire Smith, Frances M. Platt, and Paolo Tammaro: "Lipid-mediated control of the TMEM16A Ca²⁺- gated Cl⁻ channel by the lysosomal NPC1 protein" Poster presentation, Biophysical Society - 65th Annual Meeting 2021

Lara F. Scofano, Kathryn E. Acheson, Claire Smith, Frances M. Platt, and Paolo Tammaro: "The TMEM16A Ca²⁺- gated Cl⁻ channel is regulated by the lysosomal NPC1 protein" Selected Oral Communication, British Pharmacological Society - Pharmacology 2020

Lara F. Scofano, Kathryn E. Acheson, Claire Smith, Frances M. Platt, and Paolo Tammaro: "TMEM16A is a lipid sensitive ion channel and is controlled by the lysosomal NPC1 protein" Poster Presentation, OXION: Ion Channels and Disease Initiative 2019

Awards

Covid-19 Scholarship Extensions Scheme, 2021, Medical Science Division, University of Oxford

Goodger and Schorstein Research Scholarship in Medical Sciences, 2020, University of Oxford, UK

Virtual Travel Award, 2020, The Biophysical Society, Annual Meeting

The Waverley Scholarship, 2018, The Queen's College, University of Oxford, UK

Industrial Studentship, 2018, Autifony Therapeutics, UK

References

- Aaronson, P. I. and S. V. Smirnov (1996). Membrane ion channels in vascular smooth muscle excitation-contraction coupling.
- Abbott, N. J., A. A. Patabendige, D. E. Dolman, S. R. Yusof and D. J. Begley (2010). "Structure and function of the blood-brain barrier." Neurobiol Dis **37**(1): 13-25.
- Adomaviciene, A., K. J. Smith, H. Garnett and P. Tammaro (2013). "Putative pore-loops of TMEM16/anoctamin channels affect channel density in cell membranes." J Physiol **591**(14): 3487-3505.
- Afzali, M., M. Hashemi, S. P. Tabatabaei, K. T. Fakheri and A. Nakhaee (2017). "Association between the rs1805081 polymorphism of Niemann-Pick type C1 gene and cardiovascular disease in a sample of an Iranian population." Biomedical reports **6**(1): 83-88.
- Afzali, M., A. Nakhaee, S. P. Tabatabaei, K. Tirgar-Fakheri and M. Hashemi (2013). "Aberrant promoter methylation profile of Niemann-pick type C1 gene in cardiovascular disease." Iranian biomedical journal **17**(2): 77-83.
- Akaike, N., H. Kanaide, T. Kuga, M. Nakamura, J. Sadoshima and H. Tomoike (1989). "Low-voltage-activated calcium current in rat aorta smooth muscle cells in primary culture." The Journal of physiology **416**: 141-160.
- Akatsuka, Y., K. Egashira, Y. Katsuda, T. Narishige, H. Ueno, H. Shimokawa and A. Takeshita (1994). "ATP sensitive potassium channels are involved in adenosine A2 receptor mediated coronary vasodilatation in the dog." Cardiovasc Res **28**(6): 906-911.
- Alaimo, A. and A. Villarroel (2018). "Calmodulin: A Multitasking Protein in Kv7.2 Potassium Channel Functions." Biomolecules **8**(3).
- Amberg, G. C. and M. F. Navedo (2013). "Calcium dynamics in vascular smooth muscle." Microcirculation **20**(4): 281-289.
- Armulik, A., A. Abramsson and C. Betsholtz (2005). "Endothelial/pericyte interactions." Circ Res **97**(6): 512-523.
- Armulik, A., G. Genové, M. Mäe, M. H. Nisancioglu, E. Wallgard, C. Niaudet, L. He, J. Norlin, P. Lindblom, K. Strittmatter, B. R. Johansson and C. Betsholtz (2010). "Pericytes regulate the blood-brain barrier." Nature **468**(7323): 557-561.
- Arnould, T., C. Michiels, I. Alexandre and J. Remacle (1992). "Effect of hypoxia upon intracellular calcium concentration of human endothelial cells." J Cell Physiol **152**(1): 215-221.
- Askew Page, H. R., T. Dalsgaard, S. N. Baldwin, T. A. Jepps, O. Povstyan, S. P. Olesen and I. A. Greenwood (2019). "TMEM16A is implicated in the regulation of coronary flow and is altered in hypertension." Br J Pharmacol **176**(11): 1635-1648.
- Attwell, D., A. M. Buchan, S. Charkak, M. Lauritzen, B. A. Macvicar and E. A. Newman (2010). "Glial and neuronal control of brain blood flow." Nature **468**(7321): 232-243.
- Attwell, D., A. Mishra, C. N. Hall, F. M. O'Farrell and T. Dalkara (2016). "What is a pericyte?" J Cereb Blood Flow Metab **36**(2): 451-455.
- Ávalos Prado, P., S. Häfner, Y. Comoglio, B. Wdziekonski, C. Duranton, B. Attali, J. Barhanin and G. Sandoz (2021). "KCNE1 is an auxiliary subunit of two distinct ion channel superfamilies." Cell **184**(2): 534-544.e511.
- Ayuyan, A. G. and F. S. Cohen (2018). "The Chemical Potential of Plasma Membrane Cholesterol: Implications for Cell Biology." Biophys J **114**(4): 904-918.
- Bader, C. R., D. Bertrand and E. A. Schwartz (1982). "Voltage-activated and calcium-activated currents studied in solitary rod inner segments from the salamander retina." The Journal of physiology **331**: 253-284.
- Baeyens, N., V. Bouryi and N. Morel (2014). "Extracellular calcium modulates the inhibitory effect of 4-aminopyridine on Kv current in vascular smooth muscle cells." Eur J Pharmacol **723**: 116-123.

- Bakker, A. C., P. Webster, W. A. Jacob and N. W. Andrews (1997). "Homotypic fusion between aggregated lysosomes triggered by elevated $[Ca^{2+}]_i$ in fibroblasts." J Cell Sci **110 (Pt 18)**: 2227-2238.
- Balasubramanian, L., A. Ahmed, C. M. Lo, J. S. Sham and K. P. Yip (2007). "Integrin-mediated mechanotransduction in renal vascular smooth muscle cells: activation of calcium sparks." Am J Physiol Regul Integr Comp Physiol **293(4)**: R1586-1594.
- Balreira, A., V. Boczonadi, E. Barca, A. Pyle, B. Bansagi, M. Appleton, C. Graham, I. P. Hargreaves, V. M. Rasic, H. Lochmüller, H. Griffin, R. W. Taylor, A. Naini, P. F. Chinnery, M. Hirano, C. M. Quinzii and R. Horvath (2014). "ANO10 mutations cause ataxia and coenzyme Q₁₀ deficiency." J Neurol **261(11)**: 2192-2198.
- Barish, M. E. (1983). "A transient calcium-dependent chloride current in the immature *Xenopus* oocyte." J Physiol **342**: 309-325.
- Bayliss, W. M. (1902). "On the local reactions of the arterial wall to changes of internal pressure." J Physiol **28(3)**: 220-231.
- Bell, R. D., E. A. Winkler, A. P. Sagare, I. Singh, B. LaRue, R. Deane and B. V. Zlokovic (2010). "Pericytes control key neurovascular functions and neuronal phenotype in the adult brain and during brain aging." Neuron **68(3)**: 409-427.
- Bennett, M. V., J. E. Contreras, F. F. Bukauskas and J. C. Sáez (2003). "New roles for astrocytes: gap junction hemichannels have something to communicate." Trends Neurosci **26(11)**: 610-617.
- Benussi, A., M. S. Cotelli, V. Cantoni, V. Bertasi, M. Turla, A. Dardis, J. Biasizzo, R. Manenti, M. Cotelli, A. Padovani and B. Borroni (2019). "Clinical and neurophysiological characteristics of heterozygous NPC1 carriers." JIMD Rep **49(1)**: 80-88.
- Bergers, G. and S. Song (2005). "The role of pericytes in blood-vessel formation and maintenance." Neuro-oncology **7(4)**: 452-464.
- Bergers, G. and S. Song (2005). "The role of pericytes in blood-vessel formation and maintenance." Neuro Oncol **7(4)**: 452-464.
- Billaud, M., V. S. Donnemberg, B. W. Ellis, E. M. Meyer, A. D. Donnemberg, J. C. Hill, T. D. Richards, T. G. Gleason and J. A. Phillippi (2017). "Classification and Functional Characterization of Vasa Vasorum-Associated Perivascular Progenitor Cells in Human Aorta." Stem Cell Reports **9(1)**: 292-303.
- Billig, G. M., B. Pál, P. Fidzinski and T. J. Jentsch (2011). "Ca²⁺-activated Cl⁻ currents are dispensable for olfaction." Nat Neurosci **14(6)**: 763-769.
- Blaustein, M. P. and W. J. Lederer (1999). "Sodium/calcium exchange: its physiological implications." Physiol Rev **79(3)**: 763-854.
- Blocki, A., S. Beyer, F. Jung and M. Raghunath (2018). "The controversial origin of pericytes during angiogenesis - Implications for cell-based therapeutic angiogenesis and cell-based therapies." Clin Hemorheol Microcirc **69(1-2)**: 215-232.
- Boccaccio, A., J. Scholz-Starke, S. Hamamoto, N. Larisch, M. Festa, P. V. Gutla, A. Costa, P. Dietrich, N. Uozumi and A. Carpaneto (2014). "The phosphoinositide PI(3,5)P₂ mediates activation of mammalian but not plant TPC proteins: functional expression of endolysosomal channels in yeast and plant cells." Cell Mol Life Sci **71(21)**: 4275-4283.
- Bock, J., I. Szabó, N. Gamper, C. Adams and E. Gulbins (2003). "Ceramide inhibits the potassium channel Kv1.3 by the formation of membrane platforms." Biochem Biophys Res Commun **305(4)**: 890-897.
- Brailoiu, E., D. Churamani, X. Cai, M. G. Schrlau, G. C. Brailoiu, X. Gao, R. Hooper, M. J. Boulware, N. J. Dun, J. S. Marchant and S. Patel (2009). "Essential requirement for two-pore channel 1 in NAADP-mediated calcium signaling." Journal of Cell Biology **186(2)**: 201-209.
- Brailoiu, E., T. Rahman, D. Churamani, D. L. Prole, G. C. Brailoiu, R. Hooper, C. W. Taylor and S. Patel (2010). "An NAADP-gated two-pore channel targeted to the plasma

- membrane uncouples triggering from amplifying Ca²⁺ signals." J Biol Chem **285**(49): 38511-38516.
- Brauchi, S., G. Orta, C. Mascayano, M. Salazar, N. Raddatz, H. Urbina, E. Rosenmann, F. Gonzalez-Nilo and R. Latorre (2007). "Dissection of the components for PIP₂ activation and thermosensation in TRP channels." Proc Natl Acad Sci U S A **104**(24): 10246-10251.
 - Bright, N. A., L. J. Davis and J. P. Luzio (2016). "Endolysosomes Are the Principal Intracellular Sites of Acid Hydrolase Activity." Current biology : CB **26**(17): 2233-2245.
 - Brini, M. and E. Carafoli (2011). "The plasma membrane Ca²⁺ ATPase and the plasma membrane sodium calcium exchanger cooperate in the regulation of cell calcium." Cold Spring Harb Perspect Biol **3**(2).
 - Brooks, M. B., J. L. Catalfamo, R. MacNguyen, D. Tim, S. Fancher and J. A. McCardle (2015). "A TMEM16F point mutation causes an absence of canine platelet TMEM16F and ineffective activation and death-induced phospholipid scrambling." J Thromb Haemost **13**(12): 2240-2252.
 - Brown, D. A. and E. London (1998). "Functions of lipid rafts in biological membranes." Annu Rev Cell Dev Biol **14**: 111-136.
 - Brown, D. A. and G. M. Passmore (2010). "Some new insights into the molecular mechanisms of pain perception." J Clin Invest **120**(5): 1380-1383.
 - Brozovich, F. V., C. J. Nicholson, C. V. Degen, Y. Z. Gao, M. Aggarwal and K. G. Morgan (2016). "Mechanisms of Vascular Smooth Muscle Contraction and the Basis for Pharmacologic Treatment of Smooth Muscle Disorders." Pharmacological reviews **68**(2): 476-532.
 - Brunner, J. D., N. K. Lim, S. Schenck, A. Duerst and R. Dutzler (2014). "X-ray structure of a calcium-activated TMEM16 lipid scramblase." Nature **516**(7530): 207-212.
 - Bulley, S. and J. H. Jaggar (2014). "Cl⁻ channels in smooth muscle cells." Pflugers Archiv : European journal of physiology **466**(5): 861-872.
 - Burkhardt, J. K., C. J. Echeverri, T. Nilsson and R. B. Vallee (1997). "Overexpression of the dynamitin (p50) subunit of the dynactin complex disrupts dynein-dependent maintenance of membrane organelle distribution." The Journal of cell biology **139**(2): 469-484.
 - Bushell, S. R., A. C. W. Pike, M. E. Falzone, N. J. G. Rorsman, C. M. Ta, R. A. Corey, T. D. Newport, J. C. Christianson, L. F. Scofano, C. A. Shintre, A. Tessitore, A. Chu, Q. Wang, L. Shrestha, S. M. M. Mukhopadhyay, J. D. Love, N. A. Burgess-Brown, R. Sitsapesan, P. J. Stansfeld, J. T. Huiskonen, P. Tammara, A. Accardi and E. P. Carpenter (2019). "The structural basis of lipid scrambling and inactivation in the endoplasmic reticulum scramblase TMEM16K." Nat Commun **10**(1): 3956.
 - Caputo, A., E. Caci, L. Ferrera, N. Pedemonte, C. Barsanti, E. Sondo, U. Pfeffer, R. Ravazzolo, O. Zegarra-Moran and L. J. Galletta (2008). "TMEM16A, a membrane protein associated with calcium-dependent chloride channel activity." Science **322**(5901): 590-594.
 - Caputo, A., I. Piano, G. C. Demontis, N. Bacchi, S. Casarosa, L. Della Santina and C. Gargini (2015). "TMEM16A is associated with voltage-gated calcium channels in mouse retina and its function is disrupted upon mutation of the auxiliary $\alpha 2\delta 4$ subunit." Front Cell Neurosci **9**: 422.
 - Carstea, E. D., J. A. Morris, K. G. Coleman, S. K. Loftus, D. Zhang, C. Cummings, J. Gu, M. A. Rosenfeld, W. J. Pavan, D. B. Krizman, J. Nagle, M. H. Polymeropoulos, S. L. Sturley, Y. A. Ioannou, M. E. Higgins, M. Comly, A. Cooney, A. Brown, C. R. Kaniski, E. J. Blanchette-Mackie, N. K. Dwyer, E. B. Neufeld, T. Y. Chang, L. Liscum, J. F. Strauss, 3rd, K. Ohno, M. Zeigler, R. Carmi, J. Sokol, D. Markie, R. R. O'Neill, O. P. van Diggelen, M. Elleder, M. C. Patterson, R. O. Brady, M. T. Vanier, P. G. Pentchev and D. A. Tagle (1997). "Niemann-Pick C1 disease gene: homology to mediators of cholesterol homeostasis." Science **277**(5323): 228-231.

- Carstea, E. D., M. H. Polymeropoulos, C. C. Parker, S. D. Deterra-Wadleigh, R. R. O'Neill, M. C. Patterson, E. Goldin, H. Xiao, R. E. Straub, M. T. Vanier and et al. (1993). "Linkage of Niemann-Pick disease type C to human chromosome 18." Proc Natl Acad Sci U S A **90**(5): 2002-2004.
- Casares, D., P. V. Escribá and C. A. Rosselló (2019). "Membrane Lipid Composition: Effect on Membrane and Organelle Structure, Function and Compartmentalization and Therapeutic Avenues." Int J Mol Sci **20**(9).
- Casteels, R., K. Kitamura, H. Kuriyama and H. Suzuki (1977). "Excitation-contraction coupling in the smooth muscle cells of the rabbit main pulmonary artery." J Physiol **271**(1): 63-79.
- Cendelin, J. (2016). "Transplantation and Stem Cell Therapy for Cerebellar Degenerations." Cerebellum **15**(1): 48-50.
- Cenedella, R. J. (2009). "Cholesterol synthesis inhibitor U18666A and the role of sterol metabolism and trafficking in numerous pathophysiological processes." Lipids **44**(6): 477-487.
- Centeio, R., I. Cabrita, R. Benedetto, K. Talbi, J. Ousingsawat, R. Schreiber, J. K. Sullivan and K. Kunzelmann (2020). "Pharmacological Inhibition and Activation of the Ca(2+) Activated Cl(-) Channel TMEM16A." Int J Mol Sci **21**(7).
- Chadha, P. S., F. Zunke, H. L. Zhu, A. J. Davis, T. A. Jepps, S. P. Olesen, W. C. Cole, J. D. Moffatt and I. A. Greenwood (2012). "Reduced KCNQ4-encoded voltage-dependent potassium channel activity underlies impaired β -adrenoceptor-mediated relaxation of renal arteries in hypertension." Hypertension **59**(4): 877-884.
- Chen, F. W., C. Li and Y. A. Ioannou (2010). "Cyclodextrin induces calcium-dependent lysosomal exocytosis." PLoS One **5**(11): e15054.
- Chen, O. C. W., A. Colaco, L. C. Davis, F. N. Kiskin, N. Y. Farhat, A. O. Speak, D. A. Smith, L. Morris, E. Eden, P. Tynan, G. C. Churchill, A. Galione, F. D. Porter and F. M. Platt (2020). "Defective platelet function in Niemann-Pick disease type C1." JIMD reports **56**(1): 46-57.
- Chen, Q. Y., C. Y. Tan, Y. Wang, K. T. Ma, L. Li and J. Q. Si (2019). "Mechanism of persistent hyperalgesia in neuropathic pain caused by chronic constriction injury." Neural Regen Res **14**(6): 1091-1098.
- Chevallier, J., Z. Chamoun, G. Jiang, G. Prestwich, N. Sakai, S. Matile, R. G. Parton and J. Gruenberg (2008). "Lysobisphosphatidic acid controls endosomal cholesterol levels." J Biol Chem **283**(41): 27871-27880.
- Chipperfield, A. R. and A. A. Harper (2000). "Chloride in smooth muscle." Prog Biophys Mol Biol **74**(3-5): 175-221.
- Cho, C. H., S. Lee, A. Kim, O. Yarishkin, K. Ryoo, Y. S. Lee, H. G. Jung, E. Yang, D. Y. Lee, B. Lee, H. Kim, U. Oh, H. I. Im, E. M. Hwang and J. Y. Park (2020). "TMEM16A expression in cholinergic neurons of the medial habenula mediates anxiety-related behaviors." EMBO Rep **21**(2): e48097.
- Christensen, K. A., J. T. Myers and J. A. Swanson (2002). "pH-dependent regulation of lysosomal calcium in macrophages." J Cell Sci **115**(Pt 3): 599-607.
- Chun, Y. S. and S. Chung (2020). "High-Cholesterol Diet Decreases the Level of Phosphatidylinositol 4,5-Bisphosphate by Enhancing the Expression of Phospholipase C (PLC β 1) in Rat Brain." International journal of molecular sciences **21**(3): 1161.
- Chun, Y. S., H. G. Oh, M. K. Park, T.-W. Kim and S. Chung (2013). "Increasing Membrane Cholesterol Level Increases the Amyloidogenic Peptide by Enhancing the Expression of Phospholipase C." Journal of neurodegenerative diseases **2013**: 407903-407903.
- Chun, Y. S., S. Shin, Y. Kim, H. Cho, M. K. Park, T.-W. Kim, S. V. Voronov, G. Di Paolo, B.-C. Suh and S. Chung (2010). "Cholesterol modulates ion channels via down-regulation of phosphatidylinositol 4,5-bisphosphate." Journal of neurochemistry **112**(5): 1286-1294.

- Cil, O., X. Chen, H. R. Askew Page, S. N. Baldwin, M. C. Jordan, P. Myat Thwe, M. O. Anderson, P. M. Haggie, I. A. Greenwood, K. P. Roos and A. S. Verkman (2021). "A small molecule inhibitor of the chloride channel TMEM16A blocks vascular smooth muscle contraction and lowers blood pressure in spontaneously hypertensive rats." Kidney Int **100**(2): 311-320.
- Cipolla, M. J., D. S. Liebeskind and S. L. Chan (2018). "The importance of comorbidities in ischemic stroke: Impact of hypertension on the cerebral circulation." J Cereb Blood Flow Metab **38**(12): 2129-2149.
- Clément-Chomienne, O., M. P. Walsh and W. C. Cole (1996). "Angiotensin II activation of protein kinase C decreases delayed rectifier K⁺ current in rabbit vascular myocytes." J Physiol **495 (Pt 3)**(Pt 3): 689-700.
- Coisne, C., D. Hallier-Vanuxeem, M.-C. Boucau, J. Hachani, S. Tilloy, H. Bricout, E. Monflier, D. Wils, M. Serpelloni, X. Parissaux, L. Fenart and F. Gosselet (2016). "β-Cyclodextrins Decrease Cholesterol Release and ABC-Associated Transporter Expression in Smooth Muscle Cells and Aortic Endothelial Cells." Frontiers in physiology **7**: 185-185.
- Coisne, C., S. Tilloy, E. Monflier, D. Wils, L. Fenart and F. Gosselet (2016). "Cyclodextrins as Emerging Therapeutic Tools in the Treatment of Cholesterol-Associated Vascular and Neurodegenerative Diseases." Molecules **21**(12).
- Contreras-Vite, J. A., S. Cruz-Rangel, J. J. De Jesús-Pérez, I. A. A. Figueroa, A. A. Rodríguez-Menchaca, P. Pérez-Cornejo, H. C. Hartzell and J. Arreola (2016). "Revealing the activation pathway for TMEM16A chloride channels from macroscopic currents and kinetic models." Pflugers Archiv : European journal of physiology **468**(7): 1241-1257.
- Cook, D. P., M. V. Rector, D. C. Bouzek, A. S. Michalski, N. D. Gansemer, L. R. Reznikov, X. Li, M. R. Stroik, L. S. Ostedgaard, M. H. Abou Alaiwa, M. A. Thompson, Y. S. Prakash, R. Krishnan, D. K. Meyerholz, C. Y. Seow and D. A. Stoltz (2016). "Cystic Fibrosis Transmembrane Conductance Regulator in Sarcoplasmic Reticulum of Airway Smooth Muscle. Implications for Airway Contractility." American journal of respiratory and critical care medicine **193**(4): 417-426.
- Cooke, J. P., E. Rossitch, Jr., N. A. Andon, J. Loscalzo and V. J. Dzau (1991). "Flow activates an endothelial potassium channel to release an endogenous nitrovasodilator." The Journal of clinical investigation **88**(5): 1663-1671.
- Costes, S. V., D. Daelemans, E. H. Cho, Z. Dobbin, G. Pavlakis and S. Lockett (2004). "Automatic and Quantitative Measurement of Protein-Protein Colocalization in Live Cells." Biophysical Journal **86**(6): 3993-4003.
- Cox, T., R. Lachmann, C. Hollak, J. Aerts, S. van Weely, M. Hrebíček, F. Platt, T. Butters, R. Dwek, C. Moyses, I. Gow, D. Elstein and A. Zimran (2000). "Novel oral treatment of Gaucher's disease with N-butyldeoxynojirimycin (OGT 918) to decrease substrate biosynthesis." Lancet **355**(9214): 1481-1485.
- Coyan, F. C., F. Abderemane-Ali, M. Y. Amarouch, J. Piron, J. Mordel, C. S. Nicolas, M. Steenman, J. Mérot, C. Marionneau, A. Thomas, R. Brasseur, I. Baró and G. Loussouarn (2014). "A long QT mutation substitutes cholesterol for phosphatidylinositol-4,5-bisphosphate in KCNQ1 channel regulation." PLoS One **9**(3): e93255.
- Crocker, A. C. and S. Farber (1958). "Niemann-Pick disease: a review of eighteen patients." Medicine (Baltimore) **37**(1): 1-95.
- Crousillac, S., J. Colonna, E. McMains, J. S. Dewey and E. Gleason (2009). "Sphingosine-1-phosphate elicits receptor-dependent calcium signaling in retinal amacrine cells." J Neurophysiol **102**(6): 3295-3309.
- Cruz-Rangel, S., J. J. De Jesus-Perez, I. A. Arechiga-Figueroa, A. A. Rodriguez-Menchaca, P. Perez-Cornejo, H. C. Hartzell and J. Arreola (2017). "Extracellular protons enable activation of the calcium-dependent chloride channel TMEM16A." J Physiol **595**(5): 1515-1531.

- Cruz Hernández, J. C., O. Bracko, C. J. Kersbergen, V. Muse, M. Haft-Javaherian, M. Berg, L. Park, L. K. Vinarcsik, I. Ivasyk, D. A. Rivera, Y. Kang, M. Cortes-Canteli, M. Peyrounette, V. Doyeux, A. Smith, J. Zhou, G. Otte, J. D. Beverly, E. Davenport, Y. Davit, C. P. Lin, S. Strickland, C. Iadecola, S. Lorthois, N. Nishimura and C. B. Schaffer (2019). "Neutrophil adhesion in brain capillaries reduces cortical blood flow and impairs memory function in Alzheimer's disease mouse models." Nat Neurosci **22**(3): 413-420.
- Curtis, T. M., J. Tumelty, J. Dawicki, C. N. Scholfield and J. G. McGeown (2004). "Identification and spatiotemporal characterization of spontaneous Ca²⁺ sparks and global Ca²⁺ oscillations in retinal arteriolar smooth muscle cells." Invest Ophthalmol Vis Sci **45**(12): 4409-4414.
- Dahl, N. K., K. L. Reed, M. A. Daunais, J. R. Faust and L. Liscum (1992). "Isolation and characterization of Chinese hamster ovary cells defective in the intracellular metabolism of low density lipoprotein-derived cholesterol." Journal of Biological Chemistry **267**(7): 4889-4896.
- Dam, V. S., D. M. Boedtker, J. Nyvad, C. Aalkjaer and V. Matchkov (2014). "TMEM16A knockdown abrogates two different Ca(2+)-activated Cl (-) currents and contractility of smooth muscle in rat mesenteric small arteries." Pflugers Arch **466**(7): 1391-1409.
- Daneman, R. and A. Prat (2015). "The blood-brain barrier." Cold Spring Harb Perspect Biol **7**(1): a020412.
- Dang, S., S. Feng, J. Tien, C. J. Peters, D. Bulkley, M. Lolicato, J. Zhao, K. Zuberbuhler, W. Ye, L. Qi, T. Chen, C. S. Craik, Y. N. Jan, D. L. Minor, Jr., Y. Cheng and L. Y. Jan (2017). "Cryo-EM structures of the TMEM16A calcium-activated chloride channel." Nature **552**(7685): 426-429.
- Danielsson, J., J. Perez-Zoghbi, K. Bernstein, M. B. Barajas, Y. Zhang, S. Kumar, P. K. Sharma, G. Gallos and C. W. Emala (2015). "Antagonists of the TMEM16A calcium-activated chloride channel modulate airway smooth muscle tone and intracellular calcium." Anesthesiology **123**(3): 569-581.
- Daniotti, J. L. and R. Iglesias-Bartolomé (2011). "Metabolic pathways and intracellular trafficking of gangliosides." IUBMB Life **63**(7): 513-520.
- Dart, C. (2010). "SYMPOSIUM REVIEW: Lipid microdomains and the regulation of ion channel function." The Journal of Physiology **588**(17): 3169-3178.
- Davidson, C. D., N. F. Ali, M. C. Micsenyi, G. Stephney, S. Renault, K. Dobrenis, D. S. Ory, M. T. Vanier and S. U. Walkley (2009). "Chronic cyclodextrin treatment of murine Niemann-Pick C disease ameliorates neuronal cholesterol and glycosphingolipid storage and disease progression." PLoS One **4**(9): e6951.
- Davies, J. P., F. W. Chen and Y. A. Ioannou (2000). "Transmembrane molecular pump activity of Niemann-Pick C1 protein." Science **290**(5500): 2295-2298.
- Davis, A. J., A. S. Forrest, T. A. Jepps, M. L. Valencik, M. Wiwchar, C. A. Singer, W. R. Sones, I. A. Greenwood and N. Leblanc (2010). "Expression profile and protein translation of TMEM16A in murine smooth muscle." Am J Physiol Cell Physiol **299**(5): C948-959.
- Davis, A. J., J. Shi, H. A. Pritchard, P. S. Chadha, N. Leblanc, G. Vasilikostas, Z. Yao, A. S. Verkman, A. P. Albert and I. A. Greenwood (2013). "Potent vasorelaxant activity of the TMEM16A inhibitor T16A(inh) -A01." Br J Pharmacol **168**(3): 773-784.
- Davis, P. J. and M. J. Poznansky (1987). "Modulation of 3-hydroxy-3-methylglutaryl-CoA reductase by changes in microsomal cholesterol content or phospholipid composition." Proceedings of the National Academy of Sciences of the United States of America **84**(1): 118-121.
- de Duve, C. (1983). "Lysosomes revisited." Eur J Biochem **137**(3): 391-397.
- De Jesus-Perez, J. J., S. Cruz-Rangel, A. E. Espino-Saldana, A. Martinez-Torres, Z. Qu, H. C. Hartzell, N. E. Corral-Fernandez, P. Perez-Cornejo and J. Arreola (2018). "Phosphatidylinositol 4,5-bisphosphate, cholesterol, and fatty acids modulate the calcium-activated chloride channel TMEM16A (ANO1)." Biochim Biophys Acta Mol Cell Biol Lipids **1863**(3): 299-312.

- De Matteis, M. A. and A. Luini (2008). "Exiting the Golgi complex." Nat Rev Mol Cell Biol **9**(4): 273-284.
- Deanfield, J. E., J. P. Halcox and T. J. Rabelink (2007). "Endothelial function and dysfunction: testing and clinical relevance." Circulation **115**(10): 1285-1295.
- Di Fiore, P. P. and M. von Zastrow (2014). "Endocytosis, signaling, and beyond." Cold Spring Harbor perspectives in biology **6**(8): a016865.
- Dibattista, M., A. Amjad, D. K. Maurya, C. Sagheddu, G. Montani, R. Tirindelli and A. Menini (2012). "Calcium-activated chloride channels in the apical region of mouse vomeronasal sensory neurons." J Gen Physiol **140**(1): 3-15.
- Dinsdale, R. L., T. Pipatpolkai, E. Agostinelli, A. J. Russell, P. J. Stansfeld and P. Tammaro (2021). "An outer-pore gate modulates the pharmacology of the TMEM16A channel." Proc Natl Acad Sci U S A **118**(34).
- Divangahi, M., M. Chen, H. Gan, D. Desjardins, T. T. Hickman, D. M. Lee, S. Fortune, S. M. Behar and H. G. Remold (2009). "Mycobacterium tuberculosis evades macrophage defenses by inhibiting plasma membrane repair." Nat Immunol **10**(8): 899-906.
- Dodge, A. B., H. B. Hechtman and D. Shepro (1991). "Microvascular endothelial-derived autacoids regulate pericyte contractility." Cell Motil Cytoskeleton **18**(3): 180-188.
- Dong, X.-p., D. Shen, X. Wang, T. Dawson, X. Li, Q. Zhang, X. Cheng, Y. Zhang, L. S. Weisman, M. Delling and H. Xu (2010). "PI(3,5)P(2) controls membrane trafficking by direct activation of mucolipin Ca(2+) release channels in the endolysosome." Nature communications **1**(4): 38-38.
- Du, X., I. Lukmantara and H. Yang (2017). "CRISPR/Cas9-Mediated Generation of Niemann-Pick C1 Knockout Cell Line." Methods Mol Biol **1583**: 73-83.
- Dunham, E. T. and I. M. Glynn (1961). "Adenosinetriphosphatase activity and the active movements of alkali metal ions." J Physiol **156**(2): 274-293.
- Dunn, K. W., M. M. Kamocka and J. H. McDonald (2011). "A practical guide to evaluating colocalization in biological microscopy." American Journal of Physiology-Cell Physiology **300**(4): C723-C742.
- Dunn, K. W. and F. R. Maxfield (1992). "Delivery of ligands from sorting endosomes to late endosomes occurs by maturation of sorting endosomes." J Cell Biol **117**(2): 301-310.
- Duran, C. and H. C. Hartzell (2011). "Physiological roles and diseases of Tmem16/Anoctamin proteins: are they all chloride channels?" Acta Pharmacol Sin **32**(6): 685-692.
- Durham, J. T., H. K. Surks, B. M. Dulmovits and I. M. Herman (2014). "Pericyte contractility controls endothelial cell cycle progression and sprouting: insights into angiogenic switch mechanics." Am J Physiol Cell Physiol **307**(9): C878-892.
- Dvir, M., R. Strulovich, D. Sachyani, I. Ben-Tal Cohen, Y. Haitin, C. Dessauer, O. Pongs, R. Kass, J. A. Hirsch and B. Attali (2014). "Long QT mutations at the interface between KCNQ1 helix C and KCNE1 disrupt I(KS) regulation by PKA and PIP₂." J Cell Sci **127**(Pt18): 3943-3955.
- Earley, S. and J. E. Brayden (2015). "Transient receptor potential channels in the vasculature." Physiol Rev **95**(2): 645-690.
- Eberth, C. (1871). "Handbuch der Lehre von der Gewegen des Menschen und der Tiere " Leipzig: Engelmann **Vol. 1**.
- Ebner, M., P. A. Koch and V. Haucke (2019). "Phosphoinositides in the control of lysosome function and homeostasis." Biochemical Society Transactions **47**(4): 1173-1185.
- Eggermont, J., D. Trouet, I. Carton and B. Nilius (2001). "Cellular function and control of volume-regulated anion channels." Cell Biochem Biophys **35**(3): 263-274.

- Ek-Vitorin, J. F. and J. M. Burt (2013). "Structural basis for the selective permeability of channels made of communicating junction proteins." Biochim Biophys Acta **1828**(1): 51-68.
- El-Bouri, W. K. and S. J. Payne (2016). "A statistical model of the penetrating arterioles and venules in the human cerebral cortex." Microcirculation **23**(7): 580-590.
- Elleder, M. and F. Smíd (1985). "Adrenal changes in Niemann-Pick disease: differences between sphingomyelinase deficiency and type C." Acta Histochem **76**(2): 163-176.
- Elliott, W. J. (2007). "Systemic hypertension." Curr Probl Cardiol **32**(4): 201-259.
- Enyedi, A., T. Vorherr, P. James, D. J. McCormick, A. G. Filoteo, E. Carafoli and J. T. Penniston (1989). "The calmodulin binding domain of the plasma membrane Ca²⁺ pump interacts both with calmodulin and with another part of the pump." J Biol Chem **264**(21): 12313-12321.
- Fallah, G., T. Römer, S. Detro-Dassen, U. Braam, F. Markwardt and G. Schmalzing (2011). "TMEM16A(a)/anoctamin-1 shares a homodimeric architecture with CLC chloride channels." Molecular & cellular proteomics : MCP **10**(2): M110.004697-M004110.004697.
- Falzone, M. E., M. Malvezzi, B. C. Lee and A. Accardi (2018). "Known structures and unknown mechanisms of TMEM16 scramblases and channels." J Gen Physiol **150**(7): 933-947.
- Farouque, H. M. O., G. Worthley Stephen, T. Meredith Ian, R. A. P. Skyrme-Jones and J. Zhang Michael (2002). "Effect of ATP-Sensitive Potassium Channel Inhibition on Resting Coronary Vascular Responses in Humans." Circulation Research **90**(2): 231-236.
- Fedigan, S., E. Bradley, T. Webb, R. J. Large, M. A. Hollywood, K. D. Thornbury, N. G. McHale and G. P. Sergeant (2017). "Effects of new-generation TMEM16A inhibitors on calcium-activated chloride currents in rabbit urethral interstitial cells of Cajal." Pflugers Arch **469**(11): 1443-1455.
- Feigenson, G. W. (2006). "Phase behavior of lipid mixtures." Nat Chem Biol **2**(11): 560-563.
- Ferrera, L., A. Caputo and L. J. Galiotta (2010). "TMEM16A protein: a new identity for Ca²⁺-dependent Cl⁻ channels." Physiology (Bethesda) **25**(6): 357-363.
- Ferrera, L., A. Caputo, I. Ubbly, E. Bussani, O. Zegarra-Moran, R. Ravazzolo, F. Pagani and L. J. V. Galiotta (2009). "Regulation of TMEM16A chloride channel properties by alternative splicing." The Journal of biological chemistry **284**(48): 33360-33368.
- Flores, C. A., L. P. Cid, F. V. Sepúlveda and M. I. Niemeyer (2009). "TMEM16 proteins: the long awaited calcium-activated chloride channels?" Braz J Med Biol Res **42**(11): 993-1001.
- Formigli, L., C. Sassoli, R. Squecco, F. Bini, M. Martinesi, F. Chellini, G. Luciani, F. Sbrana, S. Zecchi-Orlandini, F. Francini and E. Meacci (2009). "Regulation of transient receptor potential canonical channel 1 (TRPC1) by sphingosine 1-phosphate in C2C12 myoblasts and its relevance for a role of mechanotransduction in skeletal muscle differentiation." J Cell Sci **122**(Pt 9): 1322-1333.
- Foskett, J. K., C. White, K. H. Cheung and D. O. Mak (2007). "Inositol trisphosphate receptor Ca²⁺ release channels." Physiol Rev **87**(2): 593-658.
- Foster, M. N. and W. A. Coetzee (2016). "KATP Channels in the Cardiovascular System." Physiol Rev **96**(1): 177-252.
- Friedrich, G. and P. Soriano (1991). "Promoter traps in embryonic stem cells: a genetic screen to identify and mutate developmental genes in mice." Genes Dev **5**(9): 1513-1523.
- Fujii, T., A. Sakata, S. Nishimura, K. Eto and S. Nagata (2015). "TMEM16F is required for phosphatidylserine exposure and microparticle release in activated mouse platelets." Proceedings of the National Academy of Sciences **112**(41): 12800-12805.

- Furness, J. B. (2017). "The physiological relevance of constriction of mesenteric arteries by topically applied noradrenaline." The Journal of physiology **595**(21): 6783-6784.
- Gaengel, K., G. Genové, A. Armulik and C. Betsholtz (2009). "Endothelial-mural cell signaling in vascular development and angiogenesis." Arterioscler Thromb Vasc Biol **29**(5): 630-638.
- Galletta, L. J., P. Pagesy, C. Folli, E. Caci, L. Romio, B. Costes, E. Nicolis, G. Cabrini, M. Goossens, R. Ravazzolo and O. Zegarra-Moran (2002). "IL-4 is a potent modulator of ion transport in the human bronchial epithelium in vitro." J Immunol **168**(2): 839-845.
- Galione, A. and G. C. Churchill (2002). "Interactions between calcium release pathways: multiple messengers and multiple stores." Cell Calcium **32**(5-6): 343-354.
- Garland, C. J., C. R. Hiley and K. A. Dora (2011). "EDHF: spreading the influence of the endothelium." Br J Pharmacol **164**(3): 839-852.
- Garner, B., D. J. Harvey, L. Royle, M. Frischmann, F. Nigon, M. J. Chapman and P. M. Rudd (2001). "Characterization of human apolipoprotein B100 oligosaccharides in LDL subfractions derived from normal and hyperlipidemic plasma: deficiency of alpha-N-acetylneuraminylactosyl-ceramide in light and small dense LDL particles." Glycobiology **11**(10): 791-802.
- Garver, W. S., K. Krishnan, J. R. Gallagos, M. Michikawa, G. A. Francis and R. A. Heidenreich (2002). "Niemann-Pick C1 protein regulates cholesterol transport to the trans-Golgi network and plasma membrane caveolae." J Lipid Res **43**(4): 579-589.
- Genovese, M., A. Borrelli, A. Venturini, D. Guidone, E. Caci, G. Viscido, G. Gambardella, D. di Bernardo, P. Scudieri and L. J. V. Galletta (2019). "TRPV4 and purinergic receptor signalling pathways are separately linked in airway epithelia to CFTR and TMEM16A chloride channels." The Journal of Physiology **597**(24): 5859-5878.
- Gerasimenko, J. V., A. V. Tepikin, O. H. Petersen and O. V. Gerasimenko (1998). "Calcium uptake via endocytosis with rapid release from acidifying endosomes." Curr Biol **8**(24): 1335-1338.
- Giepmans, B. N. and S. C. van Ijzendoorn (2009). "Epithelial cell-cell junctions and plasma membrane domains." Biochim Biophys Acta **1788**(4): 820-831.
- Goldman, D. E. (1943). "POTENTIAL, IMPEDANCE, AND RECTIFICATION IN MEMBRANES." J Gen Physiol **27**(1): 37-60.
- Goldstein, J. L., R. G. Anderson and M. S. Brown (1979). "Coated pits, coated vesicles, and receptor-mediated endocytosis." Nature **279**(5715): 679-685.
- Gonzales, A. L., Y. Yang, M. N. Sullivan, L. Sanders, F. Dabertrand, D. C. Hill-Eubanks, M. T. Nelson and S. Earley (2014). "A PLC γ 1-dependent, force-sensitive signaling network in the myogenic constriction of cerebral arteries." Sci Signal **7**(327): ra49.
- Gorter, E. and F. Grendel (1925). "ON BIMOLECULAR LAYERS OF LIPOIDS ON THE CHROMOCYTES OF THE BLOOD." The Journal of experimental medicine **41**(4): 439-443.
- Grant, B. D. and J. G. Donaldson (2009). "Pathways and mechanisms of endocytic recycling." Nat Rev Mol Cell Biol **10**(9): 597-608.
- Green (2012). Molecular Cloning: A Laboratory Manual, Fourth Edition (3 Volume Set)
- Griffin, L. D., W. Gong, L. Verot and S. H. Mellon (2004). "Niemann-Pick type C disease involves disrupted neurosteroidogenesis and responds to allopregnanolone." Nat Med **10**(7): 704-711.
- Gritli-Linde, A., F. Vaziri Sani, J. R. Rock, K. Hallberg, D. Iribarne, B. D. Harfe and A. Linde (2009). "Expression patterns of the Tmem16 gene family during cephalic development in the mouse." Gene Expr Patterns **9**(3): 178-191.
- Grouleff, J., S. J. Irudayam, K. K. Skeby and B. Schiøtt (2015). "The influence of cholesterol on membrane protein structure, function, and dynamics studied by molecular dynamics simulations." Biochim Biophys Acta **1848**(9): 1783-1795.

- Grubb, S., K. A. Poulsen, C. A. Juul, T. Kyed, T. K. Klausen, E. H. Larsen and E. K. Hoffmann (2013). "TMEM16F (Anoctamin 6), an anion channel of delayed Ca(2+) activation." J Gen Physiol **141**(5): 585-600.
- Gruenberg, J. (2001). "The endocytic pathway: a mosaic of domains." Nat Rev Mol Cell Biol **2**(10): 721-730.
- Gunaratne, G. S., E. Brailoiu, S. He, E. M. Unterwald, S. Patel, J. T. Slama, T. F. Walseth and J. S. Marchant (2021). "Essential requirement for JPT2 in NAADP-evoked Ca(2+) signaling." Sci Signal **14**(675).
- Guo, C., Y. Ma, S. Ma, F. Mu, J. Deng, J. Duan, L. Xiong, Y. Yin, Y. Wang, M. Xi and A. Wen (2017). "The Role of TRPC6 in the Neuroprotection of Calycosin Against Cerebral Ischemic Injury." Scientific Reports **7**(1): 3039.
- Guyton AC, H. J. (2015). Textbook of medical physiology. Philadelphia, Elsevier Saunders.
- Gyobu, S., K. Ishihara, J. Suzuki, K. Segawa and S. Nagata (2017). "Characterization of the scrambling domain of the TMEM16 family." Proc Natl Acad Sci U S A **114**(24): 6274-6279.
- Gyobu, S., H. Miyata, M. Ikawa, D. Yamazaki, H. Takeshima, J. Suzuki and S. Nagata (2016). "A Role of TMEM16E Carrying a Scrambling Domain in Sperm Motility." Mol Cell Biol **36**(4): 645-659.
- Habibi, I., E. S. Emamian and A. Abdi (2014). "Quantitative analysis of intracellular communication and signaling errors in signaling networks." BMC Syst Biol **8**: 89.
- Hajjar, I., J. M. Kotchen and T. A. Kotchen (2006). "Hypertension: trends in prevalence, incidence, and control." Annu Rev Public Health **27**: 465-490.
- Hall, C. N., C. Reynell, B. Gesslein, N. B. Hamilton, A. Mishra, B. A. Sutherland, F. M. O'Farrell, A. M. Buchan, M. Lauritzen and D. Attwell (2014). "Capillary pericytes regulate cerebral blood flow in health and disease." Nature **508**(7494): 55-60.
- Halliday, M. R., S. V. Rege, Q. Ma, Z. Zhao, C. A. Miller, E. A. Winkler and B. V. Zlokovic (2016). "Accelerated pericyte degeneration and blood-brain barrier breakdown in apolipoprotein E4 carriers with Alzheimer's disease." J Cereb Blood Flow Metab **36**(1): 216-227.
- Hamill, O. P., A. Marty, E. Neher, B. Sakmann and F. J. Sigworth (1981). "Improved patch-clamp techniques for high-resolution current recording from cells and cell-free membrane patches." Pflugers Arch **391**(2): 85-100.
- Hanahan, D. (1983). "Studies on transformation of Escherichia coli with plasmids." J Mol Biol **166**(4): 557-580.
- Hannun, Y. A. (1996). "Functions of ceramide in coordinating cellular responses to stress." Science **274**(5294): 1855-1859.
- Harada, A., Y. Takei, Y. Kanai, Y. Tanaka, S. Nonaka and N. Hirokawa (1998). "Golgi vesiculation and lysosome dispersion in cells lacking cytoplasmic dynein." The Journal of cell biology **141**(1): 51-59.
- Hartmann, D. A., A. A. Berthiaume, R. I. Grant, S. A. Harrill, T. Koski, T. Tieu, K. P. McDowell, A. V. Faino, A. L. Kelly and A. Y. Shih (2021). "Brain capillary pericytes exert a substantial but slow influence on blood flow." Nat Neurosci **24**(5): 633-645.
- Hartwig, J. H., G. M. Bokoch, C. L. Carpenter, P. A. Janmey, L. A. Taylor, A. Toker and T. P. Stossel (1995). "Thrombin receptor ligation and activated Rac uncap actin filament barbed ends through phosphoinositide synthesis in permeabilized human platelets." Cell **82**(4): 643-653.
- Hartzell, C., I. Putzier and J. Arreola (2005). "Calcium-activated chloride channels." Annu Rev Physiol **67**: 719-758.
- Hartzell, H. C., K. Yu, Q. Xiao, L. T. Chien and Z. Qu (2009). "Anoctamin/TMEM16 family members are Ca2+-activated Cl- channels." J Physiol **587**(Pt 10): 2127-2139.
- Hastings, C., C. Vieira, B. Liu, C. Bascon, C. Gao, R. Y. Wang, A. Casey and S. Hrynkow (2019). "Expanded access with intravenous hydroxypropyl-β-cyclodextrin to

treat children and young adults with Niemann-Pick disease type C1: a case report analysis." Orphanet Journal of Rare Diseases **14**(1): 228.

- Hawn, M. B., E. Akin, H. C. Hartzell, I. A. Greenwood and N. Leblanc (2021). "Molecular mechanisms of activation and regulation of ANO1-Encoded Ca(2+)-Activated Cl(-) channels." Channels (Austin) **15**(1): 569-603.
- Heald, R. and O. Cohen-Fix (2014). "Morphology and function of membrane-bound organelles." Curr Opin Cell Biol **26**: 79-86.
- Heinemann, S. H. and F. Conti (1992). "Nonstationary noise analysis and application to patch clamp recordings." Methods Enzymol **207**: 131-148.
- Heinze, C., A. Seniuk, M. V. Sokolov, A. K. Huebner, A. E. Klementowicz, I. A. Szijarto, J. Schleifenbaum, H. Vitzthum, M. Gollasch, H. Ehmke, B. C. Schroeder and C. A. Hubner (2014). "Disruption of vascular Ca²⁺-activated chloride currents lowers blood pressure." J Clin Invest **124**(2): 675-686.
- Heinze, C., A. Seniuk, M. V. Sokolov, A. K. Huebner, A. E. Klementowicz, I. A. Szijártó, J. Schleifenbaum, H. Vitzthum, M. Gollasch, H. Ehmke, B. C. Schroeder and C. A. Hübner (2014). "Disruption of vascular Ca²⁺-activated chloride currents lowers blood pressure." J Clin Invest **124**(2): 675-686.
- Heistad, D. D. and M. L. Marcus (1979). "Role of vasa vasorum in nourishment of the aorta." Blood Vessels **16**(5): 225-238.
- Hendriksz, C. J., M. Anheim, P. Bauer, O. Bonnot, A. Chakrapani, J.-C. Corvol, T. J. de Koning, A. Degtyareva, C. Dionisi-Vici, S. Doss, T. Duning, P. Giunti, R. Iodice, T. Johnston, D. Kelly, H.-H. Klünemann, S. Lorenzl, A. Padovani, M. Pocovi, M. Synofzik, A. Terblanche, F. Then Bergh, M. Topçu, C. Tranchant, M. Walterfang, C. Velten and S. A. Kolb (2017). "The hidden Niemann-Pick type C patient: clinical niches for a rare inherited metabolic disease." Current medical research and opinion **33**(5): 877-890.
- Herring, N. P., D. J. (2018). Levick's Introduction to Cardiovascular Physiology. London; New York, Boca Raton.
- Hibbs, E., S. Love and J. S. Miners (2021). "Pericyte Contractile Responses to Endothelin-1 and A β Peptides: Assessment by Electrical Impedance Assay." Frontiers in Cellular Neuroscience **15**(331).
- Higaki, K., H. Ninomiya, Y. Sugimoto, T. Suzuki, M. Taniguchi, H. Niwa, P. G. Pentchev, M. T. Vanier and K. Ohno (2001). "Isolation of NPC1-deficient Chinese hamster ovary cell mutants by gene trap mutagenesis." J Biochem **129**(6): 875-880.
- Hill-Eubanks, D. C., M. E. Werner, T. J. Heppner and M. T. Nelson (2011). "Calcium signaling in smooth muscle." Cold Spring Harb Perspect Biol **3**(9): a004549.
- Hille, B. (2001). Ion channels of excitable membranes., Sinauer: Sunderland, Mass.
- Hirst, G. D. and F. R. Edwards (1989). "Sympathetic neuroeffector transmission in arteries and arterioles." Physiol Rev **69**(2): 546-604.
- Hla, T. (2003). "Signaling and biological actions of sphingosine 1-phosphate." Pharmacol Res **47**(5): 401-407.
- Hla, T. (2004). "Physiological and pathological actions of sphingosine 1-phosphate." Semin Cell Dev Biol **15**(5): 513-520.
- Hoglinger, D., T. Burgoyne, E. Sanchez-Heras, P. Hartwig, A. Colaco, J. Newton, C. E. Futter, S. Spiegel, F. M. Platt and E. R. Eden (2019). "NPC1 regulates ER contacts with endocytic organelles to mediate cholesterol egress." Nat Commun **10**(1): 4276.
- Hong, G. S., S. H. Lee, B. Lee, J. H. Choi, S. J. Oh, Y. Jang, E. M. Hwang, H. Kim, J. Jung, I. B. Kim and U. Oh (2019). "ANO1/TMEM16A regulates process maturation in radial glial cells in the developing brain." Proc Natl Acad Sci U S A **116**(25): 12494-12499.
- Huang, F., J. R. Rock, B. D. Harfe, T. Cheng, X. Huang, Y. N. Jan and L. Y. Jan (2009). "Studies on expression and function of the TMEM16A calcium-activated chloride channel." Proc Natl Acad Sci U S A **106**(50): 21413-21418.

- Hübner, C. A., B. C. Schroeder and H. Ehmke (2015). "Regulation of vascular tone and arterial blood pressure: role of chloride transport in vascular smooth muscle." Pflugers Arch **467**(3): 605-614.
- Hume, J. R., G. X. Wang, J. Yamazaki, L. C. Ng and D. Duan (2010). "CLC-3 chloride channels in the pulmonary vasculature." Adv Exp Med Biol **661**: 237-247.
- Infante, R. E., L. Abi-Mosleh, A. Radhakrishnan, J. D. Dale, M. S. Brown and J. L. Goldstein (2008). "Purified NPC1 protein. I. Binding of cholesterol and oxysterols to a 1278-amino acid membrane protein." J Biol Chem **283**(2): 1052-1063.
- Ioannou, Y. A. (2005). "Guilty until proven innocent: the case of NPC1 and cholesterol." Trends Biochem Sci **30**(9): 498-505.
- Ishida, Y., S. Nayak, J. A. Mindell and M. Grabe (2013). "A model of lysosomal pH regulation." The Journal of general physiology **141**(6): 705-720.
- Ishii, H., T. Takahashi, M. Toyono, M. Tamura, K. Harada, M. Yoshida, Y. Nishikawa, K. Enomoto and G. Takada (2006). "Acid sphingomyelinase deficiency: cardiac dysfunction and characteristic findings of the coronary arteries." J Inherit Metab Dis **29**(1): 232-234.
- Jackson, W. F. (2005). "Potassium channels in the peripheral microcirculation." Microcirculation **12**(1): 113-127.
- Jackson, W. F. (2020). "Ion channels and the regulation of myogenic tone in peripheral arterioles." Curr Top Membr **85**: 19-58.
- Jackson, W. F. (2021). "Calcium-Dependent Ion Channels and the Regulation of Arteriolar Myogenic Tone." Frontiers in Physiology **12**(1924).
- Jackson, W. F. and K. L. Blair (1998). "Characterization and function of Ca(2+)-activated K⁺ channels in arteriolar muscle cells." Am J Physiol **274**(1): H27-34.
- Jacobsen, L. B., S. A. Calvin, K. E. Colvin and M. Wright (2004). "FuGENE 6 Transfection Reagent: the gentle power." Methods **33**(2): 104-112.
- Jaggar, J. H., V. A. Porter, W. J. Lederer and M. T. Nelson (2000). "Calcium sparks in smooth muscle." Am J Physiol Cell Physiol **278**(2): C235-256.
- Jaiswal, J. K., N. W. Andrews and S. M. Simon (2002). "Membrane proximal lysosomes are the major vesicles responsible for calcium-dependent exocytosis in nonsecretory cells." J Cell Biol **159**(4): 625-635.
- Jeng, G., M. Aggarwal, W.-P. Yu and T.-Y. Chen (2016). "Independent activation of distinct pores in dimeric TMEM16A channels." The Journal of general physiology **148**(5): 393-404.
- Jensen, A. B., H. B. Joergensen, V. S. Dam, D. Kamaev, D. Boedtkjer, E. M. Füchtbauer, C. Aalkjaer and V. V. Matchkov (2018). "Variable Contribution of TMEM16A to Tone in Murine Arterial Vasculature." Basic Clin Pharmacol Toxicol **123**(1): 30-41.
- Jeong, M. S., J.-s. Bae and H. K. Jin (2019). "Vascular endothelial growth factor improves the therapeutic effects of cyclodextrin in Niemann-Pick type C mice." Animal Cells and Systems **23**(5): 346-354.
- Jeong, M. S., J. S. Bae and H. K. Jin (2019). "Vascular endothelial growth factor improves the therapeutic effects of cyclodextrin in Niemann-Pick type C mice." Anim Cells Syst (Seoul) **23**(5): 346-354.
- Jia, Z. and J. Chen (2021). "Specific PIP2 binding promotes calcium activation of TMEM16A chloride channels." Commun Biol **4**(1): 259.
- Jiang, T., K. Yu, H. C. Hartzell and E. Tajkhorshid (2017). "Lipids and ions traverse the membrane by the same physical pathway in the nhTMEM16 scramblase." Elife **6**.
- Jin, Y., B. S. Strunk and L. S. Weisman (2015). "Close encounters of the lysosome-peroxisome kind." Cell **161**(2): 197-198.
- Johnson, D. E., P. Ostrowski, V. Jaumouillé and S. Grinstein (2016). "The position of lysosomes within the cell determines their luminal pH." The Journal of cell biology **212**(6): 677-692.

- Jovic, M., M. Sharma, J. Rahajeng and S. Caplan (2010). "The early endosome: a busy sorting station for proteins at the crossroads." Histol Histopathol **25**(1): 99-112.
- Jurman, M. E., L. M. Boland, Y. Liu and G. Yellen (1994). "Visual identification of individual transfected cells for electrophysiology using antibody-coated beads." Biotechniques **17**(5): 876-881.
- Kalienkova, V., V. Clerico Mosina and C. Paulino (2021). "The Groovy TMEM16 Family: Molecular Mechanisms of Lipid Scrambling and Ion Conduction." J Mol Biol **433**(16): 166941.
- Kar, P. and A. Parekh (2013). "STIM proteins, Orai1 and gene expression." Channels (Austin) **7**(5): 374-378.
- Kilkenny, C., W. Browne, I. C. Cuthill, M. Emerson and D. G. Altman (2010). "Animal research: reporting in vivo experiments: the ARRIVE guidelines." Br J Pharmacol **160**(7): 1577-1579.
- Kisler, K., A. R. Nelson, S. V. Rege, A. Ramanathan, Y. Wang, A. Ahuja, D. Lazic, P. S. Tsai, Z. Zhao, Y. Zhou, D. A. Boas, S. Sakadžić and B. V. Zlokovic (2017). "Pericyte degeneration leads to neurovascular uncoupling and limits oxygen supply to brain." Nat Neurosci **20**(3): 406-416.
- Klabunde (2012). Cardiovascular physiology concepts. Philadelphia, PA, Lippincott Williams & Wilkins/Wolters Kluwer.
- Kloner, R. A., K. S. King and M. G. Harrington (2018). "No-reflow phenomenon in the heart and brain." Am J Physiol Heart Circ Physiol **315**(3): H550-h562.
- Klumperman, J. and G. Raposo (2014). "The complex ultrastructure of the endolysosomal system." Cold Spring Harb Perspect Biol **6**(10): a016857.
- Kmit, A., R. van Kruchten, J. Ousingsawat, N. J. Mattheij, B. Senden-Gijsbers, J. W. Heemskerk, R. Schreiber, E. M. Bevers and K. Kunzelmann (2013). "Calcium-activated and apoptotic phospholipid scrambling induced by Ano6 can occur independently of Ano6 ion currents." Cell Death Dis **4**(4): e611.
- Ko, D. C., M. D. Gordon, J. Y. Jin and M. P. Scott (2001). "Dynamic movements of organelles containing Niemann-Pick C1 protein: NPC1 involvement in late endocytic events." Mol Biol Cell **12**(3): 601-614.
- Koga, J. and M. Aikawa (2012). "Crosstalk between macrophages and smooth muscle cells in atherosclerotic vascular diseases." Vascul Pharmacol **57**(1): 24-28.
- Kolter, T. (2012). "Ganglioside biochemistry." ISRN Biochem **2012**: 506160.
- Kolter, T. and K. Sandhoff (2010). "Lysosomal degradation of membrane lipids." FEBS Lett **584**(9): 1700-1712.
- Korte, N., Z. Ilkan, C. Pearson, T. Pfeiffer, P. Singhal, J. Rock, H. Sethi, D. Gill, D. Attwell and P. Tammaro (2022). "The Ca²⁺-gated Cl⁻ channel TMEM16A amplifies capillary pericyte contraction reducing cerebral blood flow after ischemia." bioRxiv: 2022.2002.2003.479031.
- Kramer, J. and R. S. Hawley (2003). "The spindle-associated transmembrane protein Axs identifies a membranous structure ensheathing the meiotic spindle." Nat Cell Biol **5**(3): 261-263.
- Kuang, Q., P. Purhonen and H. Hebert (2015). "Structure of potassium channels." Cell Mol Life Sci **72**(19): 3677-3693.
- Kumar, N. M. and N. B. Gilula (1996). "The gap junction communication channel." Cell **84**(3): 381-388.
- Kunzelmann, K., Y. Tian, J. R. Martins, D. Faria, P. Kongsuphol, J. Ousingsawat, F. Thevenod, E. Roussa, J. Rock and R. Schreiber (2011). "Anoctamins." Pflugers Arch **462**(2): 195-208.
- Kur, J., P. Bankhead, C. N. Scholfield, T. M. Curtis and J. G. McGeown (2013). "Ca²⁺ sparks promote myogenic tone in retinal arterioles." Br J Pharmacol **168**(7): 1675-1686.

- Kuruma, A. and H. C. Hartzell (1999). "Dynamics of calcium regulation of chloride currents in *Xenopus oocytes*." *Am J Physiol* **276**(1): C161-175.
- Kuruma, A., Y. Hirayama and H. C. Hartzell (2000). "A hyperpolarization- and acid-activated nonselective cation current in *Xenopus oocytes*." *Am J Physiol Cell Physiol* **279**(5): C1401-1413.
- Kuwabara, P. E. and M. Labouesse (2002). "The sterol-sensing domain: multiple families, a unique role?" *Trends Genet* **18**(4): 193-201.
- Kwik, J., S. Boyle, D. Fooksman, L. Margolis, M. P. Sheetz and M. Edidin (2003). "Membrane cholesterol, lateral mobility, and the phosphatidylinositol 4,5-bisphosphate-dependent organization of cell actin." *Proc Natl Acad Sci U S A* **100**(24): 13964-13969.
- Lamirault, G., M. Artifoni, M. Daniel, N. Barber-Chamoux and H. Nantes University Hospital Working Group On (2020). "Resistant Hypertension: Novel Insights." *Curr Hypertens Rev* **16**(1): 61-72.
- Lange, Y. (1991). "Disposition of intracellular cholesterol in human fibroblasts." *J Lipid Res* **32**(2): 329-339.
- Langmuir, I. (1917). "THE CONSTITUTION AND FUNDAMENTAL PROPERTIES OF SOLIDS AND LIQUIDS. II. LIQUIDS.1." *Journal of the American Chemical Society* **39**(9): 1848-1906.
- Large, W. A. and Q. Wang (1996). "Characteristics and physiological role of the Ca(2+)-activated Cl⁻ conductance in smooth muscle." *Am J Physiol* **271**(2 Pt 1): C435-454.
- Larivière, R., G. Thibault and E. L. Schiffrin (1993). "Increased endothelin-1 content in blood vessels of deoxycorticosterone acetate-salt hypertensive but not in spontaneously hypertensive rats." *Hypertension* **21**(3): 294-300.
- Le, S. C., Z. Jia, J. Chen and H. Yang (2019). "Molecular basis of PIP2-dependent regulation of the Ca(2+)-activated chloride channel TMEM16A." *Nat Commun* **10**(1): 3769.
- Leblanc, N., J. Ledoux, S. Saleh, A. Sanguinetti, J. Angermann, K. O'Driscoll, F. Britton, B. A. Perrino and I. A. Greenwood (2005). "Regulation of calcium-activated chloride channels in smooth muscle cells: a complex picture is emerging." *Can J Physiol Pharmacol* **83**(7): 541-556.
- Lee, B. C., G. Khelashvili, M. Falzone, A. K. Menon, H. Weinstein and A. Accardi (2018). "Gating mechanism of the extracellular entry to the lipid pathway in a TMEM16 scramblase." *Nat Commun* **9**(1): 3251.
- Lee, W. C., M. Watanabe, H. Yokoshiki, T. Temma, R. Kamada, H. Hagiwara, Y. Takahashi, T. Koya, M. Nakao and T. Anzai (2020). "Higher Pulmonary Arterial Pressure Was Related to Non-Pulmonary Vein Atrial Tachyarrhythmia." *Int Heart J* **61**(6): 1150-1156.
- Lee, W. K., P. K. Chakraborty, E. Roussa, N. A. Wolff and F. Thévenod (2012). "ERK1/2-dependent bestrophin-3 expression prevents ER-stress-induced cell death in renal epithelial cells by reducing CHOP." *Biochim Biophys Acta* **1823**(10): 1864-1876.
- Lemmey, H. A. L., C. J. Garland and K. A. Dora (2020). "Intrinsic regulation of microvascular tone by myoendothelial feedback circuits." *Curr Top Membr* **85**: 327-355.
- Leon-Aparicio, D., A. Sánchez-Solano, J. Arreola and P. Perez-Cornejo (2022). "Oleic acid blocks the calcium-activated chloride channel TMEM16A/ANO1." *Biochim Biophys Acta Mol Cell Biol Lipids* **1867**(5): 159134.
- Levy, B. I., G. Ambrosio, A. R. Pries and H. A. J. Struijker-Boudier (2001). "Microcirculation in Hypertension." *Circulation* **104**(6): 735-740.
- Levy MN, P. A., Berne RM (2007). *Cardiovascular physiology*. Philadelphia, Pa, Mosby Elsevier.

- Li, J., S. Lü, Y. Liu, C. Pang, Y. Chen, S. Zhang, H. Yu, M. Long, H. Zhang, D. E. Logothetis, Y. Zhan and H. An (2015). "Identification of the Conformational transition pathway in PIP2 Opening Kir Channels." Sci Rep **5**: 11289.
- Li, K. X., M. He, W. Ye, J. Simms, M. Gill, X. Xiang, Y. N. Jan and L. Y. Jan (2019). "TMEM16B regulates anxiety-related behavior and GABAergic neuronal signaling in the central lateral amygdala." Elife **8**.
- Li, L., R. Wang, K. T. Ma, X. Z. Li, C. L. Zhang, W. D. Liu, L. Zhao and J. Q. Si (2014). "Differential effect of calcium-activated potassium and chloride channels on rat basilar artery vasomotion." J Huazhong Univ Sci Technolog Med Sci **34**(4): 482-490.
- Li, X., F. Lu, M. N. Trinh, P. Schmiede, J. Seemann, J. Wang and G. Blobel (2017). "3.3 Å structure of Niemann–Pick C1 protein reveals insights into the function of the C-terminal luminal domain in cholesterol transport." Proceedings of the National Academy of Sciences **114**(34): 9116.
- Li, X., J. Wang, E. Coutavas, H. Shi, Q. Hao and G. Blobel (2016). "Structure of human Niemann-Pick C1 protein." Proc Natl Acad Sci U S A **113**(29): 8212-8217.
- Lightle, S., R. Tosheva, A. Lee, J. Queen-Baker, B. Boyanovsky, S. Shedlofsky and M. Nikolova-Karakashian (2003). "Elevation of ceramide in serum lipoproteins during acute phase response in humans and mice: role of serine-palmitoyl transferase." Arch Biochem Biophys **419**(2): 120-128.
- Lim, N. K., A. K. Lam and R. Dutzler (2016). "Independent activation of ion conduction pores in the double-barreled calcium-activated chloride channel TMEM16A." J Gen Physiol **148**(5): 375-392.
- Lin, C. X., X. F. Lv, F. Yuan, X. Y. Li, M. M. Ma, C. Z. Liu, J. G. Zhou, G. L. Wang and Y. Y. Guan (2018). "Ca(2+)/Calmodulin-Dependent Protein Kinase II γ -Dependent Serine727 Phosphorylation Is Required for TMEM16A Ca(2+)-Activated Cl(-) Channel Regulation in Cerebrovascular Cells." Circ J **82**(3): 903-913.
- Lin, J. J., X. H. Liu, L. Xia, Y. L. Feng, X. H. Xi and S. H. Lu (2021). "A Niemann-pick C1 disease child with BCG-itis: a case report and analysis." BMC Pediatr **21**(1): 218.
- Lin, Y. C., M. Boone, L. Meuris, I. Lemmens, N. Van Roy, A. Soete, J. Reumers, M. Moisse, S. Plaisance, R. Drmanac, J. Chen, F. Speleman, D. Lambrechts, Y. Van de Peer, J. Tavernier and N. Callewaert (2014). "Genome dynamics of the human embryonic kidney 293 lineage in response to cell biology manipulations." Nat Commun **5**: 4767.
- Lingwood, C. A. (2011). "Glycosphingolipid functions." Cold Spring Harb Perspect Biol **3**(7).
- Liu, B. (2012). "Therapeutic potential of cyclodextrins in the treatment of Niemann-Pick type C disease." Clin Lipidol **7**(3): 289-301.
- Liu, P. Y., Z. Zhang, Y. Liu, X. L. Tang, S. Shu, X. Y. Bao, Y. Zhang, Y. Gu, Y. Xu and X. Cao (2019). "TMEM16A Inhibition Preserves Blood-Brain Barrier Integrity After Ischemic Stroke." Front Cell Neurosci **13**: 360.
- Liu, Y., H. Zhang, D. Huang, J. Qi, J. Xu, H. Gao, X. Du, N. Gamper and H. Zhang (2015). "Characterization of the effects of Cl⁻ channel modulators on TMEM16A and bestrophin-1 Ca²⁺ activated Cl⁻ channels." Pflugers Arch **467**(7): 1417-1430.
- Liu, Y., Y. Zhou and K. Zhu (2012). "Inhibition of glioma cell lysosome exocytosis inhibits glioma invasion." PloS one **7**(9): e45910-e45910.
- Lloyd-Evans, E., A. J. Morgan, X. He, D. A. Smith, E. Elliot-Smith, D. J. Sillence, G. C. Churchill, E. H. Schuchman, A. Galione and F. M. Platt (2008). "Niemann-Pick disease type C1 is a sphingosine storage disease that causes deregulation of lysosomal calcium." Nat Med **14**(11): 1247-1255.
- Lloyd-Evans, E. and F. M. Platt (2010). "Lipids on Trial: The Search for the Offending Metabolite in Niemann-Pick type C Disease." Traffic **11**(4): 419-428.
- Lockwich, T. P., X. Liu, B. B. Singh, J. Jadowiec, S. Weiland and I. S. Ambudkar (2000). "Assembly of Trp1 in a signaling complex associated with caveolin-scaffolding lipid raft domains." J Biol Chem **275**(16): 11934-11942.

- Longden, T. A. and M. T. Nelson (2015). "Vascular inward rectifier K⁺ channels as external K⁺ sensors in the control of cerebral blood flow." Microcirculation **22**(3): 183-196.
- Lopatin, A. N., E. N. Makhina and C. G. Nichols (1994). "Potassium channel block by cytoplasmic polyamines as the mechanism of intrinsic rectification." Nature **372**(6504): 366-369.
- Louwette, S., L. Regal, C. Wittevrongel, C. Thys, G. Vandeweeghde, E. Decuyper, P. Leemans, R. De Vos, C. Van Geet, J. Jaeken and K. Freson (2013). "NPC1 defect results in abnormal platelet formation and function: studies in Niemann-Pick disease type C1 patients and zebrafish." Hum Mol Genet **22**(1): 61-73.
- Lu, F., Q. Liang, L. Abi-Mosleh, A. Das, J. K. De Brabander, J. L. Goldstein and M. S. Brown (2015). "Identification of NPC1 as the target of U18666A, an inhibitor of lysosomal cholesterol export and Ebola infection." Elife **4**.
- Lucena-Aguilar, G., A. M. Sánchez-López, C. Barberán-Aceituno, J. A. Carrillo-Ávila, J. A. López-Guerrero and R. Aguilar-Quesada (2016). "DNA Source Selection for Downstream Applications Based on DNA Quality Indicators Analysis." Biopreservation and biobanking **14**(4): 264-270.
- Luissint, A. C., C. Artus, F. Glacial, K. Ganeshamoorthy and P. O. Couraud (2012). "Tight junctions at the blood brain barrier: physiological architecture and disease-associated dysregulation." Fluids Barriers CNS **9**(1): 23.
- Luzio, J. P., N. A. Bright and P. R. Pryor (2007). "The role of calcium and other ions in sorting and delivery in the late endocytic pathway." Biochem Soc Trans **35**(Pt 5): 1088-1091.
- Lydic, T. A. and Y. H. Goo (2018). "Lipidomics unveils the complexity of the lipidome in metabolic diseases." Clin Transl Med **7**(1): 4.
- Ma, Q., Z. Zhao, A. P. Sagare, Y. Wu, M. Wang, N. C. Owens, P. B. Verghese, J. Herz, D. M. Holtzman and B. V. Zlokovic (2018). "Blood-brain barrier-associated pericytes internalize and clear aggregated amyloid- β 42 by LRP1-dependent apolipoprotein E isoform-specific mechanism." Mol Neurodegener **13**(1): 57.
- Ma, W., J. Xu, Q. Wang, Y. Xin, L. Zhang, X. Zheng, H. Wang, K. Sun, R. Hui and X. Huang (2010). "Interaction of functional NPC1 gene polymorphism with smoking on coronary heart disease." BMC Med Genet **11**: 149.
- MacLennan, D. H., M. Asahi and A. R. Tupling (2003). "The regulation of SERCA-type pumps by phospholamban and sarcolipin." Ann N Y Acad Sci **986**: 472-480.
- Malathi, K., K. Higaki, A. H. Tinkelenberg, D. A. Balderes, D. Almanzar-Paramio, L. J. Wilcox, N. Erdeniz, F. Redican, M. Padamsee, Y. Liu, S. Khan, F. Alcantara, E. D. Carstea, J. A. Morris and S. L. Sturley (2004). "Mutagenesis of the putative sterol-sensing domain of yeast Niemann Pick C-related protein reveals a primordial role in subcellular sphingolipid distribution." The Journal of cell biology **164**(4): 547-556.
- Malvezzi, M., M. Chalat, R. Janjusevic, A. Picollo, H. Terashima, A. K. Menon and A. Accardi (2013). "Ca²⁺-dependent phospholipid scrambling by a reconstituted TMEM16 ion channel." Nat Commun **4**: 2367.
- Manoury, B., A. Tamuleviciute and P. Tammara (2010). "TMEM16A/anoctamin 1 protein mediates calcium-activated chloride currents in pulmonary arterial smooth muscle cells." J Physiol **588**(Pt 13): 2305-2314.
- Marino, A., G. G. Genchi, E. Sinibaldi and G. Ciofani (2017). "Piezoelectric Effects of Materials on Bio-Interfaces." ACS Applied Materials & Interfaces **9**(21): 17663-17680.
- Marques, A. R. A. and P. Saftig (2019). "Lysosomal storage disorders – challenges, concepts and avenues for therapy: beyond rare diseases." Journal of Cell Science **132**(2): jcs221739.
- Matchkov, V. V., C. Aalkjaer and H. Nilsson (2005). "Distribution of cGMP-dependent and cGMP-independent Ca(2⁺)-activated Cl(-) conductances in smooth muscle cells from different vascular beds and colon." Pflugers Arch **451**(2): 371-379.

- Matchkov, V. V., D. M. Boedtkjer and C. Aalkjaer (2015). "The role of Ca(2+) activated Cl(-) channels in blood pressure control." Curr Opin Pharmacol **21**: 127-137.
- Matchkov, V. V., P. Larsen, E. V. Bouzinova, A. Rojek, D. M. Boedtkjer, V. Golubinskaya, F. S. Pedersen, C. Aalkjaer and H. Nilsson (2008). "Bestrophin-3 (vitelliform macular dystrophy 2-like 3 protein) is essential for the cGMP-dependent calcium-activated chloride conductance in vascular smooth muscle cells." Circ Res **103**(8): 864-872.
- Matchkov, V. V., V. Secher Dam, D. M. Bodtkjer and C. Aalkjaer (2013). "Transport and function of chloride in vascular smooth muscles." J Vasc Res **50**(1): 69-87.
- Matsuda, H. (1988). "Open-state substructure of inwardly rectifying potassium channels revealed by magnesium block in guinea-pig heart cells." J Physiol **397**: 237-258.
- Mayor, S. and R. E. Pagano (2007). "Pathways of clathrin-independent endocytosis." Nat Rev Mol Cell Biol **8**(8): 603-612.
- Mayran, N., R. G. Parton and J. Gruenberg (2003). "Annexin II regulates multivesicular endosome biogenesis in the degradation pathway of animal cells." Embo j **22**(13): 3242-3253.
- McGrath, J. C. and E. Lilley (2015). "Implementing guidelines on reporting research using animals (ARRIVE etc.): new requirements for publication in BJP." Br J Pharmacol **172**(13): 3189-3193.
- McGuigan, J. A. and F. Stumpff (2013). "Calculated and measured [Ca(2+)] in buffers used to calibrate Ca(2+) macroelectrodes." Anal Biochem **436**(1): 29-35.
- Megías-Vericat, J. E., M. J. Company-Albir, A. A. García-Robles and J. L. Poveda (2018). Use of 2-Hydroxypropyl-Beta-Cyclodextrin for Niemann-Pick Type C Disease. Cyclodextrin - A Versatile Ingredient.
- Mendelsohn, M. E. (2005). "In hypertension, the kidney is not always the heart of the matter." The Journal of clinical investigation **115**(4): 840-844.
- Miledi, R. (1982). "A calcium-dependent transient outward current in *Xenopus laevis* oocytes." Proc R Soc Lond B Biol Sci **215**(1201): 491-497.
- Milenkovic, V. M., M. Brockmann, H. Stöhr, B. H. Weber and O. Strauss (2010). "Evolution and functional divergence of the anoctamin family of membrane proteins." BMC evolutionary biology **10**: 319-319.
- Millard, E. E., K. Srivastava, L. M. Traub, J. E. Schaffer and D. S. Ory (2000). "Niemann-pick type C1 (NPC1) overexpression alters cellular cholesterol homeostasis." J Biol Chem **275**(49): 38445-38451.
- Mindell, J. A. (2012). "Lysosomal acidification mechanisms." Annu Rev Physiol **74**: 69-86.
- Miners, J. S., I. Schulz and S. Love (2018). "Differing associations between A β accumulation, hypoperfusion, blood-brain barrier dysfunction and loss of PDGFRB pericyte marker in the precuneus and parietal white matter in Alzheimer's disease." J Cereb Blood Flow Metab **38**(1): 103-115.
- Mishra, A., F. M. O'Farrell, C. Reynell, N. B. Hamilton, C. N. Hall and D. Attwell (2014). "Imaging pericytes and capillary diameter in brain slices and isolated retinae." Nature Protocols **9**(2): 323-336.
- Mistry, D. K. and C. J. Garland (1999). "The influence of phenylephrine outward potassium currents in single smooth muscle cells from the rabbit mesenteric artery." Gen Pharmacol **33**(5): 389-399.
- Miyawaki, A., J. Llopis, R. Heim, J. M. McCaffery, J. A. Adams, M. Ikura and R. Y. Tsien (1997). "Fluorescent indicators for Ca²⁺ based on green fluorescent proteins and calmodulin." Nature **388**(6645): 882-887.
- Molleman, A. (2008). Patch clamping : an introductory guide to patch clamp electrophysiology. Chichester, Wiley.

- Morris, M. D., C. Bhuvaneshwaran, H. Shio and S. Fowler (1982). "Lysosome lipid storage disorder in NCTR-BALB/c mice. I. Description of the disease and genetics." Am J Pathol **108**(2): 140-149.
- Mulvany, M. J. and W. Halpern (1977). "Contractile properties of small arterial resistance vessels in spontaneously hypertensive and normotensive rats." Circ Res **41**(1): 19-26.
- Nakajo, K. and Y. Kubo (2015). "KCNQ1 channel modulation by KCNE proteins via the voltage-sensing domain." The Journal of physiology **593**(12): 2617-2625.
- Namkung, W., W. E. Finkbeiner and A. S. Verkman (2010). "CFTR-adenylyl cyclase I association responsible for UTP activation of CFTR in well-differentiated primary human bronchial cell cultures." Mol Biol Cell **21**(15): 2639-2648.
- Namkung, W., P. W. Phuan and A. S. Verkman (2011). "TMEM16A inhibitors reveal TMEM16A as a minor component of calcium-activated chloride channel conductance in airway and intestinal epithelial cells." J Biol Chem **286**(3): 2365-2374.
- Namkung, W., J. R. Thiagarajah, P. W. Phuan and A. S. Verkman (2010). "Inhibition of Ca²⁺-activated Cl⁻ channels by gallotannins as a possible molecular basis for health benefits of red wine and green tea." Faseb j **24**(11): 4178-4186.
- Neher, E. (1992). "Correction for liquid junction potentials in patch clamp experiments." Methods Enzymol **207**: 123-131.
- Nelson, A. R., M. A. Sagare, Y. Wang, K. Kisler, Z. Zhao and B. V. Zlokovic (2020). "Channelrhodopsin Excitation Contracts Brain Pericytes and Reduces Blood Flow in the Aging Mouse Brain in vivo." Frontiers in Aging Neuroscience **12**.
- Nelson, M. T., H. Cheng, M. Rubart, L. F. Santana, A. D. Bonev, H. J. Knot and W. J. Lederer (1995). "Relaxation of arterial smooth muscle by calcium sparks." Science **270**(5236): 633-637.
- Nelson, M. T., M. A. Conway, H. J. Knot and J. E. Brayden (1997). "Chloride channel blockers inhibit myogenic tone in rat cerebral arteries." J Physiol **502 (Pt 2)**(Pt 2): 259-264.
- Nelson, M. T., J. B. Patlak, J. F. Worley and N. B. Standen (1990). "Calcium channels, potassium channels, and voltage dependence of arterial smooth muscle tone." Am J Physiol **259**(1 Pt 1): C3-18.
- Neylon, C. B. (2002). "Potassium channels and vascular proliferation." Vascul Pharmacol **38**(1): 35-41.
- Ni, Y.-L., A.-S. Kuan and T.-Y. Chen (2014). "Activation and inhibition of TMEM16A calcium-activated chloride channels." PloS one **9**(1): e86734-e86734.
- Nixon, R. A., J. Wegiel, A. Kumar, W. H. Yu, C. Peterhoff, A. Cataldo and A. M. Cuervo (2005). "Extensive involvement of autophagy in Alzheimer disease: an immunoelectron microscopy study." J Neuropathol Exp Neurol **64**(2): 113-122.
- Nortley, R., N. Korte, P. Izquierdo, C. Hirunpattarasilp, A. Mishra, Z. Jaunmuktane, V. Kyrargyri, T. Pfeiffer, L. Khennouf, C. Madry, H. Gong, A. Richard-Loendt, W. Huang, T. Saito, C. Saido Takaomi, S. Brandner, H. Sethi and D. Attwell (2019). "Amyloid β oligomers constrict human capillaries in Alzheimer's disease via signaling to pericytes." Science **365**(6450): eaav9518.
- Nortley, R., N. Korte, P. Izquierdo, C. Hirunpattarasilp, A. Mishra, Z. Jaunmuktane, V. Kyrargyri, T. Pfeiffer, L. Khennouf, C. Madry, H. Gong, A. Richard-Loendt, W. Huang, T. Saito, T. C. Saido, S. Brandner, H. Sethi and D. Attwell (2019). "Amyloid β oligomers constrict human capillaries in Alzheimer's disease via signaling to pericytes." Science **365**(6450).
- Ogunbayo, O. A., J. Duan, J. Xiong, Q. Wang, X. Feng, J. Ma, M. X. Zhu and A. M. Evans (2018). "mTORC1 controls lysosomal Ca²⁺ release through the two-pore channel TPC2." Science Signaling **11**(525): eaao5775.
- Ohgami, N., D. C. Ko, M. Thomas, M. P. Scott, C. C. Y. Chang and T.-Y. Chang (2004). "Binding between the Niemann–Pick C1 protein and a photoactivatable cholesterol

analog requires a functional sterol-sensing domain." Proceedings of the National Academy of Sciences of the United States of America **101**(34): 12473-12478.

- Pallottini, V. and F. W. Pfrieger (2020). "Understanding and Treating Niemann-Pick Type C Disease: Models Matter." Int J Mol Sci **21**(23).
- Papp, R., C. Nagaraj, D. Zabini, B. M. Nagy, M. Lengyel, D. Skofic Maurer, N. Sharma, B. Egemnazarov, G. Kovacs, G. Kwapiszewska, L. M. Marsh, A. Hrzenjak, G. Höfler, M. Didiasova, M. Wygrecka, L. K. Sievers, P. Szucs, P. Enyedi, B. Ghanim, W. Klepetko, H. Olschewski and A. Olschewski (2019). "Targeting TMEM16A to reverse vasoconstriction and remodelling in idiopathic pulmonary arterial hypertension." Eur Respir J **53**(6).
- Park, W. D., J. F. O'Brien, P. A. Lundquist, D. L. Kraft, C. W. Vockley, P. S. Karnes, M. C. Patterson and K. Snow (2003). "Identification of 58 novel mutations in Niemann-Pick disease type C: correlation with biochemical phenotype and importance of PTC1-like domains in NPC1." Hum Mutat **22**(4): 313-325.
- Parton, R. G. and K. Simons (2007). "The multiple faces of caveolae." Nature Reviews Molecular Cell Biology **8**(3): 185-194.
- Patel, S. and X. Cai (2015). "Evolution of acidic Ca²⁺ stores and their resident Ca²⁺-permeable channels." Cell Calcium **57**(3): 222-230.
- Patel, S. and R. Docampo (2010). "Acidic calcium stores open for business: expanding the potential for intracellular Ca²⁺ signaling." Trends Cell Biol **20**(5): 277-286.
- Patterson, M. C., P. Clayton, P. Gissen, M. Anheim, P. Bauer, O. Bonnot, A. Dardis, C. Dionisi-Vici, H. H. Klünemann, P. Latour, C. M. Lourenço, D. S. Ory, A. Parker, M. Pocoví, M. Strupp, M. T. Vanier, M. Walterfang and T. Marquardt (2017). "Recommendations for the detection and diagnosis of Niemann-Pick disease type C: An update." Neurol Clin Pract **7**(6): 499-511.
- Patterson, M. C., W. S. Garver, R. Giugliani, J. Imrie, H. Jahnova, F. J. Meaney, Y. Nadjar, M. T. Vanier, P. Moneuse, O. Morand, D. Rosenberg, B. Schwierin and B. Héron (2020). "Long-term survival outcomes of patients with Niemann-Pick disease type C receiving miglustat treatment: A large retrospective observational study." Journal of Inherited Metabolic Disease **43**(5): 1060-1069.
- Patterson, M. C., D. Vecchio, H. Prady, L. Abel and J. E. Wraith (2007). "Miglustat for treatment of Niemann-Pick C disease: a randomised controlled study." Lancet Neurol **6**(9): 765-772.
- Paulino, C., V. Kalienkova, A. K. M. Lam, Y. Neldner and R. Dutzler (2017). "Activation mechanism of the calcium-activated chloride channel TMEM16A revealed by cryo-EM." Nature **552**(7685): 421-425.
- Peake, K. B. and J. E. Vance (2012). "Normalization of cholesterol homeostasis by 2-hydroxypropyl- β -cyclodextrin in neurons and glia from Niemann-Pick C1 (NPC1)-deficient mice." The Journal of biological chemistry **287**(12): 9290-9298.
- Pedemonte, N. and L. J. Galletta (2014). "Structure and function of TMEM16 proteins (anoctamins)." Physiol Rev **94**(2): 419-459.
- Pentchev, P. G., M. E. Comly, H. S. Kruth, M. T. Vanier, D. A. Wenger, S. Patel and R. O. Brady (1985). "A defect in cholesterol esterification in Niemann-Pick disease (type C) patients." Proc Natl Acad Sci U S A **82**(23): 8247-8251.
- Pentchev, P. G., A. E. Gal, A. D. Booth, F. Omodeo-Sale, J. Fouks, B. A. Neumeyer, J. M. Quirk, G. Dawson and R. O. Brady (1980). "A lysosomal storage disorder in mice characterized by a dual deficiency of sphingomyelinase and glucocerebrosidase." Biochim Biophys Acta **619**(3): 669-679.
- Peppiatt, C. M., C. Howarth, P. Mobbs and D. Attwell (2006). "Bidirectional control of CNS capillary diameter by pericytes." Nature **443**(7112): 700-704.
- Periasamy, M. and A. Kalyanasundaram (2007). "SERCA pump isoforms: their role in calcium transport and disease." Muscle Nerve **35**(4): 430-442.
- Persell, S. D. (2011). "Prevalence of resistant hypertension in the United States, 2003-2008." Hypertension **57**(6): 1076-1080.

- Persidsky, Y., J. Hill, M. Zhang, H. Dykstra, M. Winfield, N. L. Reichenbach, R. Potula, A. Mukherjee, S. H. Ramirez and S. Rom (2016). "Dysfunction of brain pericytes in chronic neuroinflammation." J Cereb Blood Flow Metab **36**(4): 794-807.
- Peters, C. J., J. M. Gilchrist, J. Tien, N. P. Bethel, L. Qi, T. Chen, L. Wang, Y. N. Jan, M. Grabe and L. Y. Jan (2018). "The Sixth Transmembrane Segment Is a Major Gating Component of the TMEM16A Calcium-Activated Chloride Channel." Neuron **97**(5): 1063-1077 e1064.
- Peters, S. M., M. J. Tijssen, C. H. van Os, J. F. Wetzels and R. J. Bindels (1998). "Hypoxia decreases calcium influx into rat proximal tubules." Kidney Int **53**(3): 703-708.
- Petkovic, M., J. Oses-Prieto, A. Burlingame, L. Y. Jan and Y. N. Jan (2020). "TMEM16K is an interorganelle regulator of endosomal sorting." Nat Commun **11**(1): 3298.
- Pifferi, S. (2017). "Permeation Mechanisms in the TMEM16B Calcium-Activated Chloride Channels." PLoS One **12**(1): e0169572.
- Pifferi, S., V. Cenedese and A. Menini (2012). "Anoctamin 2/TMEM16B: a calcium-activated chloride channel in olfactory transduction." Exp Physiol **97**(2): 193-199.
- Pifferi, S., M. Dibattista and A. Menini (2009). "TMEM16B induces chloride currents activated by calcium in mammalian cells." Pflugers Arch **458**(6): 1023-1038.
- Pifferi, S. and A. Menini (2021). "Paving the way for designing drugs targeting TMEM16A." Trends Pharmacol Sci.
- Pike, L. J. (2006). "Rafts defined: a report on the Keystone Symposium on Lipid Rafts and Cell Function." J Lipid Res **47**(7): 1597-1598.
- Pinton, P., T. Pozzan and R. Rizzuto (1998). "The Golgi apparatus is an inositol 1,4,5-trisphosphate-sensitive Ca²⁺ store, with functional properties distinct from those of the endoplasmic reticulum." Embo j **17**(18): 5298-5308.
- Pitt, S. J., A. K. Lam, K. Rietdorf, A. Galione and R. Sitsapesan (2014). "Reconstituted human TPC1 is a proton-permeable ion channel and is activated by NAADP or Ca²⁺." Sci Signal **7**(326): ra46.
- Plaster, N. M., R. Tawil, M. Tristani-Firouzi, S. Canún, S. Bendahhou, A. Tsunoda, M. R. Donaldson, S. T. Iannaccone, E. Brunt, R. Barohn, J. Clark, F. Deymeer, A. L. George, Jr., F. A. Fish, A. Hahn, A. Nitu, C. Ozdemir, P. Serdaroglu, S. H. Subramony, G. Wolfe, Y. H. Fu and L. J. Ptácek (2001). "Mutations in Kir2.1 cause the developmental and episodic electrical phenotypes of Andersen's syndrome." Cell **105**(4): 511-519.
- Platt, F. M. (2018). "Emptying the stores: lysosomal diseases and therapeutic strategies." Nat Rev Drug Discov **17**(2): 133-150.
- Podechard, N., E. Le Ferrec, A. Rebillard, O. Fardel and V. Lecureur (2009). "NPC1 repression contributes to lipid accumulation in human macrophages exposed to environmental aryl hydrocarbons." Cardiovasc Res **82**(2): 361-370.
- Praggastis, M., B. Tortelli, J. Zhang, H. Fujiwara, R. Sidhu, A. Chacko, Z. Chen, C. Chung, A. P. Lieberman, J. Sikora, C. Davidson, S. U. Walkley, N. H. Pipalia, F. R. Maxfield, J. E. Schaffer and D. S. Ory (2015). "A murine Niemann-Pick C1 I1061T knock-in model recapitulates the pathological features of the most prevalent human disease allele." J Neurosci **35**(21): 8091-8106.
- Pries, A. R., D. Neuhaus and P. Gaetgens (1992). "Blood viscosity in tube flow: dependence on diameter and hematocrit." Am J Physiol **263**(6 Pt 2): H1770-1778.
- Pryor, P. R., B. M. Mullock, N. A. Bright, S. R. Gray and J. P. Luzio (2000). "The role of intraorganellar Ca(2+) in late endosome-lysosome heterotypic fusion and in the reformation of lysosomes from hybrid organelles." J Cell Biol **149**(5): 1053-1062.
- Pugsley, M. K. and R. Tabrizchi (2000). "The vascular system. An overview of structure and function." J Pharmacol Toxicol Methods **44**(2): 333-340.
- Qiu, R. and R. S. Lewis (2019). "Structural features of STIM and Orai underlying store-operated calcium entry." Curr Opin Cell Biol **57**: 90-98.

- Quayle, J. M., A. D. Bonev, J. E. Brayden and M. T. Nelson (1994). "Calcitonin gene-related peptide activated ATP-sensitive K⁺ currents in rabbit arterial smooth muscle via protein kinase A." J Physiol **475**(1): 9-13.
- Rahman, M. S. (2019). "Prostacyclin: A major prostaglandin in the regulation of adipose tissue development." J Cell Physiol **234**(4): 3254-3262.
- Rainbow, R., A. Parker and N. Davies (2011). "Protein kinase C-independent inhibition of arterial smooth muscle K(+) channels by a diacylglycerol analogue." Br J Pharmacol **163**(4): 845-856.
- Rajantie, I., M. Ilmonen, A. Alminaitte, U. Ozerdem, K. Alitalo and P. Salven (2004). "Adult bone marrow-derived cells recruited during angiogenesis comprise precursors for periendothelial vascular mural cells." Blood **104**(7): 2084-2086.
- Ramu, Y., Y. Xu and Z. Lu (2007). "Inhibition of CFTR Cl⁻ channel function caused by enzymatic hydrolysis of sphingomyelin." Proc Natl Acad Sci U S A **104**(15): 6448-6453.
- Riordan, J. R., J. M. Rommens, B. Kerem, N. Alon, R. Rozmahel, Z. Grzelczak, J. Zielenski, S. Lok, N. Plavsic, J. L. Chou and et al. (1989). "Identification of the cystic fibrosis gene: cloning and characterization of complementary DNA." Science **245**(4922): 1066-1073.
- Robert, R., C. Norez and F. Becq (2005). "Disruption of CFTR chloride channel alters mechanical properties and cAMP-dependent Cl⁻ transport of mouse aortic smooth muscle cells." J Physiol **568**(Pt 2): 483-495.
- Rodríguez, A., P. Webster, J. Ortego and N. W. Andrews (1997). "Lysosomes behave as Ca²⁺-regulated exocytic vesicles in fibroblasts and epithelial cells." The Journal of cell biology **137**(1): 93-104.
- Roff, C. F., E. Goldin, M. E. Comly, A. Cooney, A. Brown, M. T. Vanier, S. P. Miller, R. O. Brady and P. G. Pentchev (1991). "Type C Niemann-Pick disease: use of hydrophobic amines to study defective cholesterol transport." Dev Neurosci **13**(4-5): 315-319.
- Roher, A. E., J. P. Debbins, M. Malek-Ahmadi, K. Chen, J. G. Pipe, S. Maze, C. Belden, C. L. Maarouf, P. Thiyyagura, H. Mo, J. M. Hunter, T. A. Kokjohn, D. G. Walker, J. C. Kruchowsky, M. Belohlavek, M. N. Sabbagh and T. G. Beach (2012). "Cerebral blood flow in Alzheimer's disease." Vasc Health Risk Manag **8**: 599-611.
- Rong, Y., C. K. McPhee, S. Deng, L. Huang, L. Chen, M. Liu, K. Tracy, E. H. Baehrecke, L. Yu and M. J. Lenardo (2011). "Spinster is required for autophagic lysosome reformation and mTOR reactivation following starvation." Proceedings of the National Academy of Sciences of the United States of America **108**(19): 7826-7831.
- Rorsman, N. J. G., C. M. Ta, H. Garnett, P. Swietach and P. Tammaro (2018). "Defining the ionic mechanisms of optogenetic control of vascular tone by channelrhodopsin-2." Br J Pharmacol **175**(11): 2028-2045.
- Rosenhouse-Dantsker, A. (2019). Regulation of Ion Channels by Membrane Lipids. Comprehensive Physiology: 31-68.
- Rosenhouse-Dantsker, A., E. Leal-Pinto, D. E. Logothetis and I. Levitan (2010). "Comparative analysis of cholesterol sensitivity of Kir channels: role of the CD loop." Channels (Austin) **4**(1): 63-66.
- Rouget, C. (1873). "Mémoire sur le développement, la structure et les propriétés physiologiques des capillaires sanguins et lymphatiques. ." Arch Physiol Norm Path **5**: 603-663.
- Ruas, M., L. C. Davis, C.-C. Chen, A. J. Morgan, K.-T. Chuang, T. F. Walseth, C. Grimm, C. Garnham, T. Powell, N. Platt, F. M. Platt, M. Biel, C. Wahl-Schott, J. Parrington and A. Galione (2015). "Expression of Ca²⁺-permeable two-pore channels rescues NAADP signalling in TPC-deficient cells." The EMBO journal **34**(13): 1743-1758.
- Ruas, M., K. Rietdorf, A. Arredouani, L. C. Davis, E. Lloyd-Evans, H. Koegel, T. M. Funnell, A. J. Morgan, J. A. Ward, K. Watanabe, X. Cheng, G. C. Churchill, M. X. Zhu, F. M. Platt, G. M. Wessel, J. Parrington and A. Galione (2010). "Purified TPC isoforms

form NAADP receptors with distinct roles for Ca(2+) signaling and endolysosomal trafficking." Curr Biol **20**(8): 703-709.

- Ryou, M. G. and R. T. Mallet (2018). "An In Vitro Oxygen-Glucose Deprivation Model for Studying Ischemia-Reperfusion Injury of Neuronal Cells." Methods Mol Biol **1717**: 229-235.
- Saba, J. D. and T. Hla (2004). "Point-counterpoint of sphingosine 1-phosphate metabolism." Circ Res **94**(6): 724-734.
- Sagare, A. P., R. D. Bell, Z. Zhao, Q. Ma, E. A. Winkler, A. Ramanathan and B. V. Zlokovic (2013). "Pericyte loss influences Alzheimer-like neurodegeneration in mice." Nature Communications **4**(1): 2932.
- Sagare, A. P., R. D. Bell, Z. Zhao, Q. Ma, E. A. Winkler, A. Ramanathan and B. V. Zlokovic (2013). "Pericyte loss influences Alzheimer-like neurodegeneration in mice." Nat Commun **4**: 2932.
- Sagheddu, C., A. Boccaccio, M. Dibattista, G. Montani, R. Tirindelli and A. Menini (2010). "Calcium concentration jumps reveal dynamic ion selectivity of calcium-activated chloride currents in mouse olfactory sensory neurons and TMEM16b-transfected HEK 293T cells." The Journal of physiology **588**(Pt 21): 4189-4204.
- Sagné, C., C. Agulhon, P. Ravassard, M. Darmon, M. Hamon, S. El Mestikawy, B. Gasnier and B. Giros (2001). "Identification and characterization of a lysosomal transporter for small neutral amino acids." Proceedings of the National Academy of Sciences of the United States of America **98**(13): 7206-7211.
- Saito, M., P. I. Hanson and P. Schlesinger (2007). "Luminal chloride-dependent activation of endosome calcium channels: patch clamp study of enlarged endosomes." J Biol Chem **282**(37): 27327-27333.
- Santiago-Mujica, E., S. Flunkert, R. Rabl, J. Neddens, T. Loeffler and B. Hutter-Paier (2019). "Hepatic and neuronal phenotype of NPC1(-/-) mice." Heliyon **5**(3): e01293.
- Sato, K., S. Kubo, H. Fujii, M. Okamoto, K. Takahashi, K. Takamatsu, A. Tanaka and M. Kuriyama (2012). "Diffusion tensor imaging and magnetic resonance spectroscopy of transient cerebral white matter lesions in X-linked Charcot-Marie-Tooth disease." J Neurol Sci **316**(1-2): 178-180.
- Sayet, I., G. Neuilly, L. Rakotoarisoa, C. Mironneau and J. Mironneau (1993). "Relation between alpha 1-adrenoceptor subtypes and noradrenaline-induced contraction in rat portal vein smooth muscle." Br J Pharmacol **110**(1): 207-212.
- Schreiber, R., J. Ousingsawat and K. Kunzelmann (2020). "Targeting of Intracellular TMEM16 Proteins to the Plasma Membrane and Activation by Purinergic Signaling." Int J Mol Sci **21**(11).
- Schroeder, B. C., T. Cheng, Y. N. Jan and L. Y. Jan (2008). "Expression cloning of TMEM16A as a calcium-activated chloride channel subunit." Cell **134**(6): 1019-1029.
- Schultz, N., E. Byman, M. Fex and M. Wennström (2017). "Amylin alters human brain pericyte viability and NG2 expression." J Cereb Blood Flow Metab **37**(4): 1470-1482.
- Scott, C. and Y. A. Ioannou (2004). "The NPC1 protein: structure implies function." Biochim Biophys Acta **1685**(1-3): 8-13.
- Scudieri, P., E. Caci, A. Venturini, E. Sondo, G. Pianigiani, C. Marchetti, R. Ravazzolo, F. Pagani and L. J. Galletta (2015). "Ion channel and lipid scramblase activity associated with expression of TMEM16F/ANO6 isoforms." J Physiol **593**(17): 3829-3848.
- Scudieri, P., E. Sondo, L. Ferrera and L. J. Galletta (2012). "The anoctamin family: TMEM16A and TMEM16B as calcium-activated chloride channels." Exp Physiol **97**(2): 177-183.
- Secomb, T. W. (2016). "Hemodynamics." Comprehensive Physiology **6**(2): 975-1003.
- Seftel, H. C., S. Johnson and E. A. Muller (1980). "Distribution and biosocial correlations of blood pressure levels in Johannesburg blacks." S Afr Med J **57**(9): 313-320.

- Seo, Y., H. K. Lee, J. Park, D. K. Jeon, S. Jo, M. Jo and W. Namkung (2016). "Ani9, A Novel Potent Small-Molecule ANO1 Inhibitor with Negligible Effect on ANO2." PLoS One **11**(5): e0155771.
- Sévin, M., G. Lesca, N. Baumann, G. Millat, O. Lyon-Caen, M. T. Vanier and F. Sedel (2007). "The adult form of Niemann-Pick disease type C." Brain **130**(Pt 1): 120-133.
- Shah, S., C. M. Carver, P. Mullen, S. Milne, V. Lukacs, M. S. Shapiro and N. Gamper (2020). "Local Ca(2+) signals couple activation of TRPV1 and ANO1 sensory ion channels." Sci Signal **13**(629).
- Shah, V. N., B. Chagot and W. J. Chazin (2006). "Calcium-Dependent Regulation of Ion Channels." Calcium Bind Proteins **1**(4): 203-212.
- Sharma, D. K., J. C. Brown, A. Choudhury, T. E. Peterson, E. Holicky, D. L. Marks, R. Simari, R. G. Parton and R. E. Pagano (2004). "Selective stimulation of caveolar endocytosis by glycosphingolipids and cholesterol." Mol Biol Cell **15**(7): 3114-3122.
- Shen, J. B., B. Jiang and A. J. Pappano (2000). "Comparison of L-type calcium channel blockade by nifedipine and/or cadmium in guinea pig ventricular myocytes." J Pharmacol Exp Ther **294**(2): 562-570.
- Sheridan, J. T., E. N. Worthington, K. Yu, S. E. Gabriel, H. C. Hartzell and R. Tarran (2011). "Characterization of the oligomeric structure of the Ca(2+)-activated Cl-channel Ano1/TMEM16A." The Journal of biological chemistry **286**(2): 1381-1388.
- Shinoda, W. (2016). "Permeability across lipid membranes." Biochim Biophys Acta **1858**(10): 2254-2265.
- Shlyonsky, V. G., F. Mies and S. Sariban-Sohraby (2003). "Epithelial sodium channel activity in detergent-resistant membrane microdomains." American Journal of Physiology-Renal Physiology **284**(1): F182-F188.
- Shyng, S. L., Q. Sha, T. Ferrigni, A. N. Lopatin and C. G. Nichols (1996). "Depletion of intracellular polyamines relieves inward rectification of potassium channels." Proc Natl Acad Sci U S A **93**(21): 12014-12019.
- Silvius, J. R. (2003). "Role of cholesterol in lipid raft formation: lessons from lipid model systems." Biochim Biophys Acta **1610**(2): 174-183.
- Sim, J. J., S. K. Bhandari, J. Shi, I. L. Liu, D. A. Calhoun, E. A. McGlynn, K. Kalantar-Zadeh and S. J. Jacobsen (2013). "Characteristics of resistant hypertension in a large, ethnically diverse hypertension population of an integrated health system." Mayo Clin Proc **88**(10): 1099-1107.
- Simons, K. and J. L. Sampaio (2011). "Membrane organization and lipid rafts." Cold Spring Harb Perspect Biol **3**(10): a004697.
- Simons, K. and G. van Meer (1988). "Lipid sorting in epithelial cells." Biochemistry **27**(17): 6197-6202.
- Singer, S. J. and G. L. Nicolson (1972). "The fluid mosaic model of the structure of cell membranes." Science **175**(4023): 720-731.
- Singh, R. D., V. Puri, J. T. Valiyaveetil, D. L. Marks, R. Bittman and R. E. Pagano (2003). "Selective caveolin-1-dependent endocytosis of glycosphingolipids." Mol Biol Cell **14**(8): 3254-3265.
- Smyth, L. C. D., J. Rustenhoven, E. L. Scotter, P. Schweder, R. L. M. Faull, T. I. H. Park and M. Dragunow (2018). "Markers for human brain pericytes and smooth muscle cells." J Chem Neuroanat **92**: 48-60.
- Sones, W. R., A. J. Davis, N. Leblanc and I. A. Greenwood (2010). "Cholesterol depletion alters amplitude and pharmacology of vascular calcium-activated chloride channels." Cardiovasc Res **87**(3): 476-484.
- Sonkusare, S. K., T. Dalsgaard, A. D. Bonev and M. T. Nelson (2016). "Inward rectifier potassium (Kir2.1) channels as end-stage boosters of endothelium-dependent vasodilators." J Physiol **594**(12): 3271-3285.
- Spiegel, R., A. Raas-Rothschild, O. Reish, M. Regev, V. Meiner, R. Bargal, V. Sury, K. Meir, M. Nadjari, G. Hermann, T. C. Iancu, S. A. Shalev and M. Zeigler (2009). "The clinical spectrum of fetal Niemann-Pick type C." Am J Med Genet A **149a**(3): 446-450.

- Spiegel, S. and S. Milstien (2003). "Exogenous and intracellularly generated sphingosine 1-phosphate can regulate cellular processes by divergent pathways." Biochem Soc Trans **31**(Pt 6): 1216-1219.
- Stutzin, A. and E. K. Hoffmann (2006). "Swelling-activated ion channels: functional regulation in cell-swelling, proliferation and apoptosis." Acta Physiol (Oxf) **187**(1-2): 27-42.
- Suenami, S., S. Iino and T. Kubo (2018). "Pharmacologic inhibition of phospholipase C in the brain attenuates early memory formation in the honeybee (*Apis mellifera* L.)." Biol Open **7**(1).
- Suh, B. C. and B. Hille (2007). "Electrostatic interaction of internal Mg²⁺ with membrane PIP₂ Seen with KCNQ K⁺ channels." J Gen Physiol **130**(3): 241-256.
- Sun, H., Y. Xia, O. Paudel, X. R. Yang and J. S. Sham (2012). "Chronic hypoxia-induced upregulation of Ca²⁺-activated Cl⁻ channel in pulmonary arterial myocytes: a mechanism contributing to enhanced vasoreactivity." J Physiol **590**(15): 3507-3521.
- Sun, X., D. L. Marks, W. D. Park, C. L. Wheatley, V. Puri, J. F. O'Brien, D. L. Kraft, P. A. Lundquist, M. C. Patterson, R. E. Pagano and K. Snow (2001). "Niemann-Pick C variant detection by altered sphingolipid trafficking and correlation with mutations within a specific domain of NPC1." Am J Hum Genet **68**(6): 1361-1372.
- Suzuki, J., T. Fujii, T. Imao, K. Ishihara, H. Kuba and S. Nagata (2013). "Calcium-dependent phospholipid scramblase activity of TMEM16 protein family members." J Biol Chem **288**(19): 13305-13316.
- Suzuki, J., M. Umeda, P. J. Sims and S. Nagata (2010). "Calcium-dependent phospholipid scrambling by TMEM16F." Nature **468**(7325): 834-838.
- Suzuki, T., Y. Suzuki, K. Asai, Y. Imaizumi and H. Yamamura (2021). "Hypoxia increases the proliferation of brain capillary endothelial cells via upregulation of TMEM16A Ca(2+)-activated Cl(-) channels." J Pharmacol Sci **146**(1): 65-69.
- Swaroop, M., N. Thorne, M. S. Rao, C. P. Austin, J. C. McKew and W. Zheng (2012). "Evaluation of cholesterol reduction activity of methyl- β -cyclodextrin using differentiated human neurons and astrocytes." Journal of biomolecular screening **17**(9): 1243-1251.
- Ta, C. M., K. E. Acheson, N. J. G. Rorsman, R. C. Jongkind and P. Tammaro (2017). "Contrasting effects of phosphatidylinositol 4,5-bisphosphate on cloned TMEM16A and TMEM16B channels." Br J Pharmacol **174**(18): 2984-2999.
- Taglieri, D. M., D. A. Delfín and M. M. Monasky (2013). "Cholesterol regulation of PIP(2): why cell type is so important." Frontiers in physiology **3**: 492-492.
- Tajima, N., Y. Itokazu, E. R. Korpi, P. Somerharju and R. Käkelä (2011). "Activity of BK(Ca) channel is modulated by membrane cholesterol content and association with Na⁺/K⁺-ATPase in human melanoma IGR39 cells." J Biol Chem **286**(7): 5624-5638.
- Tammaro, P. and F. M. Ashcroft (2007). "A mutation in the ATP-binding site of the Kir6.2 subunit of the KATP channel alters coupling with the SUR2A subunit." The Journal of physiology **584**(Pt 3): 743-753.
- Tammaro, P., A. L. Smith, B. L. Crowley and S. V. Smirnov (2005). "Modulation of the voltage-dependent K⁺ current by intracellular Mg²⁺ in rat aortic smooth muscle cells." Cardiovascular Research **65**(2): 387-396.
- Tanaka, Y., Y. Yamada, Y. Ishitsuka, M. Matsuo, K. Shiraishi, K. Wada, Y. Uchio, Y. Kondo, T. Takeo, N. Nakagata, T. Higashi, K. Motoyama, H. Arima, S. Mochinaga, K. Higaki, K. Ohno and T. Irie (2015). "Efficacy of 2-Hydroxypropyl- β -cyclodextrin in Niemann-Pick Disease Type C Model Mice and Its Pharmacokinetic Analysis in a Patient with the Disease." Biol Pharm Bull **38**(6): 844-851.
- Tasca, C. I., T. Dal-Cim and H. Cimarosti (2015). "In vitro oxygen-glucose deprivation to study ischemic cell death." Methods Mol Biol **1254**: 197-210.
- Taylor, C. W. (2002). "Controlling calcium entry." Cell **111**(6): 767-769.
- te Vruchte, D., E. Lloyd-Evans, R. J. Veldman, D. C. Neville, R. A. Dwek, F. M. Platt, W. J. van Blitterswijk and D. J. Sillence (2004). "Accumulation of glycosphingolipids in

- Niemann-Pick C disease disrupts endosomal transport." J Biol Chem **279**(25): 26167-26175.
- Teichert, M., L. Milde, A. Holm, L. Stanicek, N. Gengenbacher, S. Savant, T. Ruckdeschel, Z. Hasanov, K. Srivastava, J. Hu, S. Hertel, A. Bartol, K. Schlereth and H. G. Augustin (2017). "Pericyte-expressed Tie2 controls angiogenesis and vessel maturation." Nat Commun **8**: 16106.
 - Terashima, H., A. Picollo and A. Accardi (2013). "Purified TMEM16A is sufficient to form Ca²⁺-activated Cl⁻ channels." Proceedings of the National Academy of Sciences of the United States of America **110**(48): 19354-19359.
 - Thomas-Gatewood, C., Z. P. Neeb, S. Bulley, A. Adebisi, J. P. Bannister, M. D. Leo and J. H. Jaggard (2011). "TMEM16A channels generate Ca²⁺-activated Cl⁻ currents in cerebral artery smooth muscle cells." American journal of physiology. Heart and circulatory physiology **301**(5): H1819-H1827.
 - Thorneloe, K. S., A. L. Meredith, A. M. Knorn, R. W. Aldrich and M. T. Nelson (2005). "Urodynamic properties and neurotransmitter dependence of urinary bladder contractility in the BK channel deletion model of overactive bladder." Am J Physiol Renal Physiol **289**(3): F604-610.
 - Tian, Y., R. Schreiber and K. Kunzelmann (2012). "Anoctamins are a family of Ca²⁺-activated Cl⁻ channels." J Cell Sci **125**(Pt 21): 4991-4998.
 - Tien, J., H. Y. Lee, D. L. Minor, Jr., Y. N. Jan and L. Y. Jan (2013). "Identification of a dimerization domain in the TMEM16A calcium-activated chloride channel (CaCC)." Proceedings of the National Academy of Sciences of the United States of America **110**(16): 6352-6357.
 - Tien, J., C. J. Peters, X. M. Wong, T. Cheng, Y. N. Jan, L. Y. Jan and H. Yang (2014). "A comprehensive search for calcium binding sites critical for TMEM16A calcium-activated chloride channel activity." eLife **3**: e02772.
 - Tiscione, S. A., O. Vivas, K. S. Ginsburg, D. M. Bers, D. S. Ory, L. F. Santana, R. E. Dixon and E. J. Dickson (2019). "Disease-associated mutations in Niemann-Pick type C1 alter ER calcium signaling and neuronal plasticity." J Cell Biol.
 - Tseng, T. T., K. S. Gratwick, J. Kollman, D. Park, D. H. Nies, A. Goffeau and M. H. Saier, Jr. (1999). "The RND permease superfamily: an ancient, ubiquitous and diverse family that includes human disease and development proteins." J Mol Microbiol Biotechnol **1**(1): 107-125.
 - Tuzi, S., N. Uekama, M. Okada, S. Yamaguchi, H. Saito and H. Yagisawa (2003). "Structure and dynamics of the phospholipase C-delta1 pleckstrin homology domain located at the lipid bilayer surface." J Biol Chem **278**(30): 28019-28025.
 - Tykocki, N. R., E. M. Boerman and W. F. Jackson (2017). "Smooth Muscle Ion Channels and Regulation of Vascular Tone in Resistance Arteries and Arterioles." Compr Physiol **7**(2): 485-581.
 - Uings, I. J. and S. N. Farrow (2000). "Cell receptors and cell signalling." Mol Pathol **53**(6): 295-299.
 - Van Baelen, K., L. Dode, J. Vanoevelen, G. Callewaert, H. De Smedt, L. Missiaen, J. B. Parys, L. Raeymaekers and F. Wuytack (2004). "The Ca²⁺/Mn²⁺ pumps in the Golgi apparatus." Biochim Biophys Acta **1742**(1-3): 103-112.
 - van der Donk, W. A., A. L. Tsai and R. J. Kulmacz (2002). "The cyclooxygenase reaction mechanism." Biochemistry **41**(52): 15451-15458.
 - van Leeuwen, W., J. E. Vermeer, T. W. Gadella, Jr. and T. Munnik (2007). "Visualization of phosphatidylinositol 4,5-bisphosphate in the plasma membrane of suspension-cultured tobacco BY-2 cells and whole Arabidopsis seedlings." Plant J **52**(6): 1014-1026.
 - van Meer, G. (2005). "Cellular lipidomics." Embo j **24**(18): 3159-3165.
 - van Meer, G. and A. I. P. M. de Kroon (2011). "Lipid map of the mammalian cell." Journal of Cell Science **124**(1): 5.

- van Meer, G., D. R. Voelker and G. W. Feigenson (2008). "Membrane lipids: where they are and how they behave." Nat Rev Mol Cell Biol **9**(2): 112-124.
- Van Petegem, F. (2015). "Ryanodine receptors: allosteric ion channel giants." J Mol Biol **427**(1): 31-53.
- Van Renterghem, C. and M. Lazdunski (1993). "Endothelin and vasopressin activate low conductance chloride channels in aortic smooth muscle cells." Pflugers Arch **425**(1-2): 156-163.
- Vanier, M. T. (2010). "Niemann-Pick disease type C." Orphanet Journal of Rare Diseases **5**(1): 16.
- Vanlandewijck, M., L. He, M. A. Mäe, J. Andrae, K. Ando, F. Del Gaudio, K. Nahar, T. Lebouvier, B. Laviña, L. Gouveia, Y. Sun, E. Raschperger, M. Räsänen, Y. Zarb, N. Mochizuki, A. Keller, U. Lendahl and C. Betsholtz (2018). "A molecular atlas of cell types and zonation in the brain vasculature." Nature **554**(7693): 475-480.
- Vecsernyés, M., F. Fenyvesi, I. Bácskay, M. A. Deli, L. Szente and É. Fenyvesi (2014). "Cyclodextrins, blood-brain barrier, and treatment of neurological diseases." Arch Med Res **45**(8): 711-729.
- Vella, F. (1996). "The metabolic and molecular bases of inherited disease seventh edition: Edited by C R Scriver, A L Beaudet, W S Sly and D Valle. P 4605. McGraw-Hill, New York. 1995. ISBN 0-07-909826-6." Biochemical Education **24**(1): 65-65.
- Venkatachalam, K. and C. Montell (2007). "TRP channels." Annu Rev Biochem **76**: 387-417.
- Vermeer, S., A. Hoischen, R. P. Meijer, C. Gilissen, K. Neveling, N. Wieskamp, A. de Brouwer, M. Koenig, M. Anheim, M. Assoum, N. Drouot, S. Todorovic, V. Milic-Rasic, H. Lochmüller, G. Stevanin, C. Goizet, A. David, A. Durr, A. Brice, B. Kremer, B. P. van de Warrenburg, M. M. Schijvenaars, A. Heister, M. Kwint, P. Arts, J. van der Wijst, J. Veltman, E. J. Kamsteeg, H. Scheffer and N. Knoers (2010). "Targeted next-generation sequencing of a 12.5 Mb homozygous region reveals ANO10 mutations in patients with autosomal-recessive cerebellar ataxia." Am J Hum Genet **87**(6): 813-819.
- Vitner, E. B., F. M. Platt and A. H. Futerman (2010). "Common and uncommon pathogenic cascades in lysosomal storage diseases." J Biol Chem **285**(27): 20423-20427.
- Vivas, O., S. A. Tiscione, R. E. Dixon, D. S. Ory and E. J. Dickson (2019). "Niemann-Pick Type C Disease Reveals a Link between Lysosomal Cholesterol and PtdIns(4,5)P2 That Regulates Neuronal Excitability." Cell Rep **27**(9): 2636-2648 e2634.
- Vocke, K., K. Dauner, A. Hahn, A. Ulbrich, J. Broecker, S. Keller, S. Frings and F. Möhrlen (2013). "Calmodulin-dependent activation and inactivation of anoctamin calcium-gated chloride channels." J Gen Physiol **142**(4): 381-404.
- Vyas, A., R. Gomez-Casal, S. Cruz-Rangel, H. Villanueva, A. G. Sikora, P. Rajagopalan, D. Basu, J. Pacheco, G. R. V. Hammond, K. Kiselyov and U. Duvvuri (2022). "Lysosomal inhibition sensitizes TMEM16A-expressing cancer cells to chemotherapy." Proc Natl Acad Sci U S A **119**(12): e2100670119.
- Wainszelbaum, M. J., B. M. Proctor, S. E. Pontow, P. D. Stahl and M. A. Barbieri (2006). "IL4/PGE2 induction of an enlarged early endosomal compartment in mouse macrophages is Rab5-dependent." Exp Cell Res **312**(12): 2238-2251.
- Wang, B., C. Li, R. Huai and Z. Qu (2015). "Overexpression of ANO1/TMEM16A, an arterial Ca²⁺-activated Cl⁻ channel, contributes to spontaneous hypertension." J Mol Cell Cardiol **82**: 22-32.
- Wang, J., L. D. Carbone and M. A. Watsky (2002). "Receptor-mediated activation of a Cl⁻ current by LPA and S1P in cultured corneal keratocytes." Invest Ophthalmol Vis Sci **43**(10): 3202-3208.
- Wang, L., J. Simms, C. J. Peters, M. Tynan-La Fontaine, K. Li, T. M. Gill, Y. N. Jan and L. Y. Jan (2019). "TMEM16B Calcium-Activated Chloride Channels Regulate

- Action Potential Firing in Lateral Septum and Aggression in Male Mice." J Neurosci **39**(36): 7102-7117.
- Wang, M., H. Yang, L. Y. Zheng, Z. Zhang, Y. B. Tang, G. L. Wang, Y. H. Du, X. F. Lv, J. Liu, J. G. Zhou and Y. Y. Guan (2012). "Downregulation of TMEM16A calcium-activated chloride channel contributes to cerebrovascular remodeling during hypertension by promoting basilar smooth muscle cell proliferation." Circulation **125**(5): 697-707.
 - Wang, Z., B. Fermini, J. Feng and S. Nattel (1995). "Role of chloride currents in repolarizing rabbit atrial myocytes." Am J Physiol **268**(5 Pt 2): H1992-2002.
 - Wanitchakool, P., J. Ousingsawat, L. Sirianant, I. Cabrita, D. Faria, R. Schreiber and K. Kunzelmann (2017). "Cellular defects by deletion of ANO10 are due to deregulated local calcium signaling." Cell Signal **30**: 41-49.
 - Wardlaw, J. M., H. Benveniste, M. Nedergaard, B. V. Zlokovic, H. Mestre, H. Lee, F. N. Doubal, R. Brown, J. Ramirez, B. J. MacIntosh, A. Tannenbaum, L. Ballerini, R. L. Rungta, D. Boido, M. Sweeney, A. Montagne, S. Charpak, A. Joutel, K. J. Smith and S. E. Black (2020). "Perivascular spaces in the brain: anatomy, physiology and pathology." Nat Rev Neurol **16**(3): 137-153.
 - Wassif, C. A., J. L. Cross, J. Iben, L. Sanchez-Pulido, A. Cougnoux, F. M. Platt, D. S. Ory, C. P. Ponting, J. E. Bailey-Wilson, L. G. Biesecker and F. D. Porter (2016). "High incidence of unrecognized visceral/neurological late-onset Niemann-Pick disease, type C1, predicted by analysis of massively parallel sequencing data sets." Genet Med **18**(1): 41-48.
 - Wei, J., K. I. Galaviz, A. J. Kowalski, M. J. Magee, J. S. Haw, K. M. V. Narayan and M. K. Ali (2020). "Comparison of Cardiovascular Events Among Users of Different Classes of Antihypertension Medications: A Systematic Review and Network Meta-analysis." JAMA Netw Open **3**(2): e1921618.
 - Whitlock, J. M. and H. C. Hartzell (2016). "A Pore Idea: the ion conduction pathway of TMEM16/ANO proteins is composed partly of lipid." Pflugers Arch **468**(3): 455-473.
 - Whitlock, J. M. and H. C. Hartzell (2017). "Anoctamins/TMEM16 Proteins: Chloride Channels Flirting with Lipids and Extracellular Vesicles." Annual review of physiology **79**: 119-143.
 - Wiegand, V., T. Y. Chang, J. F. Strauss, 3rd, F. Fahrenholz and G. Gimpl (2003). "Transport of plasma membrane-derived cholesterol and the function of Niemann-Pick C1 Protein." Faseb j **17**(6): 782-784.
 - William K. Purves, D. E. S., Gordon H. Orians, H. Craig Heller (2004). Life: The Science of Biology Science.
 - Willie, C. K., Y. C. Tzeng, J. A. Fisher and P. N. Ainslie (2014). "Integrative regulation of human brain blood flow." J Physiol **592**(5): 841-859.
 - Winstone, A. M., L. A. Stelitano and C. M. Verity (2017). "Niemann-Pick type C as a cause of progressive intellectual and neurological deterioration in childhood." Dev Med Child Neurol **59**(9): 965-972.
 - Wojtanik, K. M. and L. Liscum (2003). "The transport of low density lipoprotein-derived cholesterol to the plasma membrane is defective in NPC1 cells." J Biol Chem **278**(17): 14850-14856.
 - Wolin, M. S. (1991). "Activated oxygen metabolites as regulators of vascular tone." Klin Wochenschr **69**(21-23): 1046-1049.
 - Worley, J. F., 3rd, J. W. Deitmer and M. T. Nelson (1986). "Single nisoldipine-sensitive calcium channels in smooth muscle cells isolated from rabbit mesenteric artery." Proc Natl Acad Sci U S A **83**(15): 5746-5750.
 - Wraith, J. E., N. Guffon, M. Rohrbach, W. L. Hwu, G. C. Korenke, B. Bembi, C. Luzy, R. Giorgino and F. Sedel (2009). "Natural history of Niemann-Pick disease type C in a multicentre observational retrospective cohort study." Mol Genet Metab **98**(3): 250-254.

- Wu, S. N., Y. K. Lo, B. I. Kuo and H. T. Chiang (2001). "Ceramide inhibits the inwardly rectifying potassium current in GH(3) lactotrophs." Endocrinology **142**(11): 4785-4794.
- Xiao, Q., K. Yu, P. Perez-Cornejo, Y. Cui, J. Arreola and H. C. Hartzell (2011). "Voltage- and calcium-dependent gating of TMEM16A/Ano1 chloride channels are physically coupled by the first intracellular loop." Proceedings of the National Academy of Sciences of the United States of America **108**(21): 8891-8896.
- Xie, L. H., S. A. John, B. Ribalet and J. N. Weiss (2008). "Phosphatidylinositol-4,5-bisphosphate (PIP2) regulation of strong inward rectifier Kir2.1 channels: multilevel positive cooperativity." J Physiol **586**(7): 1833-1848.
- Yamazaki, Y. and T. Kanekiyo (2017). "Blood-Brain Barrier Dysfunction and the Pathogenesis of Alzheimer's Disease." Int J Mol Sci **18**(9).
- Yang, H., A. Kim, T. David, D. Palmer, T. Jin, J. Tien, F. Huang, T. Cheng, S. R. Coughlin, Y. N. Jan and L. Y. Jan (2012). "TMEM16F forms a Ca²⁺-activated cation channel required for lipid scrambling in platelets during blood coagulation." Cell **151**(1): 111-122.
- Yang, Y. D., H. Cho, J. Y. Koo, M. H. Tak, Y. Cho, W. S. Shim, S. P. Park, J. Lee, B. Lee, B. M. Kim, R. Raouf, Y. K. Shin and U. Oh (2008). "TMEM16A confers receptor-activated calcium-dependent chloride conductance." Nature **455**(7217): 1210-1215.
- Yao, Z., W. Namkung, E. A. Ko, J. Park, L. Tradtrantip and A. S. Verkman (2012). "Fractionation of a herbal antidiarrheal medicine reveals eugenol as an inhibitor of Ca²⁺-Activated Cl⁻ channel TMEM16A." PLoS One **7**(5): e38030.
- Ye, W., T. W. Han, L. M. Nassar, M. Zubia, Y. N. Jan and L. Y. Jan (2018). "Phosphatidylinositol-(4, 5)-bisphosphate regulates calcium gating of small-conductance cation channel TMEM16F." Proc Natl Acad Sci U S A **115**(7): E1667-e1674.
- Yeagle, P. L. (1985). "Cholesterol and the cell membrane." Biochim Biophys Acta **822**(3-4): 267-287.
- Yektaeian, N., D. Mehrabani, M. Sepaskhah, S. Zare, I. Jamhiri and G. Hatam (2019). "Lipophilic tracer Dil and fluorescence labeling of acridine orange used for Leishmania major tracing in the fibroblast cells." Heliyon **5**(12): e03073.
- Yemisci, M., Y. Gursoy-Ozdemir, A. Vural, A. Can, K. Topalkara and T. Dalkara (2009). "Pericyte contraction induced by oxidative-nitrative stress impairs capillary reflow despite successful opening of an occluded cerebral artery." Nat Med **15**(9): 1031-1037.
- Yerushalmi, B., R. J. Sokol, M. R. Narkewicz, D. Smith, J. W. Ashmead and D. A. Wenger (2002). "Niemann-pick disease type C in neonatal cholestasis at a North American Center." J Pediatr Gastroenterol Nutr **35**(1): 44-50.
- Yin, Z. and M. A. Watsky (2005). "Chloride channel activity in human lung fibroblasts and myofibroblasts." Am J Physiol Lung Cell Mol Physiol **288**(6): L1110-1116.
- Yoo, S. H. (2010). "Secretory granules in inositol 1,4,5-trisphosphate-dependent Ca²⁺ signaling in the cytoplasm of neuroendocrine cells." Faseb j **24**(3): 653-664.
- Yu, K., J. M. Whitlock, K. Lee, E. A. Ortlund, Y. Y. Cui and H. C. Hartzell (2015). "Identification of a lipid scrambling domain in ANO6/TMEM16F." eLife **4**: e06901-e06901.
- Yu, K., J. Zhu, Z. Qu, Y. Y. Cui and H. C. Hartzell (2014). "Activation of the Ano1 (TMEM16A) chloride channel by calcium is not mediated by calmodulin." J Gen Physiol **143**(2): 253-267.
- Zalk, R., O. B. Clarke, A. des Georges, R. A. Grassucci, S. Reiken, F. Mancina, W. A. Hendrickson, J. Frank and A. R. Marks (2015). "Structure of a mammalian ryanodine receptor." Nature **517**(7532): 44-49.
- Zambrowicz, B. P., A. Imamoto, S. Fiering, L. A. Herzenberg, W. G. Kerr and P. Soriano (1997). "Disruption of overlapping transcripts in the ROSA beta geo 26 gene trap strain leads to widespread expression of beta-galactosidase in mouse embryos and hematopoietic cells." Proc Natl Acad Sci U S A **94**(8): 3789-3794.

- Zeisel, A., H. Hochgerner, P. Lönnerberg, A. Johnsson, F. Memic, J. van der Zwan, M. Häring, E. Braun, L. E. Borm, G. La Manno, S. Codeluppi, A. Furlan, K. Lee, N. Skene, K. D. Harris, J. Hjerling-Leffler, E. Arenas, P. Ernfors, U. Marklund and S. Linnarsson (2018). "Molecular Architecture of the Mouse Nervous System." Cell **174**(4): 999-1014.e1022.
- Zhainazarov, A. B., M. Spehr, C. H. Wetzel, H. Hatt and B. W. Ache (2004). "Modulation of the Olfactory CNG Channel by PtdIns(3,4,5)P₃." The Journal of Membrane Biology **201**(1): 51-57.
- Zhang, C. H., Y. Li, W. Zhao, L. M. Lifshitz, H. Li, B. D. Harfe, M. S. Zhu and R. ZhuGe (2013). "The transmembrane protein 16A Ca²⁺-activated Cl⁻ channel in airway smooth muscle contributes to airway hyperresponsiveness." Am J Respir Crit Care Med **187**(4): 374-381.
- Zhang, J., R. Berra-Romani, M. J. Sinnegger-Brauns, J. Striessnig, M. P. Blaustein and D. R. Matteson (2007). "Role of Cav1.2 L-type Ca²⁺ channels in vascular tone: effects of nifedipine and Mg²⁺." Am J Physiol Heart Circ Physiol **292**(1): H415-425.
- Zhang, J., X. Guan, K. Shah and J. Yan (2021). "Lsm12 is an NAADP receptor and a two-pore channel regulatory protein required for calcium mobilization from acidic organelles." Nat Commun **12**(1): 4739.
- Zhang, Q., P. Zhou, Z. Chen, M. Li, H. Jiang, Z. Gao and H. Yang (2013). "Dynamic PIP₂ interactions with voltage sensor elements contribute to KCNQ2 channel gating." Proc Natl Acad Sci U S A **110**(50): 20093-20098.
- Zhang, S., Y. Chen, H. An, H. Liu, J. Li, C. Pang, Q. Ji and Y. Zhan (2014). "A novel biophysical model on calcium and voltage dual dependent gating of calcium-activated chloride channel." J Theor Biol **355**: 229-235.
- Zhang, X., H. Li, H. Zhang, Y. Liu, L. Huo, Z. Jia, Y. Xue, X. Sun and W. Zhang (2017). "Inhibition of transmembrane member 16A calcium-activated chloride channels by natural flavonoids contributes to flavonoid anticancer effects." Br J Pharmacol **174**(14): 2334-2345.
- Zheng, W., J. Kollmeyer, H. Symolon, A. Momin, E. Munter, E. Wang, S. Kelly, J. C. Allegood, Y. Liu, Q. Peng, H. Ramaraju, M. C. Sullards, M. Cabot and A. H. Merrill, Jr. (2006). "Ceramide and other bioactive sphingolipid backbones in health and disease: lipidomic analysis, metabolism and roles in membrane structure, dynamics, signaling and autophagy." Biochim Biophys Acta **1758**(12): 1864-1884.
- Zheng, Y. M. and Y. X. Wang (2007). "Sodium-calcium exchanger in pulmonary artery smooth muscle cells." Ann N Y Acad Sci **1099**: 427-435.